Universität Stuttgart
Institut für Feuerungs- und Kraftwerkstechnik

Pfaffenwaldring 23 • 70569 Stuttgart • T +49 (0) 711 685-63487 • F +49 (0) 711 685-63491 • ifk@ifk.uni-stuttgart.de

***Master Thesis* Nr. 3566**

Cand. MSc. *Nelson Felipe Rincón Soto*

Betrieb und Simulation einer Technikumsanlage zur CO_2-Abscheidug mittels chemischer Absorption in einer Packungskolonne

Operation and Simulation of a technical-scale plant for CO_2 capture via chemical absorption in a packed column

Address: Allmandring 22C Zi. 4, 70569 - Stuttgart

Date of issue: 28.05.2018

Submission: 28.11.2018

Supervisor: MSc. Marc Oliver Schmid

Preface

I always pictured myself writing my master thesis on my childhood's all-life desktop at my parent's place while petting my cat and watching the last season of Project Runway. However, I honestly never thought that I would be writing it during a German fall with this breathtaking (Slightly too perfect) view of a European classic fairy-tale forest divisible from my window. I must say, that I own this view part of my inspiration/motivation and I would not have wanted it any other way; it is as unexpected as the number of things that I have learned writing this document.

Everybody have severe and minor problems, from the amount of sugar of the morning coffee to the finance plan to pay the mortgage of the sea-side vacation house. I profoundly believe that a series of minor problems must be cleared up before resolving the serious ones. The following document tackles one of those little problems, addressing a specific but straightforward question: What could be done to enhance the CO_2 capture of an already installed pilot plant via chemical absorption with MEA solutions? That would be my small contribution towards the topic, and I hope it enlightens further research on the subject, to eventually alleviate a significant problem: Abatement CO_2 global emissions.

I want to express my profound sense of gratitude to the Institute of Combustion and Power Plant Technology (IFK) at the University of Stuttgart for supporting all the experiments and simulations presented in this research project. A special acknowledgment to my supervisor, Marc Oliver Schmid, who was always willing to contribute to the project from his experience. Thank you for making this a colorful journey!

Task Description

Stuttgart, den 11.05.2018

Master Thesis Nr. 3566

Für Herrn cand. M.Sc. *Nelson Felipe Rincón Soto*

Betrieb und Simulation einer Technikumsanlage zur CO_2-Abscheidug mittels chemischer Absorption in einer Packungskolonne

Operation and Simulation of a technical-scale plant for CO_2 capture via chemical absorption in a packed column

Fossil befeuerte Kraftwerke sind in Deutschland für ca. 40% des Ausstoßes an klimarelevantem CO_2 verantwortlich. Zur Senkung des CO_2 Ausstoßes werden neben Maßnahmen zur Effizienzsteigerung der Kraftwerksanlagen derzeit verschiedene Verfahren zur CO_2-Rückhaltung entwickelt.

Ein mögliches Verfahren ist ein der Rauchgasreinigung nachgeschalteter chemischer Waschprozess. Dabei dienen wässrige Aminlösungen als Absorptionsmittel, mit dem das CO_2 aus dem Rauchgas entfernt wird. In einem zweiten Prozessschritt wird das Absorptionsmittel thermisch regeneriert, so dass es erneut zur Absorption eingesetzt werden kann und das CO_2 mit hoher Reinheit zur Weiterverwertung oder Speicherung zur Verfügung steht. Im Rahmen eines aktuellen Forschungsprojekts wird am IFK der Einsatz eines Packungswäschers zur CO_2 Absorption untersucht. Durch Füllkörper oder strukturierte Packungen wird eine große für den Stoffaustausch wirksame Oberfläche bei geringer Bauhöhe erreicht.

Im Rahmen der Abschlussarbeit sollen Versuche an einer bestehenden Technikumsanlage durchgeführt werden und die Anlage mit reaktiven Lösungsmitteln betrieben werden. Die CO_2-Absorption über die Höhe der Absorberkolonne soll bei verschiedenen thermischen

Leistungen zur Lösungsmittelregeneration und unterschiedlichen Gas- und Lösungsmitteldurchsätzen sowie unterschiedlichen Drücken und Temperaturen im Desorber untersucht werden. Anhand der Gaskonzentrationen und der Beladung des Lösungsmittels soll eine CO_2-Stoffmengenbilanz aufgestellt werden.

Die experimentell ermittelten Daten sollen in einem Simulationsmodell abgebildet werden. Dazu soll ein in Grundzügen bestehendes Prozessmodell in Aspen Plus® erweitert und die Technikumsanlage nachbildet werden. Abschließend sollen die Versuchsergebnisse anhand der Simulation evaluiert und Potentiale eines energetisch optimierten sowie flexiblen Abscheideprozesses aufgezeigt werden.

Die studentische Arbeit wird von *Herrn M.Sc. Marc Oliver Schmid* betreut. Das Merkblatt zur Durchführung und Anfertigung von studentischen Arbeiten am IFK ist zu beachten.

Beginn der Arbeit: 28.05.2018
Abgabetermin: 28.11.2018

(*Prof. Dr. techn. Günter Scheffknecht*) (M.Sc. *Marc Oliver Schmid*)

Adresse/Kontaktdaten des/der Studierenden:
Nelson Felipe Rincón Soto
Allmandring 22C Z4
70569 Stuttgart
E-mail: nfrincons94@gmail.com

Kurzfassung

Die Abscheidung und Speicherung von CO_2 (CCS) aus Verbrennungsprozessen ist in den letzten Jahrzehnten eine akzeptable Lösung geworden, um die Menge der atmosphärischen Emissionen zu verringern. Post-Combustion-Verfahren für die CO_2-Abscheidung gelten derzeit als eine Spitzentechnologie in diesem Bereich, besonders die chemische Absorption mit Amin-Lösungen ist eine der höchstentwickelten Techniken bis heute.

Der Betrieb einer Pilotanlage (ABIGAIL - Aminosäuresalzlösungen zur Biogas Aufbereitung mit innovativer Lösungsmittelregeneration) zur CO_2-Abscheidung mit MEA (Monoethanolamin) -Lösungen und Dampfregeneration wurde im Rahmen dieser Untersuchung durchgeführt, simuliert und optimiert. Zunächst wurde eine erste Versuchskampagne durchgeführt, um die vorläufigen Parameter und Betriebsbedingungen zu sammeln. Anschließend wurde in Aspen Plus V8.6® eine Prozesssimulation entwickelt, die die gleichen Betriebsbedingungen und Sensitivitätsanalysen der wichtigsten Variablen und deren Auswirkungen auf die CO_2-Abscheidung beinhaltet. Dann wurde der Prozess in Aspen Plus V8.6® optimiert. wobei die Kostenminimierung die Zielfunktion ist. Im Anschluss wurde eine Verbesserung des Wärmetauschnetzes mit Hilfe der HENS-Analyse im Aspen Energy Analyzer V8.6™ konzipiert. Abschließend wurde eine zweite Reihe von Experimenten durchgeführt, die die optimalen Betriebsbedingungen umsetzte.

Die experimentellen Ergebnisse wurden mit den Simulationen verglichen, wobei ein Gesamtkorrelationsindex von 97.5% aufgezeigt werden konnte. Es konnte gesehen werden, dass das L/G-Verhältnis und die Lösungsmitteleintrittstemperatur die am meisten beeinflussenden Variablen im Betrieb des Absorbers sind, während der Druck im Stripper ist. Eine Kombination von L/G gleich 5.5 l/m^3, 37ºC Einlasstemperatur und 2 bar im Desorberdruck stellte eine erhebliche Minimierung der Betriebskosten von 14.23 €/day dar, ohne den erforderlichen CO_2-Abscheidungsprozess erheblich zu beeinflussen. Eine mögliche Wärmerückgewinnungskonfiguration für die aktuelle Pilotanlage wurden konzipiert und 309 kJ/h konnten in zusätzlichen Versorgungseinrichtungen eingespart werden.

Abstract

Capture and storage of CO_2 from combustion processes (CCS) has become in the last few decades an acceptable solution to diminish the amount of greenhouse gases emitted to the atmosphere. Post-combustion processes for CO_2 capture are currently a leading-edge technology in the field, being the chemical absorption with amine solutions one of the most enhanced developments up to the date.

The strip-steam operation of a pilot plant (ABIGAIL – Aminosäuresalzlösungen zur Biogas Aufbereitung mit innovativer Lösungsmittelregeneration, in its German acronym) for the CO_2 capture with MEA (Monoethanolamine) solutions was conducted, simulated and optimized in the frame of this research. A first experimental campaign was initially carried out to gather the preliminary parameters and operation conditions. Subsequently, a process simulation was developed in Aspen Plus V8.6®, featuring the same operational conditions and sensitivity analyzes of the most relevant variables and its effects on the CO_2 capture. Afterwards, the process was optimized with Aspen Plus V8.6®, being the cost minimization the objective function. Consecutively, an improvement of the heat-exchange network was conceived using HENS analysis in the Aspen Energy Analyzer V8.6™. Finally, a second set of experiments was performed featuring the simulated optimal conditions.

The experimental results were compared to the simulations, showing an overall 97.5% correlation index. It could be seen that the L/G ratio and the inlet temperature are the most influencing variables in the operation of the absorber, whereas the reflux-ratio in the stripper. A combination of L/G equals to 5.5 l/m^3, 37ºC inlet temperature and minimization of the operational cost of 14.23 €/day without affecting considerably the required CO_2 capture process. One possible heat-recovery configurations for the current pilot plant were conceived and 309 kJ/h could be saved in additional utilities.

Contents

List of Abbreviations

Abbreviation	Meaning
ABIGAIL	Aminosäuresalzlösungen zur Biogasaufbereitung mit innovativer Lösungsmittelregeneration
CCS	Carbon capture and storage
Eq	Equivalent
ERNTL	Non-random two liquid model
ESA	Electric swing adsorption
FOLU	CO_2 from Forestry and Other Land Use
GAMUS	Unsymmetric activity coefficients
GHGs	Greenhouse gases
gPROMS	Simulation software brand
HENS	Heat Exchange Network Synthesis
IPCC	Intergovernmental Panel on Climate Change
IGCC	integrated gasification combined cycle
PC	Post Combustion
PC-SAFT	Perturbed change statistical associating fluid theory
PFD	Process flow diagram
P&ID	Process and instrumentation diagram
PSA	Pressure swing adsorption
PTP	Triple point pressure
MDGs	Millennium Development Goals
NLARX	Nonlinear ARX model
RadFrac	Separation model block in Aspen Plus®
SDGs	Sustainable Development Goals
SQP	Sequential quadratic programming
TRL9	Technology Readiness Level
TSA	Temperature swing adsorption
TTP	Triple point temperature
UNIQUAC	Universal quasichemical activity coefficient model
VLE	Vapor Liquid Equilibria
Yr	Year

List of Chemical Species

Abbreviation	Name
CH_4	Methane
CO_2	Carbon dioxide
CO_3^{2-}	Carbonate ion
1DMA2P	*1-dimethylamino-2-propanol*
2DMAE	*2-(dimethylamino)ethanol*
HCO3-	Bicarbonate ion
H2O	Water
H3O+	proton
2MAE	*2-(methylamino)ethanol*
MDEA	*methyldiethanolamine*
MEA	*Monoethanolamine*
MEAH+	Positive loaded Monoethanolamine
MEACOO-	Carbamate ion
N_2	Nitrogen
OH-	Hydroxide ion
TMDAP	*Tetramethyl-1,3-diaminopropane*

List of Symbols

Symbol	Units	Meaning
α	[gCO_2/g solv.]	CO_2 load in solvent
A	[m^2]	Surface area
a	-	Stoichiometric coefficient of component in the reaction
D	[m]	Diameter
ε	[m^3/m^3]	Void fraction
E	[kJ/mol]	Activation Energy
H	[m]	Height
k	varies	Pre-exponential factor
L/G	[l/m^3]	Liquid to gas ratio in absorber
γ	-	Component activity coefficient
m	[g]	Mass
$\bar{M}$	[g/mol]	Molecular weight
n	-	Temperature exponent
N	-	Number of components in the reaction
Pa	-	Measured parameter
ρ	[kg/m^3]	Density
r	[mol/h.l]	Reaction rate
$\bar{R}$	[kJ/kmol.K]	Universal gas constant
T	[ºC]	Temperature
$\dot{V}$	[m^3/h]	Volumetric flow
x	[g/g]	Component mass fraction
y	[m^3/m^3]	Component volumetric fraction

List of Sub-indexes

Symbol	Meaning
Abs	Absorption
CO_2	Reference to Carbon dioxide concentration or stream
c	Surface
Des	Desorption
G	Gas phase
i	Particular notation for a species
in	inlet
j	Run number
k	Run time
L	Liquid phase/solvent
MEA	Reference to monoethanolamine concentration or flow
out	Outlet
p	Packing

List of figures

List of tables

1 Introduction

Although most research projects are ideally aimed to tackle a pressing problem of society, the majority of them are also framed firstly on a political context, which intends to allocate such burning issues and redirects the research to face them properly.

For instance, “Climate Action” is the 13th aim of the Sustainable Development Goals (SDGs) of the United Nations Development Programme [1]. The SDGs were born at the United Nations Conference on Sustainable Development in Rio de Janeiro in 2012, and their objective was to produce a set of universal goals that meet the urgent environmental, political and economic challenges facing the world, replacing the well-known Millennium Development Goals (MDGs) [2]. The Climate Action goal is targeted to limit the increase in global mean temperature to two degrees Celsius above pre-industrial levels, avoiding the dramatic effects of climate change with the political will and the corresponding technological measures [1]. Further political tools to incentive the investment in new greenhouse gas reduction technologies were also developed; the Kyoto-Protocol is the best example in the subject [3, 4]. Hence, the current research focuses precisely on developing and optimizing such technological measures to alleviate the climate change, mainly caused by anthropogenic emissions.

Anthropogenic emissions of greenhouse gases (GHGs) are known for contributing to the observed changes in the climate, they are mainly composed of carbon dioxide, methane, nitrogen oxide, and fluorinated gases. Total emissions of GHGs in 2010 were estimated in 49 $GtCO_2$ eq/yr as shown in Figure 1-1 [5].

Out of the total GHGs emissions, 32 (±2.7) $GtCO_2$/yr corresponded to carbon dioxide emissions in 2010 and grew further by about 3% between 2010 and 2011, and by around 1 to 2% between 2011 and 2012. CO_2 remains the dominant anthropogenic GHG, accounting for 76% of total anthropogenic GHG emissions in 2010 [5]. Further estimations of the CO_2 emissions between 1751 to 2014 were performed by the Carbon Dioxide Information Analysis Center, stating emissions of 36.1 $GtCO_2$/yr in 2014 [6].

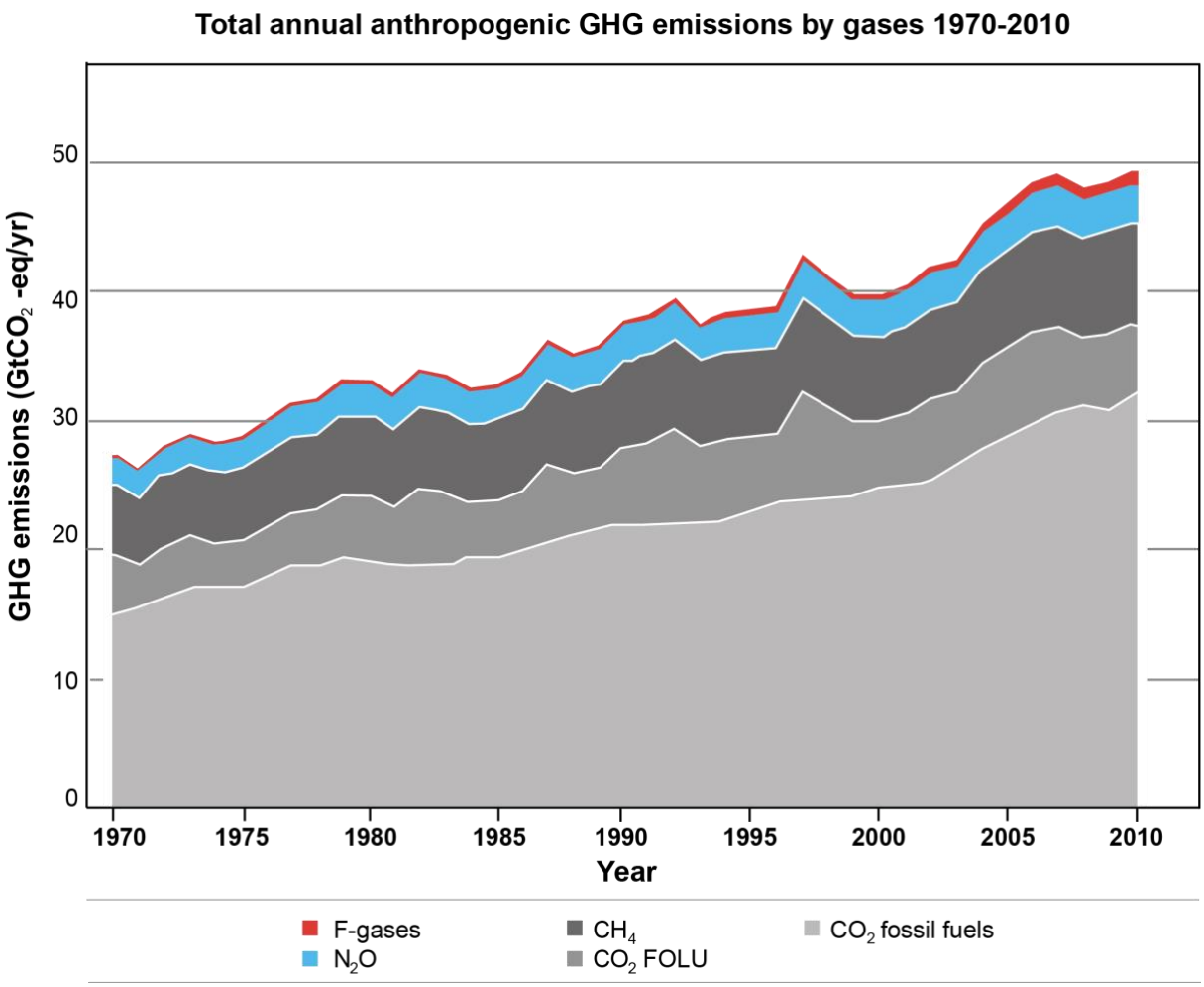

Figure 1-1: *Total anthropogenic greenhouse gas emissions 1970 – 2011 Adapted from* [5]

Furthermore, atmospheric concentrations of carbon dioxide peaked dramatically over the last centuries, going from 280 to 400 ppm CO_2 in 1750 and 2012 respectively [5], showing a clear long-term impact of anthropogenic emissions. So far, well-known general emissions values were brought up, but the purposes of this research, specific quantities relating the emissions to the amount of energy produced in power plants remain of relevance, as the studied technology, chemical absorption with MEA solutions, is mainly designed for applications in coal-fired power plants as a post-combustion step [7].

Around 40.58% of the world`s energy share in electricity generation is produced by coal, oil and gas, and peat power plants [8]. Therefore, power plants still play a crucial role in the energy network, and their impacts on the environment should be minimized. Specific CO_2 emissions of conventional (PC) power plants are estimated between 710 – 950 gCO_2 eq/kWh, whereas power plants featuring CCS processes show a substantial reduction in the specific emissions as shown in Figure 1-2 [8].

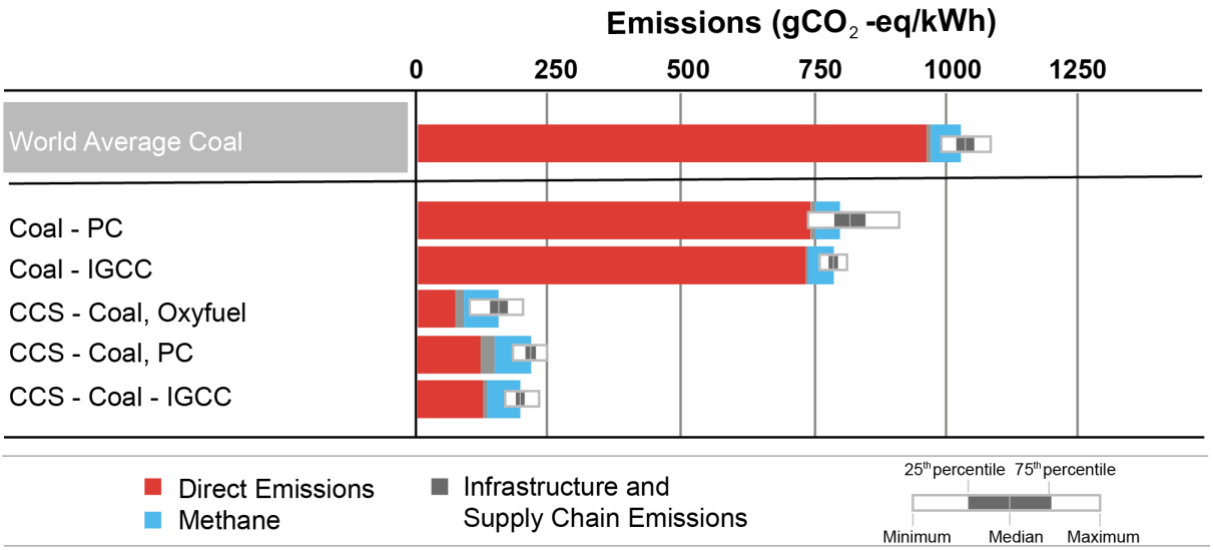

Figure 1-2: *Specific CO_2 emissions for coal-fired power plants, (2011-2013)*

Adapted from [8]

Out of all the available CCS technologies, Post-combustion is one of the most viable for implementing shortly due to the minimum effort required to install it on existing power plants [4]. As displayed in Figure 1-2, specific CO_2 emissions of 70 – 290 gCO_2 eq/kWh could be achieved when applying PC technologies [8]. Hence, an achievable reduction of approximately 84% in the specific emissions could be expected when introducing PC processes to treat the flue gases.

The sharp cutback on the emissions provided by the PC technologies makes them a target for studies and further developments. Currently, processes featuring chemical absorption with amine solutions are leading-edge technologies [9] in a pilot- and industrial scale.

Nevertheless, a profound knowledge of the operation must still be expanded before spreading the technology on a global scale. Roughly speaking, this research is aimed to contribute to this expansion through the optimization of a CO_2 chemical absorption pilot-scale plant operated with MEA solutions, hoping to correspond and help achieving to the Sustainable Development Goals of the United Nations Development Programme.

2 State of the knowledge

The relevant state of the knowledge for the research is split into two sections. On the one hand, the operation-related concepts are introduced. In this section, an overview of the emerging technologies for CO_2 capture, along with a detail description of the chemical absorption process with MEA, and a summary of the results of the conducted tests on the pilot plat ABIGAIL will be discussed. (See sections 2.1.1 to 2.1.3.)

On the other hand, the simulation-related background is reviewed during the second section. A description of the used aspenONE® Suite Software, along with the implemented thermodynamic models for the process model and a summary of the already-developed simulations for carbon capture with MEA solutions is displayed on the second part. (See sections 2.2.1 to 2.2.3.)

2.1 Operation-related state of the knowledge

The CCS process is a large-scale separation of carbon dioxide from its significant sources (Capture) followed by a long-term isolation from the atmosphere (Storage). Chemical absorption of CO_2 is just a single step during the capture phase [10]. Section 2.1.1 will broad the spectrum of the existing capture technologies, whereas section 2.1.2. aims to expand specifically on the chemical absorption process with MEA for CO_2 capture.

2.1.1 Trending processes for CO_2 capture

CO_2 capture could be categorized into three main technologies: Pre-combustion capture, Post-combustion capture, and Oxyfuel combustion [10]. The three technologies differ in their maturity level, technical advantages, and economic aspects. For instance, there are only three successful Oxyfuel-based plants in operation up to the date, whereas Post-combustion technologies have been already implemented in full-scale commercial plants around the world. A general comparison table of the current capture technologies is presented in Table 2-1 [11]. Sections 2.1.1.1 to 2.1.1.3 will expand on the technical aspects of each capture process.

Table 2-1: *Comparison of CO_2 capture technologies.*

Maturity level, technical advantages and disadvantages adapted from [12], economic aspect adapted from [12].

Aspect	Post-combustion capture	Pre-combustion capture	Oxyfuel combustion capture
Maturity level	• Highly mature. • Numerous established applications at full-scale commercial plants.	• Well-established in process industries. • Establishment of full-scale CCS plants under progress	• Only three successful plants in operation. • Limited operating data up to the date.
Technical advantages	• Highly compatible for retrofitting of existing power plants. • Available research for improving energy efficiency.	• Less energy-intensive carbon dioxide separation process due to low gas volume. • Hydrogen/syngas as alternative fuel. Compatible with conventional high efficiency steam cycle.	• Minimal emissions of pollutants. • No requirements of on-site chemical operations. High carbon capture efficiency. Compatible with conventional high efficiency steam cycle.
Technical disadvantages	• Separation constraint imposed by low carbon dioxide partial pressure in flue gas. • Significant energy consumption of amine-scrubbing process (i.e. 30% loss). Extensive water consumption	• Limited commercial availability of integrated gasification combined cycle (IGCC) technology. • High auxiliary system requirement by IGCC. Reduced efficiency due to hydrogen-fueled gas turbine.	• Infeasible development of sub-scale oxyfuel capture technology. • Net power output reduction due to energy-intensive air separation. • Air-tight installation to avoid leakage
Economic aspect	• High capital and operational cost due to large size equipment. *Capital cost*[1] Gas-fired: 748€/kW Coal-fired: 1704€/kW *Electricity cost* Gas-fired: 6.9¢/kWh Coal-fired: 6.5¢/kWh	• High capital and operational cost for sorbent technology. IGCC is more expensive than conventional coal power plant. *Capital cost* Gas-fired: 1015€/kW Coal-fired: 1566€/kW *Electricity cost* Gas-fired: 8.3¢/kWh Coal-fired: 5.9¢/kWh	• High capital cost for air separation. *Capital cost* Gas-fired: 1316€/kW Coal-fired: 1901€/kW *Electricity cost* Gas-fired: 8.6¢/kWh Coal-fired: 6.7¢/kWh

[1] Currency converted from the original [12] USD Dollars ($) to Euros (€) on the 30.09.2018

2.1.1.1 Pre-combustion capture

Pre-combustion capture is aimed to separate any possible CO_2 emissions prior to the combustion step. It is based on the principle of converting the fuel into hydrogen, a carbon-free fuel, via steam reforming or partial oxidation [4]. The entire Pre-combustion capture is divided into four main stages as shown in Figure 2-1: The reforming/partial oxidation to produce syngas, the water gas shift reaction, the CO_2 capture and compression, and last but not least, the power generation [13]

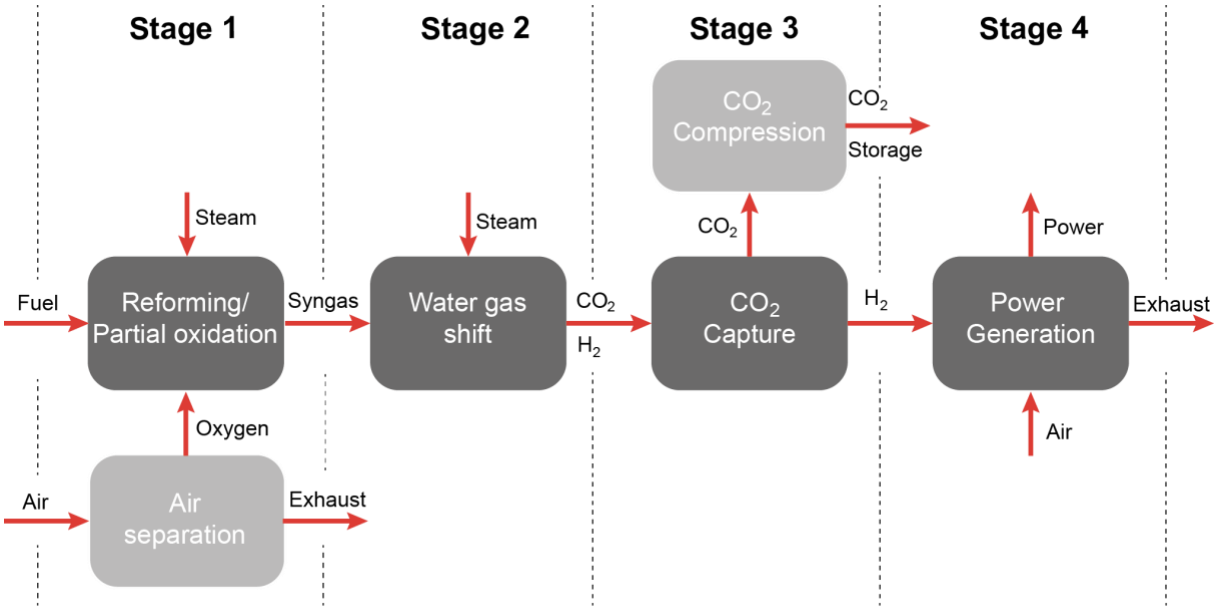

Figure 2-1: *Schematic representation of the Pre-combustion process for carbon capture*

Adapted from [13, 14]

Both processes of the first stage, so-called syngas routes, are well-known from the industry and have a broad range of applications, such as syngas, ammonia and hydrogen production. The endothermic steam reforming (Stage 1) reaction occurs typically at temperatures above 800 ºC. A portion of the fuel is burned to provide the required energy for the reaction [4]:

$$C_xH_y + xH_2O \leftrightarrow xCO + (x + y/2)H_2 \qquad \textit{Eq. 2-1}$$

The partial oxidation of fossil fuels is an exothermic reaction. It is called gasification when the fuel is oxidized from the solid state. It is carried out in the presence of oxygen, which is normally separated from the air in a previous stage [13]. The reaction could be described as:

$$C_xH_y + x/2\,O_2 \leftrightarrow xCO + (y/2)H_2 \qquad \textit{Eq. 2-2}$$

An advantage of partial oxidation over steam reforming is the absence of any additional heat source to trigger the chemical reactions. The CO produced in reactions shown in Eq. 2-1 and 2-2, is subsequently converted to CO_2 and H_2 in the presence of steam in an exothermic water-gas shift reaction (Stage 2) as displayed in Eq. 2-3 [4, 13]:

$$CO + H_2O \leftrightarrow CO_2 + H_2 \qquad \textit{Eq. 2-3}$$

Depending on the used catalyst, the chemical reaction shown in Eq. 2-3 will occur between 400-500ºC (Fe-Cr catalyst) or 180-350ºC (Cu-based catalyst). The high pressure of the water-gas shift product gas stream facilitates the CO_2 removal by conventional washing steps, as the CO_2 content at the inlet of the CO_2/H_2 separation (Stage 3) oscillates between 15 – 60%. Once the CO_2 is separated, it is compressed. Finally, the produced H_2 is used in a combined gas and steam process to generate electricity (Stage 4) [4, 13].

2.1.1.2 Oxyfuel combustion technology

Oxyfuel combustion is seen as a promising technology for CO_2 capture in thermal power plants. The Oxyfuel process is based on an Oxygen-rich atmosphere mixed with recycled flue gas (Mainly CO_2 and H_2O) to burn the fuel [15]. The basic 4 stages of the process are depicted in Figure 2-2. Initially, pure oxygen is obtained from the air separation unit (Stage 1), then coal is introduced into the oxyfuel boiler and burned in the nitrogen-free atmosphere (Stage 2) [16, 17]. Due to this fact, posterior de-NO_x and desulphurization steps are avoided [18]. The generated flue gas is directed into the gas separation step (Stage 3), where the water is separated from the CO_2 and subsequently condensed (Stage 4). On the other hand, the high-purity CO_2 stream is compressed and taken either to the final storage place or used for different applications (Such as beverages, solvent material or in fire extinguishers [17]). A part of the CO_2 is recirculated to control the temperature in the boiler.

Burning the coal in a pure oxygen atmosphere results in an adiabatic combustion temperature over 3.500ºC, which is too high for the available materials [19]. The temperature in the combustion chamber can be reduced by recycling the flue gas and the condensed water (Stage 4) back into the boiler.

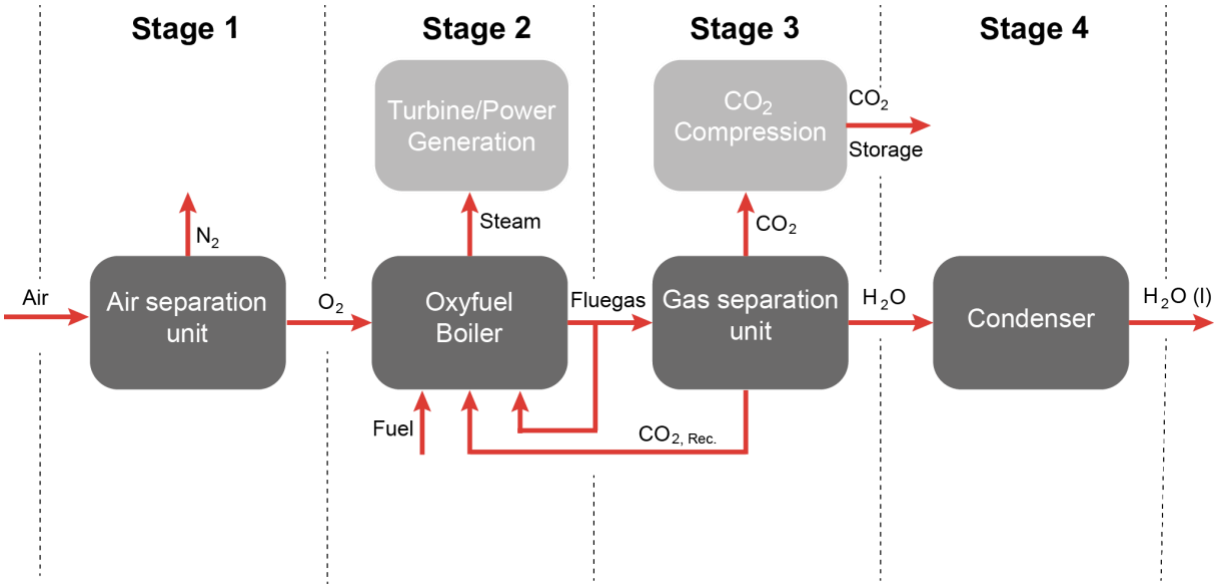

Figure 2-2: *Schematic representation of the Oxyfuel combustion process for carbon capture*

Adapted from [9]

The major disadvantage of the Oxyfuel technology is the implementation of the energy-intensive air separation step [4]. Three successful pilot plants using oxyfuel technology have already been built; The Vattenfall oxyfuel plant in Germany, which has successfully operated at 30 megawatts of thermal energy output (30MW thermal), Callide in Australia (30MW electrical) and CUIDEN in Spain (20MW thermal). Now a new oxyfuel pilot plant is going into operation in China. In a project led by the Huazhong University of Science and Technology (HUST) the first large pilot for oxyfuel combustion in the East Asia region has successfully produced a highly concentrated CO_2 stream at 3MW power output. [20]

2.1.1.3 Post-combustion capture

Post-combustion capture is the separation of CO_2 from flue gases after the power production process/combustion chamber (Stage 1). In the case of power plants, the CO_2 capture step takes place after the particle separation, De-NO_x, and De-SO_x processes (Stage 2) [4]. The most commonly applied method for post-combustion is absorption-desorption of CO_2 using the alkanol amine solutions [21]. Post-combustion can also be achieved through membrane technology, adsorption processes and cryogenic separation (Stage 3). Once the CO_2 is captured, it is compressed and taken to its final storage/application (Stage 4). A general scheme for post-combustion processes is depicted in Figure 2-3.

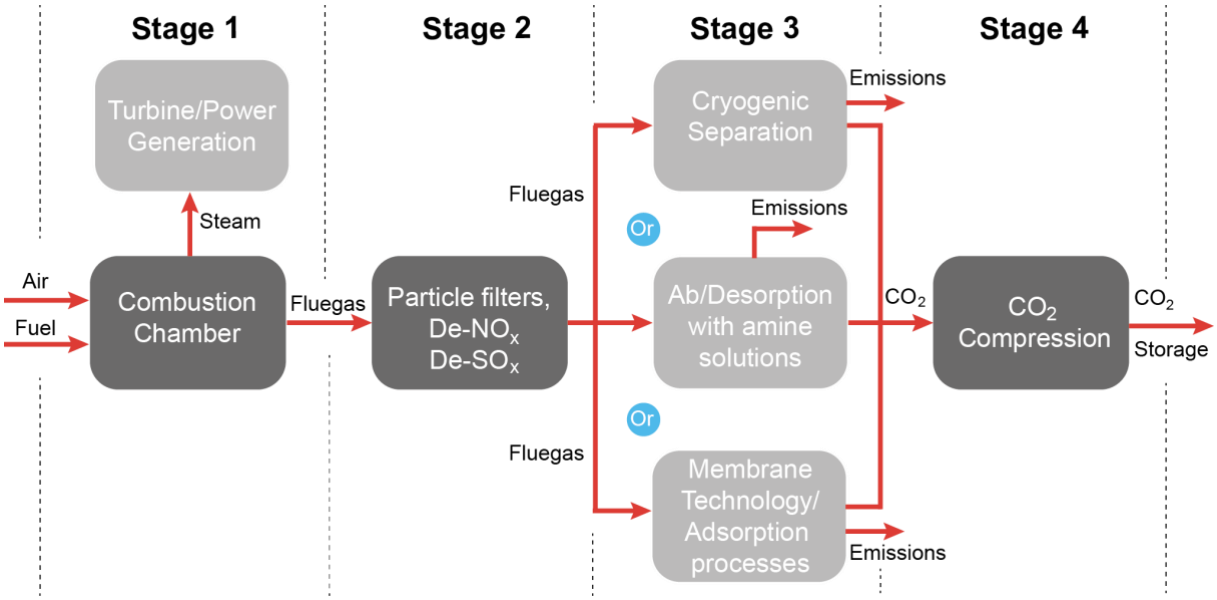

Figure 2-3: *Schematic representation of the Post-combustion process for carbon capture*

Adapted from [14]

Absorption processes (Stage 3) are usually divided into two steps. Firstly, CO_2 is separated from the flue gas through selective absorption with a physical or chemical solvent. Then, the solvent is regenerated in a desorption-stage. Around 70-80% of the capture process energy in this case is used for solvent regeneration [22]. The efficiency of the process is determined by the difference between CO_2 solubility at absorber and desorber conditions. Hence, it has limited performance at low CO_2 concentrations and high flue gas temperatures [9]. Furthermore, the main challenges for the application of this technology are the high energy demand, the degradation of the solvent, along with corrosion and further emissions [4].

In Cryogenic separation (Also stage 3), CO_2 is removed from the flue gas through condensation or sublimation at low temperatures and high pressures [22]. The principle, like any distillation process, is based on the difference of boiling points of the flue gas components. In the first step, H_2O and SO_2 are removed. Then, the flue gas is compressed and cooled to form liquid/solid CO_2 (Triple point of pure CO_2: T_{TP} = -56.6ºC, P_{TP}= 5.2 bar), which is further separated. The advantages of the process are the high purity and easy-handling of the final CO_2 product. Nevertheless, the cost associated to the flue gas compression and cooling are extremely high. Thus, the potential of cryogenic separation for large-scale processes still on the table [4, 23].

Adsorption processes are based on the strength difference of interactions between flue gas components and the surface of a solid, e.g., zeolithes, calcium oxide, activated carbon. They are either operated in cycles with several parallel solid-phase reactors, or continuously with

fluidized beds. In cyclic processes, the flue gas flows through the unloaded bed, until the equilibrium load is reached. Then, the flue gas is sent to another parallel unloaded bed, while the first one is being regenerated. Regeneration methods differ on the principle: TSA (Temperature swing adsorption) generates the adsorber through an increase of temperate; PSA (Pressure swing adsorption) is based on a substantial decrease of pressure to achieve desorption; and ESA (Electric swing adsorption) uses electrical voltage to reduce the interaction between the adsorbed molecules and the surface [4]. Adsorption processes are currently not considered attractive for large-scale application mainly due to the low loading capacity for CO_2 of the current adsorbing materials, along with the high energy demand for the regeneration stage [24].

CO_2 capture with membranes can be achieved via two different approaches: Gas permeation, and membrane absorption [25]. The principle for both cases is the membrane-selectivity towards CO_2, allowing it to pass through. In gas permeation, the selectivity is attributable to the different affinities of the flue gas components for the membrane. The mass transfer is governed by the partial pressure difference across the membrane, in such cases, a vacuum pump on the product side is needed to achieve sufficient driving force [4]. The currently available membrane-materials possess a low selectivity for CO_2, therefore, the resulting energy demand is even higher than for absorption-based processes. Hence, the potential of membrane technologies for large-scale facilities is limited. On the other hand, membrane absorption is in principle a conventional absorption process equipped with a membrane to enhance the contact area between the flue gas and the solvent. It does not present any significant advantage over conventional absorption, but features the membrane cost and a higher pressure drop [4, 9].

2.1.2 CO_2 capture through absorption with MEA solutions

After introducing the general fundamentals of the carbon capture, the sections 2.1.2.1 to 2.1.2.2. will expand specifically on the post-combustion absorption processes implementing MEA solutions. A brief description of the conventional capture process, featuring the process-controlling variables and the most-used amine species for absorption is firstly reviewed. Afterward, a detail description of the reaction mechanism and process kinetics with MEA is presented due to its major role in the simulation phase of the project.

2.1.2.1 Description of the conventional process

The most popular method among the post-combustion capture technologies is the chemical absorption with amine solutions [26]. The conventional process flow diagram is shown in Figure 2-4, it includes two main stages: The absorption, where most of the CO_2 is captured by the solvent; followed by the desorption, were the solvent is regenerated at elevated temperatures. The solvent regeneration is the most energy-intensive step of the process [27].

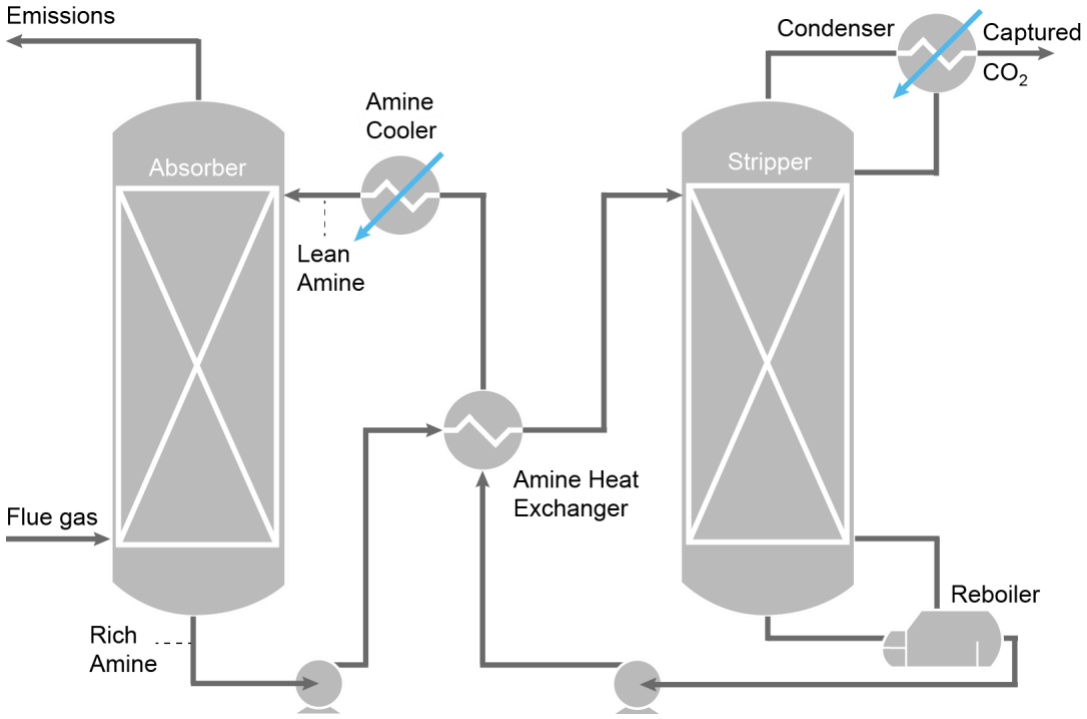

Figure 2-4: *Conventional process flow diagram (PFD) for chemical absorption with amine solutions*

Adapted from [26]

The flue gas stream enters by the bottom stage of the absorber once it has been scrubbed to remove particles, SO_X and NO_X. Furthermore, the stream is usually cooled down to approximately 40ºC before the input. Inside the absorber, the incoming gases containing CO_2 are contacted with the amine solvent flowing in counter-current (Fed at the top-stage of the column). Reactions between the absorbent and the CO_2 then take place mainly in the liquid phase. On the one hand, the clean flue gas escapes the column by the top with low CO_2 concentrations; on the other hand, the rich solvent is drawn from the column at the bottom stage and pumped through a heat exchanger to heat up the rich amine solution up to 100-110 ºC. The heat exchange occurs between the mentioned rich amine stream and the hot regenerated amine solution leaving the reboiler. Once the rich amine solution is heated up, it is fed to the stripper at the top stage for desorption to take place. The inclusion of a reboiler

provides the needed heat for the desorption and to generate a counter-current gas flow throughout the column, and the condenser is intended to increase the amount of recirculated liquid phase to promote contact between phases. The striped CO_2 is withdrawn at the top of the column as well, whereas the regenerated amine solution is recirculated to the absorption column [26].

Although different amine solvents and blends have been investigated [28] as shown in Table 2-2, and have presented higher absorption capacities than conventional solvents, the monoethanolamine (MEA) is considered the industry benchmark due to its low cost and high CO_2 reactivity. Therefore, it has been used for more than 50 years [29]. Multiple configurations and process intensification technologies, e.g. rotating packed bed absorbers, have been analyzed to reduce the overall energy consumption [26]. Nevertheless, further experiments must be conducted to determine the feasibility of such configurations [30].

Table 2-2: *CO_2 Absorption capacity of different 30% w/w amine solutions at 40ºC*

Adapted from [28]

Amine solution	***Absorption capacity [mol CO_2/mol amine]***
Monoethanolamine (MEA)	*0.58*
N-methyldiethanolamine (MDEA)	*0.52*
2-(methylamino)ethanol (2MAE)	*0.56*
2-(dimethylamino)ethanol (2DMAE)	*0.73*
1-dimethylamino-2-propanol (1DMA2P)	*0.72*
Tetramethyl-1,3-diaminopropane (TMDAP)	*1.16*

2.1.2.2 Available kinetic models for the CO_2-MEA System

To understand the reaction mechanisms and kinetic models of the MEA-CO_2 system, it is convenient to briefly introduce the fundamentals of the MEA chemistry. MEA is a primary ethanolamine, containing both: A primary amine and a primary alcohol. It is a colorless, viscous liquid with an ammonia reminiscent odor [31]. It presents a slightly basic behavior in aqueous solutions, forming the $MEAH^+$ ion. For the aim of this project, the reaction with either CO_2 or HCO_3^- are of great interest; in both cases, the ion carbamate, $MEACOO^-$, is formed [32]. It is well known as the “Loaded MEA”. The molecular structures of the three-relevant MEA species, along with their corresponding acronyms are shown in Figure 2-5:

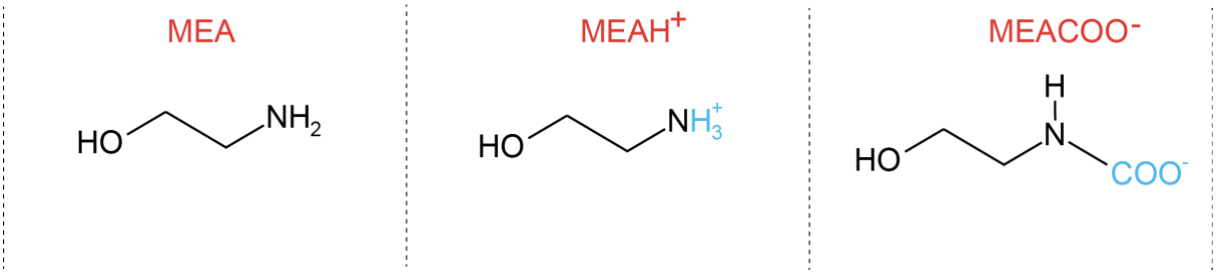

Figure 2-5: *Chemical structures of monoethanolamine relevant species for CO_2 capture*

Adapted from [33, 34, 35]

When using MEA as solvent for CO_2 capture, there are two main reaction mechanisms that must be considered for modeling the overall reaction rates of the system: On the one hand, the equilibrium reactions of the aqueous-phase electrolyte chemistry play an important role in the model, as they describe the equilibrium between the carbonate/amine ions with the aqueous phase. On the other hand, a hybrid kinetic-equilibrium chemical mechanism is more convenient to describe the chemical changes during the absorption and desorption processes [35, 32]. Figure 2-6 and 2-7 show both of the considered reaction mechanisms.

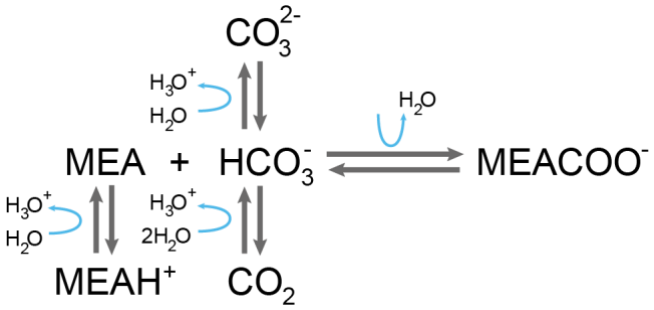

Figure 2-6: *Summary of the MEA-CO_2 mechanism - Aqueous electrolytes equilibrium*

Adapted from [32, 35]

The aqueous-phase electrolyte chemistry is described also in the equations 2-4 to 2-8. All equilibrium constants could be computed from the standard Gibbs free energy change, available in the Aspen Plus Database [32]. The first important equilibrium is an acid-base MEA reaction, where MEA protonates in aqueous solutions (Eq. 2-4). Equations 2-6 and 2-7 are carbon-related equilibriums also in aqueous solutions. The most important step of the reaction mechanism is presented in equation 2-5, as MEA is reacting with the carbonate ion to produce the carbamate ion (So called $MEACOO^-$), Last but not least, equation 2-8 depicts the liquid water equilibrium with its ions [32]

$$MEAH^+ + H_2O \leftrightarrow MEA + H_3O^+ \quad \textit{Eq. 2-4}$$

$$MEACOO^- + H_2O \leftrightarrow MEA + HCO_3^- \quad \textit{Eq. 2-5}$$

$$CO_2 + 2H_2O \leftrightarrow HCO_3^- + H_3O^+ \quad \textit{Eq. 2-6}$$

$$HCO_3^- + H_2O \leftrightarrow CO_3^{2-} + H_3O^+ \quad \textit{Eq. 2-7}$$

$$2H_2O \leftrightarrow OH^- + H_3O^+ \quad \textit{Eq. 2-8}$$

As mentioned previously, for simulation purposes it is more convenient to include a set of power-law based kinetic expressions, than only a set of equilibrium reactions [32]. Therefore, the second depicted reaction mechanism features four kinetic (Rate-based) reactions and three basic equilibriums. The summary of the mechanism is depicted in Figure 2-7, and the corresponding details in the equations 2-9 to 2-15.

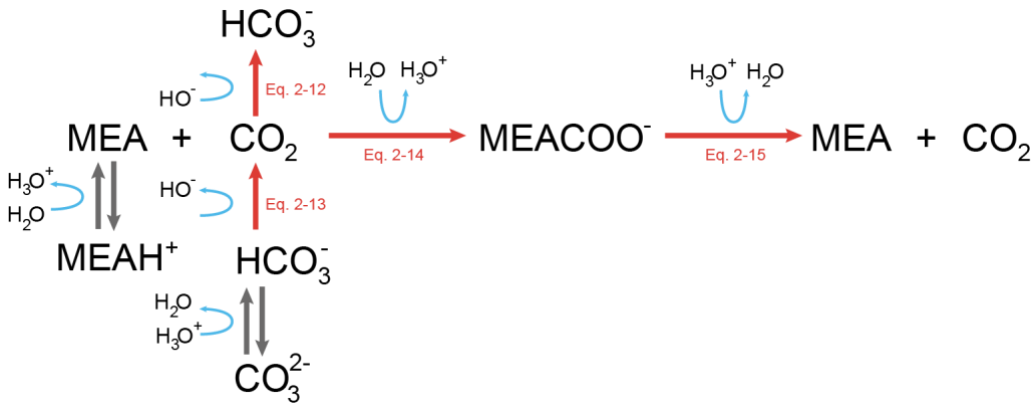

Figure 2-7: *Summary of the MEA-CO_2 mechanism – kinetic approach*

Adapted from [32, 35]

$$MEAH^+ + H_2O \leftrightarrow MEA + H_3O^+ \quad \textit{Eq. 2-9}$$

$$HCO_3^- + H_2O \leftrightarrow CO_3^{2-} + H_3O^+ \quad \textit{Eq. 2-10}$$

$$2H_2O \leftrightarrow OH^- + H_3O^+ \quad \textit{Eq. 2-11}$$

$$CO_2 + OH^- \rightarrow HCO_3^- \quad \textit{Eq. 2-12}$$

$$HCO_3^- \rightarrow CO_2 + OH^- \quad \textit{Eq. 2-13}$$

$$MEA + CO_2 + H_2O \rightarrow MEACOO^- + H_3O^+ \quad \textit{Eq. 2-14}$$

$$MEACOO^- + H_3O^+ \rightarrow MEA + CO_2 + H_2O \quad \textit{Eq. 2-15}$$

All rate-based reactions need a power law expression and a set of parameter to be modeled. The simplified power law expression for the equations 2-12 to 2-15 is presented in the expression 2-16, the detailed description of the terms is presented in the list of abbreviations:

$$r = kT^{n} exp\left(\frac{-E}{\bar{R}T}\right)\prod_{i=1}^{N}(x_i\gamma_i)^{a_i} \qquad \textit{Eq. 2-16}$$

For the reactions shown in equations 2-12 and 2-14, the n parameter is zero. Whereas the values for the pre-exponential factors, k, and the activation energies, E, are displayed in Table 2-2. The parameters of reactions 2-12 and 2-13 are derived from [36], and the parameters of reactions 2-14 and 2-15 are derived from [37]:

Table 2-3: *Kinetic Parameters of Rate-based law reactions*

Adapted from [32, 36, 37]

	k	E, [cal/mol]
Equation 2-12	1.33 x 10^{17}	13.249
Equation 2-13	6.63 x 10^{16}	25.656
Equation 2-14	3.02 x 10^{14}	9.856
Equation 2-15 (Absorber)	5.52 x 10^{23}	16.518
Equation 2-15 (Stripper)	6.50 x 10^{27}	22.786

Due to the different temperatures in the operation of the absorber and the stripper, the parameters of reaction 2-15 change as well to describe properly the chemical phenomena. The above-mentioned chemical mechanisms will be used in section 3.2.1.2.

2.1.3 Summary of the conducted experiments with the pilot plant ABIGAIL

The ABIGAIL pilot plant (Aminosäuresalzlösungen zur Biogasaufbereitung mit innovativer Lösungsmittelregeneration, in its German acronym) at the Institute of Combustion and Power Plant Technology at the University of Stuttgart was used to experimentally validate the results obtained in the simulations. So far, three fully documented experimental campaigns have been carried out using the pilot plant. Sections 2.1.3.1 and 2.1.3.2 summarize the previously-conducted experimental conditions and findings. As an important remark for the interpretation of previous results, the absorption column has multiple feeds at different packing-heights; depending on the selected solvent's feed, the so-called "Effective absorption height, H_{Abs}" is determined. A detailed description of the operation of ABIGAIL will be presented in section 3.1.

2.1.3.1 Conducted experiments during 2016

The first operation of ABIGAIL took place in 2016 by [38]. A summary of the conducted operational points is displayed in Table 2-4. It mainly focused on investigating the effect of

the L/G ratio and the effective height, H_{Abs}, of the absorption column. The detailed explanations of the used symbols could be found in the List of Abbreviations and in section 3.1:

Table 2-4: *Summary of conducted experiments with ABIGAL during 2016*

Adapted from [38]

	$\dot{V}_L$ $[l/h]$	$\dot{V}_G$ $[m^3/h]$	L/G $[l/m^3]$	y_{CO_2} $[\%v/v]$	T_{Abs}^{in} $[°C]$	H_{Abs} $[m]$	p_{Des} $[bar]$	P_{Des} $[kW]$
1	250	30,0	8,3	15	30	2,4	2	15
2	380	30,0	12,7	15	30	2,4	2	15
3	380	30,0	12,7	15	30	1,8	2	15
4	380	30,0	12,7	15	30	1,2	2	15
5	380	30,0	12,7	15	30	0,6	2	15
6	450	30,0	15,0	15	30	2,4	2	15
7	450	30,0	15,0	15	30	1,8	2	15
8	450	30,0	15,0	15	30	1,2	2	15
9	450	30,0	15,0	15	30	0,6	2	15
10	450	22,8	19,7	15	30	2,4	2	15
11	450	22,8	19,7	15	30	1.2	2	15

The first operation of the pilot plant found out outstanding performances of the absorption column when using the entire built packing height, Moreover, it was shown that higher L/G ratios influences dramatically the loading of the MEA solution, but a cost-optimum value was not found. Results regarding the stripper performance remain inconclusive, as there was not an experimental way to determine the CO_2 loading of the stripper's liquid effluent. The experience with the operation of the pilot plant also brought some adjustments to enhance the feasibility and control over the process, such as the installation of an after-stripper pump, recirculation of the clean exhaust gas in the absorber, and a cooler prior to the absorption column.

2.1.3.2 Conducted experiments during 2017

The second set of experiments was carried out in 2017 by [39]. Multiple amine acid salts were tested in this set of experiments, along with the operation of the desorption using stripping air. It was concluded that further improvements in the preheating of the stripping air must be studied to optimize its operation, and that other solvents could also be used for the CO_2 capture, as the absorption percentage is comparable. For the absorption with MEA, multiple variables were analyzed: L/G ratio, absorber's inlet temperature, reboiler's duty and

CO_2 input concentration. However, the variables were not isolated, and an optimal operation point for the absorption was not found.

The third set of experiments was conducted in 2017 by [40]**,** it was aimed to start finding optimal operational L/G values to maximize the CO_2 absorption efficiency, considering the effect on the pressure drop inside the paced column, the required reboiler heat duty, and energy for other heat transfer processes.

The set of experiments found higher absorption rates for elevated L/G, and also point out the growing energy demand when increasing the L/G. Stripping process was not analyzed in detail, and the found optimum range is only based on the absorption performance. It also leaves an open door for a cost-based optimization, considering both processes: Absorption and stripping performance. The temperature profiles of the absorption column for every operational point were also developed, and an additional water-washing device on top of the absorber was installed to facilitate a successful operation. Table 2-5 presents the summary of the operational conditions for the experiments during 2017.

Table 2-5: *Summary of conducted experiments with ABIGAL during 2017*

Adapted from [40]

	$\dot{V}_L$ $[l/h]$	$\dot{V}_G$ $[m^3/h]$	L/G $[l/m^3]$	y_{CO_2} $[\%v/v]$	$T_{Abs,in}$ $[°C]$	p_{Des} $[bar]$	P_{Des} $[kW]$
1	120	24,5	4,9	15	40	2	6,48
2	140	28,6	4,9	15	40	2	7,56
3	180	36,7	4,9	15	40	2	9,72
4	160	23,2	6,9	15	40	2	8,64
5	180	26,1	6,9	15	40	2	9,72
6	200	29,0	6,9	15	40	2	10,8
7	200	20,6	9,7	15	40	2	10,8
8	250	25,8	9,7	15	40	2	13,5
9	300	30,9	9,7	15	40	2	16,2
10	120	24,5	4,9	15	40	2	7,45
11	140	28,6	4,9	15	40	2	8,69
12	160	36,7	4,9	15	40	2	9,94
13	140	20,3	6,9	15	40	2	8,68
14	160	23,2	6,9	15	40	2	9,92
15	180	26,1	6,9	15	40	2	11,18
16	160	16,5	9,7	15	40	2	9,92
17	180	18,6	9,7	15	40	2	11,18
18	200	20,6	9,7	15	40	2	12,42
19	250	25,8	9,7	15	40	2	15,53
20	300	30,9	9,7	15	40	2	18,63
21	120	24,5	4,9	15	40	2	7,45
22	140	20,3	6,9	15	40	2	8,68
23	140	14,4	9,7	15	40	2	9,83
24	160	16,5	9,7	15	40	2	11,23

2.2 Simulation-related state of the knowledge

Sections 2.2.1 and 2.2.2 are aimed to provide an overview of the software used for simulating and optimizing the CO_2 capture process in the ABIGAIL pilot plant. Firstly, a description of the features of the aspenONE Suite is presented. Then, detailed information about Aspen Plus V8.6 and Aspen Energy Analyzer V8.6 is covered. Subsequently, the selected thermodynamic property models are described for single and multiple components. Finally, a summary of the previously conducted simulations of CO_2 capture with MEA via chemical absorption is synthetized and analyzed.

2.2.1 Description of the aspenONE® Suite V8.6

AspenTech (Short name for Aspen Technology Inc.) is an American software company founded in 1981 due to a political response of the U.S. Department of Energy to the 1970s oil crisis. It was consolidated by a group of chemical engineers of the MIT (Massachusetts Institute of Technology). AspenTech releases its first product, Aspen Plus®, in 1982, used for modeling of chemical processes. In 2004, AspenTech releases the first version of the aspenONE® suite, which brings together different simulation and optimization software for engineering, manufacturing and supply chain functions; it includes the Aspen Plus® Software. The most updated version of the aspenONE® suite was launched in 2018 and is the version 10 (V10) [41]. Figure 2-8 explains graphically the relation between the used software in the project and the developing company:

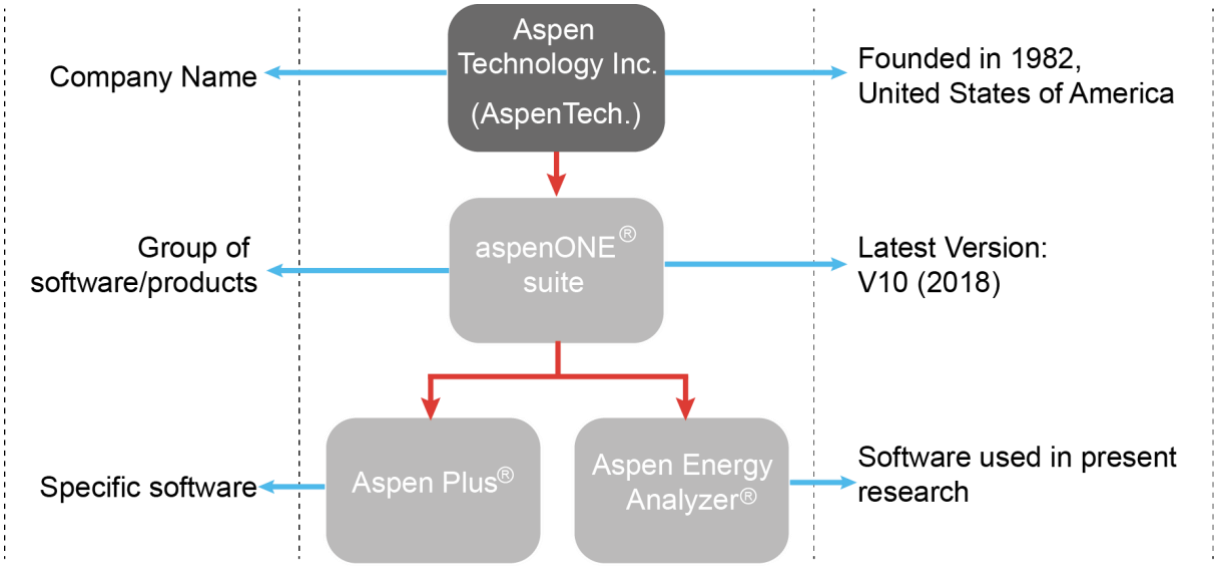

Figure 2-8: *AspenTech basic structure for current research project*

Adapted from [41]

2.2.1.1 Overview of the aspenONE® Suite V8.6.

The aspenONE® V8.6. product portfolio features software packages for different applications. Table 2-6 exhibits all available software packages for every application area. Aspen Plus® belongs to the “Process Simulation for Chemical”, whereas Aspen Energy Analyzer® to the “Energy & Utilities Optimization”. Both of the above-mentioned software were implemented to simulate the CO_2 capture process via chemical absorption in the ABIGAIL pilot plant, and are highlighted in blue in Table 2-6.

Table 2-6: *Summary of the packages per application field of the aspenONE® suite V8.6*

Adapted from [42]

Process Simulation for Energy Aspen HYSYS® • Acid Gas Cleaning • Activated Economics • Activated Energy Analysis • Activated Exchanger Design & Rating • Exchange • Sulsim™ Sulfur Recovery Aspen HYSYS® Crude Aspen HYSYS® Petroleum Refining • Refinery Reactor Models Aspen HYSYS® Upstream Aspen HYSYS® Upstream Dynamics Aspen Operator Training	**Process Simulation for Chemicals** Aspen Adsorption Aspen Batch Modeler Aspen Batch Process Developer Aspen Chromatography® Aspen Custom Modeler® Aspen Plus® • Activated Economics • Activated Energy Analysis • Activated Exchanger Design & Rating • Exchange Solids Modeling Aspen Polymers™ Aspen Process Manuals™ Aspen Properties® Distillation Modeling in Aspen Plus
Exchanger Design & Rating Aspen Air Cooled Exchanger™ Aspen Fired Heater® Aspen HTFS® Research Network™ Aspen Plate Exchanger™ Aspen Plate Fin Exchanger™ Aspen Shell & Tube Exchanger™ Aspen Shell & Tube Mechanical™ Aspen Coil Wound Exchanger	**Dynamics and Safety** Aspen Flare System Analyzer™ Aspen HYSYS® • BLOWDOWN™ Technology • Relief Sizing Aspen HYSYS® Dynamics Activated Dynamics Aspen Plus® • Relief Sizing Aspen Plus® Dynamics
Economic Evaluation Aspen Capital Cost Estimator™ Aspen In-Plant Cost Estimator™ Aspen Process Economic Analyzer™	**Energy & Utilities Optimization** Aspen Energy Analyzer™ Aspen Utilities Planner™
Operations Support Aspen OnLine® Aspen Simulation Workbook™	**Basic Engineering** Aspen Basic Engineering™
Advanced Process Control Aspen DMCplus® Aspen DMC3™ Aspen DMC3 Builder™ Aspen Inferential Qualities™ Aspen Nonlinear Controller™ Aspen Transition Management™ Aspen Watch Performance Monitor™	**Manufacturing Execution Systems** Aspen InfoPlus.21® aspenONE Process Explorer™ Aspen Production Record Manager™ Aspen Production Execution Manager™ Aspen Operations Reconciliation and Accounting™ Aspen Tank and Operations Manager™

Petroleum Supply Chain Aspen PIMS™ Aspen PIMS-AO™ aspenONE PIMS Platinum™ Aspen Assay Management™ Aspen Petroleum Scheduler™ Aspen Refinery Multi-Blend Optimizer™ Aspen Collaborative Demand Manager™ Aspen Petroleum Supply Chain Planner™ Aspen Fleet Optimizer™ **Asset Performance Management** Aspen Mtell Aspen Fidelis Reliability Aspen ProMV Aspen Column Analytics Aspen Root Cause Analytics Aspen Connect Family • Aspen Cloud Connect • Aspen Edge Connect	**Supply Chain Management** Aspen Collaborative Demand Manager™ Aspen Supply Chain Planner™ Aspen Plant Scheduler™ Family Aspen Supply Chain Connect™

2.2.1.2 Aspen Plus V8.6® for the simulation of absorption processes

"Maximize profits using a plant-wide simulation solution that combines unparalleled accuracy and engineering collaboration with time-saving workflows" is the commercial headline for advertising Aspen Plus® [43]. Which is not far from the truth, as the software is a user-friendly workflow interfaces which relies on proven physical properties and reaction models for chemicals, electrolytes, solids and polymers. Furthermore, it uses integrated modeling for batch and continuous processes. Moreover, Aspen Plus® employs seamless, integrated tools for costing, energy management, safety analysis and equipment design; Enabling lifecycle modeling from design through operations for faster troubleshooting, online performance monitoring and real-time optimization [43]. The following fields are the most suitable applications for the software:

- Bulk Chemical Process Improvement
- Concurrent Conceptual Engineering
- Distillation Improvement
- Dynamic Studies
- Energy Management

- Fast Bid Packages for Licensors
- Operations Decision Support
- Polymer Process Optimization
- Process Safety Analysis
- Project Cost Estimation
- Solid Process Optimization

A basic 5-step sequence is usually implemented when developing process simulations in Aspen Plus®, it is depicted in Figure 2-9. A simulation starts with the selection of components and their corresponding property packages depending on their chemical nature, Aspen Plus® has multiple property databases available (Step 1). Then, the reactions involved in the process must be specified, along with their kinetic parameters (Step 2). Subsequently, the process flow diagram must be defined; In this step, operation conditions and basic dimensioning of the operation units must be given (Step 3). Afterward, sensibility analysis must be carried out to identify the most influencing variables of the process and their corresponding ranges (Step 4). Finally, the optimization step allows the user to minimize/maximize the objective function by modifying one of the previously identified variables (Step 5).

Figure 2-9: *Basic 5-steps sequence for process simulation in Aspen Plus®*

Aspen Plus® features two optimization approaches as shown in Table 2-7, each one of them is based on a different algorithm to perform the iterative calculations. An effective way to override the convergence defaults, is to enter convergence specifications on Convergence forms using the SQP and Complex methods to converge optimization problems.

The value of the manipulated variable that is provided in the Stream or Block input is used as the initial estimate. Providing a good estimate for the manipulated variable helps the optimization problem converge in fewer iterations. This is especially important for optimization problems with a large number of varied variables and constraints [44]. The corresponding description of every approach is also stated in Table 2-7.

Table 2-7: *Optimization approaches in Aspen Plus® V8.6*

Adapted from [44]

Optimization Approach	Description
SQP (Sequential quadratic programming)	The sequential quadratic programming (SQP) method is used in flowsheet optimization for simultaneous convergence of optimization problems with constraints (equality or inequality) and/or tear streams. The algorithm generally follows an infeasible path (Constraints and tear streams are converged simultaneously with the optimization problem). However, a feasible path is also possible (Converging the tear streams at each iteration of the optimization). SQP is used for system generated optimization convergence blocks.
Complex Method	The Complex method is used to converge optimization problems with bounds on the manipulated variables and inequality constraints. Complex is a direct search method; it does not require numerical derivatives. It may be useful for simple problems without recycle loops or equality constraints (design specifications).

2.2.1.3 Aspen Energy Analyzer™ V8.6. for the heat exchange network

Aspen Energy Analyzer™ is an energy management software for performing optimal heat exchanger network design to minimize process energy. It provides an easy environment to perform optimal heat exchanger network design and retrofit. Using this tool, it is possible to cut down on unnecessary energy use, for a less expensive and greener process design. Utilizing either a graphical or algorithmic method, the best heat exchanger network design solutions could be identified [45]. An example of how an optimized heat exchange network looks like is depicted in Figure 2-10:

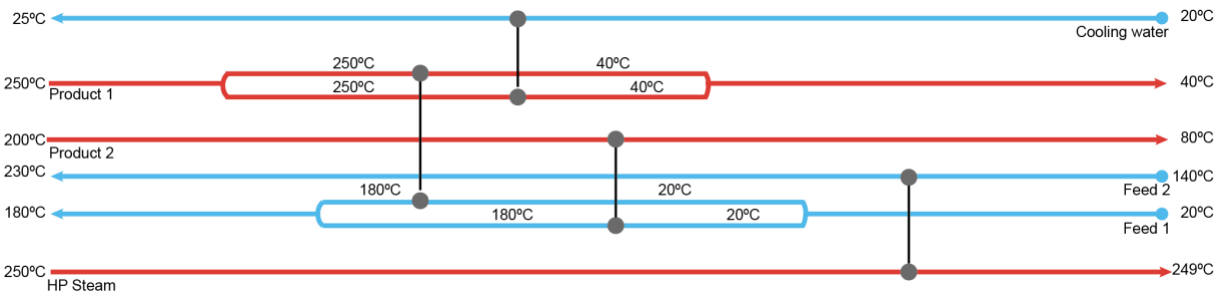

Figure 2-10: *Illustrative example of an optimized heat exchange network with Aspen Energy Analyzer™*

The upper blue straight line represents the cold utility stream available in the process, whereas the bottom red straight line depicts the hot utility stream. The four intermediate straight lines are process streams that need to be either cooled (Red lines pointing to the right), or heated up (Blue lines pointing to the left). Every vertical line represents a heat exchanger, and its terminal circles point out the stream where heat is transferred.

An optimized heat exchange network involves heat exchange not only with the utility streams, but also with the process ones. It gives essentially information regarding when and which streams should be coupled for heat transfer, providing output temperatures for each device, and the amount of flows that should be split for an optimal usage of the process utilities.

2.2.2 Available property packages for the simulation of amine solutions

One of the most challenging steps in any process simulation with Aspen Plus® is the choice of the appropriate property package. The explained property packages will be implemented in the simulations, as will be explained in section 3.2.1.1.

When using Aspen Plus® for simulating amine solutions, the unsymmetric ENRTL property method (Electrolyte non-random two liquid model – ENRTL-RK) and PC-SAFT (Perturbed change statistical associating fluid theory) equation of state are used to compute liquid and vapor properties, respectively [32].

For multiple component property modelling, a set of Henry-components (Solutes) must be selected. Out of all the different species in the model, CO_2 and N_2 are selected as Henry components. Their corresponding Henry constants are specified for these components in water and MEA, they were obtained from the literature [46, 47] and integrated to the Aspen Plus® property package. In the reaction calculations, an infinite-dilution condition is assumed for the calculations regarding the unsymmetric activity coefficients (GAMUS) [32].

The PC-SAFT parameters of MEA are regressed from the vapor pressure data [48, 49, 50, 51], the heat of vaporization data, the liquid heat capacity data [52, 53], and the liquid density data [54, 55, 56]. Those for water are obtained from [57], and those for the other components are retrieved from the Aspen Database.

The NRTL interaction parameters between MEA and H_2O are determined from the regression of binary VLE data [51, 58, 59, 60], excess enthalpy data [59, 61], and heat capacity data [54, 62]. The sources for the remaining parameters for the transport property models (Viscosity, liquid molar volume, surface tension, thermal conductivity and binary diffusivity) could be found in [32].

2.2.3 Summary of the published simulations for CO_2 –MEA absorption processes

As CO_2 chemical absorption has reached a TRL9 (Technology Readiness Level), most recent simulation studies are related to process dynamics to study the flexibility of the operation. However, several experimental validations of Aspen Plus® models have been carried out over the last years. Table 2-8 synthetizes the conducted experimental validations of the desorption processes for CO_2 capture via chemical absorption with MEA, featuring the most important facts of each and the amount of experimental conditions (runs) that each validation used:

Table 2-8: *Review of the available published simulations on desorption models for CO_2 capture processes via chemical absorption with MEA.*

Adapted from [63]

Source	Desorber Validation Parameters	Modeling details	Aims
[64]	Temperature, loading, regeneration energy	1 pilot plant (39 runs) Aspen Plus® ENRTL	Re-fitting
[65]	Temperature, CO_2 loading	1 pilot plant (19 runs) [66] gProms PC-SAFT	Prediction of desorber runs
[67]	Reboiler duty, CO_2 concentration, temperature	1 pilot plant (19 runs) Aspen Plus® ENRTL	Comparison of rate-based and equilibrium models, re-fitting
[68]	Desorbed CO_2, reflux flow rate, loading	2 pilot plants MATLAB	Validate an in-house model
[69, 70, 71]	Temperature, composition, CO_2 loading	1 pilot plant (2 runs) gProms PC-SAFT	Integration of theoretical CO_2 capture in a power plant
[72]	Reboiler duty	NA Aspen Plus® and Aspen	Validate heat consumption

		HYSYS® ERNTL	reduction by changes on absorption configurations
[73]	Loading, desorbed CO_2, solvent flow rate	1 pilot plant K-Spice, InfoChem, CO_2SIM	Dynamic changes
[74]	Reboiler duty, CO_2 loading	2 pilot plant Aspen Plus®	Validate two packings and two scales
[75]	Reboiler temperature	1 pilot plant Dymola, Modelica, Optimica	Represent dynamic changes
[76]	Heat of regeneration, temperature, CO_2 loading	1 pilot plant (2 runs) In-House ERNTL	Validate an in-house model for different CO_2 concentrations in flue gas
[77]	Temperature, vapor composition	1 pilot plant (1 run from [78]) Aspen Plus® ERNTL-RK	Enhancement of existing model
[79]	Temperature, reboiler duty	1 pilot plant (5 runs) Aspen HYSYS® ERNTL	Evaluation of performance of exhaust gas recycle and validation of simulation model
[80]	Lean temperature, CO_2 concentration on the top of the stripper, flow rate	1 pilot plant with variation of operation parameters NLARX, Simulink®	Evaluation of dynamic predictions
[81, 82, 83]	Loading, reboiler duty	1 pilot plant with variation of operation parameters Aspen Plus®, MATLAB UNIQUAC	Operation and comparison of MEA through transient response
[84]	Temperature, loading	1 pilot plant Aspen Plus®, Aspen Plus Dynamics® ERNTL	Prediction of dynamic changes

It is clear that the aspenONE® suite is the most used software for modeling the desorption stage of the process, along with the inclusion of the ERNTL model for species' properties. Nevertheless, other commercially available software has been implemented for such purposes, i.e., gProms. Overall, in the simulation models, kinetic constants, effective absorption/adsorption area or heat loss are often used to adjust the simulations to the experimental data [63]. For validation aims, the CO_2 loading and the temperature profiles are the most common comparison outputs, either in the absorption or the stripping stage.

Further research and simulations in field involve not only the model validation, but the process optimization and the analysis of different configurations, where vapor recompression plus stream-split arranges are studied, showing overall energy savings up to 19% [85]. Figure 2-11 illustrates one of the above-mentioned configurations.

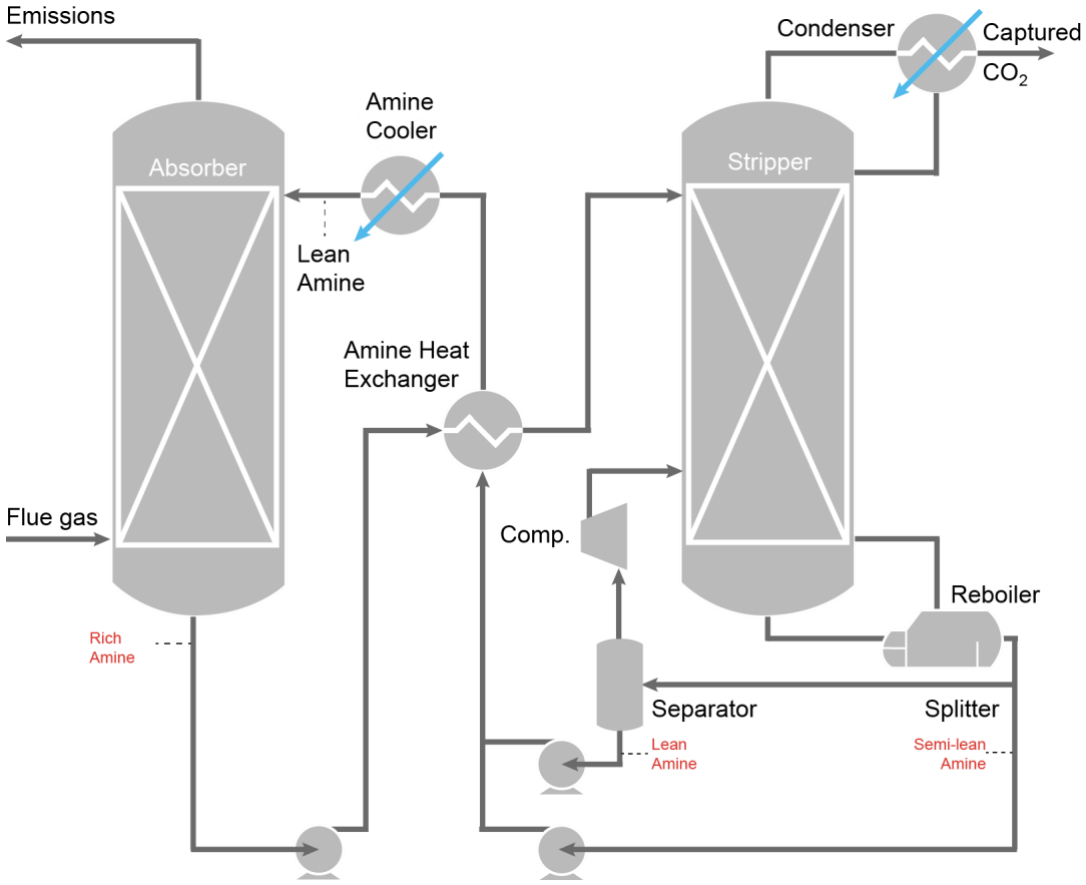

Figure 2-11: *Vapor recompression combined with split-stream process configuration*

Adapted from [85]

The innovation in the configuration plotted in Figure 2-11 is the inclusion of a compressor to recirculate back to the stripper the gas phase included in the lean amine stream. Furthermore, the lean amine stream is split to control the amount of recirculated gas. Therefore, multiple configurations for this technology must still be developed to further abate operational cost.

2.3 Problem statement

Further enhancements of the ABIGAIL pilot plant at the Institute of Combustion and Power Plant Technology of the Stuttgart University will require a computational representative process model to foresee its performance when changing process parameters/configurations. Therefore, operational cost of the pilot plant could potentially be diminished, as the trial-and-error rate will steadily decay. Moreover, an initial set of optimal operation conditions for the current configuration should be suggested for the pilot plant.

3 Methodology for the practical tests and simulations

The following section is divided into two parts: On the one hand, the operation-related procedures are explained; including a description of each component of the pilot plant, detailed start-up/shut-down routines for the strip steam operation, overview of the LabVIEW's interface for process controlling and its control loops, an exhaustive depiction of the step-by-step method for analyzing the MEA samples, and a summary of the conducted runs with their corresponding operational conditions.

On the other hand, the simulation details and parameters are listed. It summarizes all relevant inputs for every software, starting with the property packages, up to the specific block's configurations. Finally, an implementation algorithm condenses the general procedure to conduct the simulations throughout the different software.

3.1 Methods and procedures of the operation-related aspects of the pilot plant

The pilot plant ABIGAIL was built to study the different amine salt solutions for the CO_2 capture from flue gases or natural gas. Its first documented operation was carried out in 2016 by [38]. Further experiments were conducted in 2017 by [40]. For this project, a total amount of 19 strip steam runs divided in two measurement campaigns were carried out at the ABIGAIL pilot plant.

The experimental performance results were then compared with the outputs of the simulation model for each operation condition. This first section is aimed to enlighten the details concerning the operation of the pilot plant and the sample analysis.

3.1.1 Detailed description of the ABIGAIL pilot plant

The pilot plant is mainly composed by two sections: The absorber column and the stripping section. All operation units and instruments are supported inside a 4.0 metal structure as seen in Figure 3-1. Each subsystem is equipped with multiple temperature, pressure, flow and concentration measurement instruments. The P&ID of the pilot plant is shown in Figure 3-2. It is the most-updated depiction of the available instrumentation. A complete list of the instruments is synthetized in the Annex A.

In the strip steam operation, the synthetic flue gas (Composed by N_2 and CO_2) enters the bottom stage of the absorption column (ABS-1) after being transported by the compressor (GE-1). Simultaneously, the lean MEA solution is fed from the top stage of the absorber (ABS-1). Although multiple heights for feeding the solvent are available, it is not possible to use more than one at the same time. However, previous research have shown that feeding the solvent in the top stage is more suitable to achieve higher absorption rates [38]. The cleansed gas is withdrawn from the top of the column and a part sent directly to the chimney, while the other part is rinsed with water (NW-1) and recirculated to the absorber passing again by the compressor (GE-1). The gas concentration could be determined at the outlet stream of the column (yCO_2-1) and at the recirculation line (yCO_2-Rezi) by using NDIR Gas analyzers (Details is section 3.1.1.1)

The loaded MEA solution is removed by the bottom stage of the column and pumped (P-1) through the heat exchanger (WT-1). Then, it is fed to the top stage of the stripper (DES-1) and exposed to the high operational temperatures of the desorption process. As the regenerated solvent flows downwards, the concentration of MEA increases. The solution is retrieved from the bottom of the stripper and pumped (P-4) to the main solvent container (BE-1), which besides storing the solution, is also equipped with an electrical resistance to warm up the solution and generate the recirculating MEA vapors. In other words, it replaces the reboiler of conventional processes. The recirculated vapors are fed back to the desorption column in the bottom stage. As they flow upwards, the CO_2 concentration becomes higher. The CO_2 loaded gas is removed from the upper section of the column, cooled down (WT-3) and separated from any liquid phase (KO-1) before it is sent to the chimney. The separated liquid is pumped (P-3) back to the stripper.

The solvent container (BE-1) is divided into two sections, one for heating up the solution, and the other one to dispense it to the recirculation loop. Once the regenerated solvent reaches the tank, its level increases until it reaches the top of the first compartment, the supernatant is transferred to the second compartment by gravity. Afterward, the regenerated solvent is fed to the heat exchanger (WT-1) and pumped (P-2) to the upper cooler (WT-2) to finally be introduced into the absorber. The concentration of MEA in the solvent could be monitored by taking samples in any of the six different measurement points. The most recent inclusion (October 2018) to the pilot plant was precisely the sixth measuring point right at the output of the stripper after the pump (P-4).

Figure 3-1: *Picture of the ABIGAIL pilot plant on the 29.09.2018*

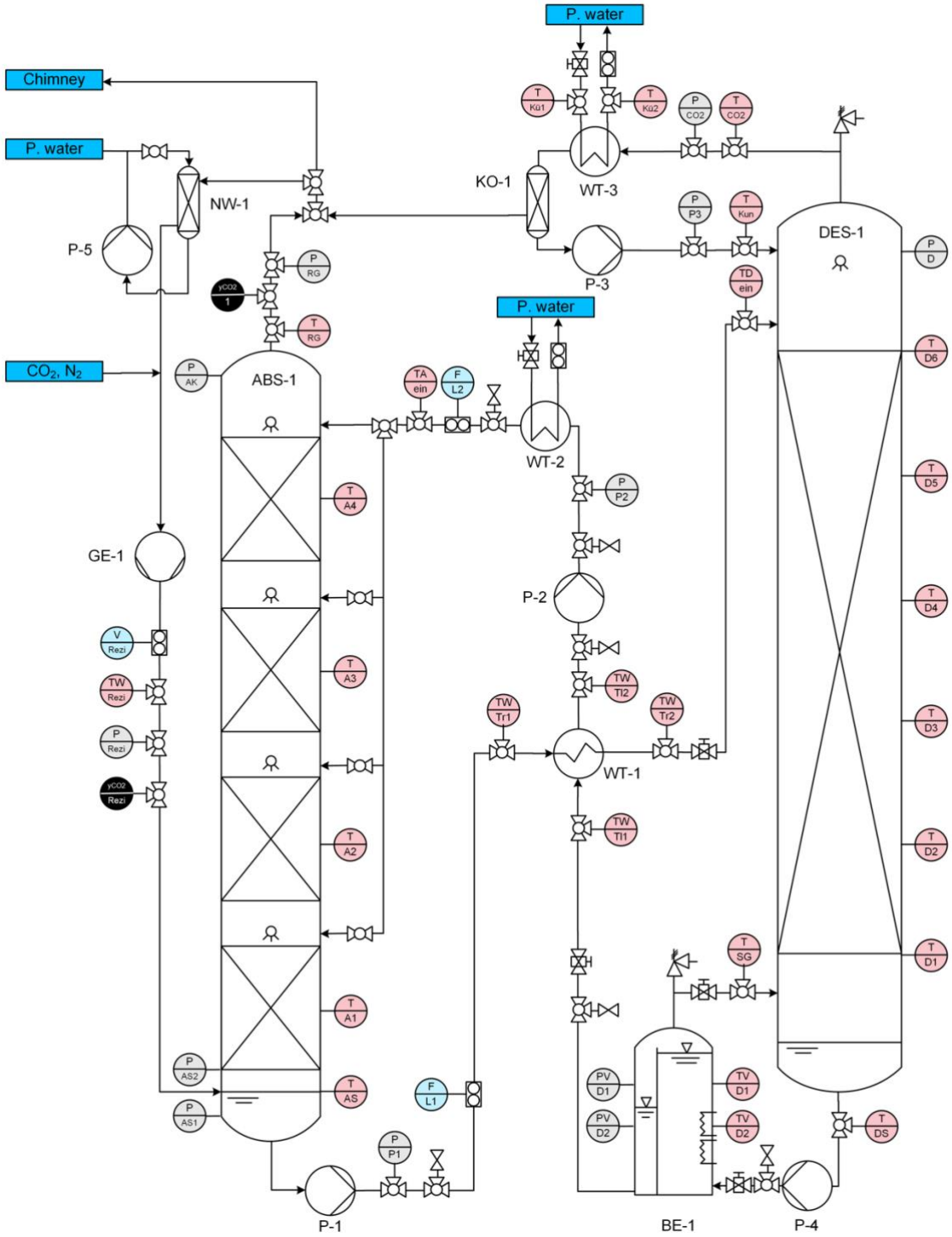

y a	Gas Analyzer	P a	Pressure sensor	F a	Flow meter	T a	Temperature sensor
WT	Heat Exchanger	P	Pump	GE	Compressor	ABS	Absorber
DES	Stripper	NW	Water washer	KO	Condenser	BE	Storage tank

Figure 3-2: *Most updated P&ID (20.10.2018) of the ABIGAIL pilot plant for the strip steam operation*

3.1.1.1 Absorption column and its components

The absorption stage is composed by the absorption column (ABS-1), along with its pre-inflow cooler (WT-2), the draining pump (P-1), the gas recirculation compressor (GE-1), and the water washer (NW-1) with its pump (P-5). Figure 3-3 simplifies the main unit operations of the absorption stage with their corresponding abbreviations.

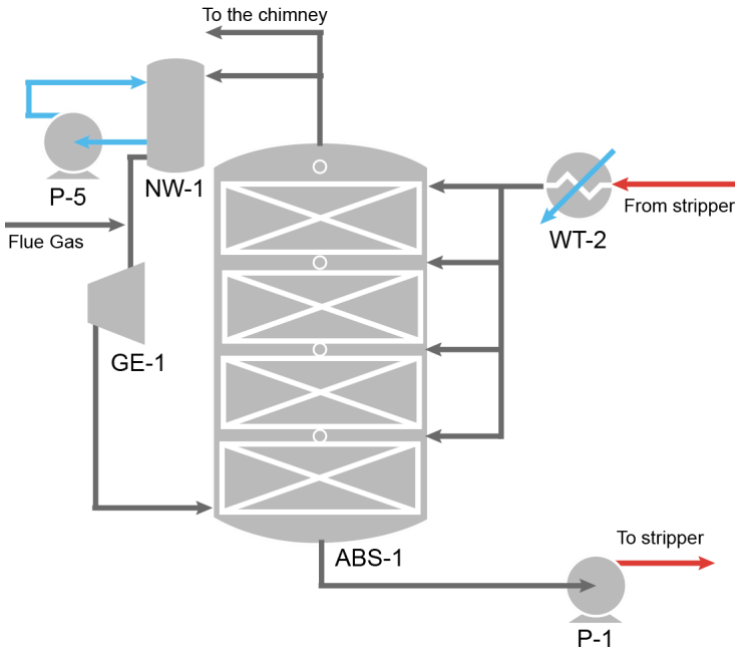

Figure 3-3: *Main unit operations of the absorption stage*

Furthermore, the absorption stage is equipped with 6 thermocouples for temperature measurements, 5 pressure gauges, 2 gas monitors for determining the CO_2 concentration, and 3 flow meters for measuring the volumetric flow from the solvent and the recirculated gas. Moreover, a sample of solvent could be withdrawn from the bottom of the column after P-1. The detailed list of the instruments could be found in Annex A. The basic technical characteristics of the operational units are listed in table 3-1.

Table 3-1: *Technical description of the absorption stage components*

Abbreviation	Function/ Description	Technical Characteristics
ABS-1	Main component of the absorption system. Captures the CO_2 present in the flue gas via chemical absorption in a countercurrent array, where the solvent (MEA Solution 30% w/w) is fed in the top stage. It is made out of Plexiglas® [86] and it has an internal plastic packing to	• Packed height (H) [m]: 3.40 • Diameter (D) [m]: 0.10 • Packing type: Hiflow® • ring 15-7 plastic from rvt [87] • Nominal packing diameter (D_p) [mm]: 15 • Surface Area (A_c) [m^2/m^3]:

	increase the contact area between the phases. Four possible heights for solvent feed could be achieved. Moreover, it is equipped with 5 internal thermocouples and 3 pressure gauges for temperature and pressure control.	313 • Void Fraction (ε) [%v/v]: 91
GE-1	The compressor is aimed to pressurize the recirculating gas to transport it inside the absorption column. Its performance is directly managed in the control room, depending on the desired gas flow, recirculation share, and inlet CO_2 concentration.	
NW-1	The water washer was built to prevent the dragged liquid MEA solution coming from the top stage of the absorber to enter the compressor. From the operational point of view, it will prevent corrosion of the internal parts of the compressor.	
P-1	The pump was installed to transport the loaded solvent through the heat exchanger up to the stripper. Its performance is manipulated at the control room based on the desired volumetric solvent flow and the level inside the absorption column.	• Peristaltic Industrial Hose Pump • Reference: D25 SW USCLSS 35R0.75K EP TF • Specifications: V 0.75 kW; 35U/min; 230/400V • Brand: Verderflex®
P-5	The pump was installed to recycle the water from the water wash.	
WT-2	The aim of the cooler is to adjust the inlet absorber's inlet temperature. It is manually operated with process cold water	• FP 05-27-1-EH-0, Plate heat exchanger. • Dimensions: 80 x 40 x 40 cm • Number of plates: 30, 0.5 mm • Brand: Funke • Operation: Countercurrent • Utility: Process water

3.1.1.2 Desorption column and its components

The stripper (DES-1) is the main component of the desorption stage. The top material reflux comprises a cooler (WT-3), a phase separation unit (KO-1) and a recirculation pump (P-3). On the other hand, the reboiler subsystem is composed by a draining pump (P-4) to overcome the static pressure of the fluid height inside the tank (BE-1) when recirculating the solvent. The tank (BE-1) is equipped with an electric resistance that provides the energy to boil the solution and generates the required steam for recirculation. The pre-heater (WT-1) exchanges heat between the high temperature solvent coming from the tank and the loaded solvent coming from the absorption process. A final transport pump (P-2) is also implemented to transfer the solvent back to the absorption stage. Figure 3-4 depicts a simplified process flow diagram of the desorption stage.

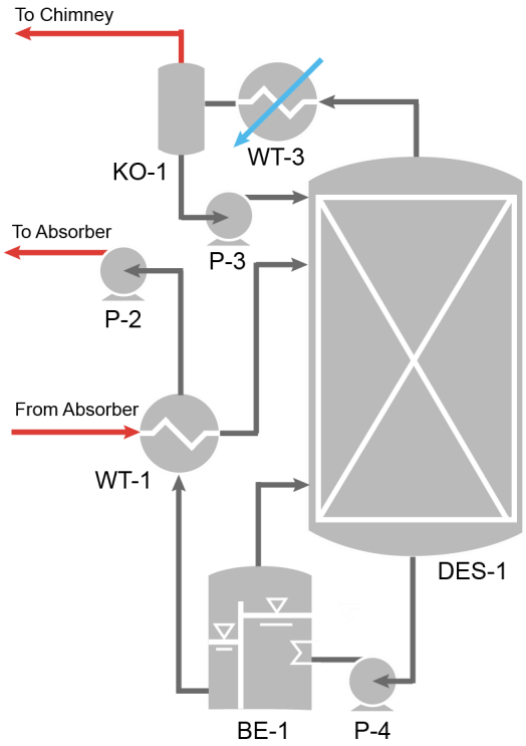

Figure 3-4: *Main Unit Operations of the desorption stage*

The desorption stage is equipped with 20 thermocouples to monitor temperature in the lines and inside the column. Furthermore, 6 pressure gauges are installed to control the operation pressure and compute the pressure drop across the packing. Additionally, four different locations could be used to withdraw solvent samples from the system, the most-recently added one was included in October 2018, right after the draining pump (P-4). The detailed list of the instruments could be found in Annex A. The basic technical characteristics of the main operational units are listed in table 3-2.

Table 3-2: *Technical description of the desorption stage components*

Abbreviation	Function/ Description	Technical Characteristics
BE-1	The solvent storage tank has two major tasks: On the one hand, it stores large amounts of the solvent. On the other hand, it is equipped with an electric resistance to generate boil-up steam for the stripper's gas recirculation. It is internally split into two sections, one operates as a reboiler, and the other one as mixing volume. The inclusion of the tank prevents pump damage due to liquid flow fluctuations.	• 200 l capacity • Equipped with copper electric resistance covered with stainless stell
DES-1	The stripper is the main component of the desorption system. The regeneration of the solvent takes place throughout the column due to its high temperatures. It possesses two recirculation systems, one at the top for a liquid recirculation, and one at the bottom for gas recirculation. The column is fully packed with metallic Raflux® rings to increase the contact area between the phases. Furthermore, it has six different thermocouples to monitor the temperature profile across the column. Only one possible input height of solvent is available in this device.	• Packed height (H) [m]: 2.70 • Diameter (D) [m]: 0.15 • Packing type: Raflux® ring 15-3 plastic from rvt [88] • Nominal packing diameter (D_p) [mm]: 15 • Surface Area (A_c) [m^2/m^3]: 313 • Void Fraction (ε) [%v/v]: 91
KO-1	The phase splitter separates the liquid from the gas phase after the cooler on top of the stripper. Its aim is to recirculate most of the water to the system.	
P-2	The pump was installed to transport the lean solvent up to the input of the absorption column. Its performance is manipulated at the control room based on the desired volumetric solvent flow and the level inside the absorption column.	• Peristaltic Industrial Hose Pump • Reference: D15 SW USCLSS 28R0.75K EP TF • Specifications: V 0.37kW; 28/U/min; 230/400V • Brand: Verderflex®
P-3	The pump was installed to recycle the condensed water from the phase	

	splitter inside the desorption column.	
P-4	The pump was installed to enable the re-filling of the solvent tank with the regenerated solution. Its aim is to overcome the static pressure inside the tank, allowing the fluid to flow towards the inside.	
WT-1	The heat exchanger between the rich and the lean MEA solution is intended to pre-heat the CO_2-loaded stream utilizing the high temperature of the regenerated solution. Hence, a reduction in the utilities' cost is achieved	• Z2-51, Plate heat exchanger • Dimensions: 48 x 18 x 18 cm • Brand: Zilmet® • Operation: Countercurrent • Utility: N/A, works with process streams
WT-3	Aimed to recovery part of the evaporated water during the desorption process, the cooler on top of the stripper was installed.	• FP 05-27-1-EH-0, Plate heat exchanger. • Dimensions: 80 x 40 x 40 cm • Number of plates: 30, 0.5 mm • Brand: Funke • Operation: Countercurrent • Utility: Process water

3.1.2. Strip steam operation procedures and protocols

To operate properly the ABIGAIL pilot plant, a start-up, a steady state operation, and a shut-down protocol must be taken into account. The simplified process flow diagram, including both subsystems, absorption and desorption, is shown in Figure 3-5 with its corresponding notation of the most important streams.

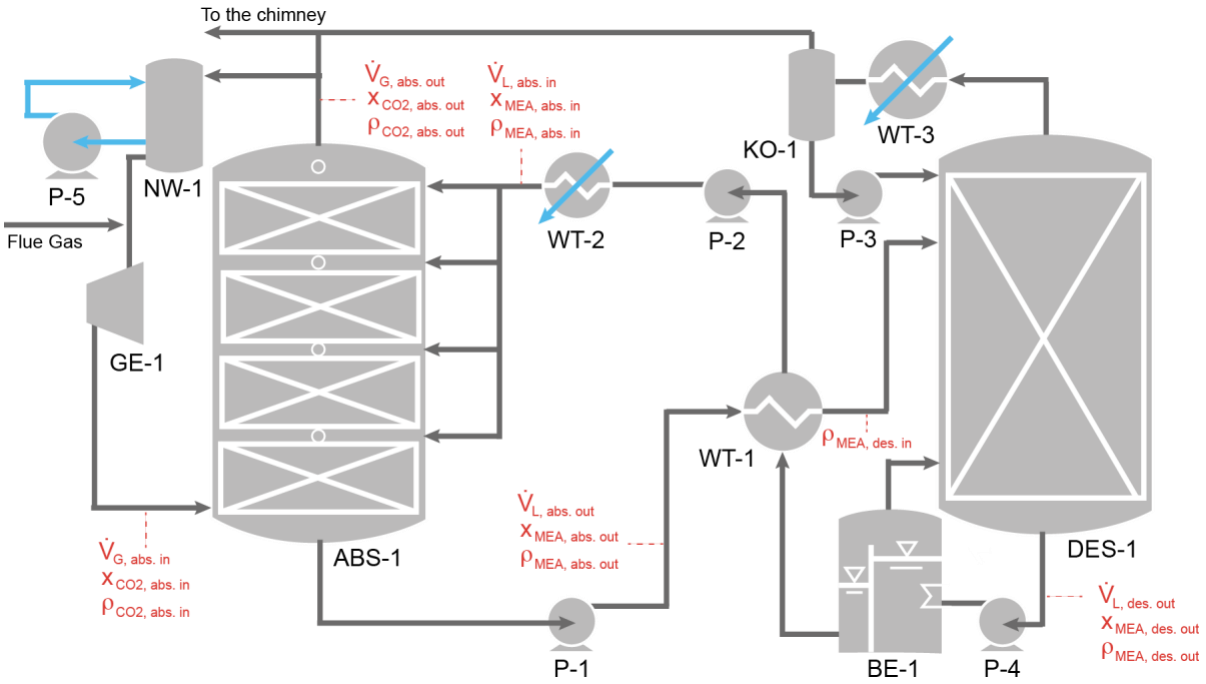

Figure 3-5: *Simplified Process Flow Diagram of the ABIGAIL pilot plant*

The following three subsections depict the protocols of every part of the operation through step-by-step flow chart algorithms. The Start-up protocol explain the main steps to turn on the pilot plant and to reach the stationary state. The steady state operation flow chart indicates how to vary the L/G ratio, CO_2 inlet concentration, desorption pressure, inlet absorber temperature, and boil-up/reflux in the stripper. Finally, the shut-down protocol states the recommended order to stop the operation of the pilot plant.

3.1.2.1 Start-up protocol

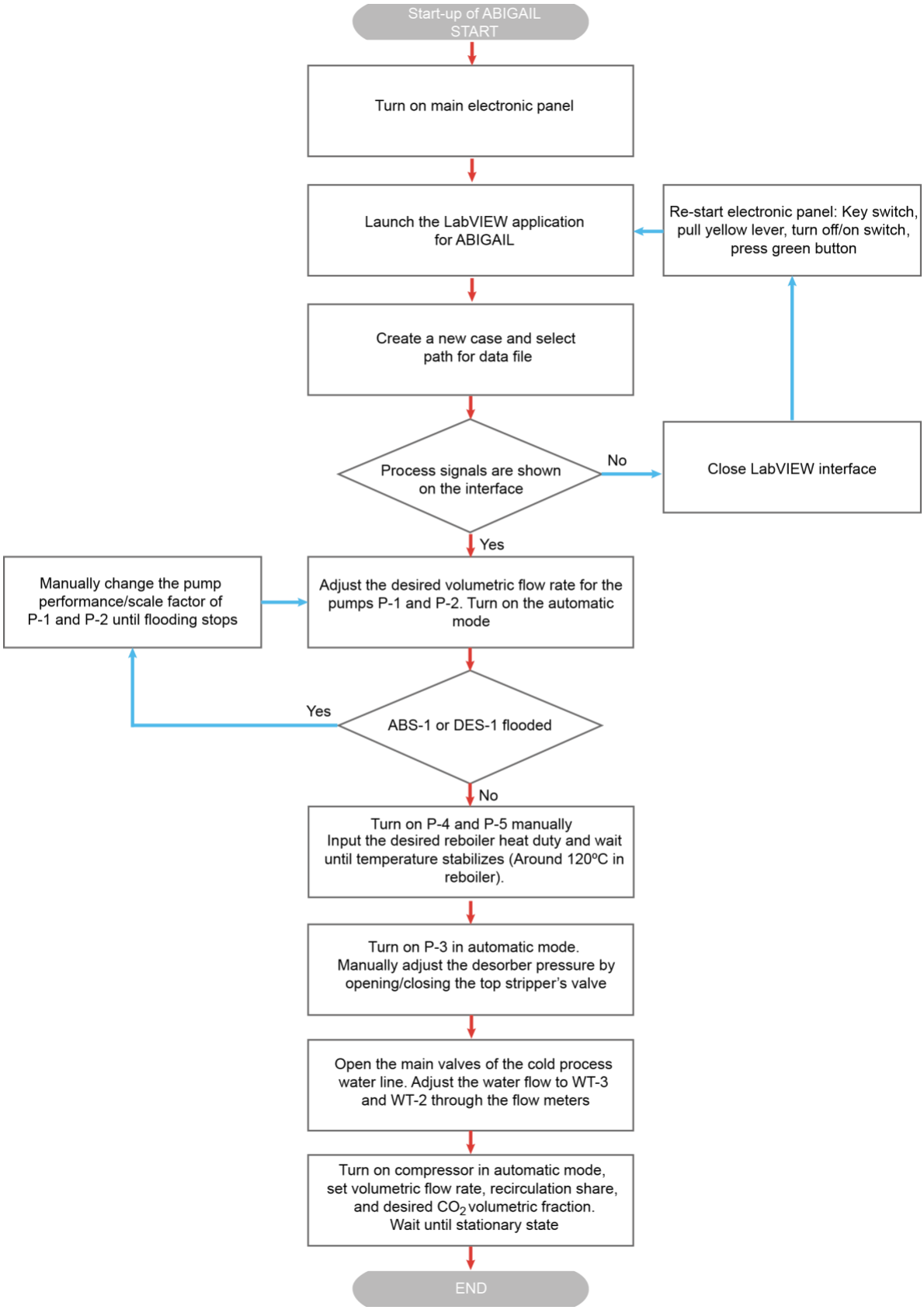

Figure 3-6: *Flow chart algorithm for the Start-up protocol*

3.1.2.2 Steady state operation protocols

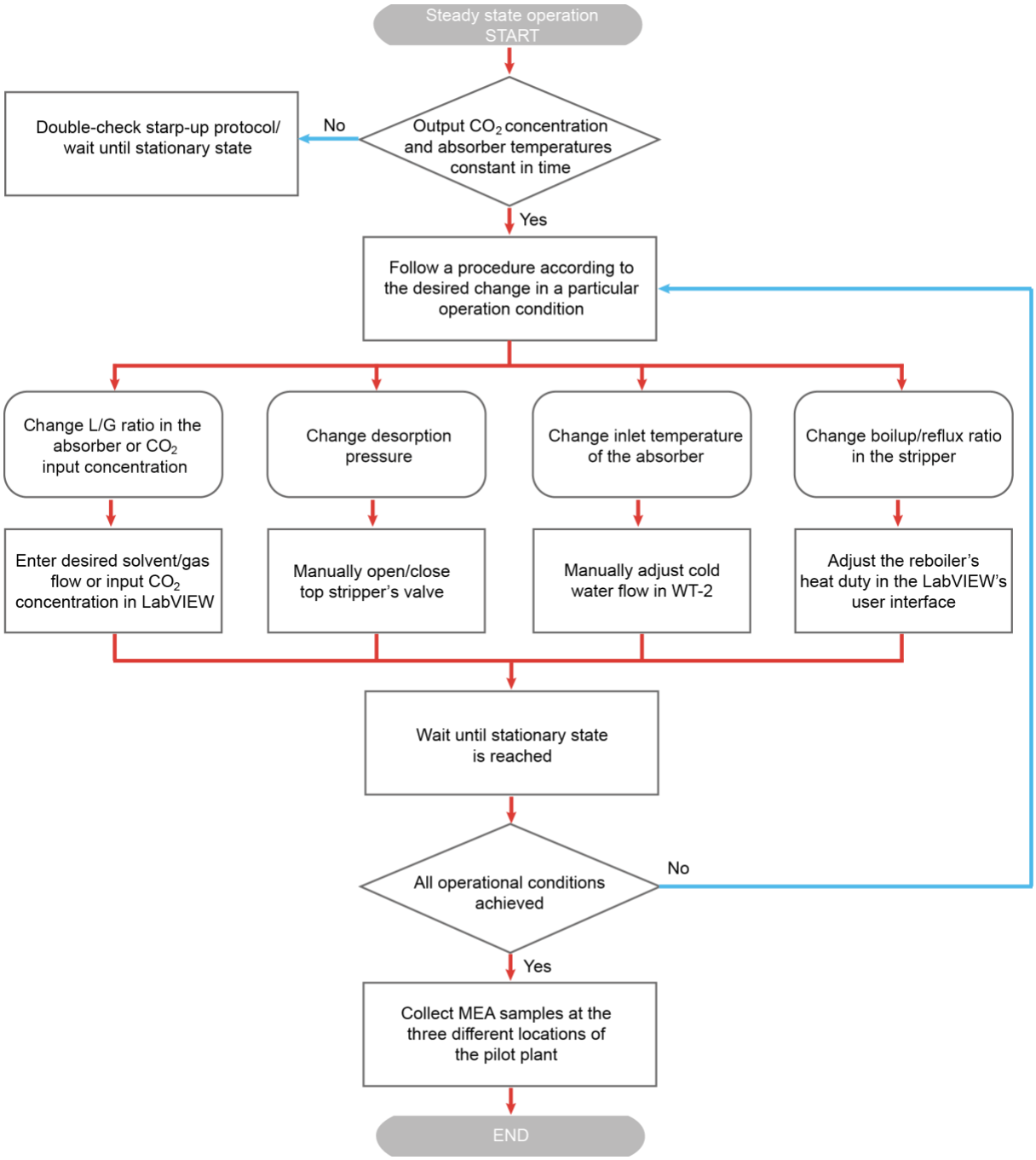

Figure 3-7: *Flow chart algorithm for the Stationary state operation protocol*

3.1.2.2 Shut-down protocol

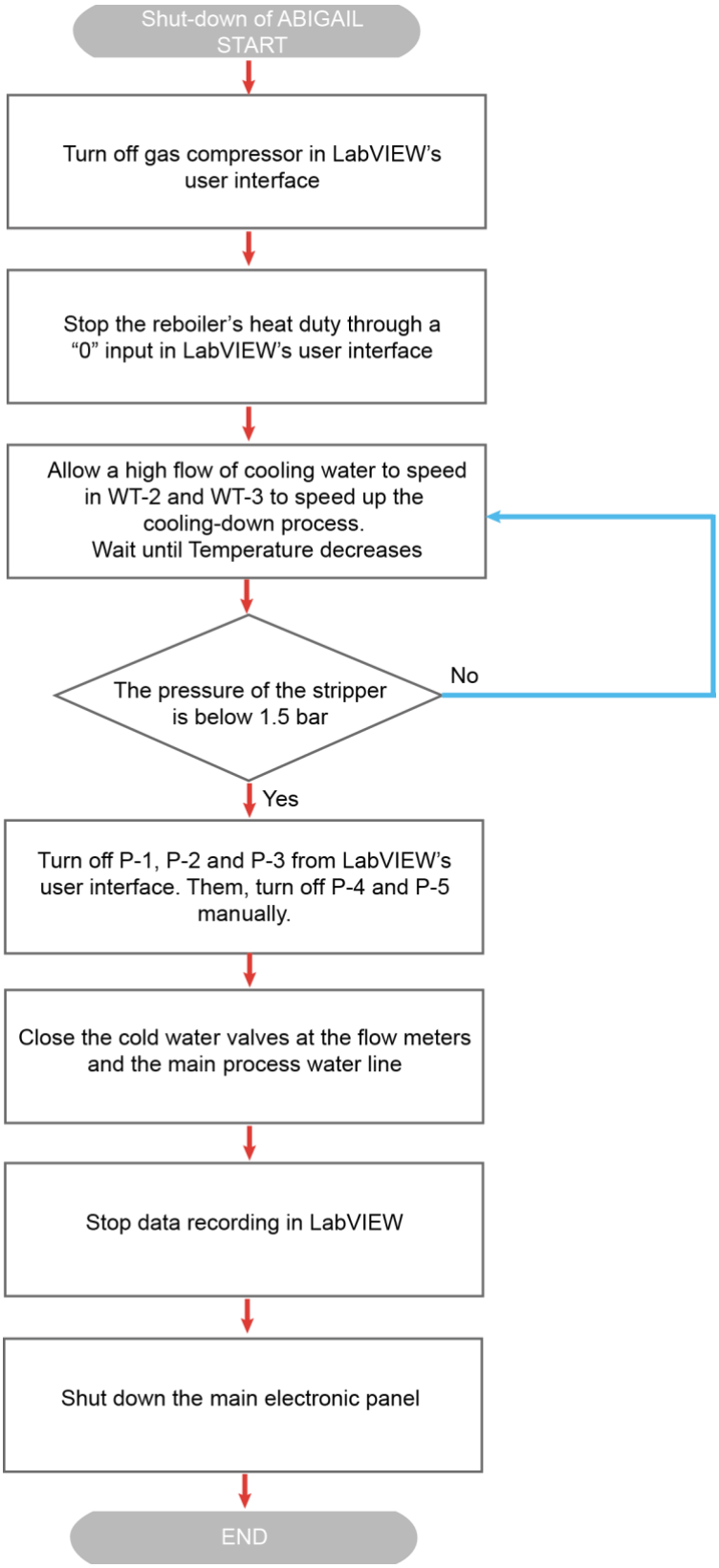

Figure 3-8: *Flow chart algorithm for the Shut-down protocol*

3.1.3. Developed LabVIEW software for data analysis and process control

LabVIEW is a systems engineering software for applications that require test, measurement, and control with rapid access to hardware and data insights [89]. An application was developed to monitor, control and record the data of the available instruments of the pilot plant.

Section 3.1.3.1 describes the user's interface of the developed LabVIEW's applications, stating the main screens and what could be done in each, whereas section 3.1.3.2 provides details regarding the manipulated, measured and controlled variables of the process

3.1.3.1 Description of the LabVIEW's User Interface

The main user's interface of the developed LabVIEW application shows the strip steam process flow sheet along with an schematic representation of all instruments and the measured signals. An adapted screenshot of the user's interface could be seen in Figure 3-9. It could be seen that the liquid streams are depicted in blue, and the gas streams in red. The interface is also equipped with the displaying of safety operation parameters, such as liquid level in the columns, tank, and condenser, as well as flow warnings at the exit of each pump, to ensure liquid flow through each.

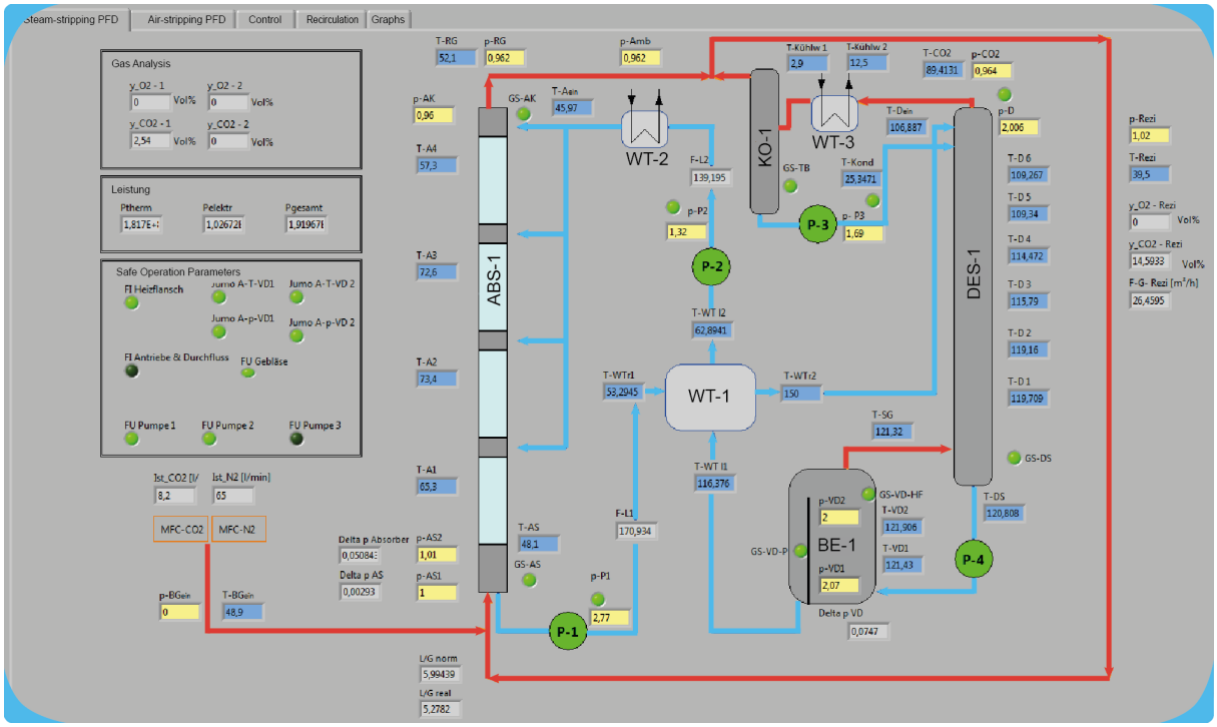

Figure 3-9: *Strip steam process flow sheet in LabVIEW*

The second tab of the developed LabVIEW application is the control interface. It is illustrated in Figure 3-10. Its main aim is to adjust the solvent flow of the pumps P-1 and P-2. It could be done in automatic mode by inputting the desired volumetric flow, or manually by controlling the pump's performance or the scale factor. P-3 could also be turned on through this interface. Furthermore, the pumps' control parameters could also be tuned in.

Moreover, the control tab allows the user to define the maximum pressure in the system. As soon as this pressure is reached, a safety valve on top of the stripper will release some of the accumulated gas to lower the pressure. Last but not least, any remarks during the operation could be added at any time and recorded with the data.

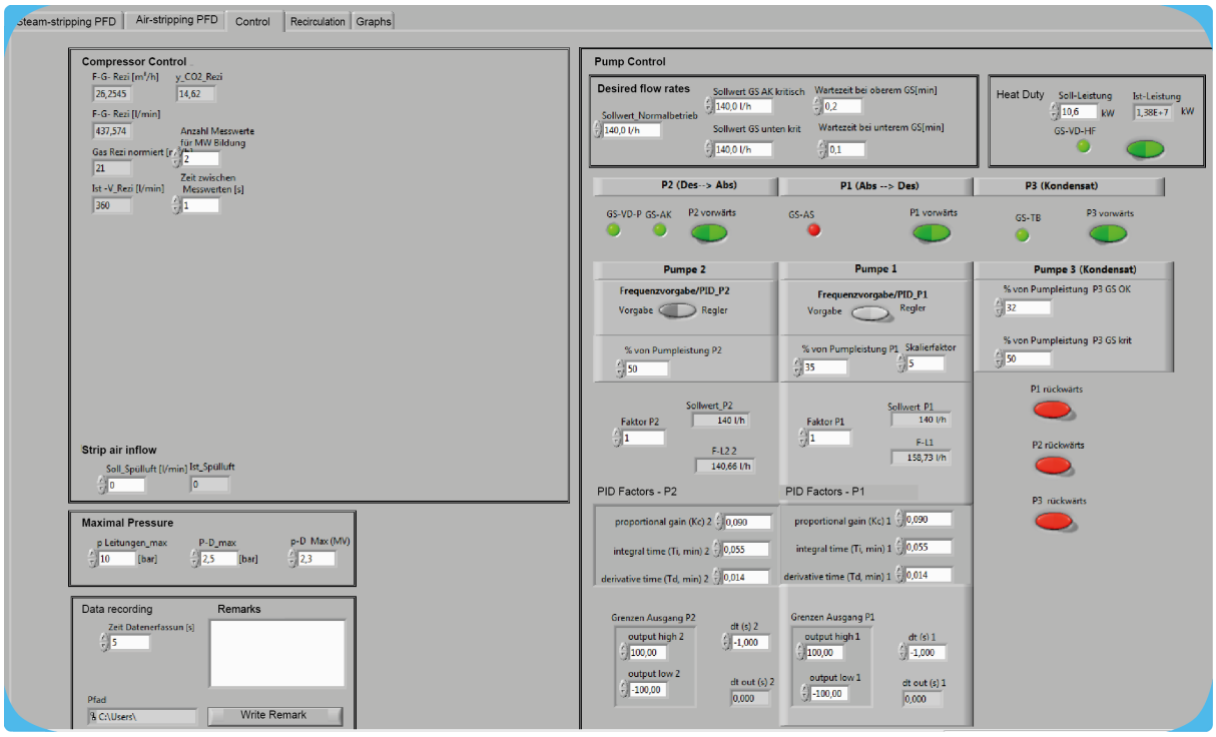

Figure 3-10: *Control interface in LabVIEW for liquid and air flow rates*

The third tab "Recirculation" is intended to operate the gas recirculation to the absorber. It is shown in Figure 3-11. Firstly, the gas volumetric flow could be defined, along with the recirculation percentage and the desired gas concentration. Automatic mode is usually implemented to find the right quantities of fresh gas that must be retrieved to the system. The controller's parameters could also be tuned in this interface.

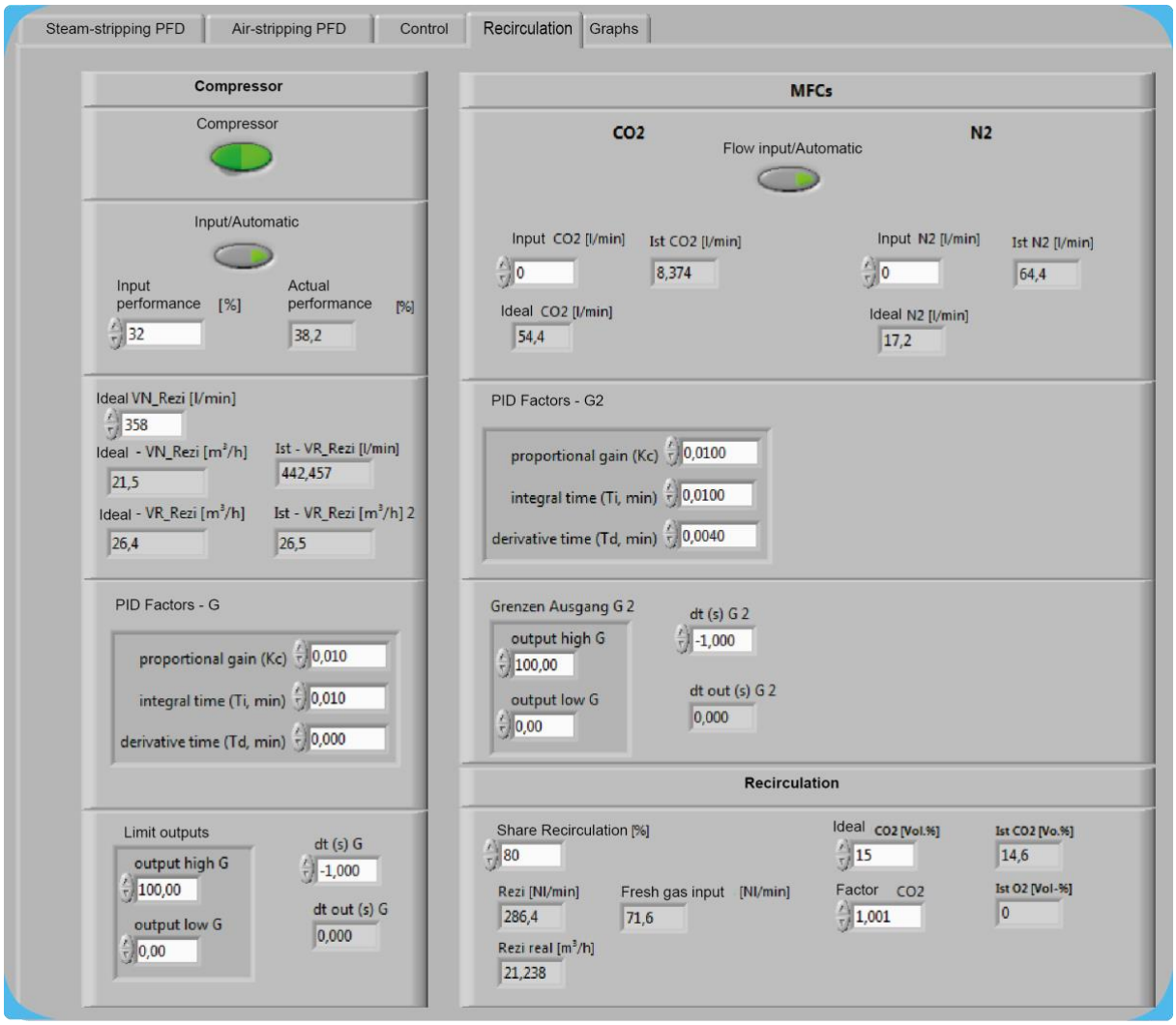

Figure 3-11: *Control interface in LabVIEW for gas composition and flow rate*

Once the pilot plant is fully operating, the LabVIEW application allows the user to appreciate the operation outputs in time-functioned plots, as depicted in Figure 3-12. The three graphs to the left, plot the CO_2 concentrations in the measuring points: Inflow and outflow of the absorption column. The middle three graphs display the temperature profiles in the absorber, stripper, and in the heat exchangers. The final two graphs to the right illustrate the pressure in particular points of the system and the volumetric liquid flows.

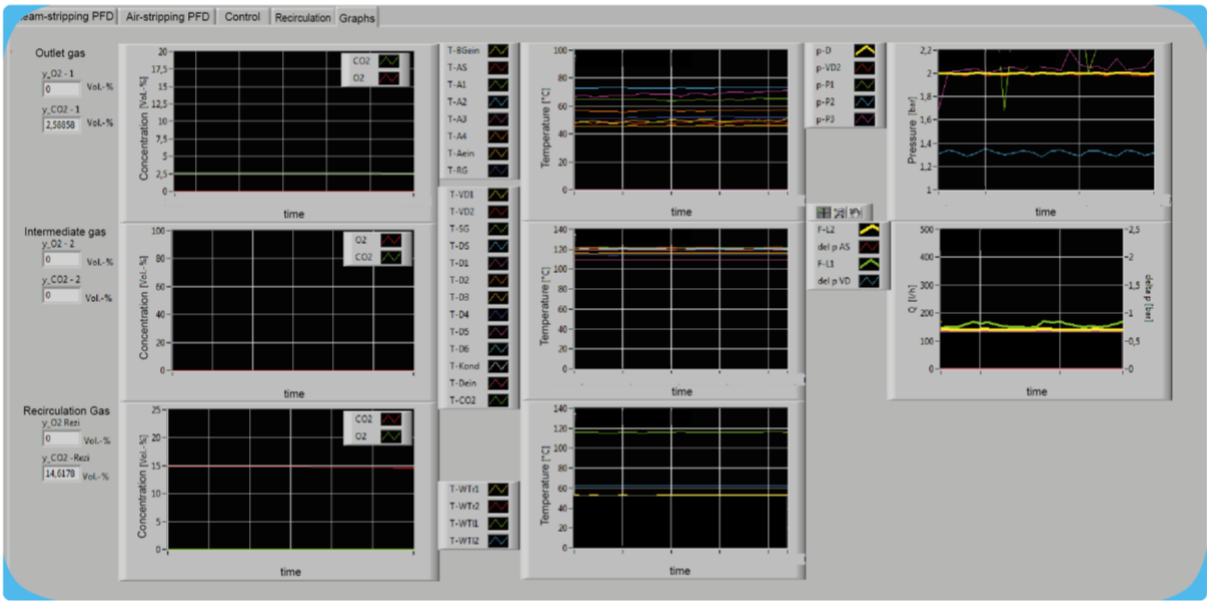

Figure 3-12: *Real-time plotting of measured variables LabVIEW interface*

Once all operation points are carried out, the data recoding must be stopped by pressing the “Stop“ button. A .txt file will be created containing all data from every available instrument/analyzer.

3.1.3.2 Manipulated and controlled variables

Besides monitoring process variables and parameters, LabVIEW allows the user to manipulate certain variables to control operation conditions. The control loops of the process are shown schematically in Figure 3-13.

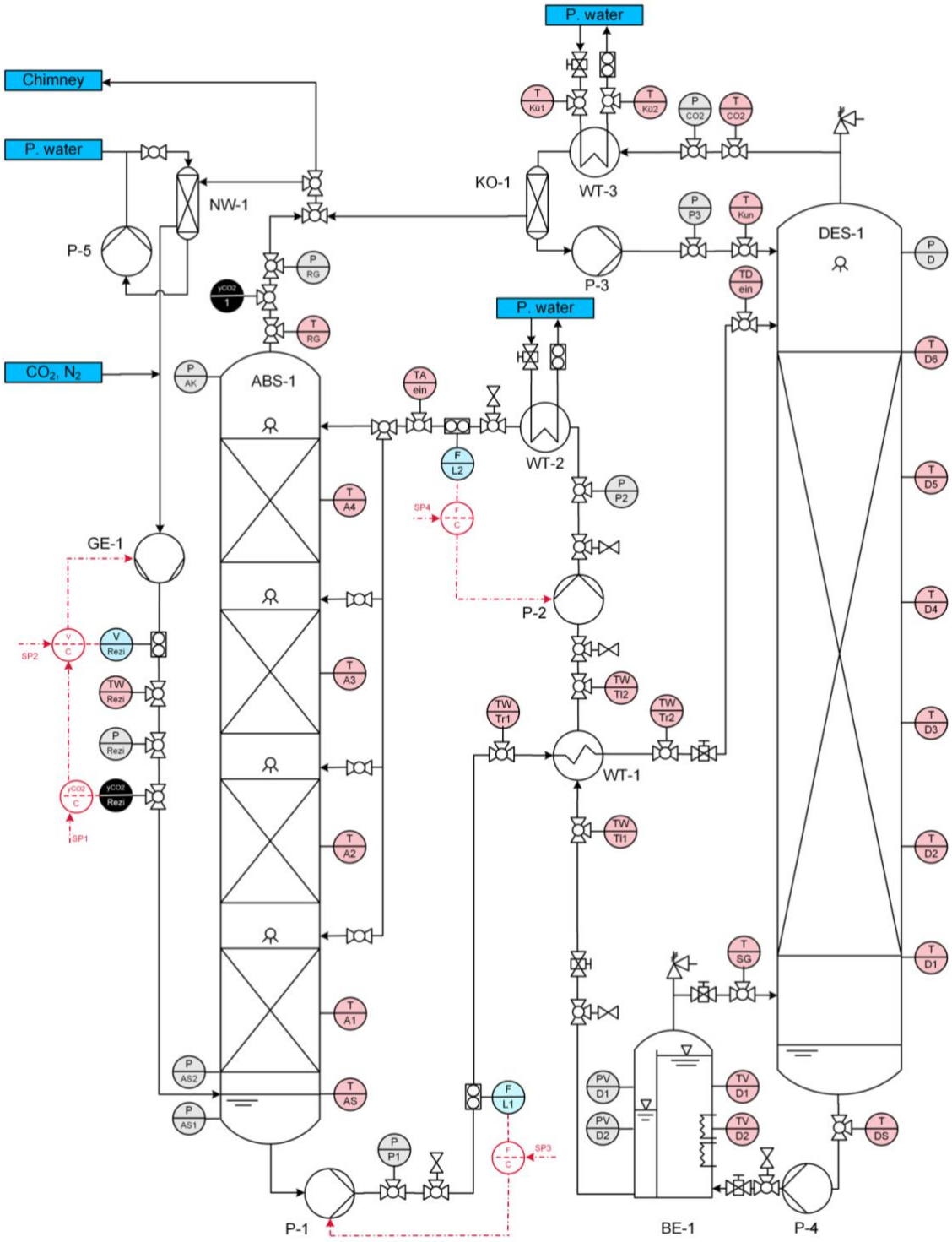

Figure 3-13: *Control loops in the ABIGAIL pilot plant*

The first control loop is composed by the flow meter after P-1 and P-1 itself. The process flow signal is processed in the controller, which compares it with the set point provided in the LabVIEW interface. Then, the signal is converted in pump performance and sent to P-1. The level of the absorber is not considered in the control loop. Hence, it must be adjusted manually when flooding.

A second control loop is aimed to control the volumetric flow of the solvent's inflow in the absorber by manipulating P-2. It operates the same way as the first loop, and neither the absorber's nor reboiler's level is included in the loop. To control them, manual adjustments on the pump's performance must be conducted.

The most complex loop pretends to control the volumetric gas flow to the absorber an its CO_2 concentration. It operates in a cascade mode, gathering initial concentration information from the gas analyzer in the recirculation stream. Then, the signal is compared with the concentration input provided by the user, and the amount of required CO_2 is calculated. Simultaneously, the flow meter placed after the compressor provides a second controller with the volumetric flow signal. The second controller emits a signal to finally adjust the compressor's setting to satisfy the concentration and flow requirements.

Other process variables must be changed manually. For instance, the inlet temperature of the absorber is modified by manipulating the utility water flor in WT-2; the stripper's pressure is controlled by manually adjusting the upper stage valve of the column, and the boil-up ratio is controlled by manually manipulating the reboiler's duty from the LabVIEW interface. A complete list of the measured variables and parameters in LabVIEW is summarized in Table 3-3.

Table 3-3: *Measured variables and parameters in LabVIEW*

Measured Parameter and units	Meaning
F-L2 [l/h]	Fresh solvent flow
F-L1[l/h]	Loaded solvent flow
FL ideal normal [l/h]	Desired solvent flow
FL Upper ideal [l/h]	Upper limit of solvent flow
FL Lower ideal[l/h]	lower limit of solvent flow
Psoll [kWh]	Reboiler's heat duty
T-Bgein [°C]	Absorber's gas input temperature
T-AS [°C]	Temperature at absorber's bottom stage
T-A1 [°C]	Temperature profile in absorber
T-A2 [°C]	Temperature profile in absorber
T-A3 [°C]	Temperature profile in absorber
T-A4 [°C]	Temperature profile in absorber
T-Aein [°C]	Absorber's liquid input temperature
T-RG [°C]	Absorber's top stage temperature
T-WTr1 [°C]	Loaded solvent input temperature
T-WTr2 [°C]	Loaded solvent output temperature
T-WTl1 [°C]	Lean solvent input temperature

T-WT2 [°C]	Lean solvent output temperature
T-VD1 [°C]	Top reboiler's stage temperature
T-VD2 [°C]	Bottom reboiler's stage temperature
T-SG [°C]	Stripper's gas recirculation temperature
T-DS [°C]	Stripper's bottom stage temperature
T-D1 [°C]	Temperature profile in stripper
T-D2 [°C]	Temperature profile in stripper
T-D3 [°C]	Temperature profile in stripper
T-D4 [°C]	Temperature profile in stripper
T-D5 [°C]	Temperature profile in stripper
T-D6 [°C]	Temperature profile in stripper
T-Kond [°C]	Condenser's temperature
T-Dein [°C]	Stripper's input temperature
TCO2 [°C]	Stripper's top stage temperature
p-Amb [bar]	Ambient pressure
p-Bgein [bar]	Gas inflow pressure in absorber
p-AS2 [bar]	Absorber's bottom stage pressure
p-AS1 [bar]	Absorber's bottom stage pressure
Delta p AS [bar]	Pressure drop in absorber's bottom stage
p-AK [bar]	Absorber's top stage pressure
p-RG [bar]	Absorber's top outflow pressure
p-CO2 [bar]	Stripper's top outflow pressure
p-P1 [bar]	P-1 output pressure
p-D [bar]	Stripper's top stage pressure
p-VD2 [bar]	Pressure in bottom of the tank
p-VD1 [bar]	Pressure in top of the tank
Delta p VD[bar]	Pressure drop in tank
p-P2 [bar]	P-2 output pressure
p-P3 [bar]	P-3 output pressure
y-CO2 1 [%v/v]	CO_2 concentration at absorber's gas outflow
y O2 1 [%v/v]	O_2 concentration at absorber's gas outflow
y-CO2 2 [%v/v]	CO_2 concentration at absorber's gas outflow 2
y -O2 2 [%v/v]	O_2 concentration at absorber's gas outflow 2
y-CO2 Rezi [%v/v]	CO_2 concentration at absorber's gas inflow
y - O2 Rezi [%v/v]	O_2 concentration at absorber's gas inflow
ideal CO2 (MFC)	Calculated amount of recirculated CO_2
real CO2 (MFC)	Real amount of recirculated CO_2
ideal N2 (MFC)	Calculated amount of recirculated N_2
real N2 (MFC)	Real amount of recirculated N_2
GS-TB	Level indicator in condenser
GS-AK	Overflow indicator in absorber
GS-AS	Level indicator in absorber
GS-VD-P	Level indicator in reboiler
GS-VD-HF	Overflow indicator in reboiler
Ideal P2 [l/h]	Desired solvent flow in P2
Ideal P1 [l/h]	Desired solvent flow in P1
p Recy [bar]	Pressure of the recycled gas

T Recy [°C]	Temperature of the recycled gas
V Recy [m^3/h]	Recycled gas volumetric flow
V Recy norm [m^3/h]	Recycled gas normal volumetric flow
% Comp. Performance	Compressor's energy performance
T-Cool 1	Inlet temperature of process water in WT-3
T-Cool 2	Outlet temperature of process water in WT-3
L/G real [l/m^3]	Computed Liquid to Gas ratio
L/G norm [l/m^3]	Computed normal Liquid to Gas ratio

3.1.3.3 Data export and processing

For data processing purposes, the .txt file containing the recorded data from LabVIEW is exported to a Microsoft® Excel for Mac 2016 sheet for further calculations. The first step in the data processing is the identification of each stationary state from the raw data. Once the time intervals of each stationary state (Or "Run") are fixed (k_{j0} and k_{jf}), an average value of every measured parameter is computed as follows:

$$\overline{Pa_j} = \frac{\sum_{t=k_{j0}}^{t=k_{jf}} Pa_k}{(j_f - j_0)} \qquad \textit{Eq. 3-1}$$

Pa_J: Measured parameter in j run

j: Run number

k: time

After computing the average values of the measured parameters for each run, the characteristic performance indicators for the absorption and desorption are calculated. Firstly, the liquid-to gas ratio (L/G) is considered at the process conditions:

$$\left.\frac{L}{G}\right]_j = \frac{\dot{V}_{L,abs,in}}{\dot{V}_{G,abs,in}} \qquad \textit{Eq. 3-2}$$

A schematic placement of the used symbols for each process stream could be found in Figure 3-5. The second absorption performance parameter is the percentage of absorbed CO_2, which could be determined with the experimental data in two different ways. On the one hand, it could be computed with the gas-phase data as stated in Equation 3-3. Later on this section, the percentage of absorption will be computed used only the liquid-phase experimental data:

$$\%Abs_{jG} = \frac{\left(x_{CO_2,abs,in}\right)\left(\dot{V}_{G,abs,in}\right)\left(\rho_{G,abs,in}\right) - \left(x_{CO_2,abs,out}\right)\left(\dot{V}_{G,abs,out}\right)\left(\rho_{G,abs,out}\right)}{\left(x_{CO_2,abs,in}\right)\left(\dot{V}_{G,abs,in}\right)\left(\rho_{G,abs,in}\right)} \quad \textit{Eq. 3-3}$$

Due to operational constrictions, it is not possible to measure the volumetric gas outflow of the absorber. Therefore, it is assumed that the gas flow through the absorption column is kept constant during the operation, hence:

$$\%Abs_{jG} = \frac{\left(x_{CO_2,abs,in}\right)\left(\rho_{G,abs,in}\right) - \left(x_{CO_2,abs,out}\right)\left(\rho_{G,abs,out}\right)}{\left(x_{CO_2,abs,in}\right)\left(\rho_{G,abs,in}\right)} \quad \textit{Eq. 3-4}$$

As the gas density stills highly dependent on the process temperature, its change must be considered. The CO_2 mass fraction is not measured during the operation, thus, the volume fractions must be converted to its corresponding mass fraction:

$$x_{CO_2} = y_{CO_2}\left(\frac{\rho_{CO_2}}{\rho_G}\right) \quad \textit{Eq. 3-5}$$

Assuming that the gas phase could be modeled with the ideal gas law:

$$x_{CO_2} = y_{CO_2}\left(\frac{\bar{M}_{CO_2}}{\bar{M}_G}\right) \quad \textit{Eq. 3-6}$$

The molecular weight of the gas is determined as follows, assuming nitrogen and CO_2 as the only components:

$$\bar{M}_G = \left(y_{CO_2}\right)\left(\bar{M}_{CO_2}\right) + \left(1 - y_{CO_2}\right)\left(\bar{M}_{N_2}\right) \quad \textit{Eq. 3-7}$$

The experimental determination of the MEA samples provides two relevant results for the data analysis. On the one hand, the CO_2 load (α) of the samples is determined [gCO_2/gSolvent]; on the other hand, the MEA mass fraction is also measured. Using the CO_2 load, it is also possible to compute a percentage of absorbed CO_2 based on the liquid-phase measured values. It could be calculated by following Equation 3-9:

$$\%Abs_j = \frac{CO_2\ removed\ from\ the\ gas\ phase}{Initial\ CO_2} = \frac{CO_2\ integrated\ to\ the\ liquid\ phase}{Initial\ CO_2} \quad \textit{Eq. 3-8}$$

$$\%Abs_{jL} = \frac{\left(\alpha_{CO_2,abs,out}\right)\left(\dot{V}_{L,abs,out}\right)\left(\rho_{L,abs,out}\right) - \left(\alpha_{CO_2,abs,in}\right)\left(\dot{V}_{L,abs,in}\right)\left(\rho_{L,abs,in}\right)}{\left(x_{CO_2,abs,in}\right)\left(\dot{V}_{G,abs,in}\right)\left(\rho_{G,abs,in}\right) + \left(\alpha_{CO_2,abs,in}\right)\left(\dot{V}_{L,abs,in}\right)\left(\rho_{L,abs,in}\right)} \quad \textit{Eq. 3-9}$$

The absorption percentages calculated with equations 3-8 and 3-4 should be similar. However, the one computed with Equation 3-8 tends to be more precise, as the volumetric flow rate is a measured variable, and no constant flow assumption must be considered.

The percentage of MEA regeneration is a representative parameter of the stripper's performance. It is a ratio between the amount of regenerated MEA in the stripper and consumed MEA the absorption.

$$\%Des_j = \frac{(x_{MEA,des,out})(\dot{V}_{L,des,out})(\rho_{L,des,out}) - (x_{MEA,abs,out})(\dot{V}_{L,abs,out})(\rho_{L,abs,out})}{(x_{MEA,abs,in})(\dot{V}_{L,abs,in})(\rho_{L,abs,in}) - (x_{MEA,abs,out})(\dot{V}_{L,abs,out})(\rho_{L,abs,out})} \quad \textit{Eq.3-10}$$

Eq. 3-10 has a limitation, as the volumetric flow going out of the stripper ($V_{L,des,out}$) is not experimentally measured. Therefore, it is assumed that its value is equal to the amount of recirculated solvent ($V_{L,abs,in}$).

3.1.4 Experimental analysis of MEA Samples

The experimental determination of the CO_2 load and the MEA concentration is conducted via potentiometric titration of the samples. The method is essentially based in the reaction between MEA and a strong acid, HCl. It starts with the determination of the CO_2 loading in the solvent ($\square_{CO2}$), which measures the mass content of CO_2 per gram of solvent [gCO_2/gSolvent]. During the first experimental campaign, two samples (One at the absorber's inlet –so called lean sample, and the other one at its outlet –so called rich sample) were taken in every run. An additional outlet valve was installed for the second experimental campaign at the outflow of the stripper (so called regenerated sample). Therefore, three solvent samples were taken during the last set of operations.

To determine the CO_2 loading, approximate 10g of the sample (m_{sample}) are mixed with an excess (Approx. 15.0 ml) of HCl solution 5.0 M (m_{HCl}). Consequently, the CO_2 is stripped from the sample as shown in Equation 3-11:

$$MEACOO^- + HCl \rightarrow MEA++ Cl^- + CO_{2(g)} \quad \textit{Eq.3-11}$$

Once the CO_2 is removed from the sample, its weight is determined again (m_{final}). The corresponding mass of CO_2 would be approximate the mass difference between the final mass and the mass of the sample plus the HCl mass:

$$m_{CO_2\ j} = m_{sample\ j} + m_{HCl\ j} - m_{final\ j} \quad \textit{Eq.3-12}$$

The mass of the CO_2-free solvent ($m_{solvent}$) could also be computed as follows:

$$m_{solvent\ j} = m_{sample\ j} - m_{CO_2\ j} \quad \textit{Eq.3-13}$$

Finally, the CO_2 load could be determined with the measured values as shown in equation 3-14:

$$\alpha_{CO_2\ j} = \frac{m_{CO_2\ j}}{m_{solvent\ j}} \quad \textit{Eq.3-14}$$

After the CO_2 loading is computed, the MEA concentration of every sample is determined by following a double-equivalence point automatic titration of the sample with HCl 1.0 [90]. Firstly, 5.0g of the sample are weighted and mixed with approximately 15.0 ml of a 5M HCl solution, the CO_2 is subsequently stripped as shown in Eq. 3-11. Moreover, the present carbamate is reduced back to MEA (Also Eq. 3-11), and the remaining MEA reacts with the excess of acid to produce the protonated $MEAH^+$, as displayed in Equation 3-15. This comprises the first preparation stage of the procedure:

$$MEA + HCl \rightarrow MEAH^+ + Cl^- \quad \textit{Eq.3-15}$$

To carry out the automatic titration, the excess HCl, along with the total $MEAH^+$ must be neutralized with a 50.0% w/w solution of KOH. Around 10.0 ml of the solution are added to the sample until a 13.0 pH is reached. The neutralization process is described by Equations 3-16 and 3-17, and corresponds to the second preparation stage of the procedure:

$$MEAH^+ + KOH \rightarrow MEA + H_2O + K^+ \quad \textit{Eq.3-16}$$

$$HCl + KOH \rightarrow H_2O + KCl \quad \textit{Eq.3-17}$$

Once the pH is around 13.0, the sample is submitted to an automatic titration with a 1.0M HCl solution. The first equivalence point indicates the required amount of HCl to neutralize the excess of KOH. The second equivalence point reveals the total amount of HCl needed to neutralize both, the KOH and the MEA. Hence, the difference between these two volumes is proportional to the content of MEA in the sample. Equations 3-15 and 3-17 describe this third stage. A summary of the double equivalence point is depicted in Figure 3-14:

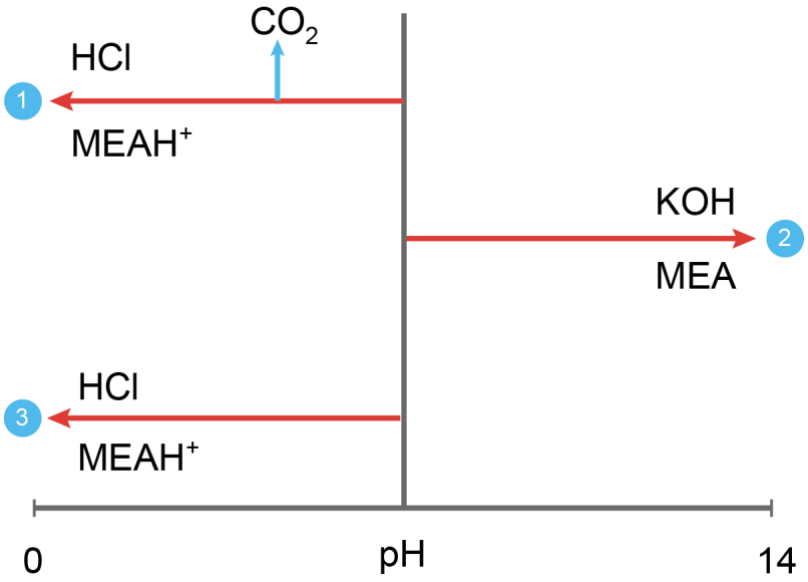

Figure 3-14: *Schematic representation of the double equivalence point titration*

Figure 3-15 presents an example of an obtained titration curve for the lean sample from the run 134. Both equivalence points are clearly visible. The remaining titration curves for the rest of the samples could be found in the digital annex.

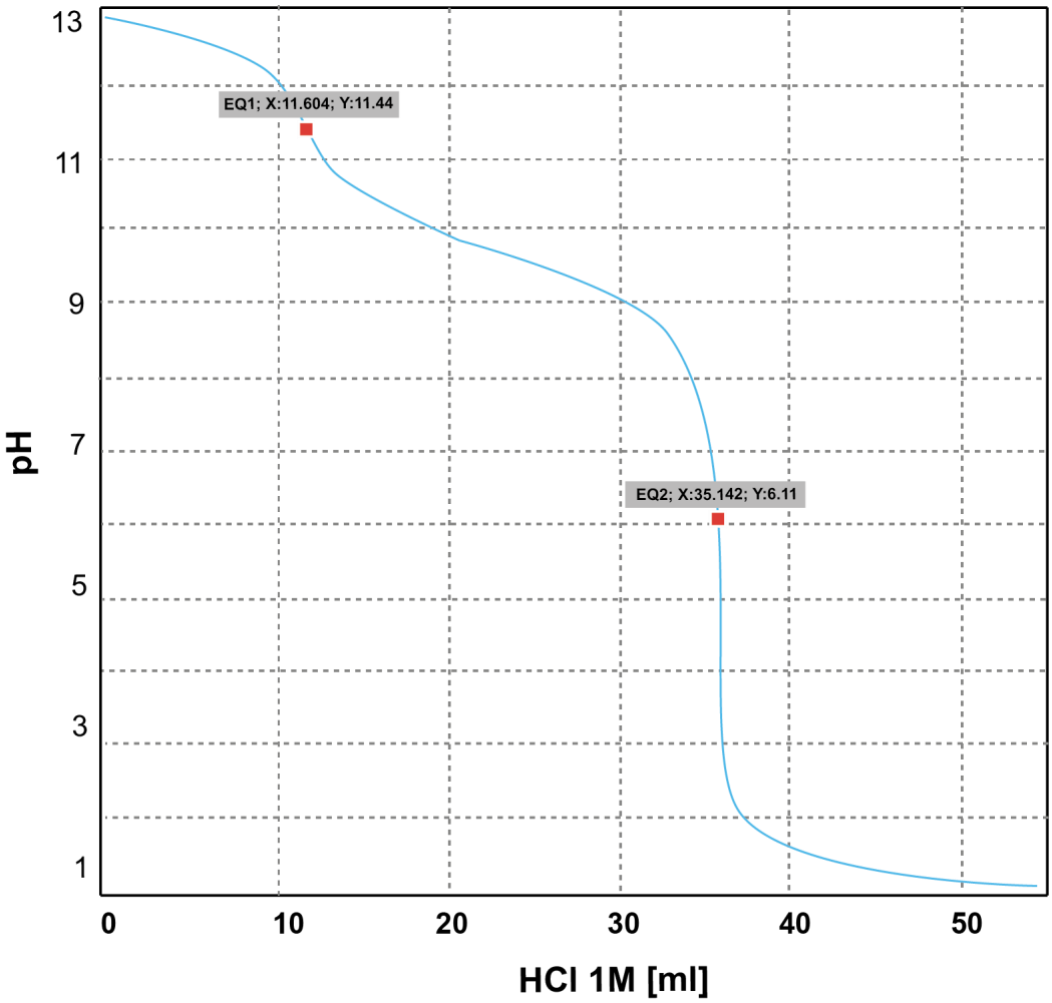

Figure 3-15: *Titration curve example of lean sample from run 134*

To determine the mass fraction of MEA in the solution, the CO_2-free mass of the solvent is computed with the previously calculated CO_2 load:

$$m_{solvent\ j} = m_{sample\ j}\left(1 - \alpha_{CO_2\ j}\right) \qquad \textit{Eq.3-18}$$

The total amount of MEA in the sample is determined with the difference between the equivalence volumes and the stoichiometry of the reaction shown in Eq. 3-15. The detail factor is presented in eq. 3-19:

$$x_{MEAT\ j} = \left(V_{2j} - V_{1j}\right)\left(\frac{1mol\ HCl}{1l\ sln.HCl}\right)\left(\frac{1l}{1000ml}\right)\left(\frac{1molMEA}{1molHCl}\right)\left(\frac{1}{m_{solvent\ j}}\right)\bar{M}_{MEA} \qquad \textit{Eq.3-19}$$

The amount of available MEA for each sample, which does not include the initially present loaded carbamate ($MEACOO^-$), could be determined by considering the stoichiometry of the reaction shown in Eq. 3-11. The final expression is illustrated in Eq. 20:

$$x_{MEA\,j} = \left[\frac{n_{MEAT\,j}\left(\alpha_{CO_2\,j}+1\right)\bar{M}_{CO_2} - \alpha_{CO_2\,j} m_{sample\,j}}{\left(\alpha_{CO_2\,j}+1\right)\bar{M}_{CO_2}}\right]\frac{\bar{M}_{MEA}}{m_{solvent\,j}} \qquad \textit{Eq.3-20}$$

The experimentally determined loads and compositions for every run are directly implemented on the calculations of section 3.1.3.3.

3.1.5 Summary of the conducted experiments

To summarize the methodology of the research project, a simplified Gantt diagram is shown in Figure 3-14. The methodology is split into two main procedures: The experimental and the simulation phase. The experimental part is composed by four main stages, including two experimental campaigns (Conducted on the 24.09.2018 and 11.10.2018 respectively), a preliminary operation of the pilot plant (03.07.2018), and the analysis of the solvent samples in the lab (30.10.2018).

The simulation phase is composed by three main stages, the basic simulation model, the sensibility and optimization, and the data analysis. Further details will be explained in section 3.2.1.

Figure 3-16: *Schematic Gantt diagram for the experimental campaigns and simulations*

The detailed operation conditions for every run is displayed in Table 3-4. A total of 19 runs were conducted over two measuring campaigns. Three different liquid to gas ratios, combined with three inlet absorber's temperatures and 2 stripper's pressures were studied in all possible combinations. As a remark, Table 3-4 displays just the "Ideal" value of each operation condition, the planned experimental values for each parameter are summarized in the Annex B. The first run of the project starts in 127, as a continuation of previous experimental campaign. The simulations were not based on the ideal values of Table 3-4, but in the real averaged values of Annex B for every run.

Table 3-4: *Summary of the operational conditions of each run for both experimental campaigns*

Experiment number	$T_{Abs,in}$ $[°C]$	p_{Des} $[bar]$	P_{Des} $[kW/l]$	y_{CO_2} $[\%v/v]$	$\dot{V}_G$ $[m^3/h]$	$\dot{V}_L$ $[l/h]$	L/G $[l/m^3]$
127	35	1,8	0,076	15	28,6	140	4,90
128	40	1,8	0,076	15	28,6	140	4,90
129	45	1,8	0,076	15	28,6	140	4,90
130	50	1,8	0,076	15	28,6	140	4,90
131	45	1,8	0,076	15	25,4	140	5,51
132	40	1,8	0,076	15	25,4	140	5,51
133	35	1,8	0,076	15	25,4	140	5,51
134	35	1,8	0,076	15	21,5	140	6,51
135	40	1,8	0,076	15	21,5	140	6,51
136	45	1,8	0,076	15	21,5	140	6,51
137	40	2,0	0,076	15	28,6	140	4,90
138	40	2,0	0,076	15	25,4	140	5,51
139	40	2,0	0,076	15	21,5	140	6,51
140	45	2,0	0,076	15	21,5	140	6,51
141	45	2,0	0,076	15	25,4	140	5,51
142	45	2,0	0,076	15	28,6	140	4,90
143	35	2,0	0,076	15	28,6	140	4,90
144	35	2,0	0,076	15	25,4	140	5,51
145	35	2,0	0,076	15	21,5	140	6,51

3.2 Simulation and optimization parameters with aspenONE Suite V8.6.

The following section is aimed to explain the procedures conducted to carry out every simulation step. Figure 3-15 complements Figure 2-9 by summarizing the aims and details regarding every stage of the simulation process. It differs from the Gantt representation of the simulation (Figure 3-14), as it is quite more specific. All stages were conducted in Aspen Plus® V8.6, and a part (HENS) of the fifth stage was carried out in Aspen Energy Analyzer™ V8.6.

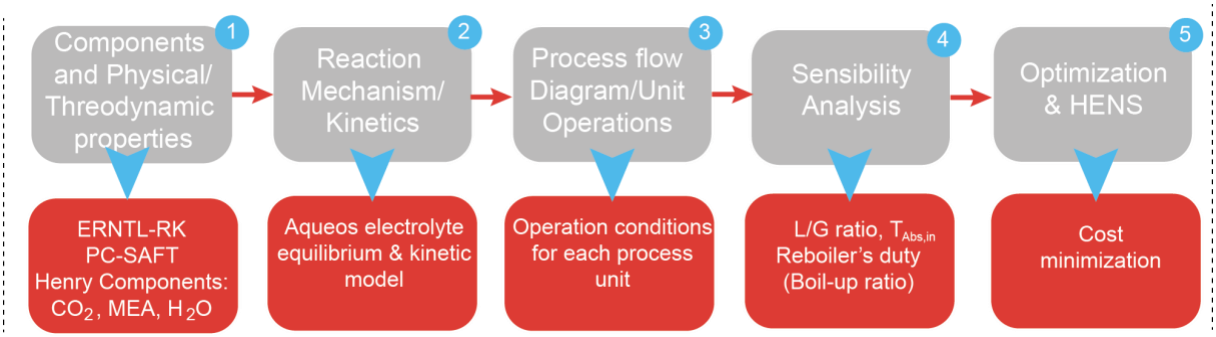

Figure 3-17: *Summarized procedure of the conducted simulations*

The detail inputs for every stage will be shown in the upcoming sections.

3.2.1. Simulation parameters with Aspen Plus® V8.6.

To consolidate a simulation in Aspen Plus® V8.6 several steps must be fulfilled: First, the property packages and components must be selected. Then, the reaction mechanisms and their kinetic parameters must be defined. Afterward, the flowsheet must be developed, featuring the operational conditions and the characteristic parameters of each operation unit. Finally, once the simulation converges, a sensibility analysis could be conducted to identify the most influencing variables in the overall performance of the CO_2 capture model. The mentioned steps comprise stages 1 to 4 in Figure 3-15.

3.2.1.1 Property packages and components

The following components were considered to represent the chemistry of the CO_2 capture process via chemical absorption with MEA when developing the model in Aspen Plus® V8.6:

Table 3-5: *Components used in the CO_2 capture model in Aspen Plus® V8.6*

ID	Type	Name	Formula
MEA	Conventional	Monoethanolamine	C_2H_7NO
H2O	Conventional	Water	H_2O
CO2	Conventional	Carbon Dioxide	CO_2
H3O+	Conventional	Hydron ion	H_3O^+
OH-	Conventional	Hydroxide ion	OH^-
HCO3-	Conventional	Bicarbonate ion	HCO_3^-
CO3-2	Conventional	Carbonate ion	CO_3^{-2}
MEAH+	Conventional	Monoethanolamine ion	$C_2H_8NO^+$
MEACOO-	Conventional	Carbamate ion	$C_3H_6NO_3^-$
N2	Conventional	Nitrogen	N_2
O2	Conventional	Oxygen	O_2
CO	Conventional	Carbon monoxide	CO

The unsymetric electrolyte NRTL equation property method (ENRTL-RK) and PC-SAFT equation of state are used to compute liquid and vapor properties. CO_2 and N_2 are selected as solutes or “Henry components” to which Henry’s law is applied. Henry constants are specified for this components with water and MEA as solvents. The parameters are already integrated in the property package once the Henry compounds are selected.

3.2.1.2 Reaction mechanism

As explained in section 2.1.2.2, a reaction mechanism fully comprised by 5 equilibrium reactions was used to model the electrolyte chemistry. In the simulation, this reaction mechanism is identified with CHEMISTRY ID = MEA. It is used as the global electrolyte calculation option. Hence, it is specified on the “Global” sheet of the Properties/Specification form.

CHEMISTRY ID = MEA

$$MEAH^+ + H_2O \leftrightarrow MEA + H_3O^+ \quad \textit{Eq. 3-21}$$

$$MEACOO^- + H_2O \leftrightarrow MEA + HCO_3^- \quad \textit{Eq. 3-22}$$

$$CO_2 + 2H_2O \leftrightarrow HCO_3^- + H_3O^+ \quad \textit{Eq. 3-23}$$

$$HCO_3^- + H_2O \leftrightarrow CO_3^{2-} + H_3O^+ \quad \textit{Eq. 3-24}$$

$$2H_2O \leftrightarrow OH^- + H_3O^+ \quad \textit{Eq. 3-25}$$

In addition, two reaction models called Absorber (Used in the absorber, 30-80ºC) and Stripper (Used in the stripper, 80-120ºC) were also created. In both reaction models, all reactions are assumed in chemical equilibrium except those of CO_2 with OH^- and CO_2 with MEA. Both models differ only in the kinetic parameters (Activation energy and kinetic constant) of the Eq. 3-21. The magnitude of the parameters in the stripper’s model is higher, making the reaction highly temperature dependent.

CHEMISTRY ID = Absorber/Stripper

$$MEAH^+ + H_2O \leftrightarrow MEA + H_3O^+ \quad \textit{Eq. 3-26}$$

$$HCO_3^- + H_2O \leftrightarrow CO_3^{2-} + H_3O^+ \quad \textit{Eq. 3-27}$$

$$2H_2O \leftrightarrow OH^- + H_3O^+ \quad \textit{Eq. 3-28}$$

$$CO_2 + OH^- \rightarrow HCO_3^- \quad \textit{Eq. 3-29}$$

$$HCO_3^- \rightarrow CO_2 + OH^- \quad \textit{Eq. 3-30}$$

$$MEA + CO_2 + H_2O \rightarrow MEACOO^- + H_3O^+ \quad \textit{Eq. 3-31}$$

$$MEACOO^- + H_3O^+ \rightarrow MEA + CO_2 + H_2O$$ *Eq. 3-32*

3.2.1.3 Parameters of each operation unit

Once the property packages and the reaction mechanism are set, the flow sheet must be established. It is composed by streams and unit operations. The input streams must be defined according to the operation conditions. Then, each operation unit must be specified with its corresponding dimensioning/design parameters. Two flow sheet arranges were developed on the frame of this project: On the one hand, a closed loop flow sheet for considering the effects of the recycles of the process. On the other hand, an open loop flow sheet to compare the performance of the absorption and desorption processes under different operational conditions with the experimental results. Figure 3-16 shows the developed closed loop flow sheet, featuring the names of every stream and unit operation

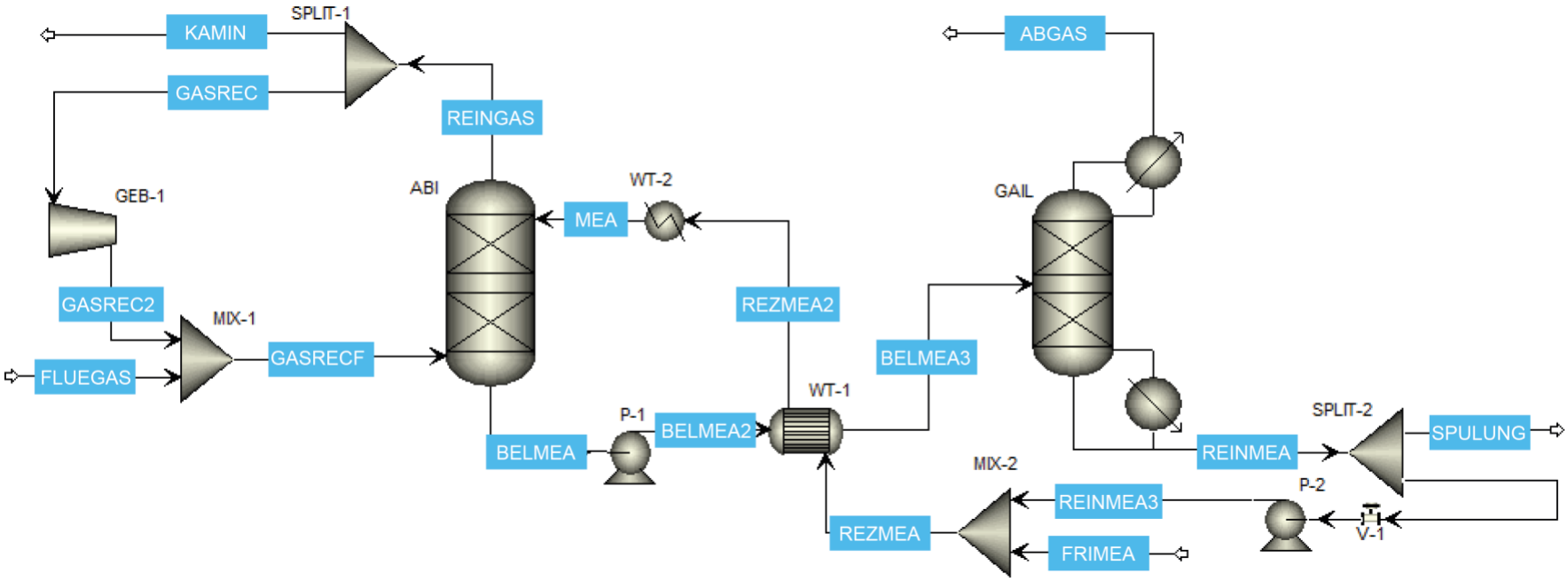

Figure 3-18: *Closed loop flow sheet in Aspen Plus® for simulation the CO_2 capture process*

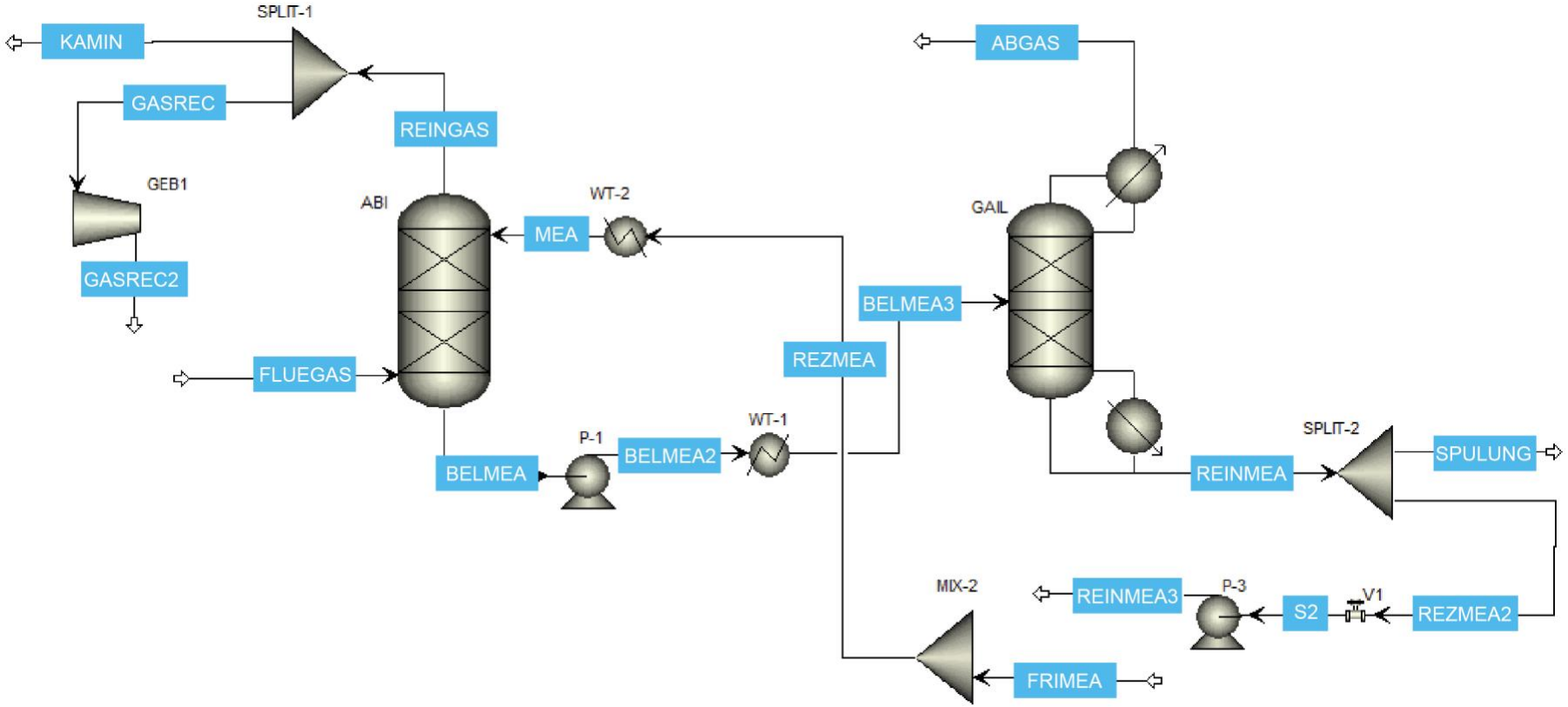

Figure 3-19: *Open loop flow sheet in Aspen Plus® for simulation the CO_2 capture process*

The closed loop flow sheet is composed by two columns (Radfracs), “ABI” and “GAIL”. The absorber (ABI) is fed by the stream “GASRECF” at the bottom stage, which is adjusted to satisfy the volumetric flow and CO_2 concentration at the absorber’s inlet by varying the CO_2 flow in the “FLUEGAS” stream. Therefore, the stream “FLUEGAS” must be adjusted for every operation point, and its initial input is required.

This is the First and Second design specifications of the process, which are specified in Aspen Plus® under the tab “Design specifications”. The gas recirculation in the absorber is set to 80% of the total outlet gas flow of the column. A compressor (GEB-1) is used in the simulation to ensure that the recycled gas “GASREC” has enough pressure to flow back inside “ABI”. The remaining 20% of the gas is directed to the chimney, “KAMIN”, in its German translation.

A Second inlet is needed for “ABI”: The solvent. It is done through the stream “MEA” in the top stage of the column. As the solvent is recirculated back to the absorber after the regeneration in the stripper, part of the MEA and water are removed during the stripping. Therefore, afresh-solvent stream “FRIMEA” is required to adjust the desired flow and MEA concentration at the input of the absorption column. This corresponds to the third adjustable process specification. The temperature of “MEA” is manually adjusted through the specifications of “WT-2”. The solvent is removed from the bottom stage of the absorber through the stream “BELMEA”, which is pumped through the main heat exchanger (WT-1) to be preheated with the high temperature regenerated solvent stream “REZMEA”.

The preheated solvent stream “BELMEA3” is fed to “GAIL” in the upper stage. The CO_2 desorption occurs throughout the column. The column is equipped with a top reflux system, which condenses part of the stripped gas to be recirculated back into the column. In the operation, this is done as well. The non-condensed gas is emitted in the stream “ABGAS”. On the other hand, the tank-reboiler of the operation is simulated by a classic reboiler model in the column, which heats the outgoing solvent stream through an electric resistance, and recirculates the evaporated vapors back the stripper. Around 10% of the solvent must be removed from the system for convergence purposes (“SPULUNG”). In the operation, all the regenerated solvent is fed to the tank, where large amounts of the solvent make the concentration uniform again before recycling it back to the absorber.

As could be seen in Figure 3-16, the closed loop flow sheet does not completely match all devices in the P&ID of the ABIGAIL pilot plant, but it represents the most important

processes carried out in the operation. Annex C presents the detailed parameters for every operation unit of the open loop flow sheet. As there is no recirculation in the open loop scheme, GEB-1, P-2, V-1 and MIX-1 are not considered among the units as seen in Figure 3-19.

As the studied variables in the operation are limited, only changes of the input streams “FLUEGAS” and “FRIMEA”, along with the pressure of the stripper, its heat duty and the outlet temperature of WT-2 are considered for every operation point. The specification details of the input streams are shown in Annex D, along with the results of all process streams.

3.2.1.4. Solver settings

When defining the solver settings in Aspen Plus® V8.6, a general convergence input must be introduced along with the specific settings for the complex blocks, for instance the columns. The general convergence of the simulation followed a sequential modular method. The default converge methods for each scenario of the simulation are displayed in Table 3-5. Furthermore, the parameters for tear stream convergence and tearing sequencing are shown as well.

Table 3-6: *Solver settings and default convergence methods*

Default methods	
Tears	Wegstein
Single design spec.	Broyden
Multiple design specs	Broyden
Tear & design specs	Broyden
Optimization	SQP
Tear stream convergence parameters	
Tolerance	0.00001
Trace threshold	0.00002
Trace option	Cutoff
State	Pressure & enthalpy
Tearing and sequencing parameters	
Design spec nesting	Inside
User nesting	Outside
Variable weight	1
Loop weight	1

The settings shown in Table 3-6 were implemented for the solver of each column:

Table 3-7: *Solver settings and default convergence methods for the process columns*

Basic Convergence	
Algorithm	Standard
Maximum iterations	100
Methods	
Initialization method	Standard
Damping level	Medium
Liquid-liquid phase splitting method	Gibbs
Solids handling	Overall
Salt precipitation handling	Include

The solver general and block solver settings were chosen based on the recommendations of previous simulations in Aspen Plus® V8.6 of the CO_2 capture process with MEA solutions [32].

3.2.1.5. Sensibility Analysis

The sensibility analysis was carried out for both blocks: The absorber (ABI) and the stripper (GAIL). Its aim is to identify the most influencing variables for each subsystem; hence they could be further optimized. During the sensibility analysis, the absorption and desorption percentages are of great interest. The absorption and desorption percentages are computed according to the expressions presented in section 3.1.2. The studied variables and their corresponding ranges for analysis could be found in Table 3-8.

Table 3-8: *Studied variables and ranges during sensibility analysis*

Studied variable	**Range**
Inlet absorber's temperature	35 – 55ºC
L/G ratio in absorber	3.5 – 7.1
Pressure in stripper	1.7 – 2.1 bar
Reboiler's heat duty	8 – 15 kW

Furthermore, a quantifiable parameter is incorporated to numerically determine the most influencing variables in the process. It is named "Relative sensibility" and its definition is shown in Equation 3-33

$$Relative\ sensibility = \left|\frac{\Delta Output\ parameter}{\Delta Selected\ variable}\right| \qquad \textit{Eq. 3-33}$$

3.2.2 Parameters of the process optimization with Aspen Plus V8.6.

The utilities used for simulating the process are cooling process water (For WT-2, and the stripper's condenser), along with electrical energy (For the pumps, compressor, and reboiler).

Table 3-9: *Description of the implemented utilities for cost optimization*

Utility	Description	Cost
PROWATER	Process water used for cooling WT-2	0.0019 €/kg
REBOILER	Electric duty used to operate the reboiler of the stripping section	0.39 €/kg
CONDENS	Process water used for condensing the top stream of the stripper	0.0019 €/kg
PUMP	Electric duty used to operate Pumps	0.39 €/kg
PUMP2	Electric duty used to operate Compressor	0.39 €/kg
Lost MEA	Amount of lost MEA during the process	9.11€/kg

The main aim of the optimization is precisely to minimize the total operation cost associated to the utilities mentioned in Table 3-9. The objective function utilized in Aspen Plus® V8.6 is displayed in Equation 3-33:

$$min = \sum_{P=1}^{2} W_i €_i + \sum_{WT=1}^{2} \dot{V}_{H_2O_i} \rho_{H_2O} €_i + W_{i,GEB} €_i + \dot{V}_{L\,lost} \rho_L €_i \qquad \textit{Eq. 3-34}$$

The L/G ratio, along with the inlet absorber's temperature (T_{Abs}) and the stripper's pressure were selected as the manipulated variables to minimize the daily operational cost of the pilot plant. Two constrains were taken into account for the optimization: The percentage of absorption and desorption (Eq. 3-9 and 3-10) were kept over 90 and 60% respectively.

3.2.3 Parameters of the optimization of the heat-exchange network with Aspen Energy Analyzer™ V8.6.

The aim of using Aspen Energy Analyzer™ is to consider alternative configurations for the heat exchange network of the process. The following streams were considered for the semi-quantitative analysis: REINMEA, MEA, ABGAS, RECGAS, FLUEGAS. The required input of every stream in Aspen Energy Analyzer™ consists of the mass flow of each stream. Along with their temperatures and average calorific capacity. The detailed information for every selected stream could be found in the electronic annex.

4 Results and discussions

The following section presents the results and discussions of both experimental campaigns. Initially, the search for the stationary states during every measuring campaign is displayed to identify the time interval were the key measured parameters remain constant. Then, the temperature and concentration profiles throughout the column are shown. Afterwards, the absorption and stripping efficiency is analysed for every run, along with the MEA concentration and its CO_2 load. Finally, the general validation graphs compared all the simulated outputs with their corresponding measured variables. It Is worth to mention, that for every result, a contrast between the simulated and the measured values is always available.

4.1 First experimental campaign

The first experimental campaign was conducted on the 24.09.2018 with a total amount of 10 runs or different stationary states. The initial operation conditions were chosen based on the work of [40]. Every run is carried out at a constant reboiler's duty and pressure in the stripper. The varying parameters were the inlet absorber's temperature and the L/G ratio.

4.1.1 Stationary states

The dynamic profile for all the runs of the first experimental campaign is shown in Figure 4-1. It could be appreciated that the varying parameters of each run are displayed (Absorber's inlet temperature and gas volumetric flow, affecting the L/G ratio). Furthermore, the outlet CO_2 concentration is also shown. It is assumed that a stationary state is reached once the three above-mentioned parameters reach a plateau for over 3 minutes.

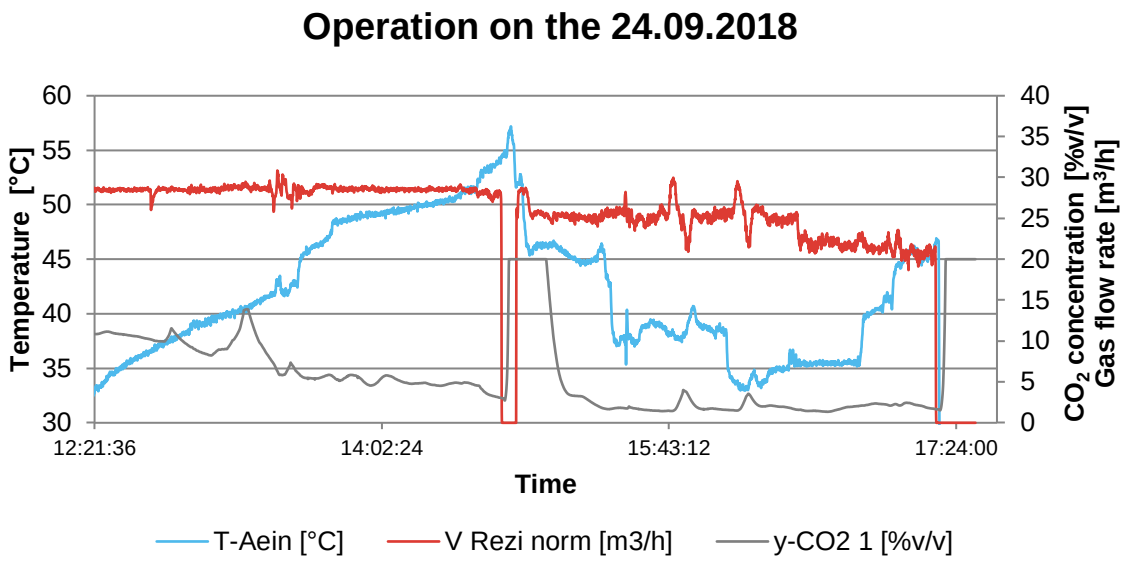

Figure 4-1: *Dynamic profile of the main process outputs during the first experimental campaign, 10.68 kW and 1.8 bar*

The time intervals for every run are presented in table 4-1. An average value of all measured parameters was then computer for each time frame.

Table 4-1: *Time intervals for every run during the first experimental campaign*

Run	Tabs (°C)	Pdes (bar)	Reboiler's duty (kW/l)	L/G	Initial Time	Final Time
127	35	1,8	0,076	4,90	12:29:01	12:33:56
128	40	1,8	0,076	4,90	13:05:01	13:08:31
129	45	1,8	0,076	4,90	13:34:16	13:39:11
130	50	1,8	0,076	4,90	14:20:36	14:27:46
131	45	1,8	0,076	5,51	15:12:01	15:20:11
132	40	1,8	0,076	5,51	15:34:06	15:41:31
133	35	1,8	0,076	5,51	16:19:01	16:23:31
134	35	1,8	0,076	6,51	16:33:01	16:43:41
135	40	1,8	0,076	6,51	16:53:46	16:56:51
136	45	1,8	0,076	6,51	17:10:51	17:14:01

4.1.2 Temperature profile throughout the columns

Figure 4-2 illustrated the temperature profile in the absorber for the first four runs (127 to 130). The specific conditions of each run are also displayed in the graph. The dotted lines represent the simulated data, whereas the squared-shaped data series correspond to the experimentally determined quantities. The error bars within the experimental series represent the minimum and maximum measured valued in each time interval.

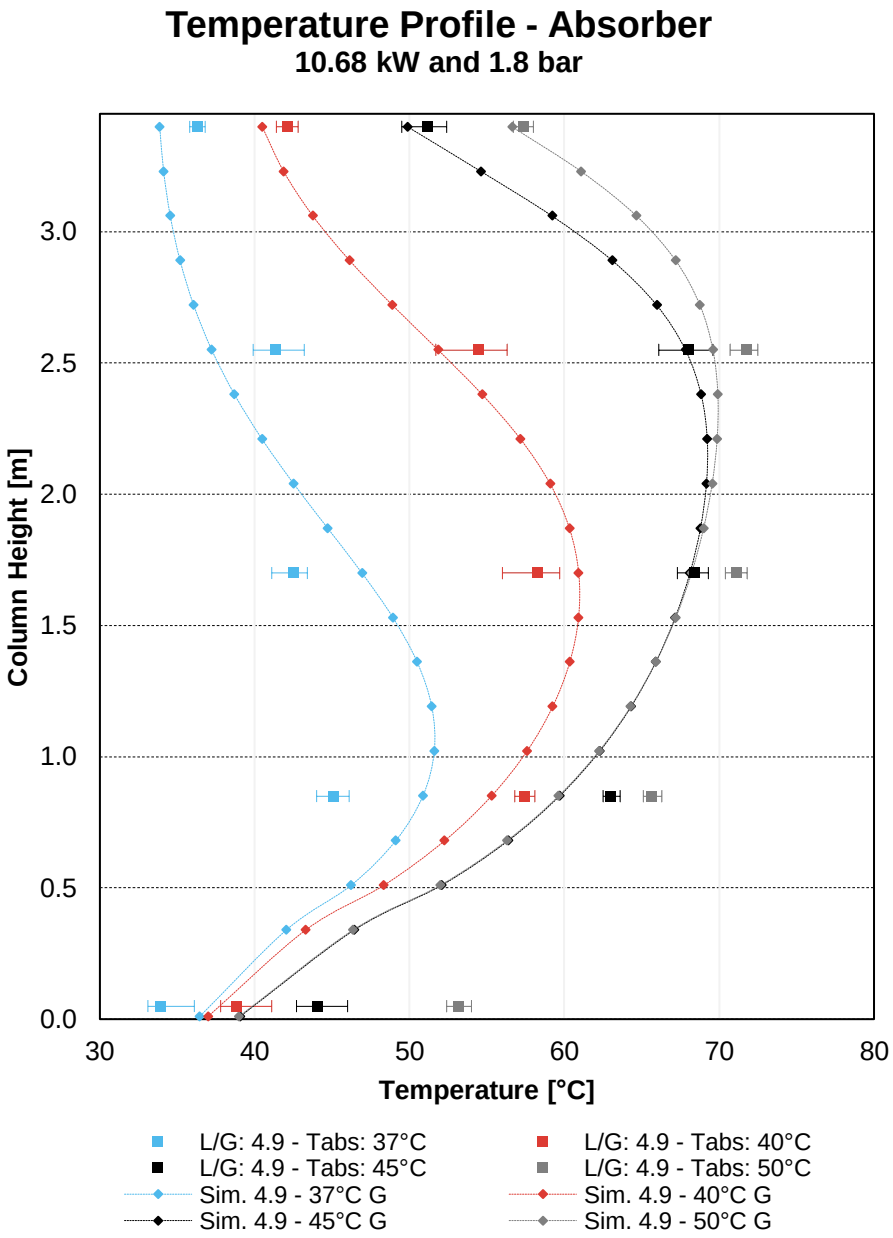

Figure 4-2: *Temperature profiles for runs 127 to 130 – Absorber*

In figure 4-2 it is clear that the simulated outputs match the trend of the experimental quantities for all runs. Slight deviations could be seen in the bottom of the column, especially for the run 130. It is also clear that the highest temperatures are reached somewhere in between the column's height, a possible explanation for this fact is the correlation with the reaction rate: Higher reaction rates release larger energy amounts. Hence, the temperature tends to increase in the points where the heat is released. Figure 4-2 also displays the effect of the inlet absorption temperature in the general development of the profile: The higher the inlet temperature, the upper the maximum temperature could be located in the column, as well as the higher its magnitude.

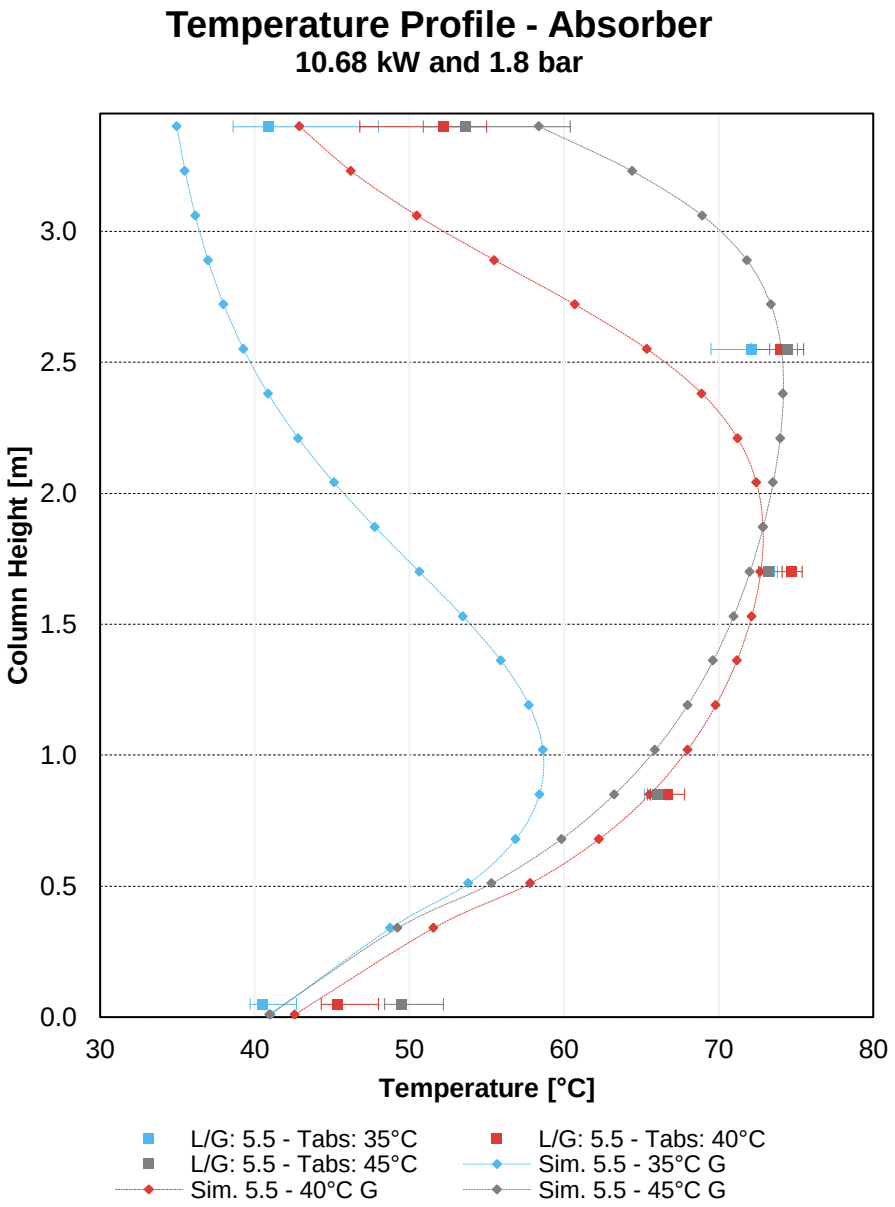

Figure 4-3: *Temperature profiles for runs 131 to 133 - Absorber*

Figure 4-3 presents the temperature profiles for the runs 131 to 133. The main difference with the respect to Figure 4-2 is the L/G ratio, which is higher for the case of Figure 4-3. In general, the maximum temperature in the column tends to increase for higher L/G ratios. As the gas volumetric flow is reduced to reach a L/G ratio of 5.5, the CO_2 amount is affected. Hence, less CO_2 could be solubilized in the solvent and reactions take place at a lower reaction rate. That is the case of L/G=5.5 and T_{abs} of 35ºC, where it is clear that the reactions did not take place at the same high rate for the simulation scenario.

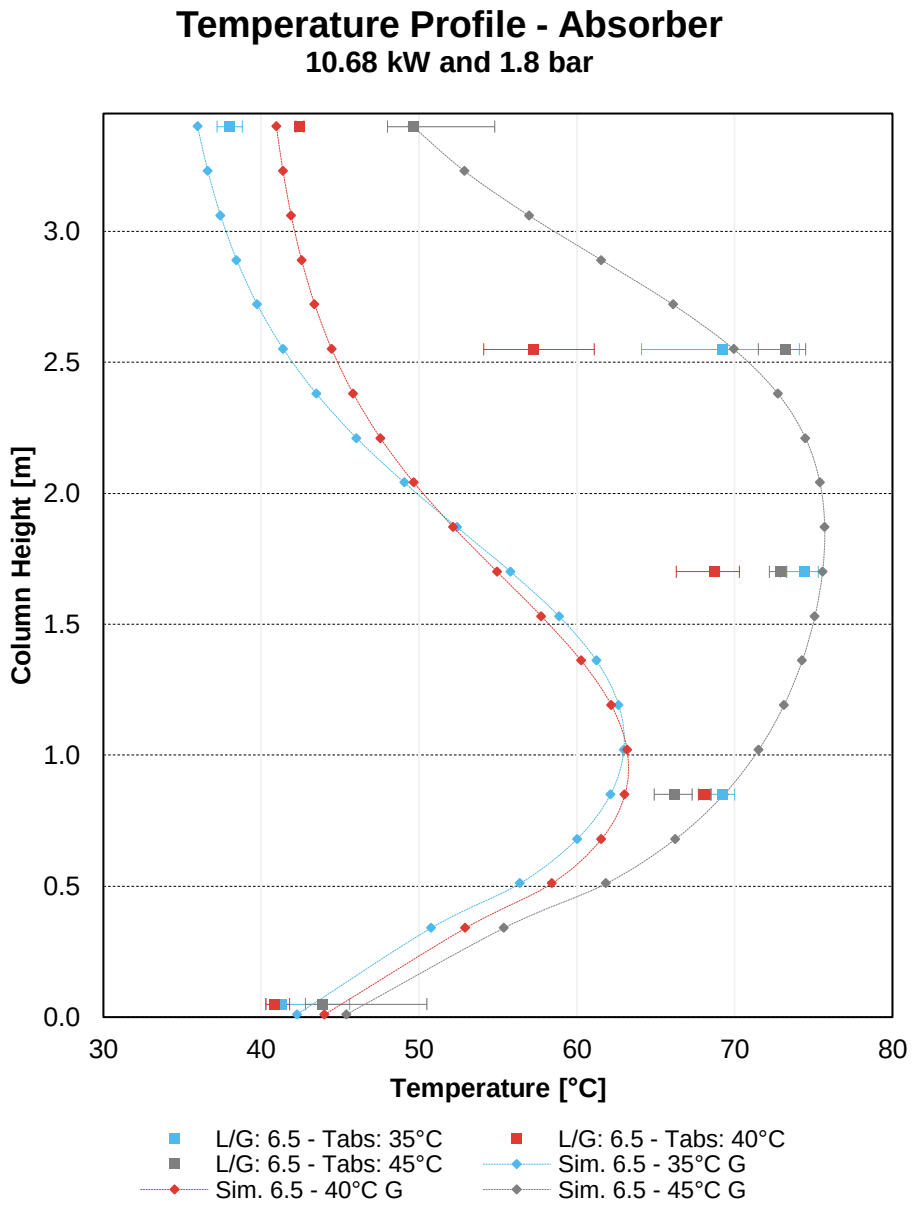

Figure 4-4: *Temperature profiles for runs 134 to 136 - Absorber*

Figure 4-4 presents the temperature profiles for the runs 134 to 136. The main difference with the respect to Figure 4-3 is the L/G ratio, which is higher for the case of Figure 4-4. In general, the maximum temperature in the column tends to increase for higher L/G ratios. The discrepancy between the simulated outputs and the measured values is greater for lower $T_{abs,in}$. Nevertheless, the general trend remains for both, experimental and simulated magnitudes.

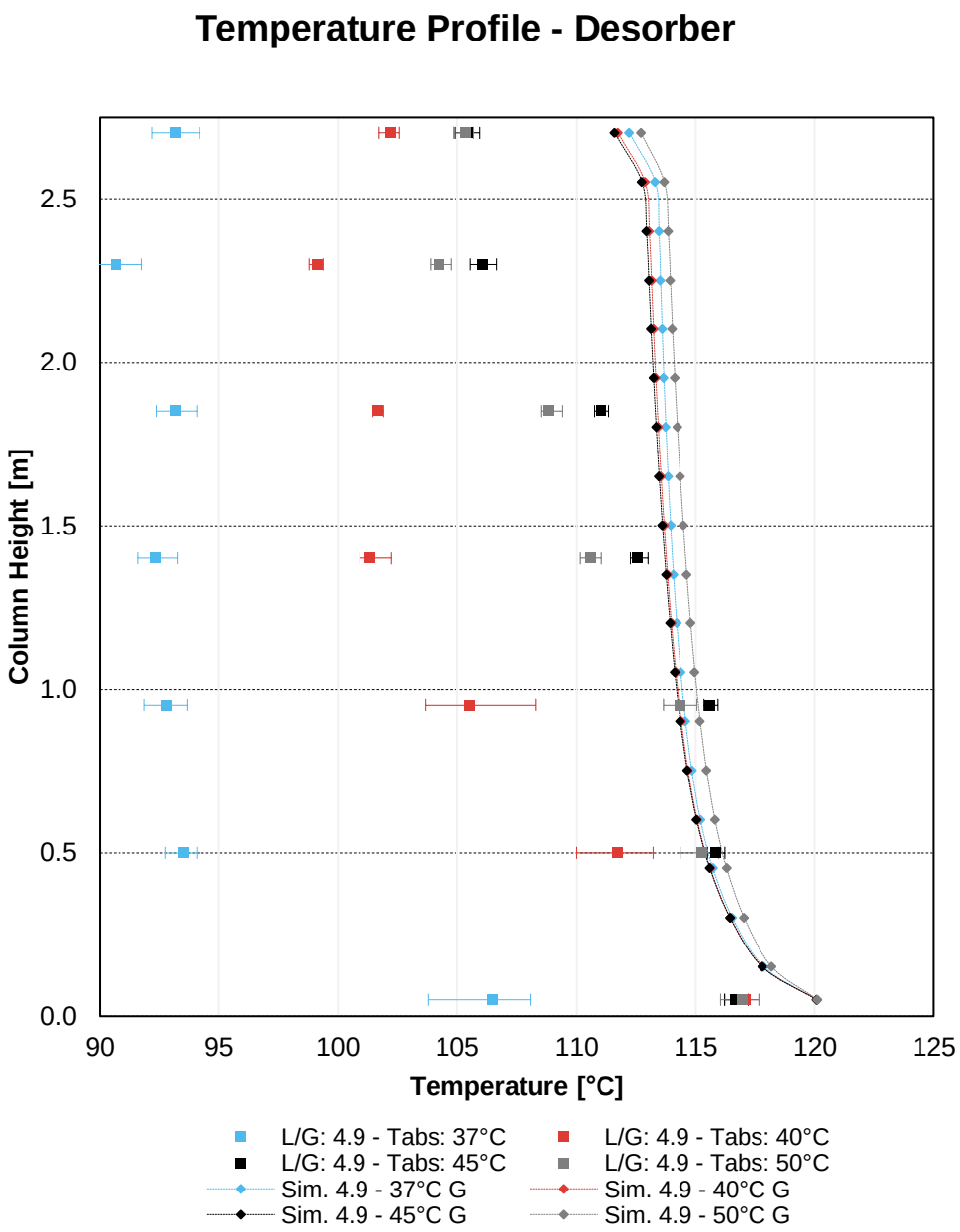

Figure 4-5: *Temperature profiles for runs 127 to 130 - Stripper*

On the other hand, the stripper's temperature profiles were also determined. Figure 4-5 shows the profiles for the runs 127 to 130. A clear discrepancy between the simulated outputs and the measured values is appreciated for the first four runs. A possible explanation for this fact is the warming-up process of the stripper: Once it reaches the corresponding temperature for a given operation pressure, it tends to stabilize. It is assumed that the stripper was warming up during the first two runs, hence, higher discrepancy is observed for those particular stationary states. The higher magnitude of the error bars of the first runs, precisely show the unstable state of the temperature in the stripper.

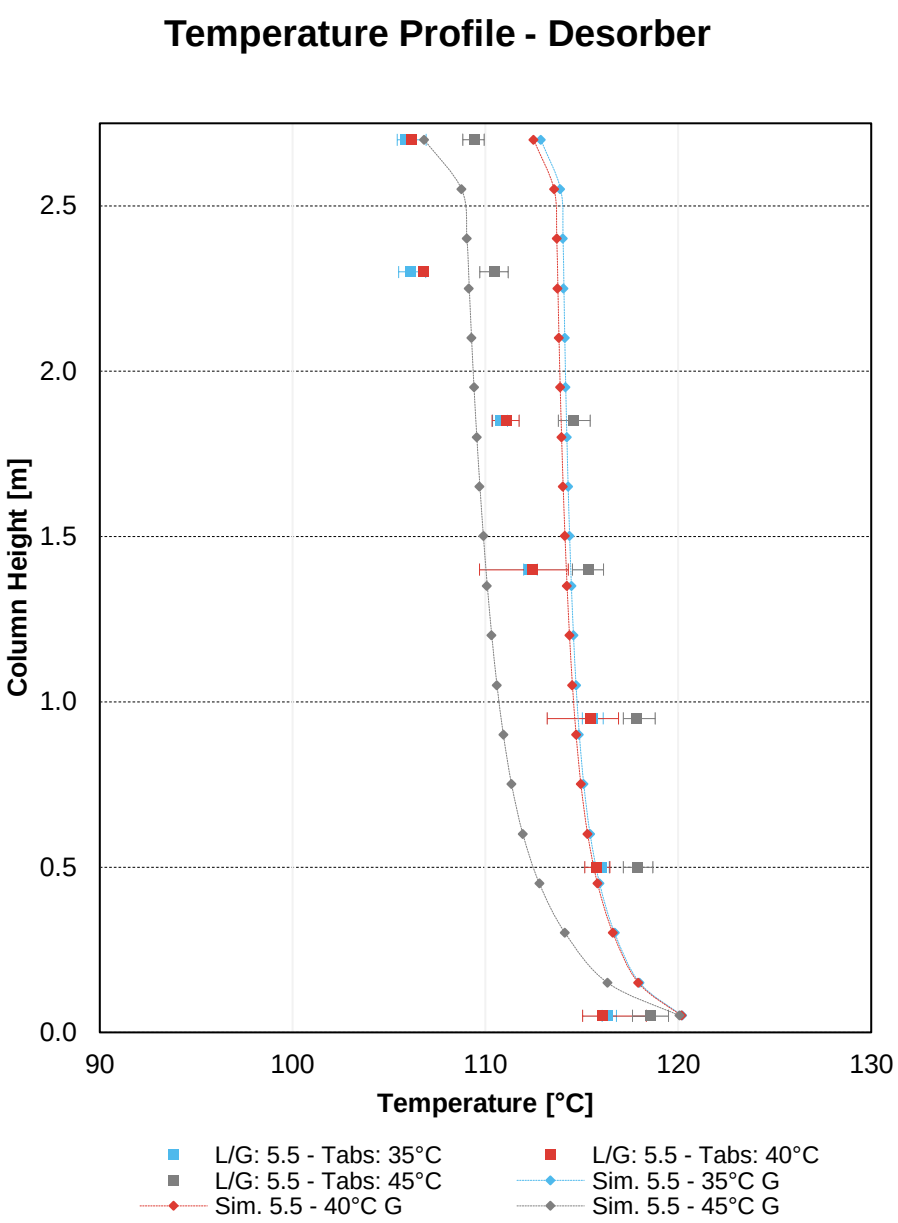

Figure 4-6: *Temperature profiles for runs 131 to 133 – Stripper*

Once the temperature in the stripper stabilizes, it becomes clear that the simulated outputs and the measured values match and tend to remain constant throughout the entire height of the column. The highest temperatures could be found in the vicinity of the reboiler. This behaviour could be appreciated in Figure 4-6. Furthermore, the inlet temperature of the absorber its L/G ratio present a minimum influence in the temperature profile of the stripper.

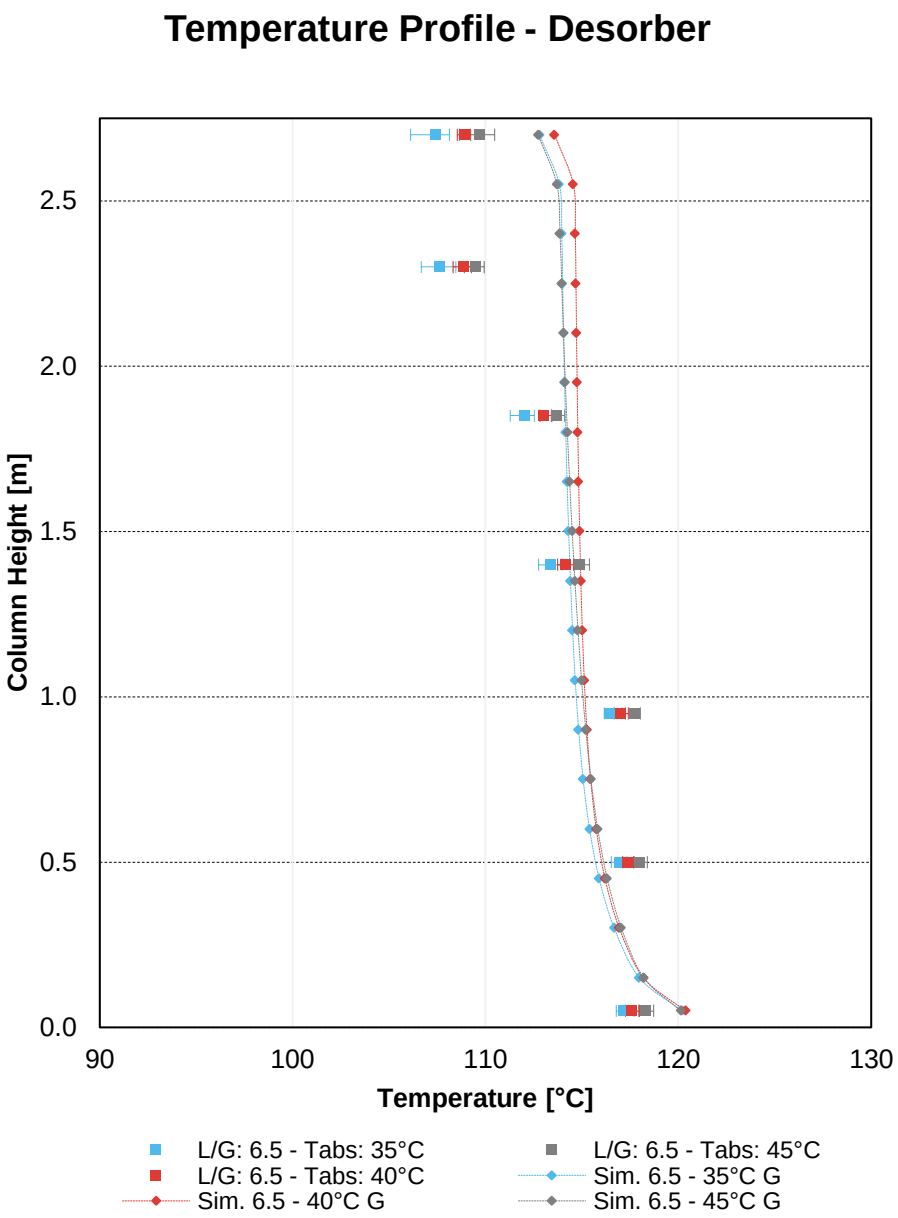

Figure 4-7: *Temperature profiles for runs 134 to 136 - Stripper*

Figure 4-7 is the perfect example of a fully-developed temperature profile in the stripper, as the simulated and experimental values match. However, the top-second temperature sensor clearly shows a deviation regarding to the general trend. The feed of the condensed reflux right at its height might explain such fact.

4.1.3 Concentration profiles throughout the columns

The concentration profiles throughout the columns will be shown in this section. Every graph represents only one run, as multiple concentration profiles are plotted in the same diagram.

For instance, in the absorber, the MEA concentration in the liquid phase, along with the loaded MEA (MEACOO-) and the CO_2 in the gas phase are displayed. On the other hand, the absorber's concentration profile also plots the CO_2 consumption reaction rate.

The concentration profiles for the stripper show the MEA concentration at every specific height of the column, along with the corresponding CO_2 concentration in the gas phase and the MEA regeneration reaction rate on a second horizontal axis. The aim of this profile is to qualitatively assess the desorption in the stripper.

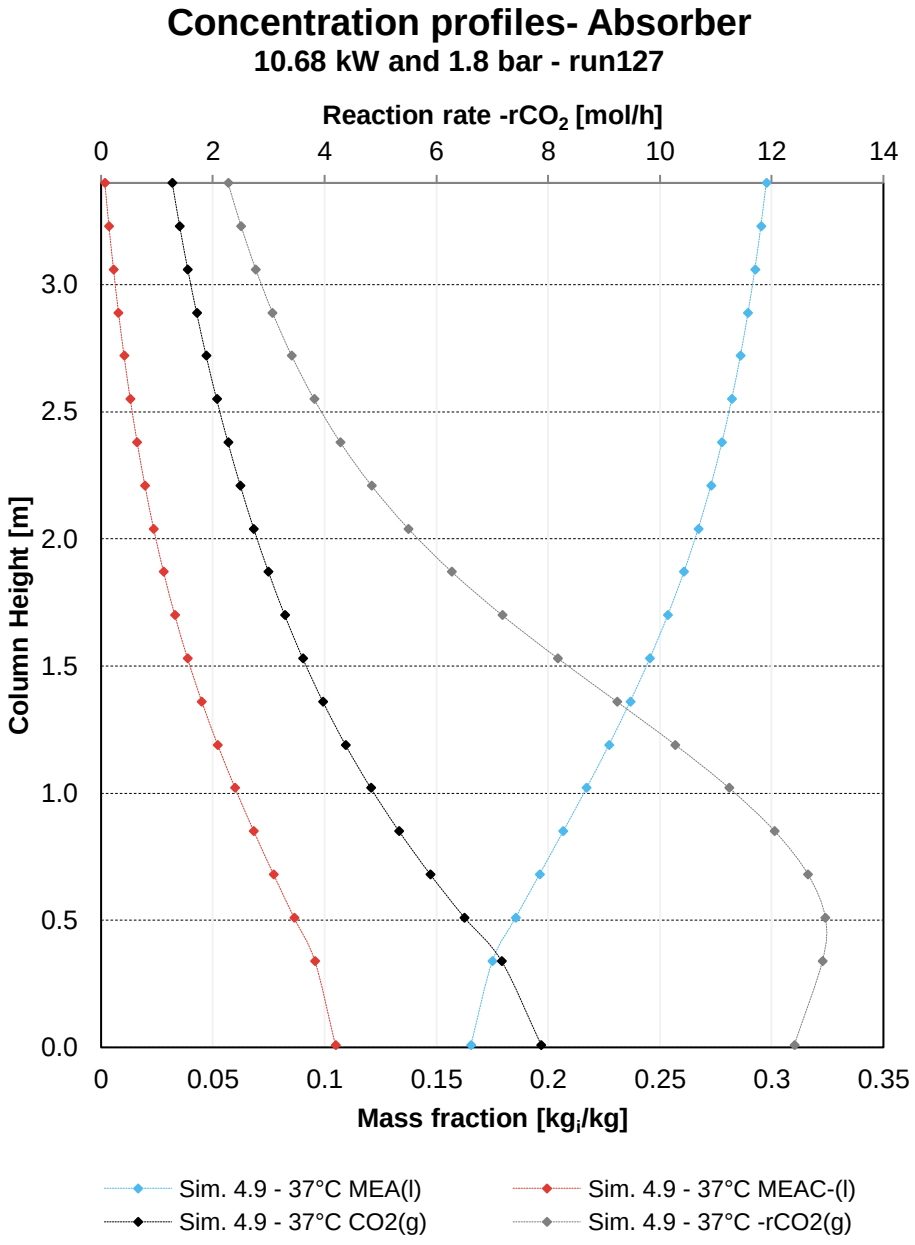

Figure 4-8: *Concentration and reaction rate profiles for run 127 – Absorber*

Figure 4-5 presents the concentration profiles in the absorber for the run 127. It is clear that the CO_2 reaction rate shows a maximum magnitude at a given column height, matching the trend of the temperature profile. The reaction rate is also a function of the CO_2 concentration, according to the rate law. Therefore, the maximum values could be found in the bottom of the column, where the dissolved CO_2 concentration is higher. On the one hand, a logical decreasing CO_2 and $MEACOO^-$ concentration as the top of the column is approached could be appreciated. On the other hand, a decreasing MEA concentration as the bottom of the column is approached was determined.

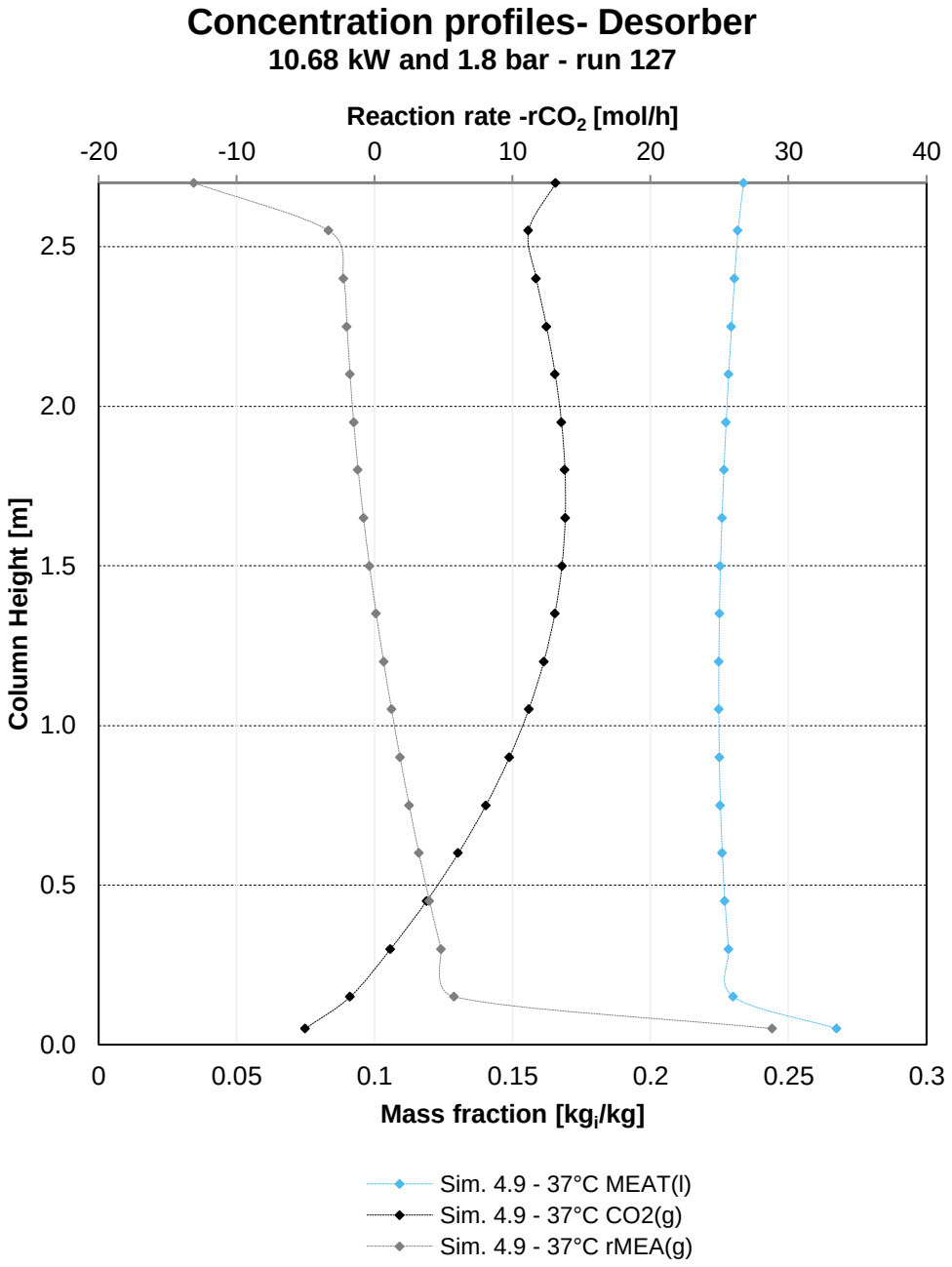

Figure 4-9: *Concentration and reaction rate profiles for run 127 – Absorber*

In the case of the stripper, the highest MEA regeneration rates could be found in the vicinity of the reboiler, where the temperature is at its maximum. Negative magnitudes of the reaction rate were found in the top stages of the stripper, as the temperature is low, along with the MEA concentration. The most considerable increase in the MEA concentration occurs also near the reboiler. The CO_2 concentration finds its maximum magnitude in an intermediate height of the column. Hence, the stripper's height might be over design. The remaining concentration profiles for every run could be found in the Annex E, they all present the same trends.

4.1.4 Abs- and desorption percentages

The definitions of the absorption and desorption percentages were defined in section 3. The results regarding the firs experimental campaign are shown in the following section. During the first experimental campaign it was not possible to determine the CO_2 load and MEA concentration of the solvent stream leaving the stripper. Thus, the desorption percentage could only be determined based on the simulation outputs.

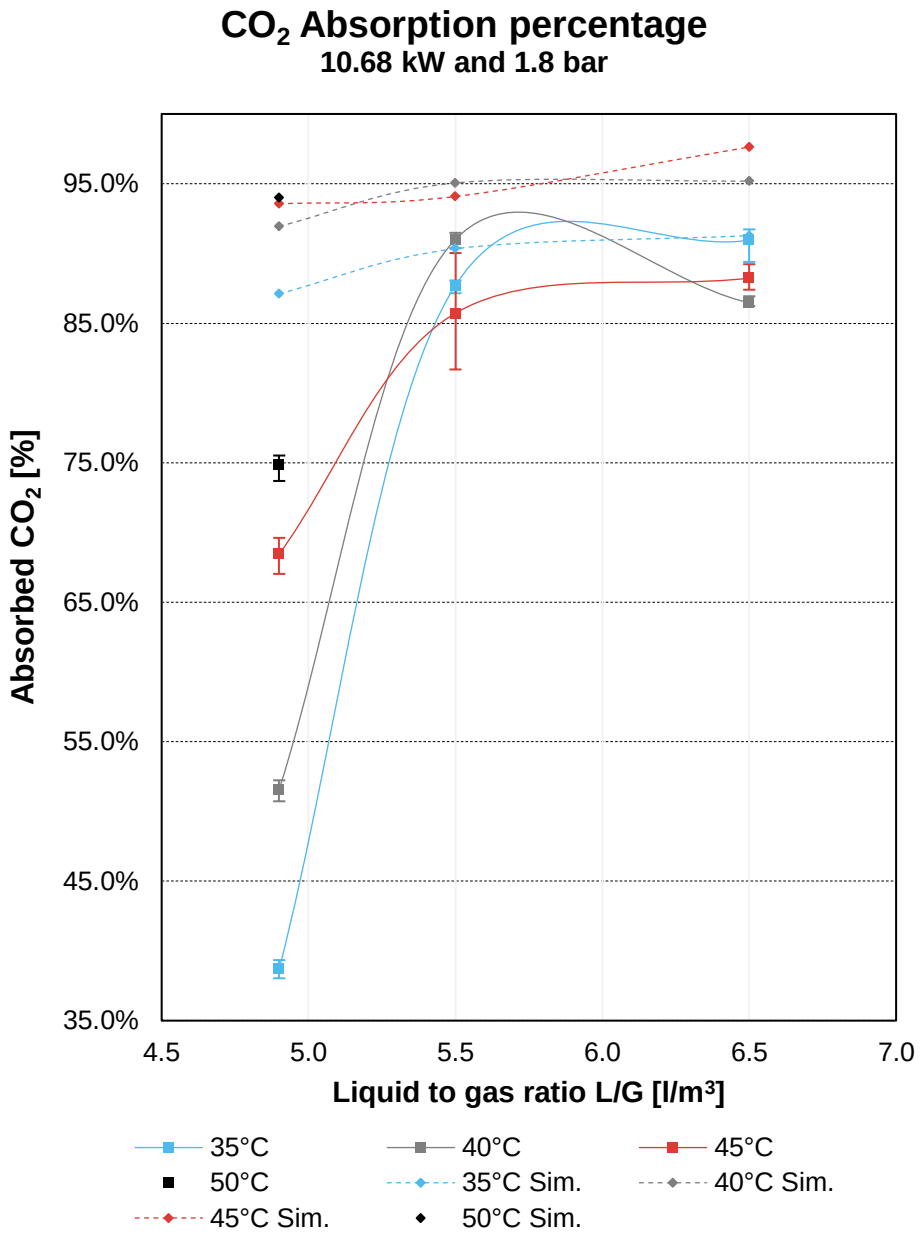

Figure 4-10: *CO_2 absorption percentage for runs 127 – 136*

Figure 4-10 presents the percentage amount of absorbed CO_2 for all the runs of the first experimental campaign. It is clear that the simulated outputs are most of the times above the measured values, and that major discrepancies are presented for low L/G rations. Hence, it is advisable to use the model at L/G ratios above 5 l/m^3. The high amounts of gas when operating with low L/G rations reach the solubility limit. Hence, absorption is limited and the flue gas leaves the column with high CO_2 concentrations.

Nevertheless, the percentages match the general trend: a plateau is reached after L/G = 5.5 l/m^3 for most of the absorber's inlet temperatures. CO_2 absorption percentage above 85% could be easily reached in the operation.

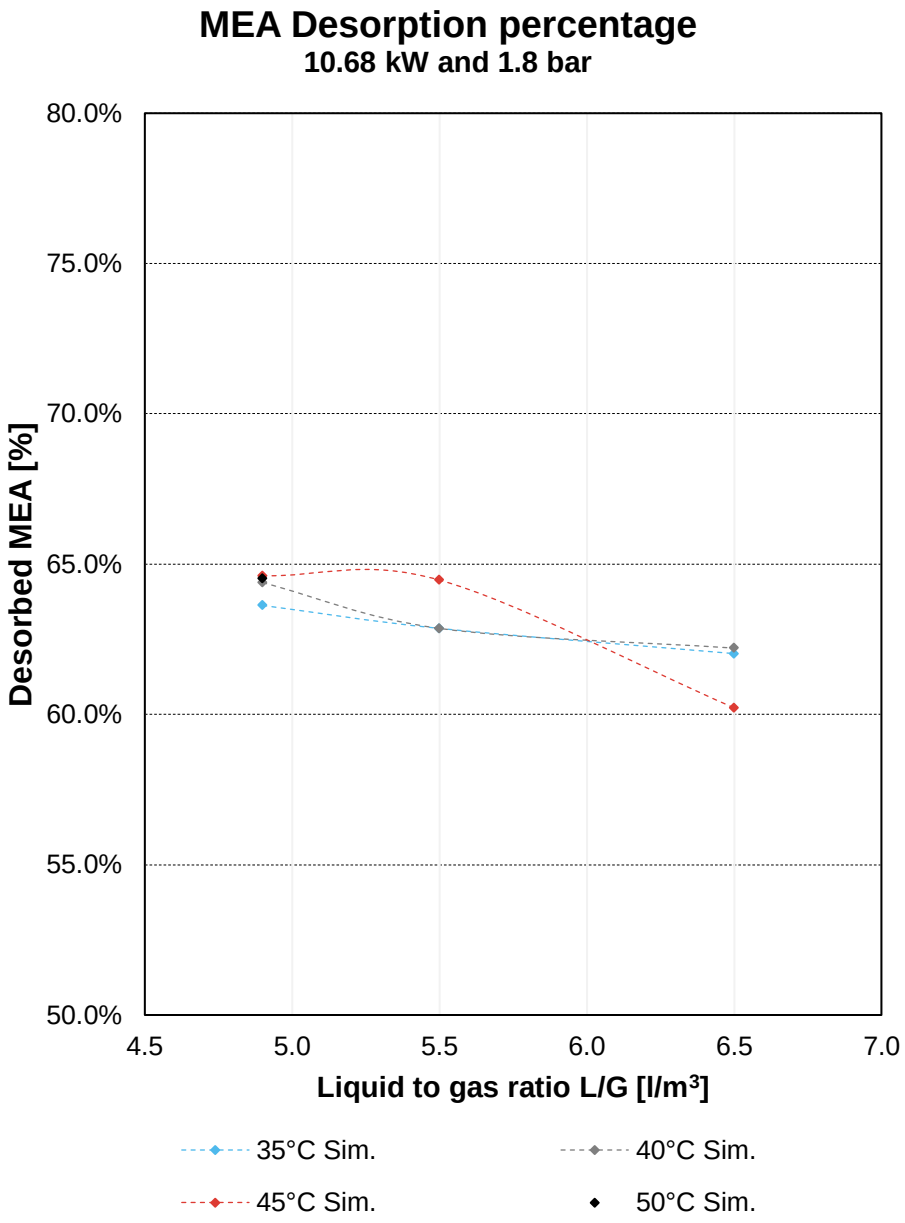

Figure 4-11: *MEA desorption percentage for runs 127 – 136*

Figure 4-11 shows exclusively the desorption percentages computed with the simulation outputs. It could be seen that the L/G ration and the absorber's inlet temperature have a minimum effect over the desorption. The general trend states that the desorption is favoured when the L/G ratio decreases. However, it is not as considerable as the effect of the L/G over the absorption percentage.

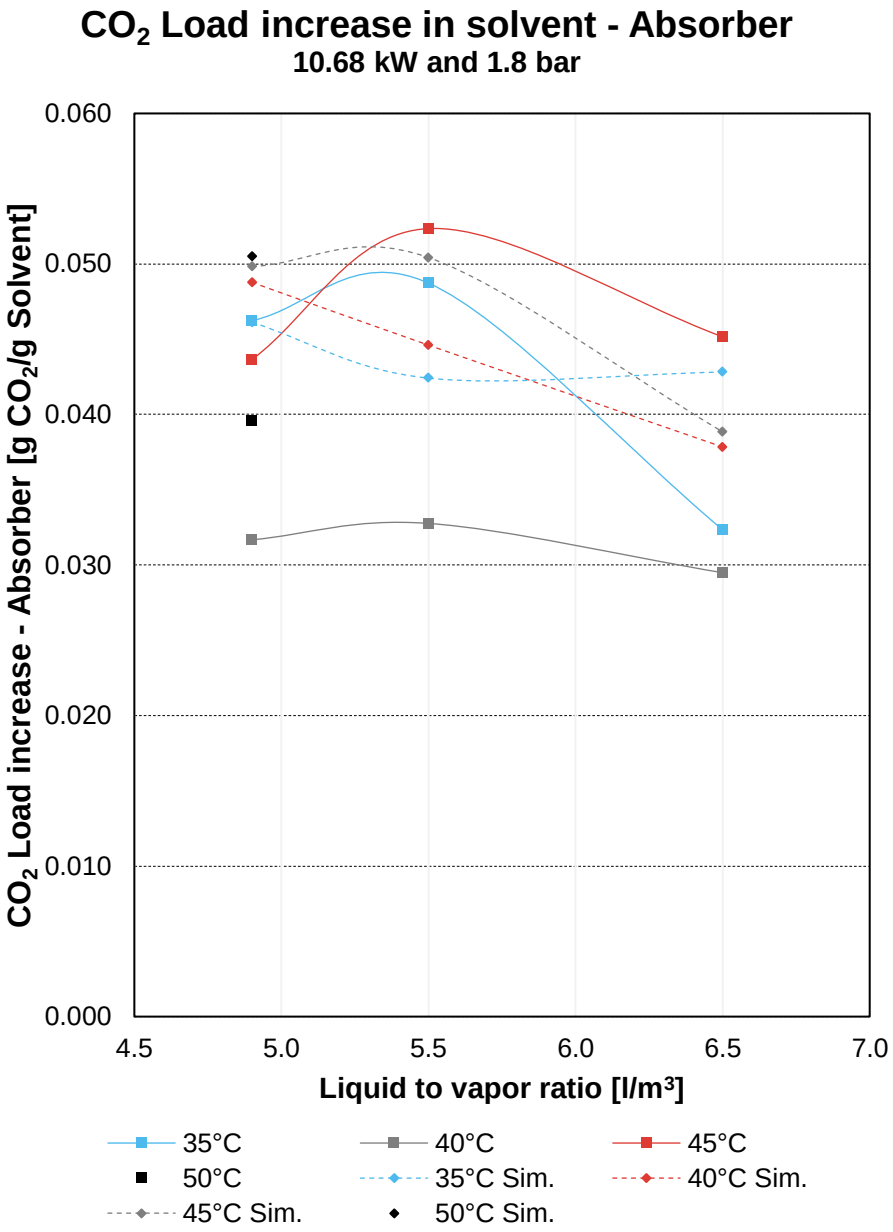

Figure 4-12: *CO_2 load increase in solvent for runs 127 – 136*

Another way to analyse the performance of the absorption process is through the CO_2-load increase within the absorber. The more the CO_2-load increases, the better the absorption performance. Figure 4-12 displays the results on the CO_2 load increase for all runs of the first experimental campaigns. Experimentally, it is clear that the higher increase in the load could be allocated in a L/V of 5.5 l/m^3. Which matches the behaviour of almost all of the simulation outputs. In general, an initial operation optimum of L/G = 5.5 l/m^3 could be identified.

4.1.5 MEA mass fraction

Besides the CO_2-load in the solvent, the total MEA concentration was also monitored during the operation and simulation. As explained in section 3, the pilot plant has three available spots to take a solvent sample: One before the inlet to the absorber (So-called lean sample), another at the outlet of the absorber (So-called rich sample), and a last new-installed one at the outlet of the stripper (So-called regenerated sample). The results of the concentration monitoring are shown in the following section.

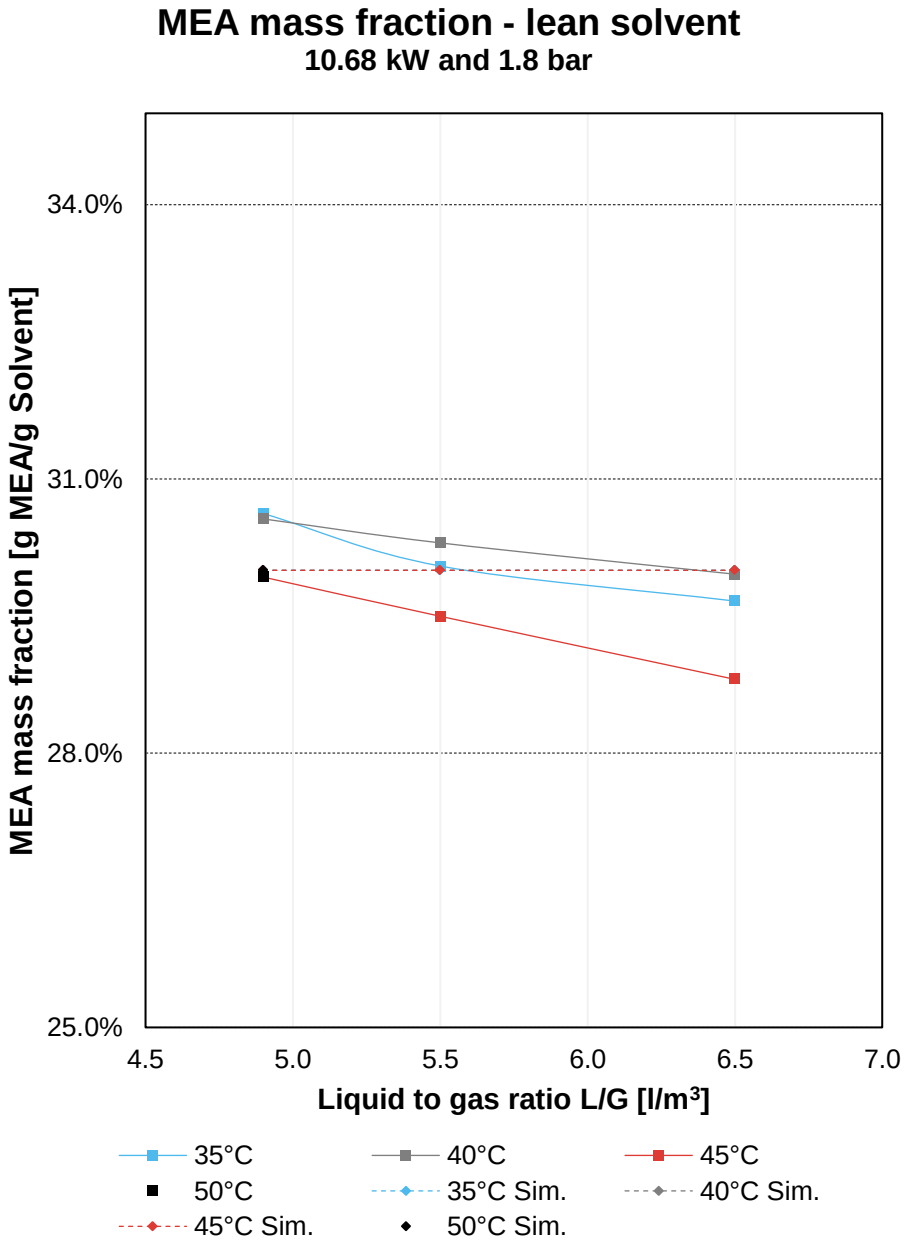

Figure 4-13: *MEA fraction (lean) for runs 127 – 136*

Figure 4-12 shows the MEA concentration for the lean samples of every run. It could be seen that not considerable chance in the concentration is presented throughout the entire campaign, as the magnitudes oscillate between 28.5 and 30.8 %w/w. The simulated outputs do not change, as the input MEA concentration was defined as one of the process specifications. On the other hand, a clear trend is presented in the experimental data: The MEA concentration tends to decrease as the L/G ratio increases. This might be explained based on the desorption process, as seen in Figure 4-11, the desorption is not favoured at high L/G ratios.

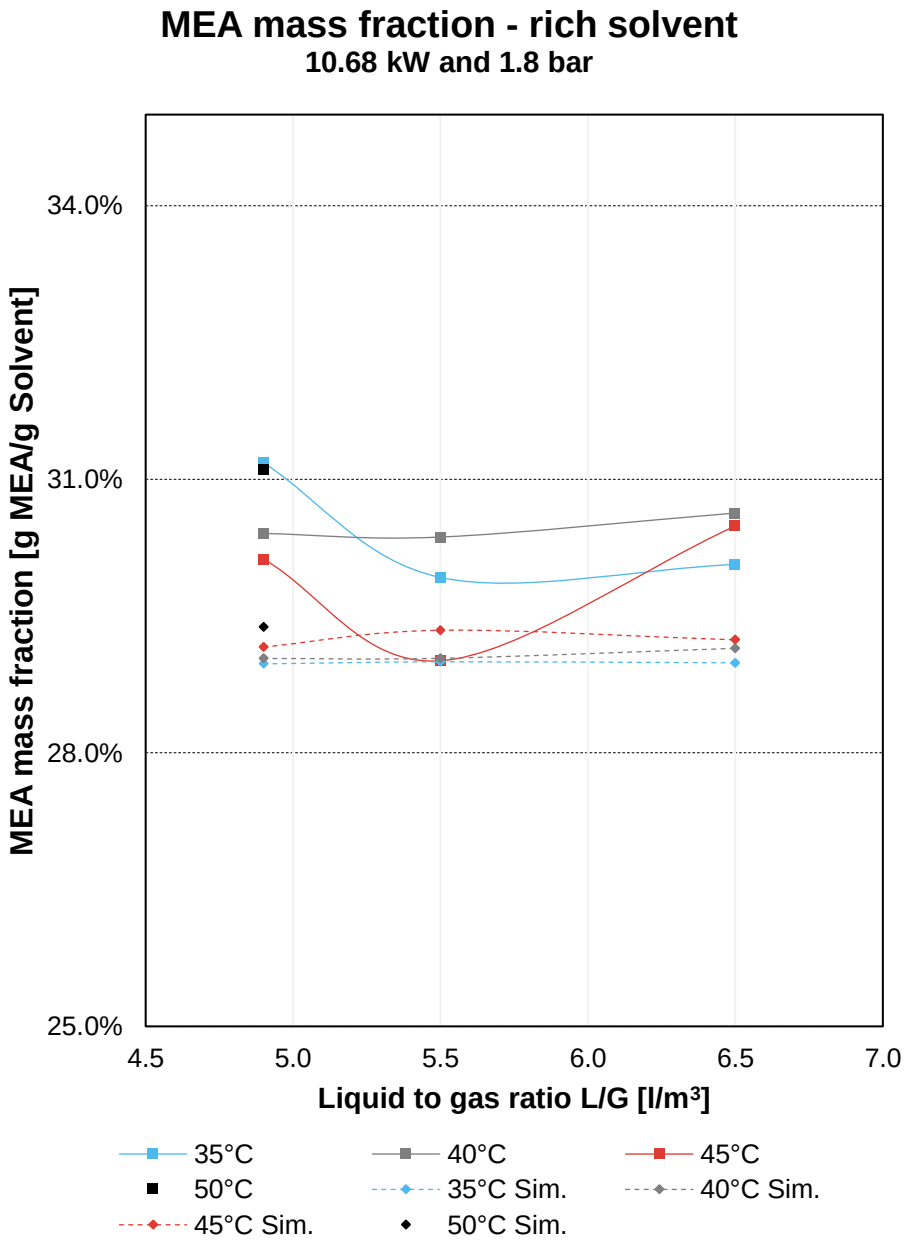

Figure 4-14: *MEA fraction (rich) for runs 127 – 136*

Figure 4-13 displays the MEA concentration for the rich samples. As the experimental method is designed to determine the total amount of MEA, all the loaded solvent (MEACOO-)

is desorbed back to MEA. Therefore, it is expected that the MEA concentrations correspond to the ones of the lean sample. In the simulation, the fractions of MEA, $MEAH^+$ and $MEACOO^-$ were added to enable comparisons with the experimental results. In general, the simulation outputs and the experimental magnitudes match. No clear trend could be identified in the experimental data series.

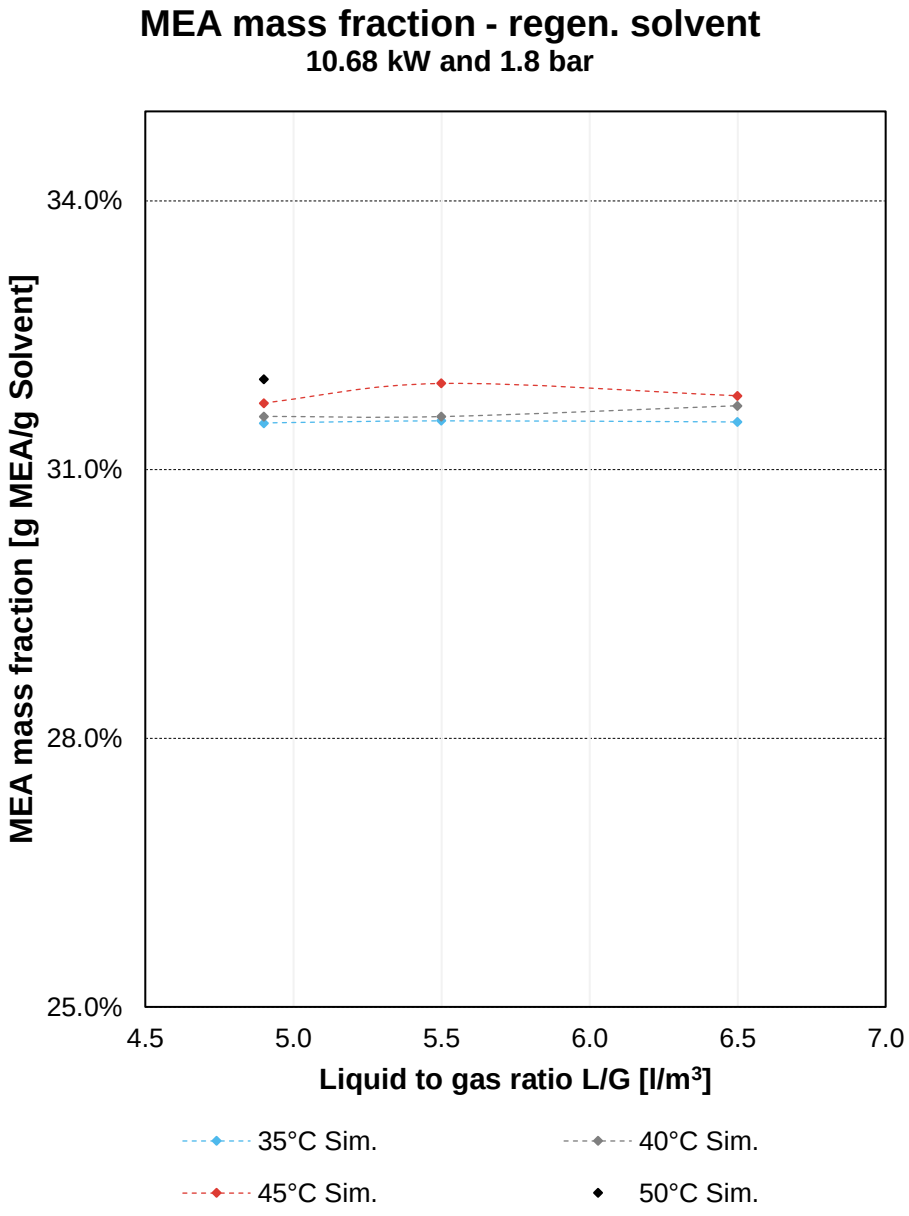

Figure 4-15: *MEA fraction (regen.) for runs 127 – 136*

Figure 4-14 presents the results for the regenerated samples. As said, the experimental values could only be measured after the installation of a valve at the stripper's outlet, which was carried out before the second experimental campaign. The simulation outputs show a relatively higher concentration of MEA in the stripper's outlet stream. This may be due to the

fact that water is removed from the stripper's top, and the MEA remains in the solvent. Therefore, its concentration increases.

4.1.6 General validation graphs

To completely verify the matching of the model to the experimental data, a general validation graph is presented in Figure 4-15. The graph is composed by the output temperatures, the MEA concentrations of every sample, the CO_2 load of every sample, and the absorption/desorption percentages, which are the parameters that could be compared.

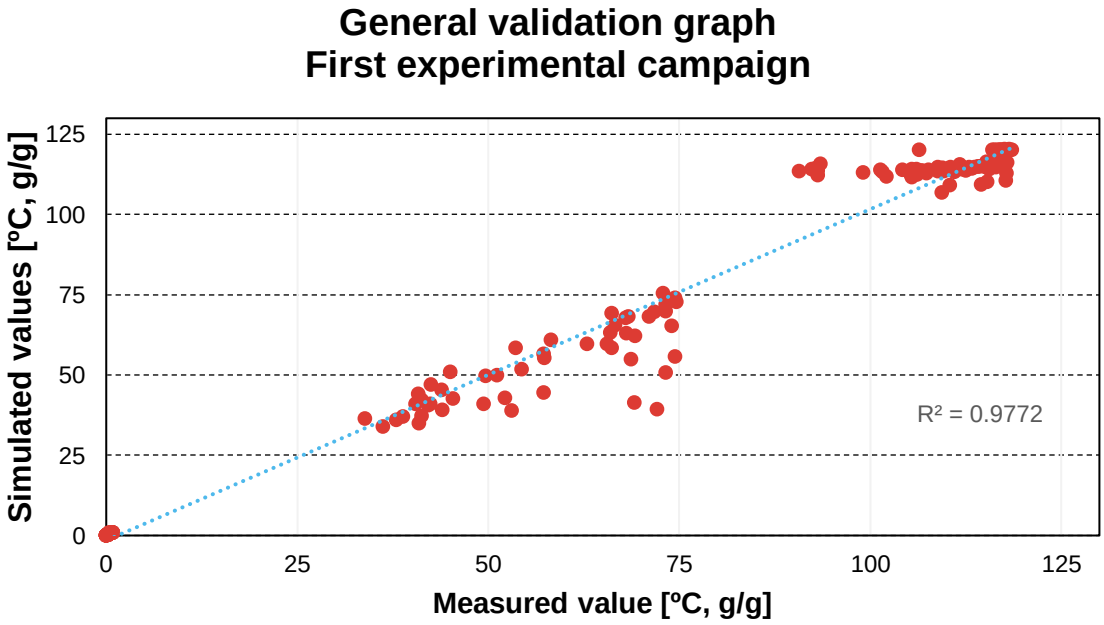

Figure 4-16: *Model validation graph for runs 127 – 136*

It could be seen that despite some discrepancies in the temperatures, a 0.977 coefficient of determination could be reached, pointing out that the simulated outputs match the experimental measured values. Therefore, the developed model could be used to represent the operation of the pilot plant ABIGAIL.

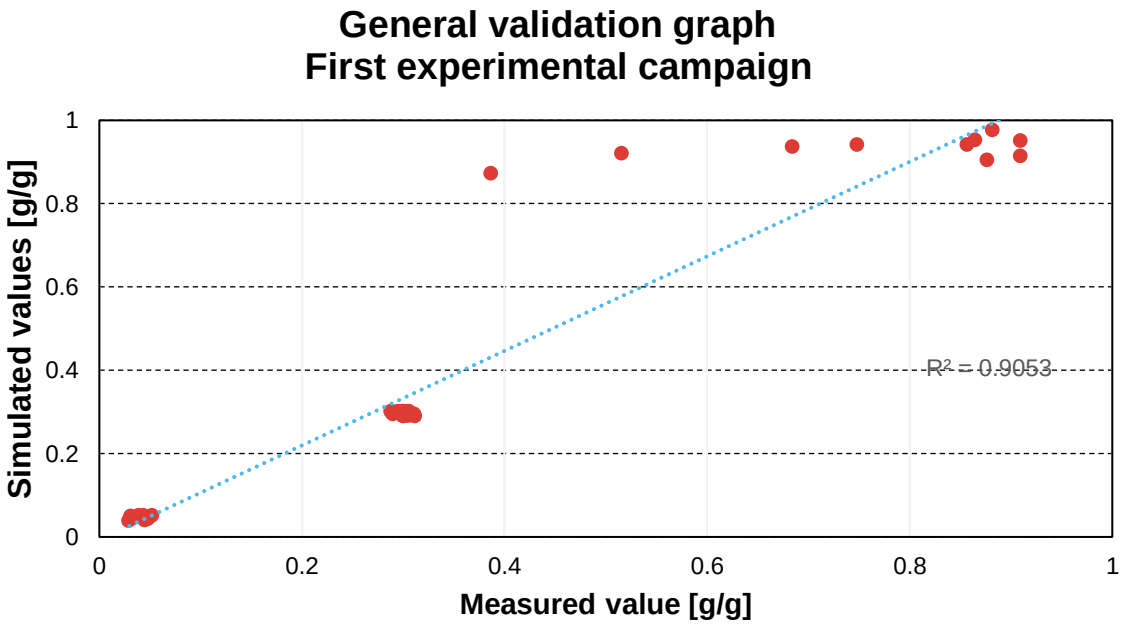

Figure 4-17: *Model validation graph for runs 127 – 136 – smaller scale*

Figure 4-16 zooms the validation of the absorption/desorption percentages, along with the MEA concentration and load. It could be appreciated that the data fitting of only these parameters is not as accurate as the general fitting of the process.

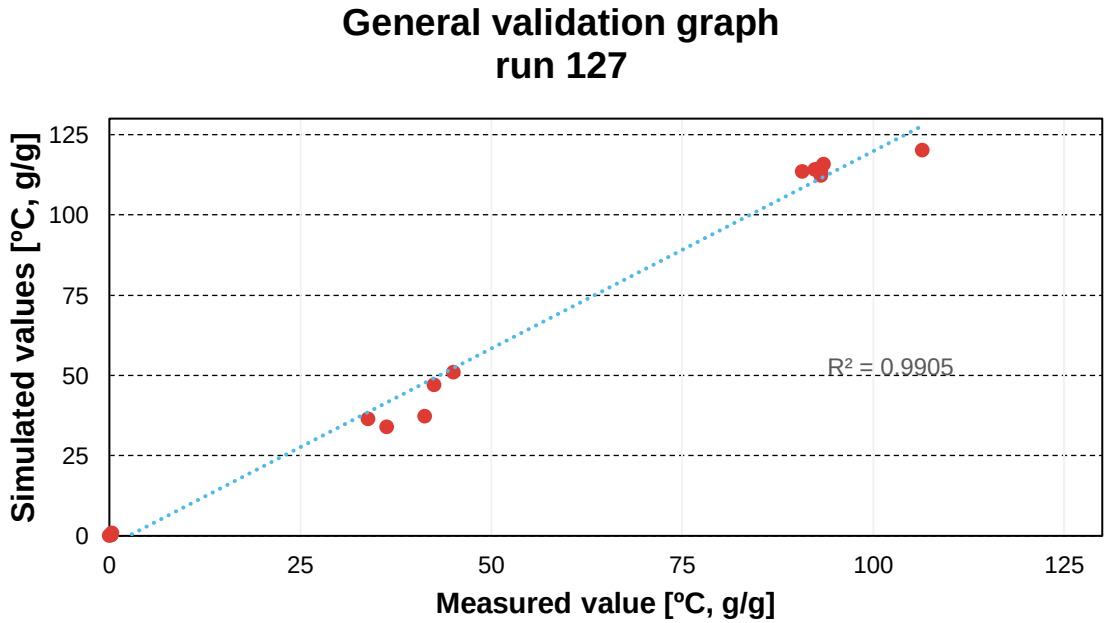

Figure 4-18: *Model validation graph for run 127*

Furthermore, individual validation graphs were also built for every run, as shown in Figure 4-17 for the case of run 127. It could be seen that a coefficient of determination of 99% could

be reached for individual stationary states. The remaining validations graphs for the rest of runs could be found in the Annex E.

4.2 Sensitivity Analysis

The sensibility analysis was aimed to determine the most influencing variables of the process in terms of CO_2 absorption and MEA desorption percentages. On the one hand, the absorber's inlet temperature and its L/G ratio were analysed for the CO_2 absorption percentage. On the other hand, the pressure of the stripper and the rebuilder's duty were selected as the variables to be analysed for the MEA desorption percentage. It is worth to mention that the results of the sensibility analysis were merely obtained from the simulation once the model was verified with the first experimental campaign.

4.2.1 L/G ratio and absorption inlet temperature

Figure 4.18 displays the results of the sensibility analysis for the absorber's inlet temperature and the L/G ratio. It could be seen that higher inlet temperatures affect positively the percentage of absorbed CO_2. Nevertheless, temperature rises over 55ªC do not have a considerable influence in the final output. Furthermore, higher temperatures decrease the CO_2 solubility in the solvent, hence, the reaction rates in the liquid phase dramatically shrink. Hence, simulation results with temperatures over 45ºC are considered not reliable, as multiple convergence issues arise.

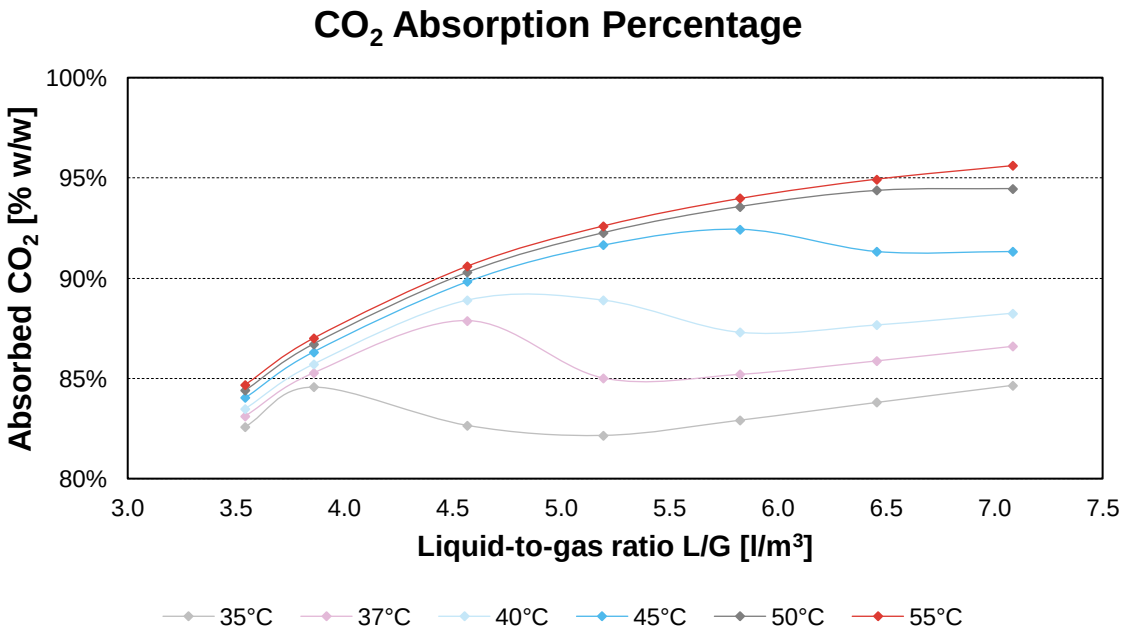

Figure 4-19: *Sensibility analysis for absorber*

Although the inlet temperature clearly influences the amount of absorbed CO_2, the L/G ratio presented a relatively higher influence in the overall absorption. An optimum L/G magnitude for every inlet temperature must be found, and its rage varies between 4 and 5.7 l/m^3.

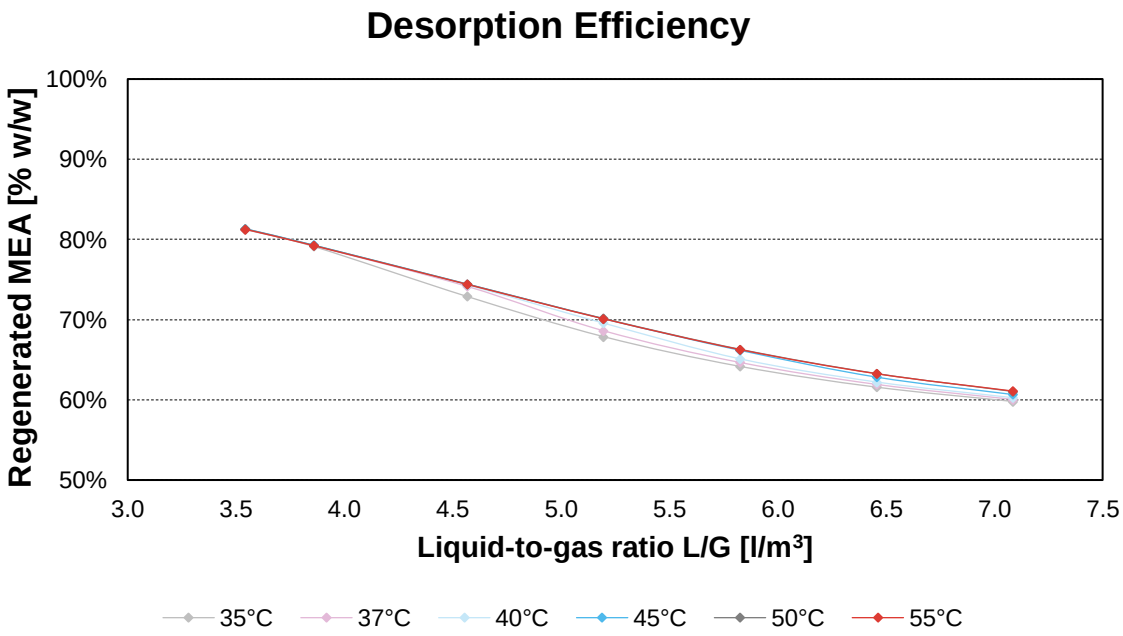

Figure 4-20: *Sensibility analysis for stripper regarding L/G*

On the other hand, Figure 4.19 illustrates the effects of the above mentioned variables in the stripper. It is initially clear, that the inlet absorber's temperature does not have an influence in the desorption performance, but the increase in the L/G ratio affects it negatively. The larger amounts of loaded solvent entering the stripper might be one of the reasons why the desorption efficiency is influenced negatively by the higher L/G ratios.

4.2.2 Stripper's pressure and reboiler's heat duty

The following sensibility analysis was only applied to the stripper. Figure 4-20 displays the effect of the stripper's pressure and the reboiler's heat duty on the overall amount of regenerated MEA. It is clear that both variables influence the process: as the heat duty increases, the amount of recirculated steam peaks, enhancing the contact between the phases, hence, the mass transfer during desorption is favoured. This is also achieved by operating the column at higher pressures, which has its advantages (cost-effective) and its drawbacks (Risky operation).

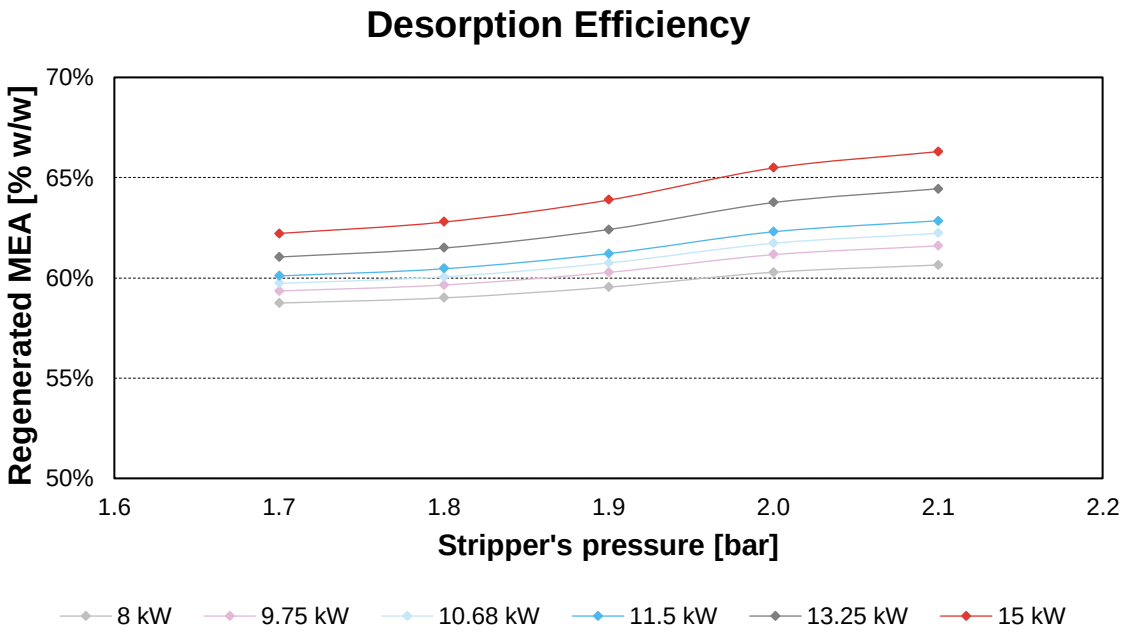

Figure 4-21: *Sensibility analysis for stripper regarding pressure and reboiler duty*

To quantify the effect of every variable in the final outputs, a relative sensibility was computed for every scenario. Results are shown in Table 4-2. The higher the magnitude of the relative sensibility, the higher the effect of the variable in the process output. In this case, the L/G ratio is the most influencing variable in terms of percentage of absorption and desorption, whereas the stripper's pressure affects exclusively the desorption performance.

Table 4-2: *Dimensionless relative sensitivity for different process variables and outputs*

	% Absorbed CO_2	% Desorbed MEA
Inlet absorption temperature	5,15E-03	9,50E-04
L/G ratio	2,88E-02	6,19E-02
Stripper's pressure	-	1,16E-01
Reboiler's heat duty	-	6,26E-03

Therefore, the L/G ration, along with the inlet absorption temperature ($T_{abs,\ in}$) and the stripper's pressure were chosen as the manipulated variables for the optimization.

4.3 Optimization to minimize operational cost

The results of the optimization are shown as daily operational cost in Table 4-3. The initial state corresponds to the operation conditions of the run 128. The found optimized state indicates a cost reduction of 14.23 €/day by operating the plant at an L/G =5.5, Tabs, in =37°C, and a stripper's pressure of 2.03 bar. This operation point was investigated during the second experimental campaign to verify the model and the found optimal point. Based on the optimization's constrains, absorption and desorption percentages above 90% and 60% +- 0.05 respectively are expected in the operation as well.

Table 4-3: *Detailed summary of the optimization results*

Variable	Initial State (€/day)	Optimized State (€/day)
PROWATER	11,10 €	11,10 €
REBOILER	101,37 €	95,56 €
CONDENS	1,19 €	1,00 €
PUMP	0,14 €	0,14 €
PUMP2	0,17 €	0,12 €
COMPRESS	0,46 €	0,46 €
Lost MEA Amount [kg/day]	2,83	2,02
Lost MEA	25,81 €	18,43 €
Total Cost	**143,06 €**	**128,83 €**

Figure 4-2 presents a summary of the optimization results. It compares the initial and the optimized state, showing not only the operation cost for each case, but also the simulated values for CO_2 absorption and desorption percentages. It could be seen that the optimization constrains are fulfilled for both cases, and that even the desorption percentage was clearly improved (Around 5.6%) with the optimal conditions.

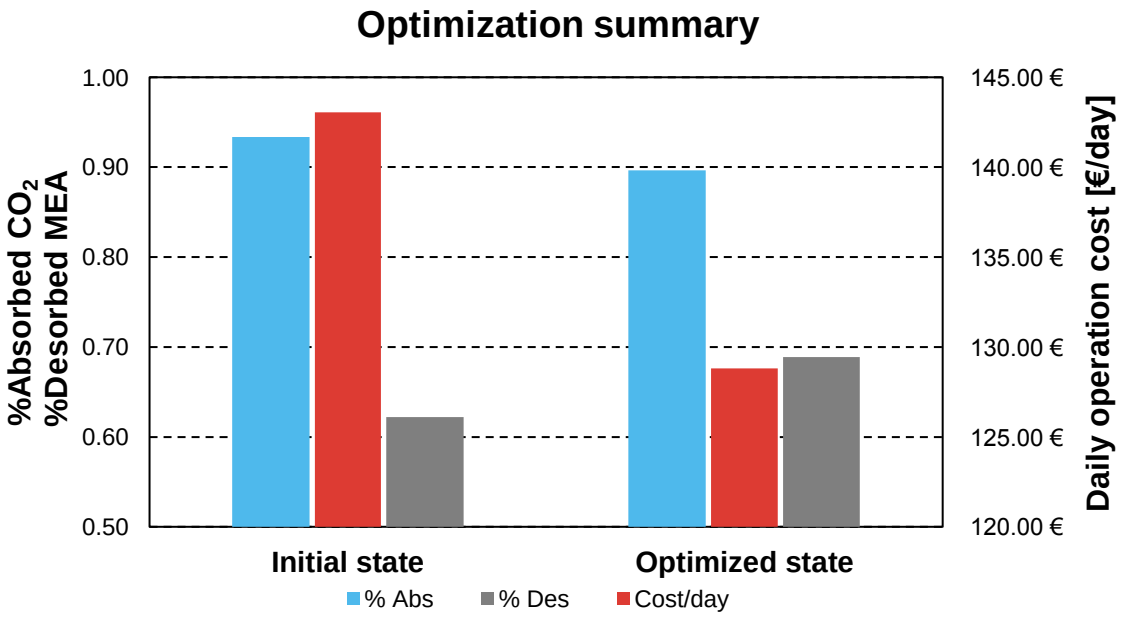

Figure 4-22: *Summary of the optimization results*

Based on the found optimum point, a second experimental campaign was designed to validate the results of the optimization.

4.4 Second experimental campaign

As the validation of the data was conducted in a similar way as for the first experimental campaign, most of the results present the same trend and illustrate similar physical-chemical

phenomena. To avoid re-stating arguments, the most relevant discrepancies are only cleared in the following section.

4.4.1 Stationary states

The second experimental campaign was carried out on the 11.10.2018 with a total of 9 different stationary states or operational conditions. The run number 144 matches the optimum found the previous section. Figure 4-22 and Table 4-4 present a summary of the operation conditions.

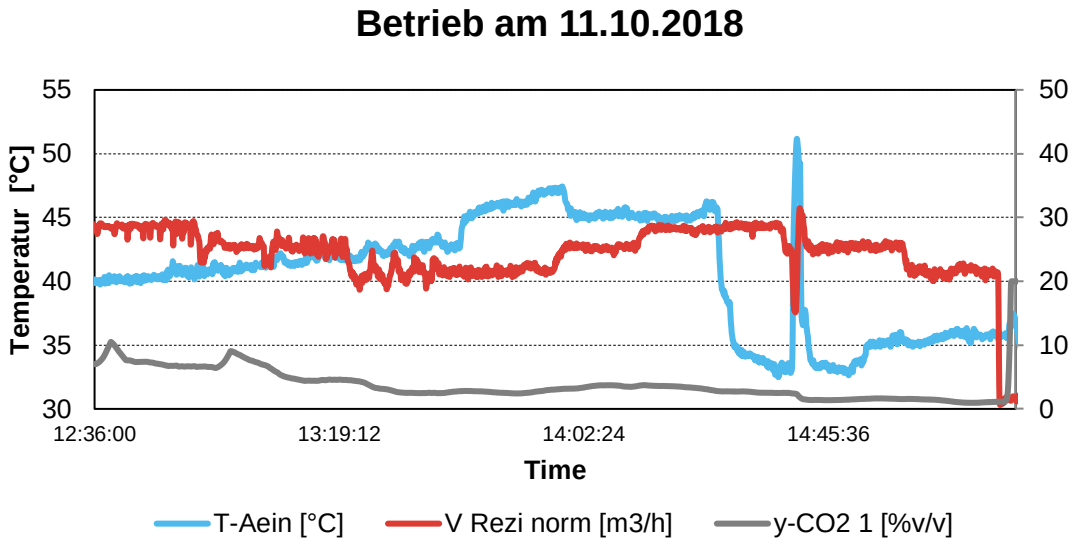

Figure 4-23: *Dynamic profile of the main process outputs during the first experimental campaign, 10.68 kW and 2.0 bar*

Table 4-4: *Time intervals for every run during the second experimental campaign*

Run number	Tabs (°C)	Pdes (bar)	Verdampfer (kW/l)	L/G	Initial Time	Final Time
137	40	2	0,076	4,90	12:45:19	12:48:19
138	40	2	0,076	5,51	13:10:29	13:13:44
139	40	2	0,076	6,51	13:36:14	13:39:39
140	45	2	0,076	6,51	13:48:24	13:52:49
141	45	2	0,076	5,51	13:59:49	14:05:24
142	45	2	0,076	4,90	14:15:49	14:20:24
143	35	2	0,076	4,90	14:30:04	14:35:14
144	35	2	0,076	5,51	14:52:59	14:56:04
145	35	2	0,076	6,51	15:02:04	15:05:19

4.4.2 Temperature profiles throughout the columns

Figure 4-23 presents the temperature profiles for the runs 134 to 139. The main difference regarding the temperature profiles of the first section is the representation: In this temperature profiles the inlet temperature of the absorber remains constant for each graph, and only the L/G ratio changes. Which is the opposite as in the previous temperature profiles.

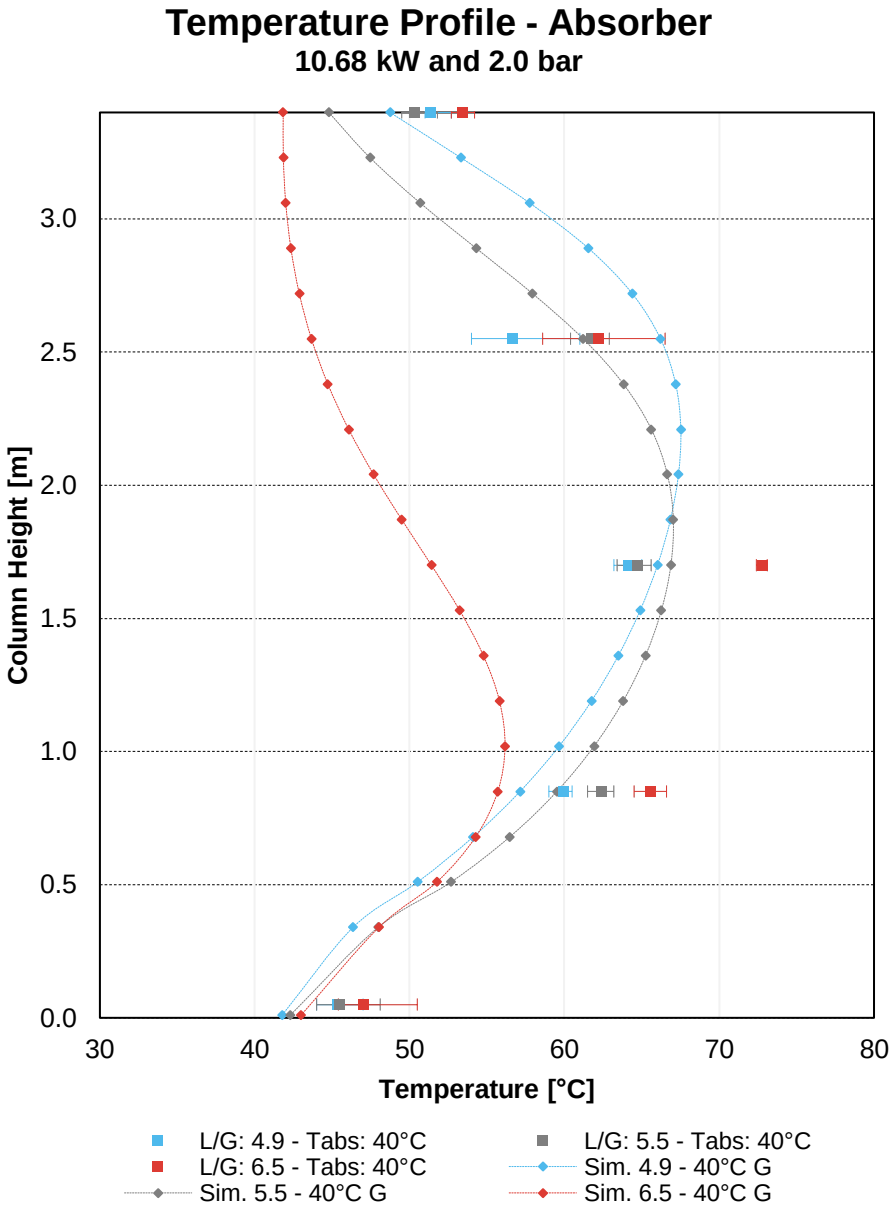

Figure 4-24: *Temperature profiles for runs 137 to 139 – Absorber*

It could be seen that some discrepancies between the model and the experimental data are present when the L/G increases. The model requires a large concentration of CO_2 to "Activate" the reaction rate and increate the temperature in the column. As the Gas volumetric flow was the only parameter changed, its low amount produced an overall low

CO_2 partial pressure in the model. Thus, a minimum amount was dissolved in the liquid and the reaction could not be activated, as shown in the red doted line.

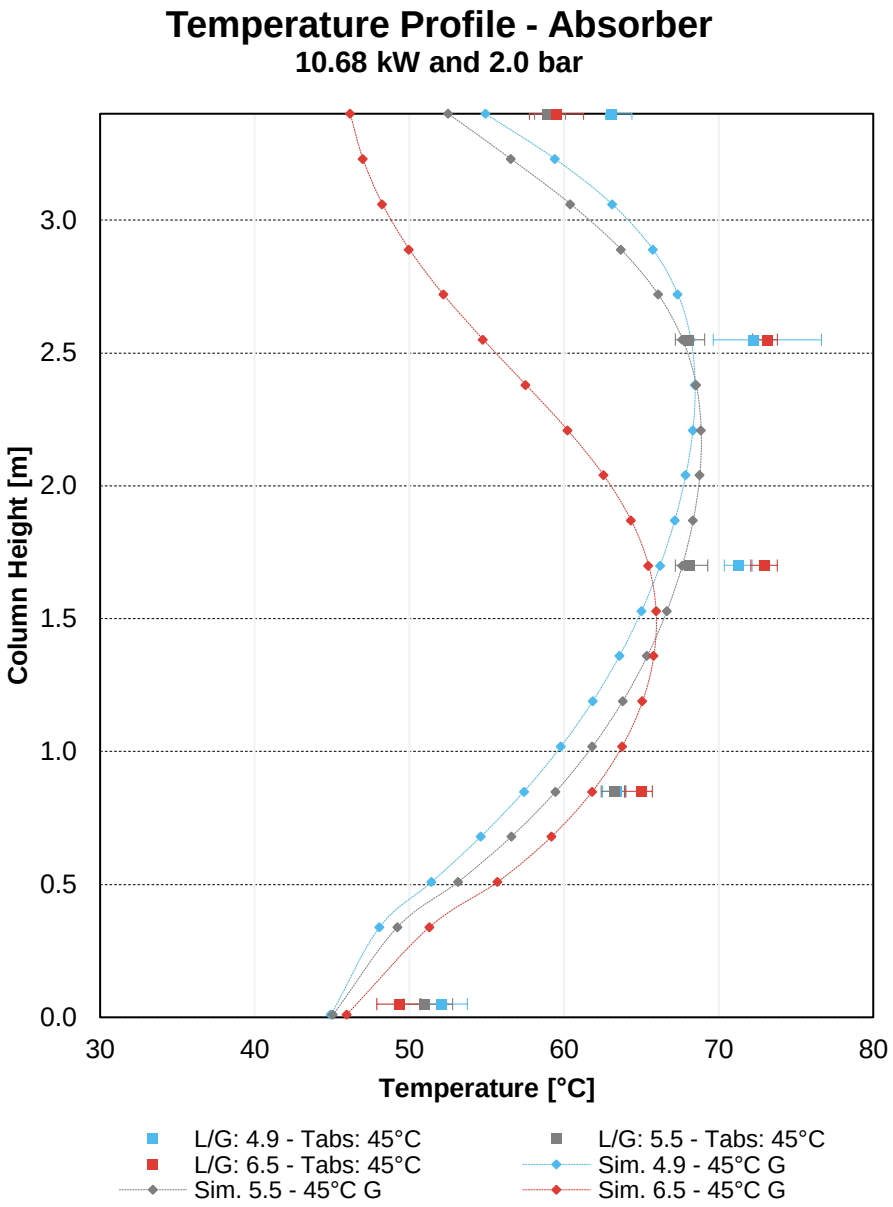

Figure 4-25: *Temperature profiles for runs 140 to 142 – Absorber*

As seen in Figure 4-24, an inlet temperature of 45°C in the absorber favored the matching of the model and experimental-data. Some discrepancies could also be found at high L/G ratios.

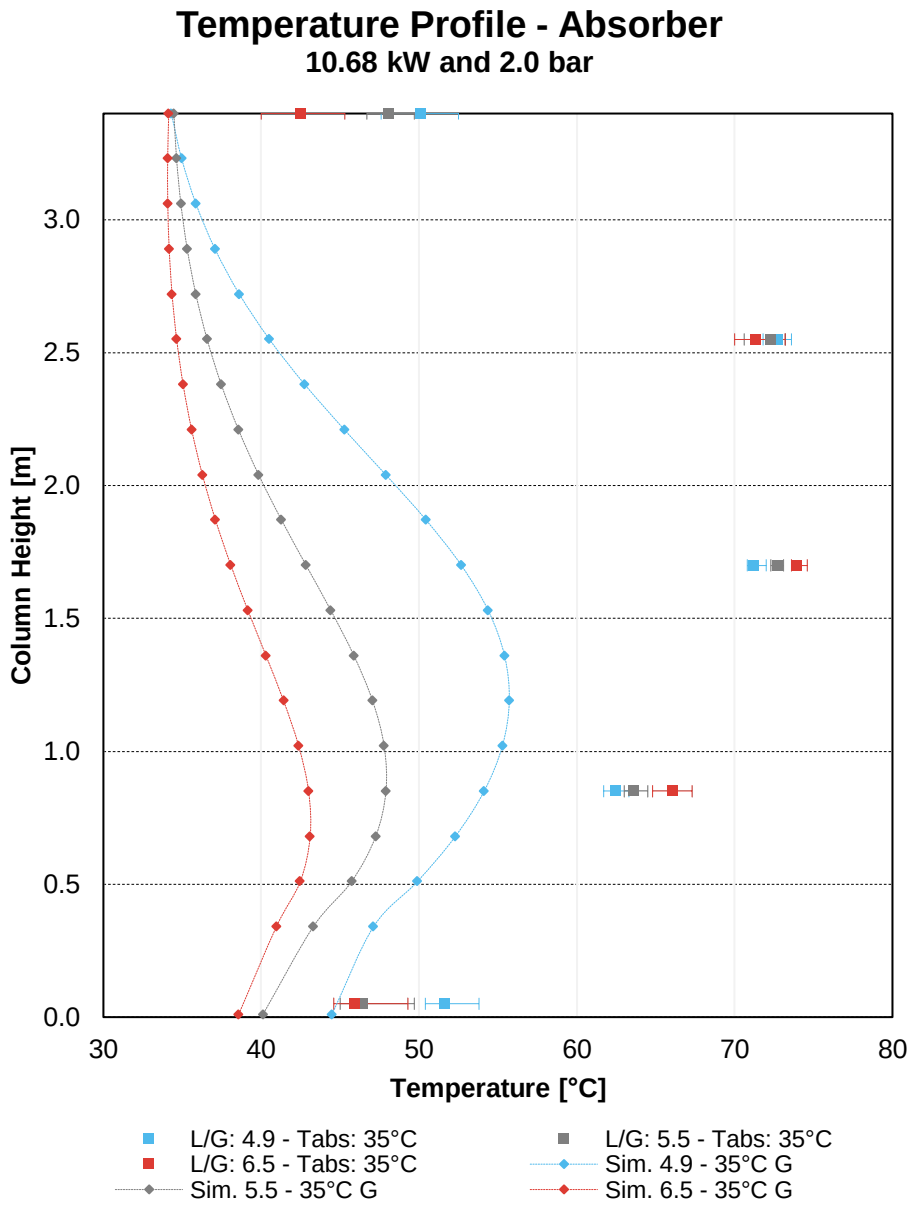

Figure 4-26: *Temperature profiles for runs 143 to 145 – Absorber*

Figure 4-24 is a clear example of a discrepancy between the model and the experimental data, as all the experiments were conducted at the lowest absorber's inlet temperature, the model predicted that the activation energy to start the reaction mechanism was not reached. Therefore, the temperature peaks do not match.

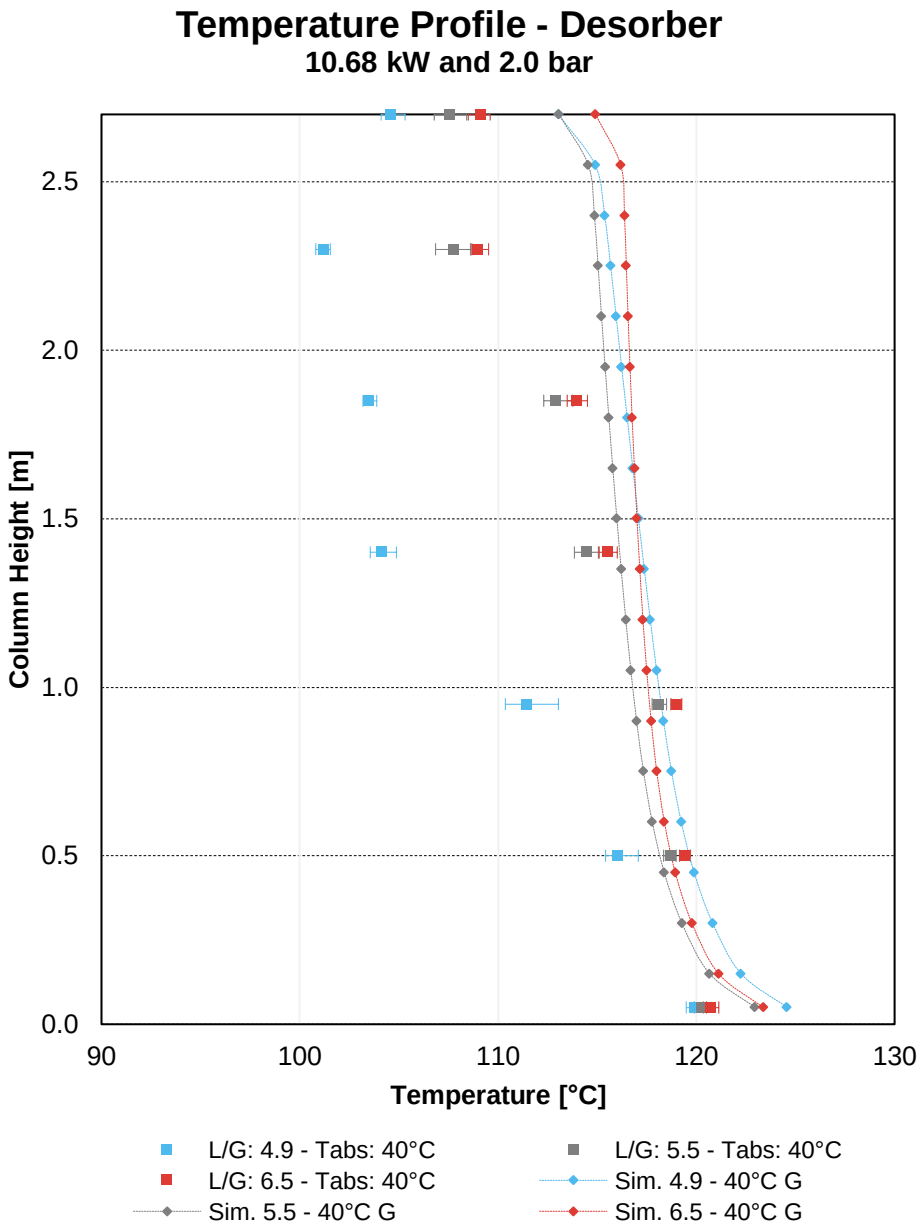

Figure 4-27: *Temperature profiles for runs 137 to 139 – Stripper*

In the case of the stripper, the warming-up process is clear in Figure 4-26. As the run 137 was the first one, possible the stripper did not reach its stationary-state temperature within the time the experimental samples were taken. The same deviation in the second top temperature measurement instrument could be appreciated during the second experimental campaign.

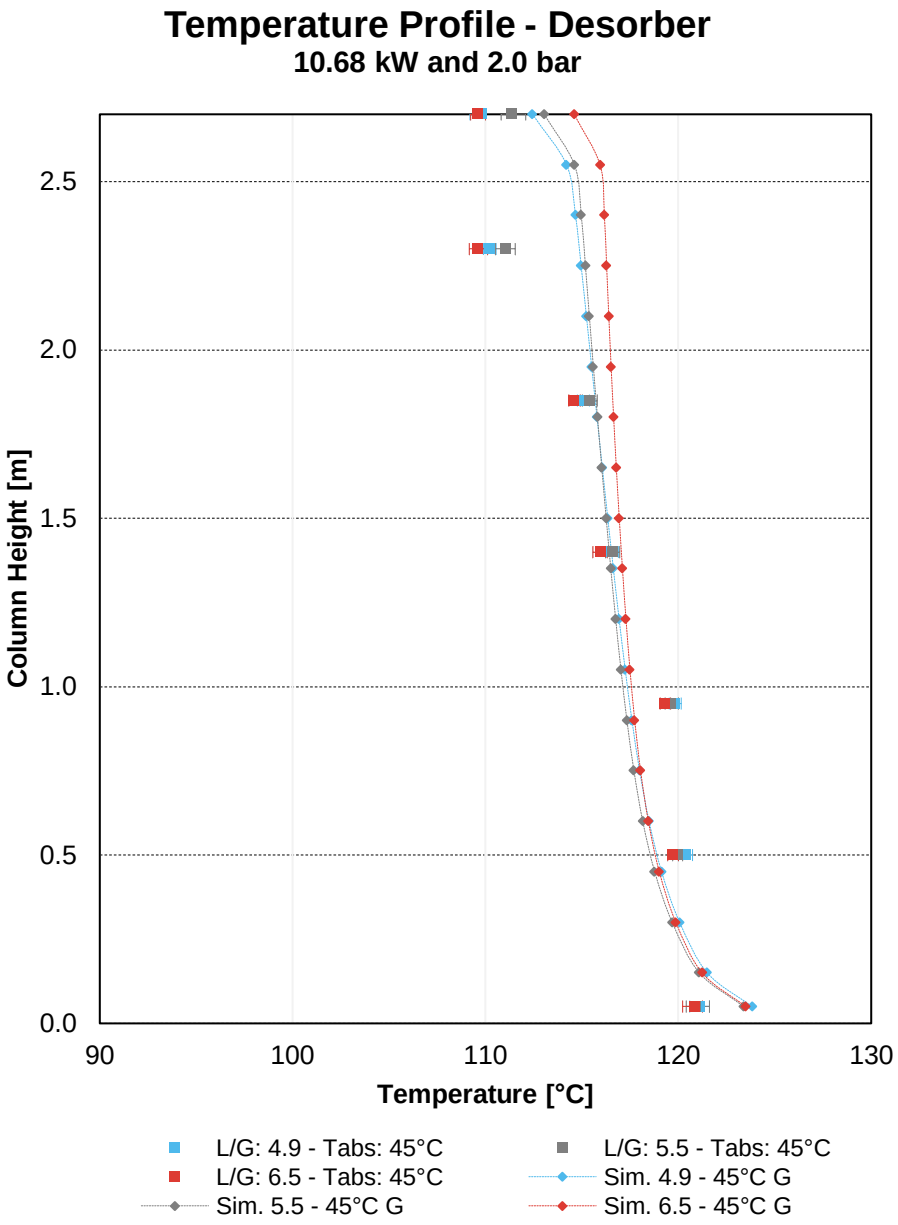

Figure 4-28: *Temperature profiles for runs 140 to 142 – Stripper*

Once the temperature stabilizes in the stripper, the experimental data and the model present a fair fit to each other. This could be seen in Figure 4-27.

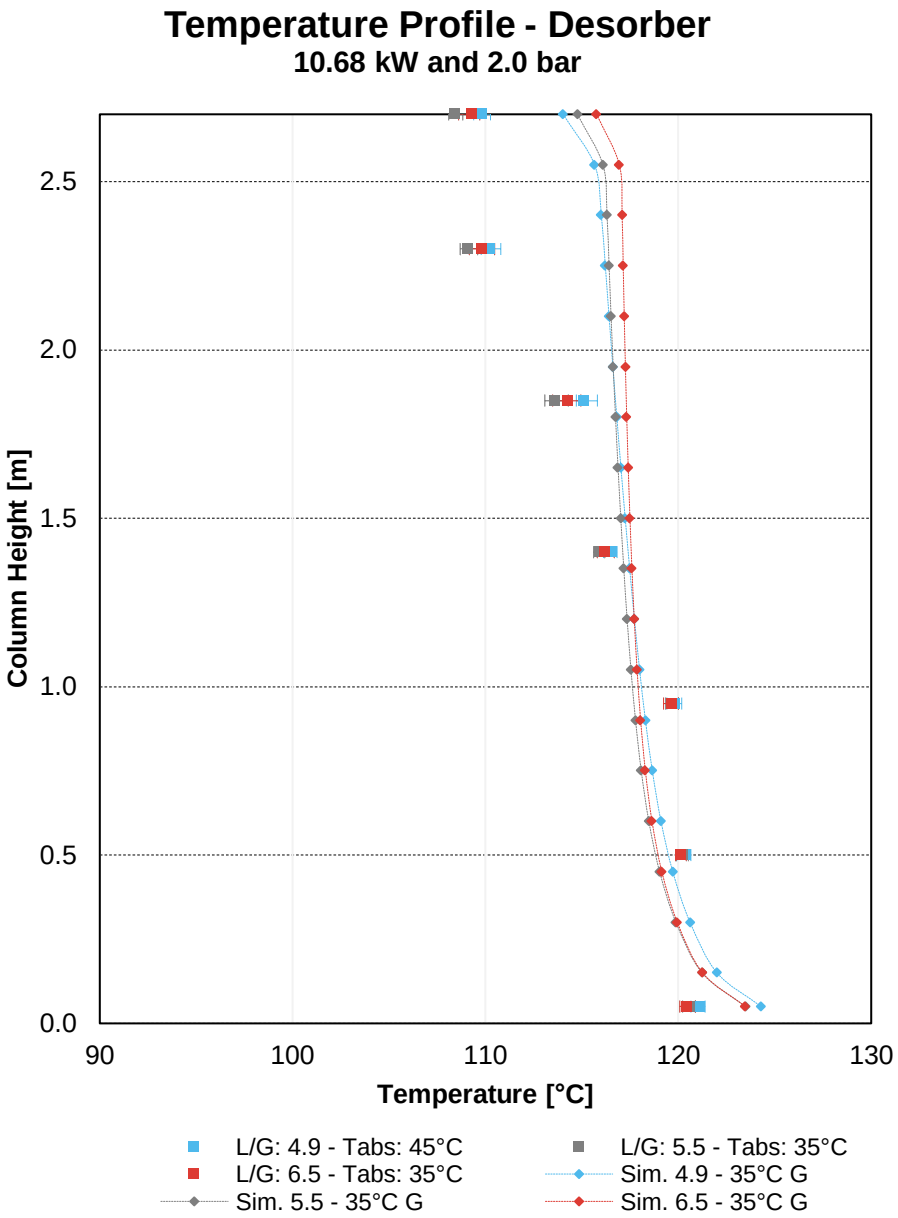

Figure 4-29: *Temperature profiles for runs 143 to 145 – Stripper*

In general, the temperatures in the stripper during the second experimental campaign were higher than during the first one. This is due to the highest pressure in the operation of the stripper.

4.4.3 Concentration profiles throughout the columns

The concentration profiles during the second experimental campaign present a similar behaviour as during the second campaign. The main differences are their magnitudes. Figures 4-29 and 4-30 show the profiles for the run 138. The rest of the profiles could be found in the Annex E.

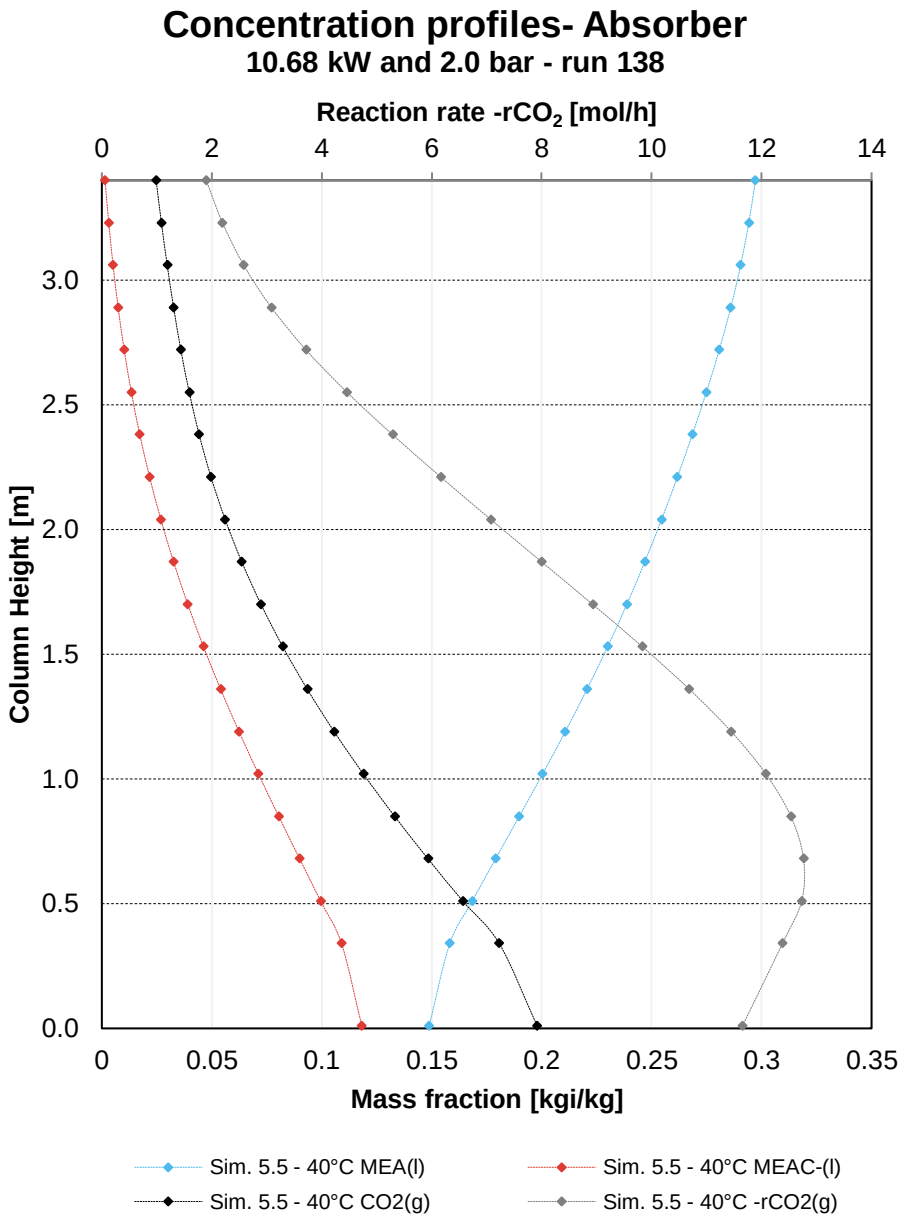

Figure 4-30: *Concentration and reaction rate profiles for run 138– Absorber*

As could be seen in Figure 4-29. The reaction rate presents a maximum magnitude somewhere close to the absorber's bottom, where the CO_2 concentration peaks. In the case of considering multiple feeds in the absorber, the bottom stages of the column are great points for the feed of the solvent in case a temperature control in absorber wants to be implemented.

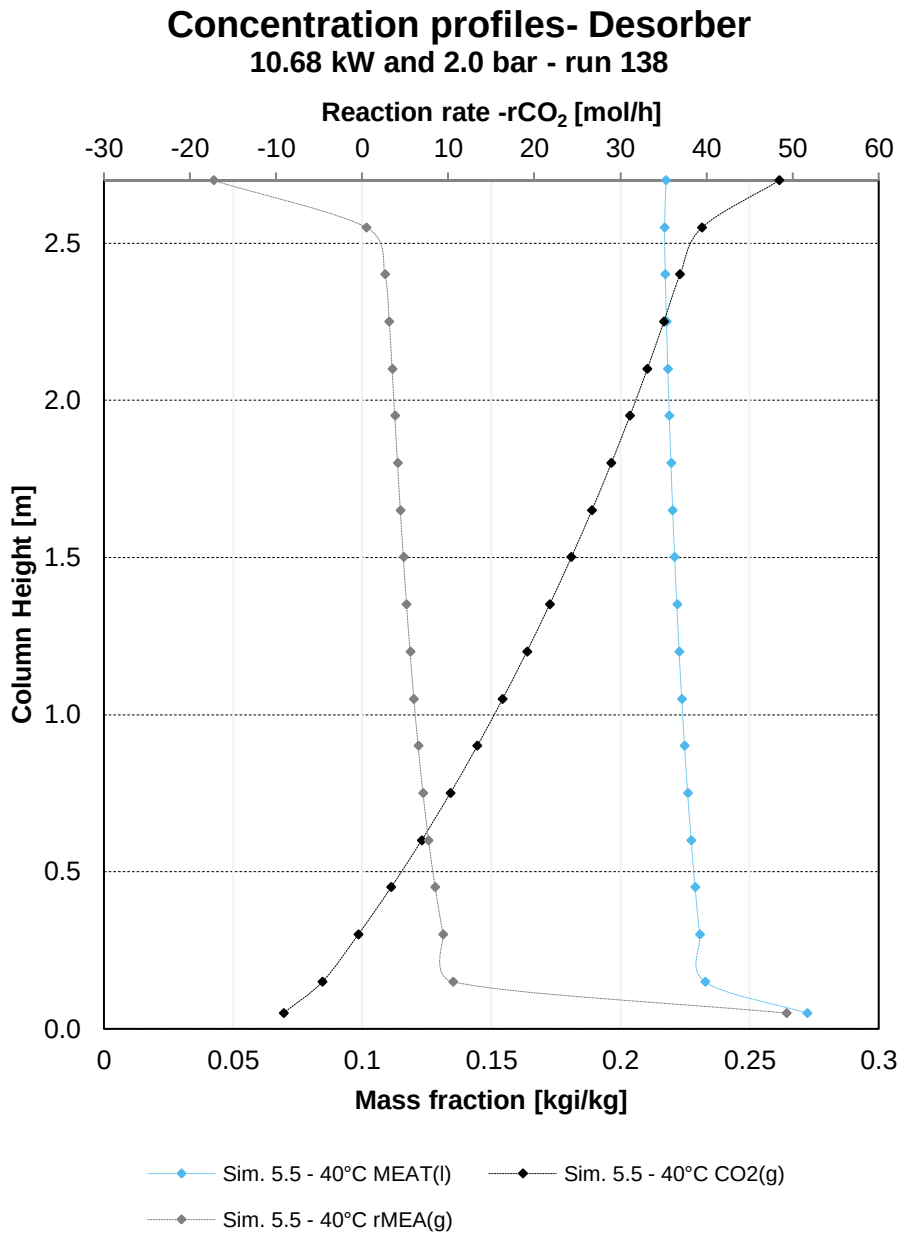

Figure 4-31: Concentration and reaction rate profiles for run 138– Stripper

As the pressure in the stripper was increased during the second experimental campaign, higher temperatures could also be reached inside it. Hence, a steepest change in the concentration of the involved species (CO_2 and MEA) is expected. For instance, the CO_2 concentration in the gas phase almost doubles the concentration when operating the stripper at 1.8 bar.

4.4.4 Abs- and desorption rates along the columns

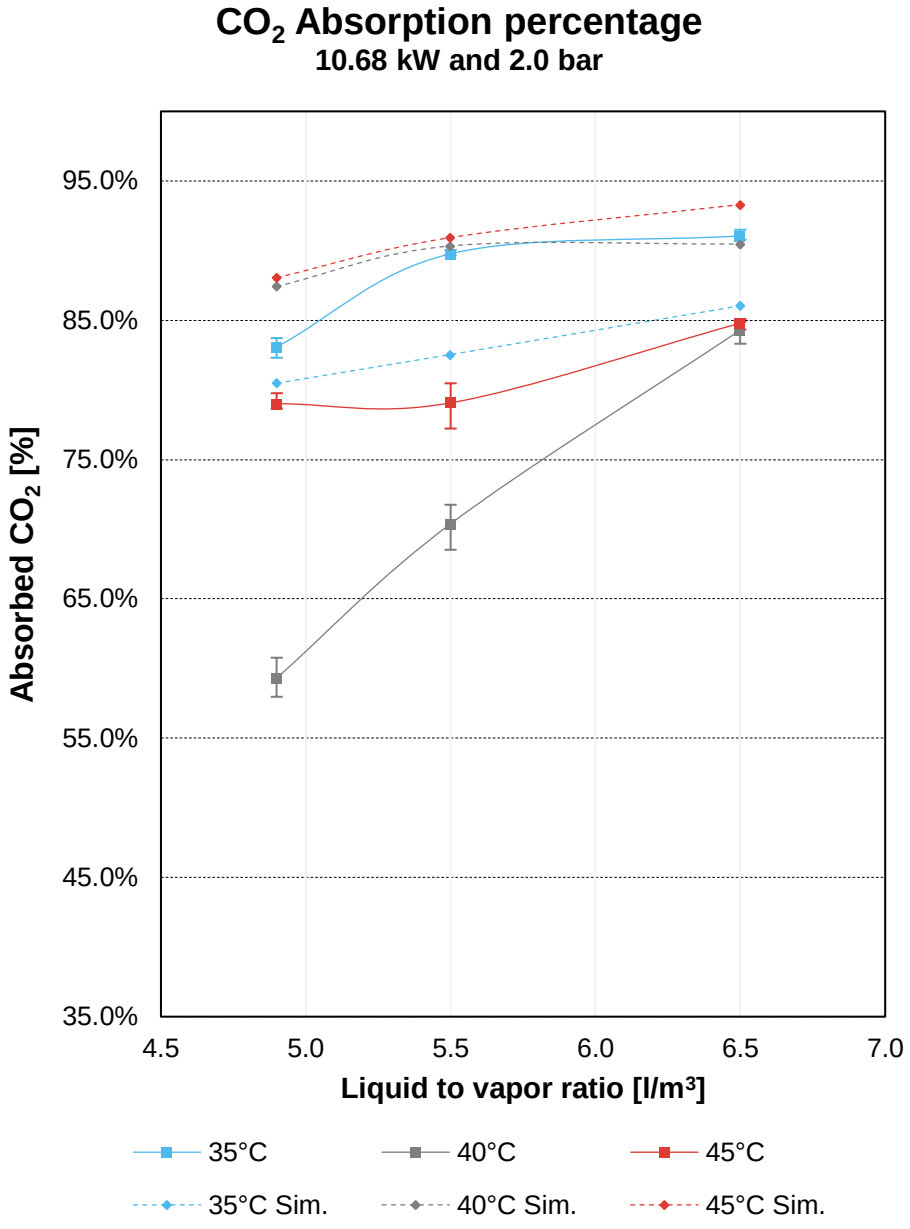

Figure 4-32: CO_2 absorption percentage for runs 137 to 145

Figure 4-32 presents the percentage amount of absorbed CO_2 for all the runs of the second experimental campaign. It is clear that the simulated outputs are most of the times above the measured values, and that major discrepancies are presented for low L/G rations. Hence, it is advisable to use the model at L/G ratios above 5 l/m^3. The high amounts of gas when operating with low L/G rations reach the solubility limit. Hence, absorption is limited and the flue gas leaves the column with high CO_2 concentrations.

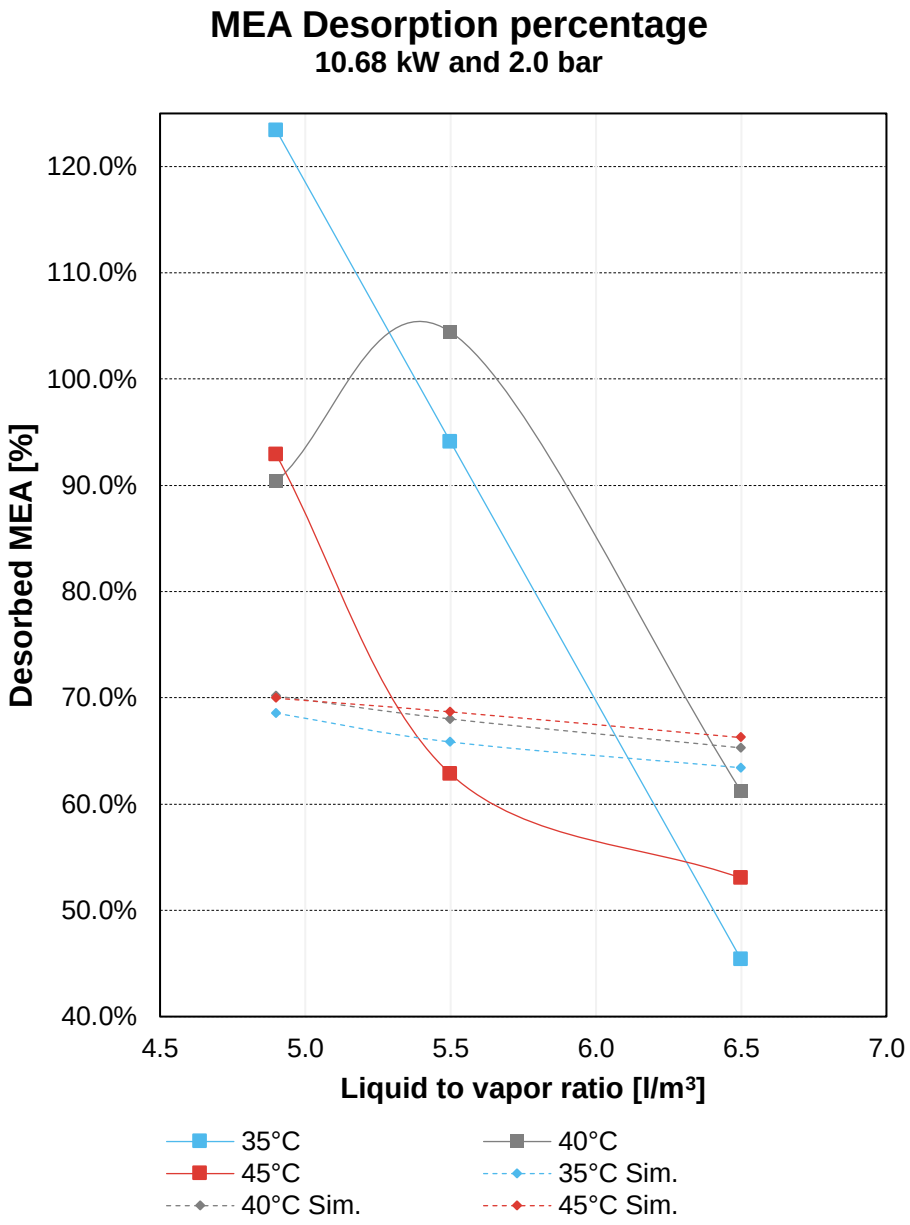

Figure 4-33: MEA desorption percentage for runs 137 to 145

The desorption percentage was determined for all the runs taking into account the new-installed valve to determine the load and concentration of the solvent. The model predicts a decreasing trend as the L/G ratio peaks which could be appreciated for T_{Abs} = 45°C and 35°C. A clear discrepancy between the model and the experimental method could be appreciated, featuring desorption percentages over 100%. The explanation for such alarming values is the assumption regarding the solvent-volumetric flow exiting the stripper: As there is no measuring instrument, it is assumed that its volumetric flow is the same as the lean solvent, which based on the experimental results, should not be assumed, as part of the water exit the column from its top.

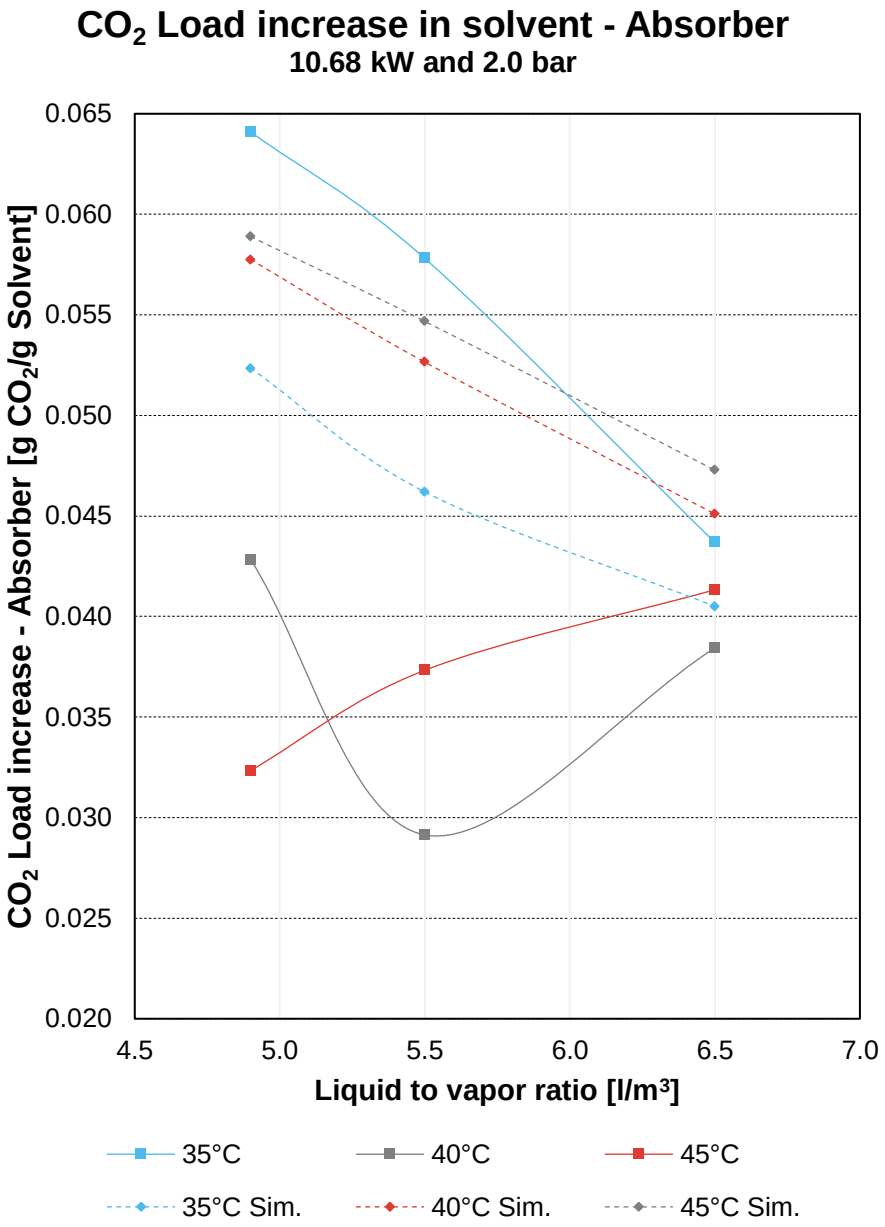

Figure 4-34: CO_2 load increase in solvent for runs 137 to 145

The load increase compares the amount of absorbed CO_2 between the lean and the rich samples. The model predicts a decreasing trend regarding the CO_2 load in the solvent as the L/G ratio increases. As a Gravimetric method was used for the CO2 load determination, its uncertainty affects the results shown in Figure 4-34, and might explain the mismatching trend of the experimental points with $T_{Abs,\ in}$ = 40ºC.

4.4.5 MEA mass fraction

The MEA mass fraction was determined to make sure that the conditions were kept constant during the entire operation. The concentration was monitored in three different points for the second experimental campaign (Lean sample, rich, and regenerated sample).

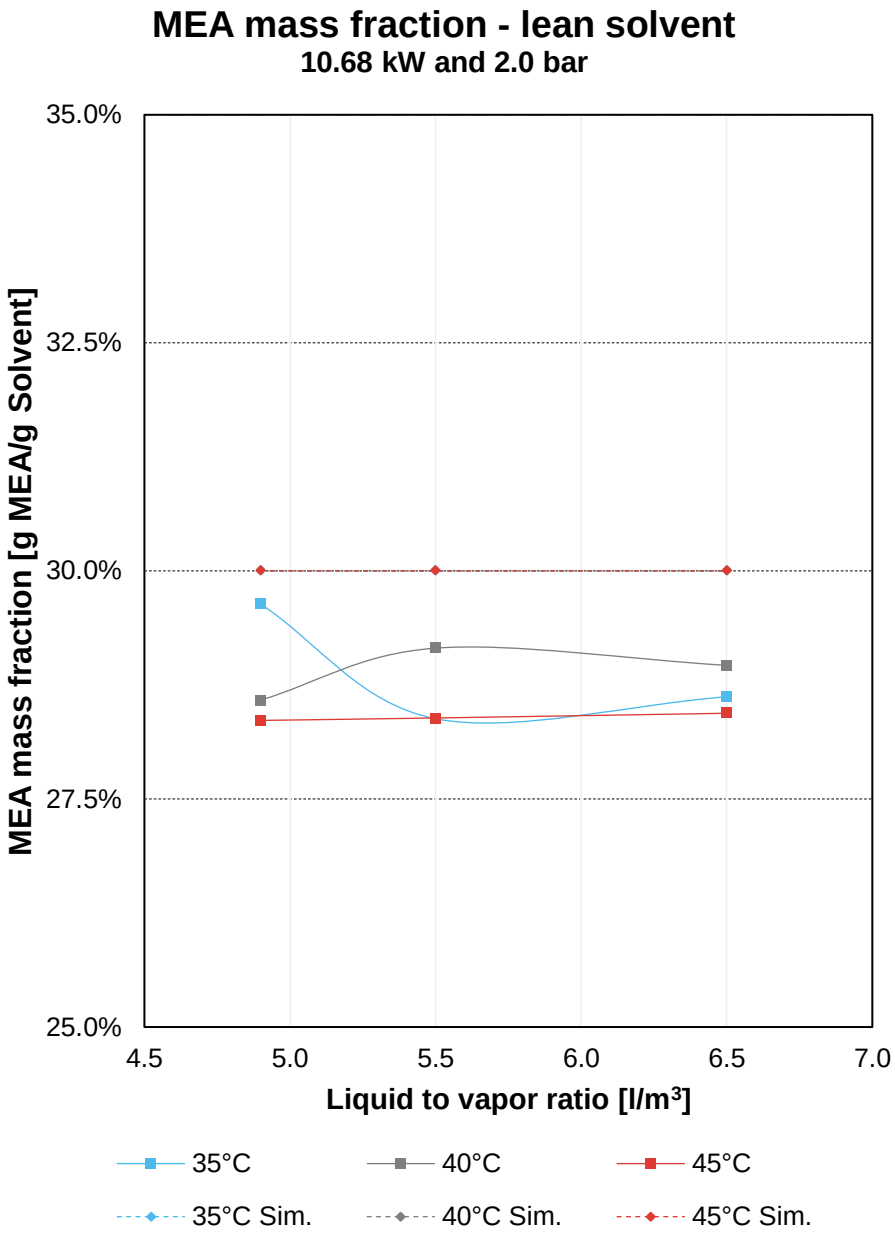

Figure 4-35: MEA concentration – lean solvent for runs 137 to 145

No deviation is ideally expected regarding the MEA concentration of the lean sample. The mass fraction is a process specification in the simulation, therefore it is kept constant through an adjustable stream of fresh solvent. No considerable deviation is appreciated in the simulation output.

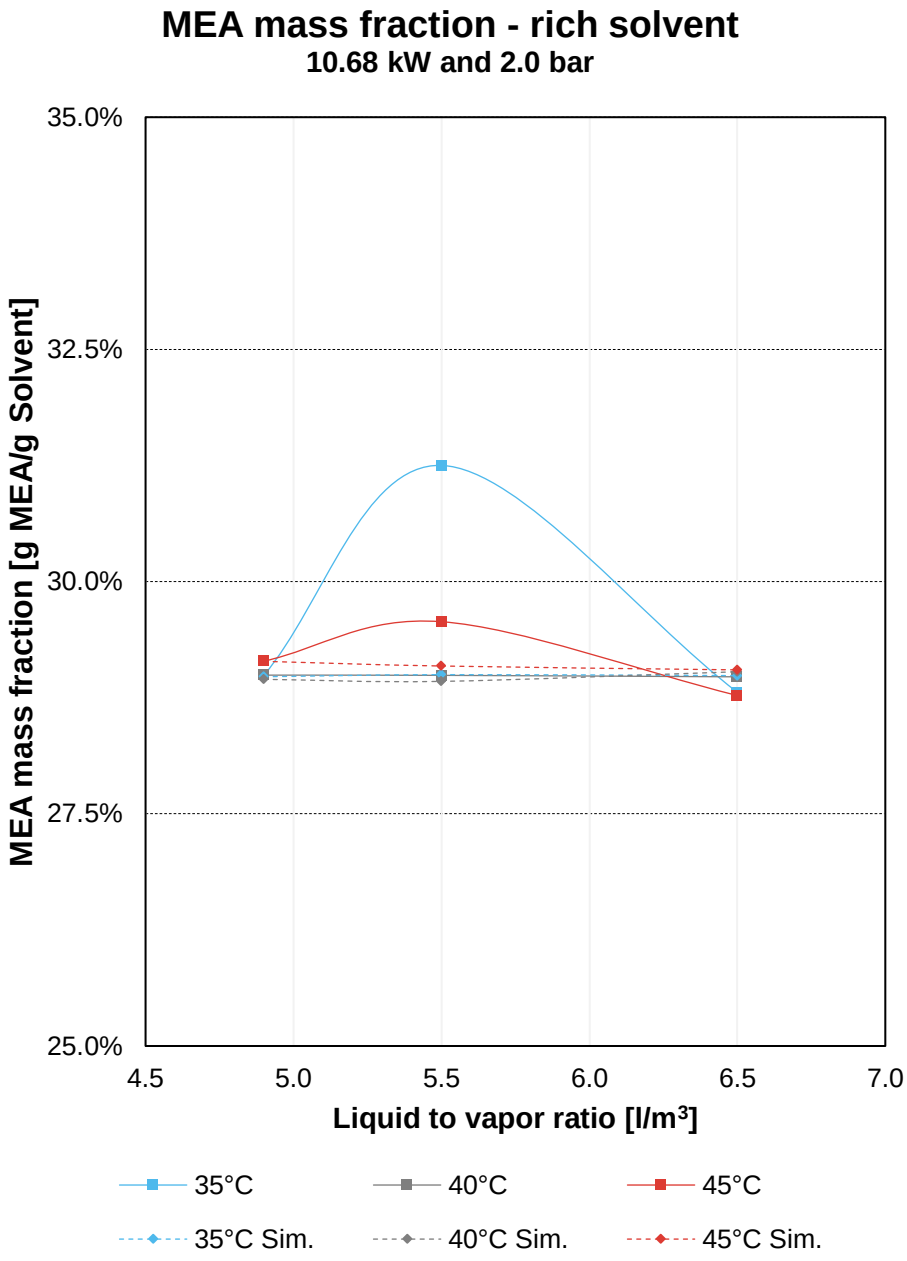

Figure 4-36: MEA concentration – rich solvent for runs 137 to 145

Regarding the rich solvent, Figure 4-36 shows that its concentration also tends to remain constant. A particularly close match was found in the samples with an inlet temperature of 40ºC. A constant concentration was expected, as the method is designed to determine the total amount of MEA, including the loaded.

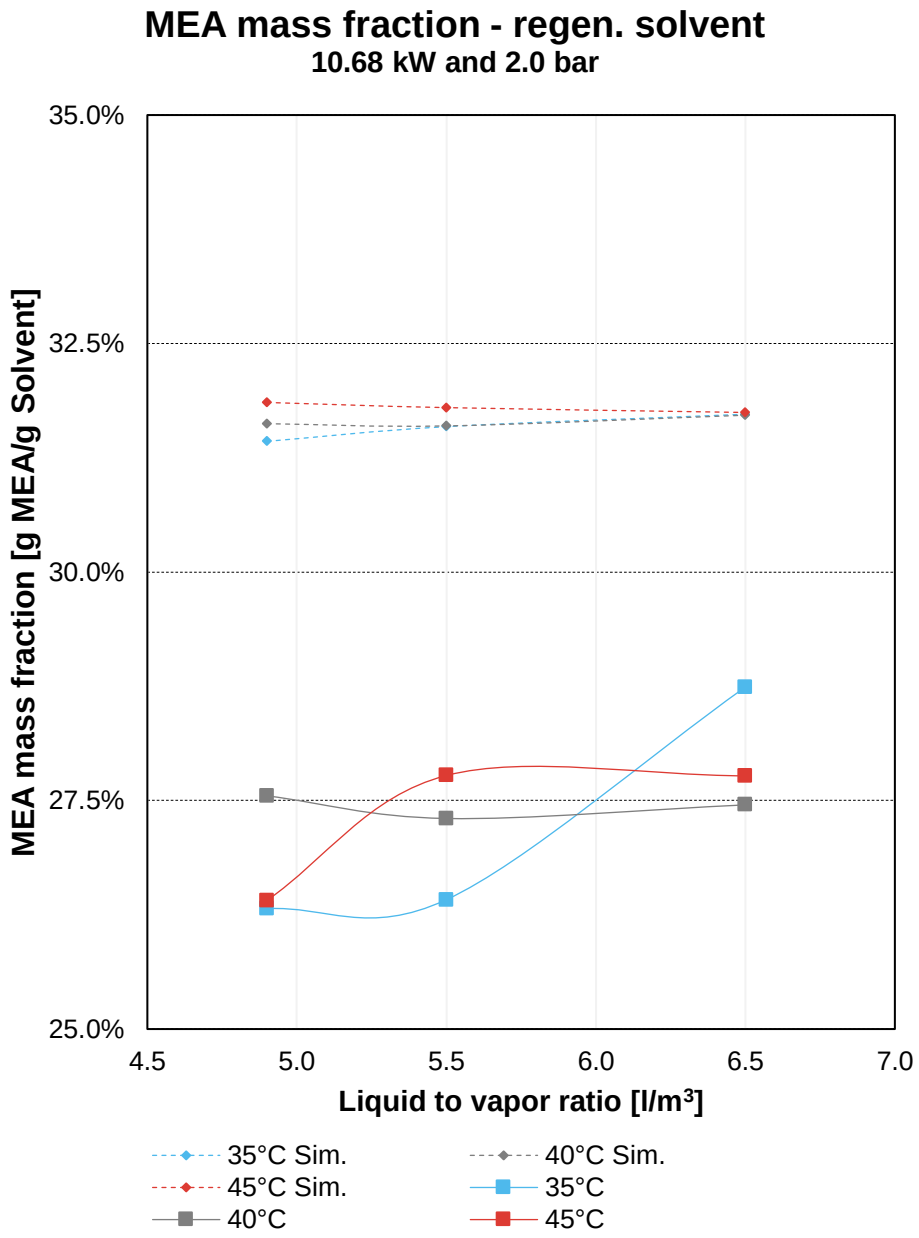

Figure 4-37: *MEA concentration –regen. solvent for runs 137 to 145*

The regenerated MEA in the simulation also differ from the operation. The operation points show a clear lower magnitude, indicating both: That the total amount of MEA was not fully regenerated in the stripper, or that other components integrate the solvent (Besides CO_2), diluting the initial amount of MEA.

4.4.6 General validation graphs

To completely verify the matching of the model to the experimental data, a general validation graph is presented in Figure 4-38. The graph is composed by the output temperatures, the

MEA concentrations of every sample, the CO_2 load of every sample, and the absorption/desorption percentages, which are the parameters that could be compared.

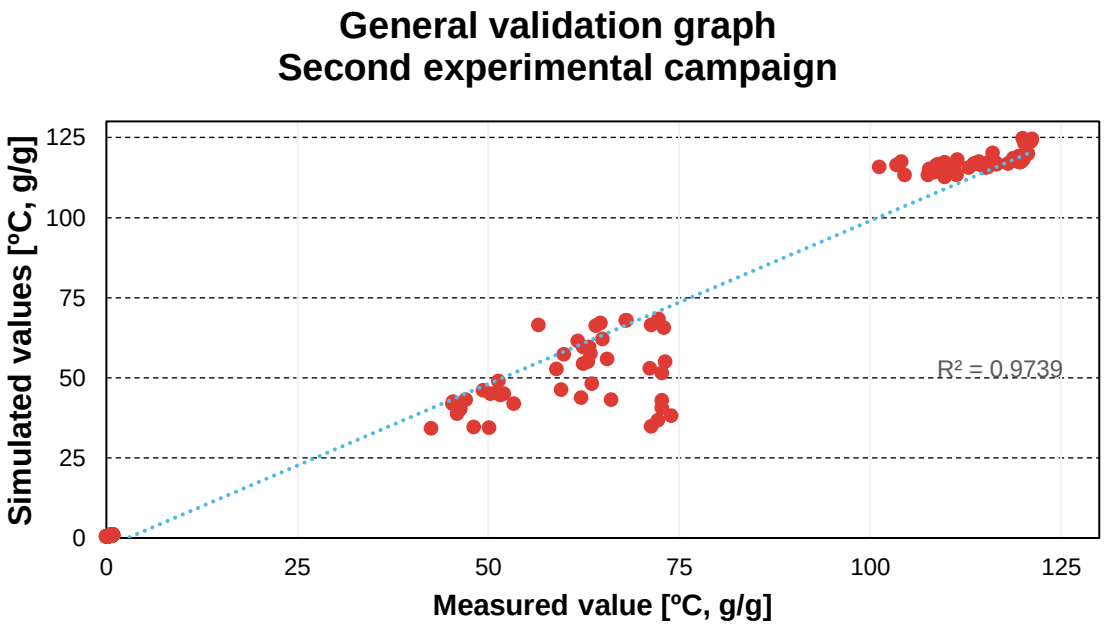

Figure 4-38: *Model validation graph for runs 137 – 145*

It could be seen that despite some discrepancies in the temperatures, a 0.973 coefficient of determination could be reached, pointing out that the simulated outputs match the experimental measured values. Therefore, the developed model could be used to represent the operation of the pilot plant ABIGAIL.

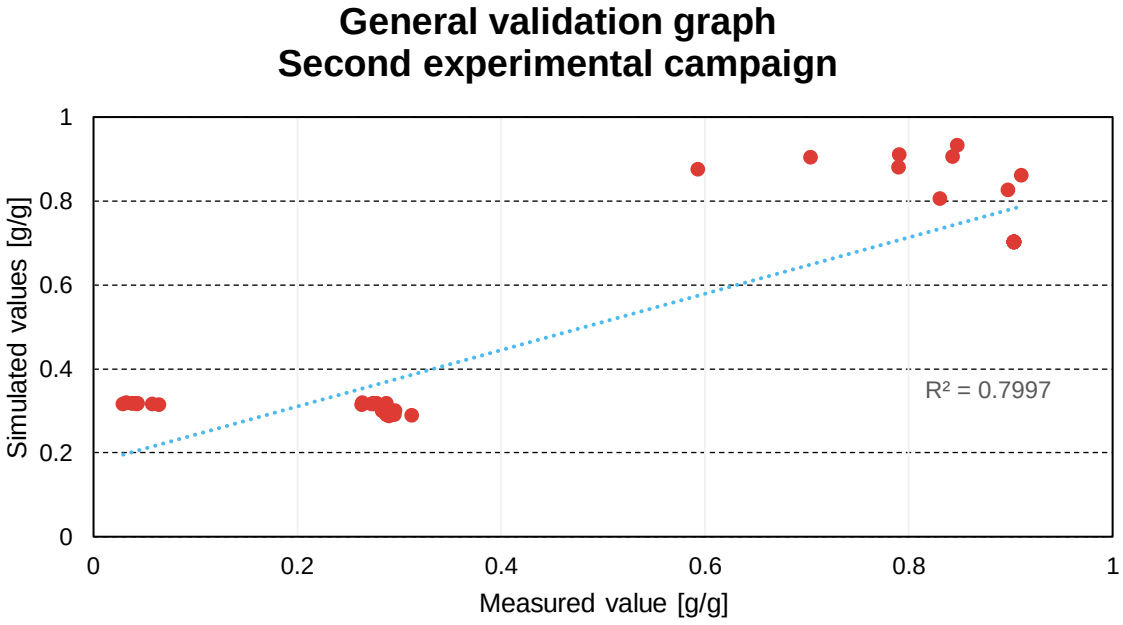

Figure 4-39: *Model validation graph for runs 137 – 145 – Smaller scale*

Figure 4-39 zooms the validation of the absorption/desorption percentages, along with the MEA concentration and load. It could be appreciated that the data fitting of only these parameters is not as accurate as the general fitting of the process.

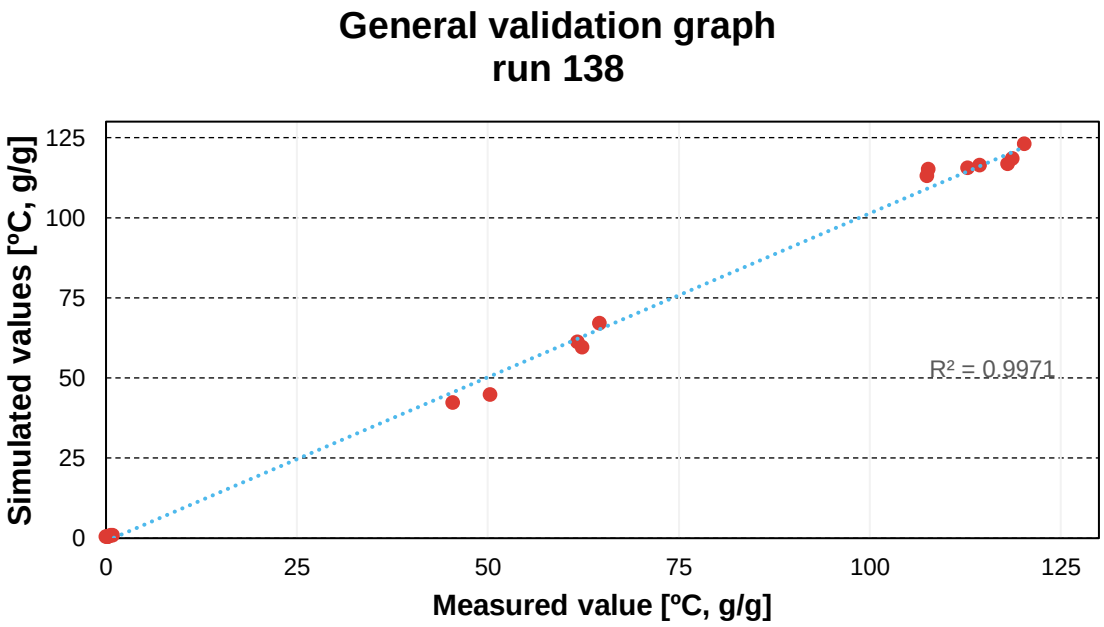

Figure 4-40: *Model validation graph for runs 137 – 145*

Furthermore, individual validation graphs were also built for every run, as shown in Figure 4-17 for the case of run 127. It could be seen that a coefficient of determination of 99% could be reached for individual stationary states. The remaining validations graphs for the rest of runs could be found in the Annex E.

4.5 Optimization of the heat-exchange network

Figure 4-41 displays the qualitative results of the synthesis of the heat exchange network of the pilot plant. The upper blue arrow corresponds to the needed cooling utilities by the process, and the bottom red arrow represents the heating utilities. Two streams were considered as “Cold streams”, meaning that they needed to be heated, as explained in section 3.2.3. These streams are depicted in blue in figure 4-41, and correspond to the loaded solvent exiting the absorber that must be preheated before entering the stripper, and the flue gas that must be preheated before entering the absorber.

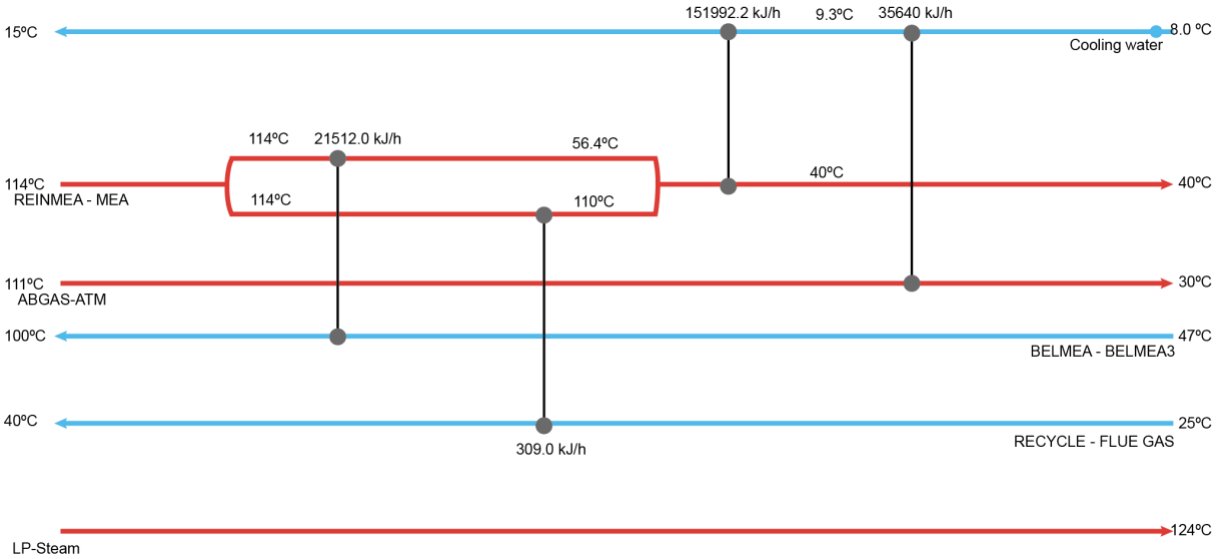

Figure 4-41: *Results of HENS analysis – plausible configuration*

Two so called “Hot streams” are represented by the internal red arrows. These streams must be cooled down during the process. The first hot stream is the solvent exiting the reboiler/storage tank, which must be cooled from around 114ºC to 40ºC. The second hot stream involves the cooling down of the outlet gas stream of the stripper to the ambient temperature. Only one additional possible configuration was found using Aspen Energy Analyzer™, it states an energy integration between the loaded solved and the lean solvent exiting the reboiler, just as it was built in the pilot plant.

However, the high energy content of the lean solvent stream is more than enough to reach the desired temperature of the loaded solvent. Hence, the lean stream could be split, and just a part can be used for that purpose. The remaining split stream could be used for preheating the incoming flue gas. Although multiple heat exchanges are conducted on the lean stream, the remaining energy must be removed by a cold utility to reach the desired 40ºC. However, the amount of cooling utility is not considerable lower than in the initial scenario, and the costs of installing a new heat exchanger for the flue gas preheating are high. Therefore, no particular alteration in the actual heat exchange network is proposed.

5 Summary and conclusions

A simulation model to represent the operation of the Pilot Plant ABIGAIL for CO_2 capture with amine solutions was developed and validated. For the initial operation campaign, a 97.7% correlation index (R^2) was achieved; whereas 97.3% for the optimized operation. An overall 97.5% correlation index (R^2) was found. Therefore, the open loop model is suitable for future simulations of the pilot plant, particularly useful to analyze stationary states, and to conceive modifications in the pilot plant.

Specifically, the temperature profiles in the absorber and stripper match for most of the stationary states. Discrepancies are found when operating at low CO_2 inlet volumetric flows, and low inlet temperatures of the solvent for the absorber; and when the data is retrieved during the warming-up process of the stripper.

The simulated concentration and reaction rate profiles in the absorber show a clear correlation with the temperature profiles, as the maximum temperature could be found somewhere in between the column's height, slightly above the maximum reaction rates. Regarding the stripper, the steepest changes are directly correlated with the operation pressure, as the higher the pressure, the enhanced the desorption percentage and the steepest the concentration changes of the main species.

Some improvements were carried out regarding the operation of the pilot plant, as an additional measuring point to test the load and concentration of the solvent was installed at the outlet of the stripper.

Regarding the overall performance of the absorption and desorption, the L/G ratio, along with $T_{Abs,\ in}$ and P_{Des} were the most influencing variables, as shown during the sensibility analysis, and through the experimentally collected data. It is also clear that a cost-effective operation point could be found without affecting significantly the performance of the capture process. Nevertheless, an analysis over the stripper's performance is still not accurate, as the exit solvent volumetric flow cannot be measured, and the constant volumetric flow assumption throughout the column must

be assumed. Therefore, the computed experimental desorption percentages are not fully reliable. The installation of a flow meter at the exit of the stripper, would definitely enhance its analysis.

A 14.3 € reduction in the daily operation cost could be achieved by operating the pilot plant at L/G= 5.5, $T_{Abs,in}$= 37°C and P_{Des}= 2.03 bar, achieving absorption and desorption percentages above 90% and 60% respectively. No further changes in the heat exchange network should be implemented in the pilot plant.

6 Bibliography

[1] (UNDP), United Nations Development Programme, "Sustainable Development Goals Booklet," in *United Nations Conference on Sustainable Development*, Río de Janeiro, 2012.

[2] Background of the Sustainable Development Goals, "(UNDP) United Nations Development Programme," 2015. [Online]. Available: http://www.undp.org/content/undp/en/home/sustainable-development-goals/background/. [Accessed 15 09 2018].

[3] United Nations, "Kyoto protocol to the United Nations framework," in *Convention on Climate Change*, Kyoto, 1998.

[4] R. Notz, I. Tönnies, N. McCann, G. Scheffknecht and H. Hasse, "CO_2 capture for fossil fuel-fired power plants," *Chemical Engineering Technology,* vol. II, no. 34, pp. 163-172, 2010.

[5] Intergovernmental Panel on Climate Change, "IPCC 2014: Synthesys Report - Fifth Assessment Report of the Intergovernmental Panel on Climate Change," R.K. Pachauri and L.A. Meyer, Geneva, 2014.

[6] Carbon Dioxide Information Analysis Center, "Global CO_2 Emissions from Fossil-Fuel Burning, Cement Manufacture, and Gas Flaring: 1751-2014," Oak Ridge National Laboratory, Oak Ridge, 2014.

[7] C. Dinca, N. Slavu and A. Badea, "Benchmarking of the pre/post-combustion chemical absorption for the CO_2 capture," *Journal of the Energy Institute,* vol. I, no. 91, pp. 445-456, 2018.

[8] Intergovernmental Panel on Climate Change, "IPCC 2014: Chapter 7, Energy Systems - Fifth Assessment Report of the Intergovernmental Panel on Climate Change," Cambridge University Press, New York, 2014.

[9] M. Anwar, A. Fayyaz, N. Sohail, M. Khokhar, M. Baqar, W. Khan, K. Rasool, M. Rehan and A. Nizami, "CO_2 capture and storage: A way forward for sustainable environment," *Journal of Environmental Management,* vol. 226, pp. 131 - 144, 2018.

[10] W. L. Theo, J. S. Lim, H. Hashim, A. A. Mustaffa and W. S. Ho, "Review of pre-combustion capture and ionic liquid in carbon capture and storage," *Applied Energy,* no. 183, pp. 1633-1663, 2016.

[11] S. Mills, "Coal-fired CCS demonstration plants, 2012," © IEA Clean Coal Centre, London, 2012.

[12] International Energy Agency - IEA Greenhouse Gas R&D Programme, "CO_2 capture as a factor in power station investment decisions," IEA Greenhouse Gas R&D Programme, Cheltenham, 2007.

[13] D. Jansenc, M. Gazzani, G. Manzolini, E. van Dijk and M. Carbo, "Pre-combustion CO_2 capture," *International Journal of Greenhouse Gas Control,* vol. 40, p. 167–187, 2015.

[14] D. Leung, G. Caramanna and M. Maroto-Valer, "An overview of current status of carbon dioxide capture and storage technologies," *Renewable and Sustainable Energy Reviews,* no. 39, p. 426–443, 2014.

[15] C. Yin and J. Yan, "Oxy-fuel combustion of pulverized fuels: Combustion fundamentals and modeling," *Applied Energy,* no. 162, pp. 742-762, 2016.

[16] M. B. Toftegaarda, J. Brix, P. A. Jensen, P. Glarborg and A. D.Jensen, "Oxy-fuel combustion of solid fuels," *Progress in Energy and Combustion Science,* vol. 36, no. 5, pp. 581-625, 2010.

[17] L. Chen, S. Z. Yong and A. F.Ghoniem, "Oxy-fuel combustion of pulverized coal: Characterization, fundamentals, stabilization and CFD modeling," *Progress in Energy and Combustion Science,* vol. 38, no. 2, pp. 156-214, 2012.

[18] T. Wall, Y. Liu, C. Spero, L. Elliott, S. Khare, R. Rathnam, F. Zeenathal, B. Moghtaderi, B. Buhre, C. Sheng, R. Gupta, T. Yamada, K. Makino and J. Yuag, "An overview on oxyfuel coal combustion—State of the art research and technology development," *Chemical Engineering Research and Design,* vol. 87, no. 8, pp. 1003-1016, 2009.

[19] B. Metz, O. Davidson, H. Conick, M. Loon and L. Meyer, "IPCC Special Report on Carbon Dioxide Capture and Storage," Cambridge University Press, Cambridge, 2007.

[20] Global Carbon Carbon and Storage Institute, "Milestone Oxyfuel Plant Going into Operation in Hubei, China," Global Carbon Carbon and Storage Institute, 05 05 2016. [Online]. Available: https://www.globalccsinstitute.com/insights/authors//2016/05/05/milestone-oxyfuel-plant-going-operation-hubei-china. [Accessed 30 09 2018].

[21] A. Kazemi and A. Mehrabani-Zeinabad, "Post combustion carbon capture: Does optimization of the processing system based on energy and utility requirements warrant the lowest possible costs?," *Energy, Elsevier,* vol. 112, pp. 353-363, 2016.

[22] D. Aaron and C. Tsouris, "Separation of CO_2 from Flue Gas: A Review," *Separation Science and Technology,* vol. 40, no. 1-3, pp. 321-348, 2005.

[23] L. I. Eide and D. W. Bailey, "Precombustion Decarbonisation Processes," *Oil & Gas Science and Technology,* vol. 60, no. 3, pp. 475 - 484.

[24] D. C. Thomas, Carbon Dioxide Capture for Storage in Deep Geologic Formations: Results from the CO_2 Capture Project, First Edition ed., Amsterdam: Elsevier, 2005.

[25] B. McKee, "Solutions for the 21st Century, Zero Emissions Technologies for Fossil Fuels," International Energy Agency, Paris, 2002.

[26] S.-Y. Oh, M. Binns and H. K. J.-K. Cho, "Energy minimization of MEA-based CO_2 capture process," *Applied Energy,* vol. 169, pp. 353-362, 2016.

[27] H. P. Mangalapally, R. Notz, S. Hoch, N. Asprion, G. Sieder, H. Garcia and H. Hasse, "Pilot plant experimental studies of post combustion CO_2 capture by reactive absorption with MEA and new solvents," *Energy Procedia,* vol. 1, no. 1, pp. 963-970, 2009.

[28] A. Al Hinai and M. Abu Zahra, "Study of novel solvents and 2MAE blends for CO_2 Post-Combustion Capture," *Energy Procedia,* vol. 114, p. 686–692, 2017.

[29] Z. Liang, H. Gao, W. Rongwong and Y. Na, "Comparative studies of stripper overhead vapor integration-based configurations for post-combustion CO_2 capture," *International Journal of Greenhouse Gas Control,* vol. 34, pp. 75-84, 2015.

[30] M. Wang, A. S. Joel, C. Ramshaw, D. Eimer and N. M. Musaa, "Process intensification for post-combustion CO_2 capture with chemical absorption: A critical review," *Applied Energy,* vol. 158, no. 15, pp. 275-291, 2015.

[31] M. Frauenkron, J.-P. Melder, G. Ruider, R. Rossbacher and H. Höke, "Ethanolamines and Propanolamines," in *Ullmann's Encyclopedia of Industrial Chemistry*, Weinheim: Wiley-VCH, 2002.

[32] Aspen Technology, Inc., "Rate-Based Model of the CO_2 Capture Process by MEA using Aspen Plus," Aspen Technology, Inc., Burlington, 2014.

[33] Sigma-Aldrich®, "Products - Ethanolamine," [Online]. Available: https://www.sigmaaldrich.com/catalog/product/aldrich/411000?lang=de&region=DE. [Accessed 14 10 2018].

[34] Chemspider, "Chemspider - 2-Hydroxyethanaminium," [Online]. Available: http://www.chemspider.com/Chemical-Structure.392552.html. [Accessed 14 10 2018].

[35] B. Lv, B. Guo, Z. Zhou and G. Jing, "Mechanisms of CO_2 Capture into Monoethanolamine Solution with Different CO_2 Loading during the Absorption/Desorption Processes," *Environ. Sci. Technol.,* vol. 48, no. 17, p. 10728–10735, 2015.

[36] B. R. Pinsent, L. Pearson and F. J. W. Roughton, "The Kinetics of Combination of Carbon Dioxide with Hydroxide Ions," *Transactions of the Faraday Society,* vol. 52, pp.

1512-1520, 1956.

[37] H. Hikita, S. Asai, H. Ishikawa and M. Honda, "The Kinetics of Reactions of Carbon Dioxide with Monoethanolamine, Diethanolamine, and Trietanolamine by a Rapid Mixing Method," *Chemical Engineering,* vol. 13, pp. 7-12, 1977.

[38] J. Korherr, "First operation of an experimental plant for biogas upgrading via chemical absorption," University of Stuttgart, Stuttgart, 2016.

[39] J. Hilpert, "Operation of an experimental plant for Biogas upgrading via chemical absorption and innovative solvent regeneration," University of Stuttgart, Stuttgart, 2017.

[40] P. Schüle, "Operation of a technical-scale plant for CO_2 capture via chemical absoprtion in a packed column," Stuttgart, 2017.

[41] AspenTech, " Milestones and Innovations," 2018. [Online]. Available: https://www.aspentech.com/en/about-aspentech/milestones-and-innovations. [Accessed 15 10 2018].

[42] AspenTech, "aspenONE Product portfolio," 2018. [Online]. Available: https://www.aspentech.com/en/products/full-product-listing. [Accessed 16 10 2018].

[43] AspenTech, "Aspen Plus," 2018. [Online]. Available: https://www.aspentech.com/en/products/engineering/aspen-plus. [Accessed 16 10 2018].

[44] Aspen Tech, "Aspen Plus V8.6, User Guide - Optimization," 2014.

[45] Aspen Tech, "Aspen Energy Analyzer," 2018. [Online]. Available: https://www.aspentech.com/en/products/pages/aspen-energy-analyzer. [Accessed 17 10 2018].

[46] Y. Yan and C. Chen, "Thermodynamic Modeling of CO_2 Solubility in Aqueous Solutions of NaCl and Na2SO4," *Journal of Supercritical Fluids,* vol. 66, pp. 623-634, 2010.

[47] Y. Zhang and C. Chen, "Thermodynamic Modeling for CO_2 Absorption in Aqueous MDEA Solution with Electrolyte NRTL Model," *Ind. Eng. Chem. Res.,* vol. 50, pp. 176-187, 2011.

[48] J. B. Matthews, J. F. Sumner and E. A. Moelwyn-Hughes, "The Vapor Pressures of Certain Liquids," *Trans. Faraday Soc.,* vol. 46, pp. 797-803, 1950.

[49] S. M. Danov, N. B. Mashin, R. V. Efremov and K. K. Slashchinina, "Vapor Pressure of Ethanol Amines," *Zh. Fiz. Khim.,* vol. 43, pp. 733-736, 1969.

[50] T. E. Daubert, J. W. Jalowka and V. Goren, "Vapor Pressure of 22 Pure Industrial

Chemicals," *AIChE Symp. Ser.,* vol. 83, pp. 128-158, 1987.

[51] K. Tochigi, K. Akimoto, K. Ochi, F. Liu and Y. Kawase, "Isothermal VaporLiquid Equilibria for Water+2-Aminoethanol+Dimethyl Sulfoxide and Its Constituent Three Binary Systems," *J. Chem. Eng. Data,* vol. 44, pp. 588-590, 1999.

[52] Y. Maham, L. G. Hepler, A. E. Mather, A. W. Hakin and R. A. Marriott, "Molar Heat Capacities of Alkanolamines from 299.1 to 397.8K, Group Additivity and Molecular Connectivity Analysis," *J. Chem. Soc. Faraday Trans.,* vol. 93, pp. 1747- 1750, 1997.

[53] L. F. Chiu, H. F. Liu and M. H. Li, "Heat Capacity of Alkanolamines by Differential Scanning Calorimetry," *J. Chem. Eng. Data.,* vol. 33, pp. 631-636, 1999.

[54] F. Murrieta-Guevara and A. Trejo Rodriguez, "A Liquid Density as a Function of Temperature for Five Organic Solvents," *J. Chem. Eng. Data,* vol. 29, no. 29, pp. 204-206, 1984.

[55] M. H. Li and K. P. Shen, "Densities and Solubilities of Solutions of Carbon Dioxide in Water+Monoethanolamine+N-methyldiethanolamine," *J. Chem. Eng. Data,* vol. 37, pp. 288-290, 1992.

[56] A. Valtz, C. Coquelet and D. Richon, "Volumetric Properties of the Monoethamolamine Methanol Mixture at Atmospheric Pressure from 283.15 to 353.15K," *Thermochimica Acta,* vol. 428, pp. 185-191, 2005.

[57] J. Gross and G. Sadowski, "Application of the Perturbed-Chain SAFT Equation of State to Associating Systems," *Ind. Eng. Chem. Res.,* vol. 41, pp. 5510-5515, 2002.

[58] H. Touhara, S. Okazaki, F. Okino, H. Tanaka, K. Ikari and K. Nakanishi, "Thermodynamic Properties of Aqueous Mixtures of Hydrophilic Compounds. 2. Aminoethanol and Its Methyl Derivatives”," *J. Chem. Thermodyn.,* vol. 14, pp. 145-156 , 1982.

[59] A. Nath and F. Bender, "Isothermal Vapor-Liquid Equilibria of Binary and Ternay Mxitures Containing Alcohol, Alkanolamine and Water with a New Static Device," *J. Chem. Eng. Data,* vol. 28, pp. 370-375, 1983.

[60] Z. Cai, R. Xie and Z. Wu, "Binary Isobaric Vapor-Liquid Equilibria of Ethanolamines + Water," *J. Chem. Eng. Data,* vol. 41, pp. 101-1103, 1996.

[61] M. L. P. Posey, "Thermodynamic Model for Acid Gas Loaded Aqueous Alkanolamine Solutions," Austin, 1996.

[62] M. Page, J. Y. Huot and C. Jolicoeur, "A Comprehensive Thermodynamic Investigation of Water-Ethanolamine Mixtures ata 10, 25, and 40 C," *J. Can. J. Chem.,* vol. 71, pp. 1064-1072, 1993.

[63] M. Garcia, H. K. Knuutila and S. Gu, "ASPEN PLUS simulation model for CO2 removal with MEA: Validation of desorption model with experimental data," *Journal of Environmental Chemical Engineering,* vol. 5, p. 4693–4701, 2017.

[64] Y. Lim, J. Kim, J. Jung, C. Lee and C. Han, "Modeling and simulation of CO2 capture process for coal- based power plant using amine solvent in South Korea," *Energy Procedia,* vol. 37, p. 1855–1862, 2013.

[65] H. Ahn, M. Luberti, Z. Liu and S. Brandani, "Process simulation of aqueous MEA plants for postcombustion capture from coal-fired power plants," *Energy Procedia,* vol. 37, p. 1523–1531, 2013.

[66] F. Tobiesen, O. Juliussen and H. Svendsen, "Experimental validation of a rigorous desorber model for post-combustion capture," *Chem. Eng. Sci.,* vol. 63, pp. 2641-2656, 2008.

[67] Y. Zhang and C.-C. Chen, "Modeling CO_2 absorption and desorption by aqueous monoethanolamine solution with aspen rate-based model," vol. 37, p. 1584–1596, 2013.

[68] M. Saimpert, G. Puxty, S. Qureshi, L. Wardhaugh and A. Cousins, "A new rate based absorber and desorber modelling tool," *Chem. Eng. Sci.,* vol. 96, pp. 10-25, 2013.

[69] N. Mac Dowell, N. Samsatli and N. Shah, "Dynamic modelling and analysis of an amine-based post-combustion CO_2 capture absorption column," *Int. J. Greenh. Gas Control,* vol. 12, pp. 247-258, 2013.

[70] N. Mac Dowell and N. Shah, "The multi-period optimisation of an amine-based CO_2 capture process integrated with a super-critical coal-fired power station for flexible operation," *Comput. Chem. Eng.,* vol. 74, pp. 169-183, 2015.

[71] N. Mac Dowell and N. Shah, "Dynamic modelling and analysis of a coal-fired power plant integrated with a novel split-flow configuration post-combustion CO_2 capture process," *Int. J. Greenh. Gas Control,* vol. 27, pp. 103-119, 2014.

[72] L. Øi and S. Kvam, "Comparison of energy consumption for different CO_2 ab- sorption configurations using different simulation tools".

[73] N. Enaasen, L. Zangrilli, A. Mangiaracina, T. Mejdell, H. Kvamsdal and M. Hillestad, "Validation of a dynamic model of the brindisi pilot plant," *Energy Procedia,* vol. 63, pp. 1040-1054, 2014.

[74] I. von Harbou, M. Imle and H. Hasse, "Modeling and simulation of reactive absorption of CO2 with MEA: Results for four different packings on two different scales," *Chem. Eng. Sci.,* vol. 105, p. 179–190, 2014.

[75] S. Gardarsdóttir, F. Normann, K. Andersson, K. Prölß, S. Emilsdóttir and F. Johnsson, "Post-combustion CO2 capture applied to a state-of-the-art coal-fired power plant- The influence of dynamic process conditions," *Int. J. Greenh. Gas Control 33 (2015) 51–62.*

[76] T. Nagy and P. Mizsey, "Model verification and analysis of the CO2-MEA absorber/desorber system," *Int. J. Greenh. Gas Control,* vol. 39, pp. 236-244, 2015.

[77] B.-H. Li, N. Zhang and R. Smith, "Simulation and analysis of CO2 capture process with aqueous monoethanolamine solution," *Appl. Energy,* vol. 161, p. 707–717, 2015.

[78] R. Notz, H. Mangalapally and H. Hasse, "Post combustion CO_2 capture by reactive absorption: pilot plant description and results of systematic studies with MEA," *Int. J. Greenh. Gas Control 6 (2012) 84–112,* vol. 6, pp. 84-112, 2012.

[79] M. Akram, U. Ali, T. Best, S. Blakey, K. Finney and M. Pourkashanian, "Performance evaluation of PACT Pilot-plant for CO_2 capture from gas turbines with Exhaust Gas Recycle," *Int. J. Greenh. Gas Control,* vol. 47, pp. 137-150, 2016.

[80] N. Abdul Manaf, A. Cousins, P. Feron and A. Abbas, "Dynamic modelling, identification and preliminary control analysis of an amine-based post-combustion CO_2 capture pilot plant," *J. Clean. Prod.,* vol. 113, pp. 635-653, 2016.

[81] J. Gaspar, L. Ricardez-Sandoval, J. Jorgensen and P. Fosb, "Dynamic simulation and analysis of a pilot-scale CO2 post-combustion capture unit using piperazine and MEA," *IFAC-PapersOnLine,* vol. 49, pp. 645-650, 2016.

[82] J. Gaspar and P. Fosbøl, "Simulation and multivariable optimization of post-combustion capture using piperazine," *Int. J. Greenh. Gas Control,* vol. 49, p. 227–238, 2016.

[83] J. Gaspar, L. Ricardez-Sandoval, J. Jorgensen and P. Fosbol, "Controllability and flexibility analysis of CO2 post-combustion capture using piperazine and MEA," *Int. J. Greenh. Gas Control,* vol. 51, p. 276–289, 2016.

[84] A. Chinen, J. Morgan, B. Omell, D. Bhattacharyya and D. Miller, "Dynamic data reconciliation and model validation of a MEA-Based CO2 capture system using pilot plant data," *IFAC-PapersOnLine,* vol. 49, p. 639–644, 2016.

[85] S. Aromada and L. Oi, "Simulation of improved absorption configurations for CO2 capture," in *Proceedings of the 56th SIMS*, Linköping, 2015.

[86] Expresszuschnitt, "PLEXIGLAS® Platten im Zuschnitt," Expresszuschnitt, [Online]. Available: https://expresszuschnitt.de/PLEXIGLAS?gclid=CjwKCAjwx7DeBRBJEiwA9MeX_AGqYVWoDpuBR0yq8Z1Qp0U3irt83PHq1uHTdLXgF1lDB9hSqAgfXhoCNGMQAvD_BwE. [Accessed 21 10 2018].

[87] rvt, "Plastic, Hiflow® ring 15-7," 2015. [Online]. Available: https://rvtpe.com/wp-content/uploads/2015/03/HR-15-7-PP1.pdf. [Accessed 21 10 2018].

[88] rvt, "Raflux ring 15-3 metal," 2013. [Online]. Available: https://rvtpe.com/wp-content/uploads/2013/01/RR-15-3-stainl-steel.pdf. [Accessed 21 10 2018].

[89] N. Instruments, "What Is LabVIEW?," 2018. [Online]. Available: http://www.ni.com/en-us/shop/labview.html. [Accessed 23 10 2018].

[90] Y.-C. Chang, "Potentiometric Titration of Free Amine and Amine Carbonate in Carbonated Monoethanolamine Solutions," *Anal. Chem.,* vol. 30, no. 6, pp. 1095-1097, 1958.

[91] C. Kunze and H. Spliethoff, "Assessment of oxy-fuel, pre- and post-combustion-based carbon capture for future IGCC plants," *Applied Energy,* vol. 94, pp. 109-116, 2012.

Annexes

Annex A: Complete list of instruments and operation units of the ABIGAIL pilot plant

Operation Units	
Abbreviation	**Description**
ABS-1	Packed absorption column
BE-1	Solvent storage tank and stripper reboiler
DES-1	Packed stripping column
GE-1	Compressor for gas recirculation and feed
KO-1	Phase separator for stripper's exhaust gas
NW-1	Water rinsing device for recirculated gas to the absorber
P-1	Rich solvent transport pump from the absorber to the stripper
P-2	Lean solvent transport pump from tank to the top of the absorber
P-3	Liquid recirculation pump for condensed part of loaded gas
P-4	Stripper's outflow pump
P-5	Pump for water recirculation in the water rinsing device
WT-1	Heat exchanger between lean and rich MEA streams
WT-2	Cooler prior to the absorber's input
WT-3	Cooler from CO_2 loaded gas at the top of the stripper
Instruments	
F-L1	Rich MEA Flow meter
F-L2	Lean MEA Flow meter
P-AK	Absorber's top stage pressure gauge
P-AS1	Absorber's gas inflow pressure gauge
P-AS2	Absorber's bottom stage pressure gauge
P-CO2	Pressure gauge at the CO_2 loaded gas line
P-D	Stripper's top stage pressure gauge
PV-D1	Tank's top part pressure gauge
PV-D2	Tank's bottom part pressure gauge
P-P1	Outlet P-1 pressure gauge
P-P2	Outlet P-3 pressure gauge
P-P3	Outlet P-1 pressure gauge, inlet of recycled gas to the stripper
P-Rezi	Gas recirculation line pressure gauge
P-RG	Cleansed gas line pressure gauge
T-A1	Absorber's stage thermocouple
T-A2	Absorber's stage thermocouple
T-A3	Absorber's stage thermocouple
T-A4	Absorber's stage thermocouple
T-Aein	Absorber's inflow thermocouple
T-AS	Absorber's bottom stage thermocouple
T-CO2	Stripper´s exhaust gas thermocouple
T-D1	Stripper's stage thermocouple
T-D2	Stripper's stage thermocouple
T-D3	Stripper's stage thermocouple
T-D4	Stripper's stage thermocouple

T-D5	Stripper's stage thermocouple
T-D6	Stripper's stage thermocouple
T-Dein	Stripper's inflow thermocouple
T-DS	Stripper's bottom stage thermocouple
T-Kü1	Inflow refrigerant thermocouple
T-Kü2	Outflow refrigerant thermocouple
T-Kun	Stripper's recycle inflow thermocouple
T-RG	Absorber's gas outflow thermocouple
T-SG	Stripper's gas recycle thermocouple
TV-D1	Tank's top part thermocouple
TV-D2	Tank's bottom part thermocouple
TW-Tl1	Heat exchanger's lean inflow thermocouple
TW-Tl2	Heat exchanger's lean outflow thermocouple
TW-Tr1	Heat exchanger's rich inflow thermocouple
TW-Tr2	Heat exchanger's rich outflow thermocouple
yCO2-1	Cleansed gas CO_2 monitor
yCO2-Rezi	Recycled gas CO_2 monitor

Annex B: Summary of the real averaged measured parameters for every run

The number of the experimental runs start on the 127, as that represents the overall operation point of the pilot plant since it was built.

	Run Number – First Experimental Campaign									
Measured parameter	**127**	**128**	**129**	**130**	**131**	**132**	**133**	**134**	**135**	**136**
F-L2 [l/h]	140,1	139,7	139,9	140,0	140,1	140,0	140,0	140,0	140,0	140,0
F-L1[l/h]	156,0	154,9	155,1	155,8	150,5	154,2	153,4	165,2	158,2	148,5
FL ideal normal [l/h]	140,0	140,0	140,0	140,0	140,0	140,0	140,0	140,0	140,0	140,0
FL Upper ideal [l/h]	140,0	140,0	140,0	140,0	140,0	140,0	140,0	140,0	140,0	140,0
FL Lower ideal[l/h]	140,0	140,0	140,0	140,0	140,0	140,0	140,0	140,0	140,0	140,0
Psoll [kWh]	10,7	10,7	10,7	10,7	10,7	10,7	10,7	10,7	10,7	10,7
T-Bgein [°C]	41,5	43,2	49,2	54,2	49,3	42,7	38,9	39,4	44,3	49,1
T-AS [°C]	37,8	38,8	44,1	53,1	49,5	45,4	40,5	41,3	40,9	43,9
T-A1 [°C]	51,2	57,4	63,0	65,6	66,0	66,7	66,2	69,3	68,1	66,2
T-A2 [°C]	47,9	58,3	68,4	71,1	73,3	74,7	73,3	74,5	68,7	72,9
T-A3 [°C]	47,0	54,4	68,0	71,8	74,5	74,0	72,1	69,2	57,3	73,3
T-A4 [°C]	39,2	42,2	51,2	57,3	53,6	52,2	40,9	38,0	42,4	49,7
T-Aein [°C]	37,6	39,8	45,8	50,3	45,1	39,0	34,9	35,5	40,3	45,0
T-RG [°C]	39,5	43,7	55,2	61,7	56,3	51,4	42,3	38,7	43,0	50,3
T-WTr1 [°C]	41,7	44,4	48,4	54,3	52,7	51,0	49,0	51,3	51,0	51,7
T-WTr2 [°C]	99,9	103,4	103,1	103,4	105,6	104,6	150,0	150,0	150,0	117,4
T-WTl1 [°C]	108,9	111,6	110,8	112,4	115,8	115,4	115,9	117,0	117,1	117,6
T-WT2 [°C]	52,0	54,8	58,8	63,7	64,2	62,1	60,2	60,9	61,6	63,5
T-VD1 [°C]	113,7	118,8	117,5	117,7	119,3	117,7	118,2	119,0	119,2	119,8
T-VD2 [°C]	115,2	118,9	117,5	117,7	119,4	118,2	118,6	119,4	119,8	120,2
T-SG [°C]	114,4	118,3	117,1	117,4	118,8	116,9	117,3	118,2	118,4	118,4
T-DS [°C]	112,9	117,1	116,7	117,0	118,6	116,1	116,3	117,2	117,6	118,3
T-D1 [°C]	103,2	111,7	115,8	115,3	117,9	115,8	116,0	116,9	117,4	118,0
T-D2 [°C]	98,5	105,5	115,6	114,3	117,8	115,5	115,6	116,5	117,0	117,7
T-D3 [°C]	97,2	101,4	112,6	110,6	115,3	112,4	112,3	113,4	114,1	114,9

T-D4 [°C]	98,0	101,7	111,0	108,9	114,6	111,1	110,8	112,0	113,0	113,7
T-D5 [°C]	95,5	99,1	106,1	104,3	110,5	106,8	106,1	107,6	108,9	109,5
T-D6 [°C]	98,5	102,2	105,4	105,4	109,4	106,2	105,9	107,4	108,9	109,7
T-Kond [°C]	33,0	35,0	44,2	22,7	23,8	23,6	23,3	23,2	23,2	23,4
T-Dein [°C]	98,7	102,4	102,8	103,5	106,2	104,0	103,6	103,6	104,7	106,0
TCO2 [°C]	77,8	80,4	89,5	87,9	93,2	90,9	89,3	90,1	91,2	91,6
p-Amb [bar]	1,0	1,0	1,0	1,0	1,0	1,0	1,0	1,0	1,0	1,0
p-Bgein [bar]	0,0	0,0	0,0	0,0	0,0	0,0	0,0	0,0	0,0	0,0
p-AS2 [bar]	1,0	1,0	1,0	1,0	1,0	1,0	1,0	1,0	1,0	1,0
p-AS1 [bar]	1,0	1,0	1,0	1,0	1,0	1,0	1,0	1,0	1,0	1,0
Delta p AS [bar]	0,0	0,0	0,0	0,0	0,0	0,0	0,0	0,0	0,0	0,0
p-AK [bar]	1,0	1,0	1,0	1,0	1,0	1,0	1,0	1,0	1,0	1,0
p-RG [bar]	1,0	1,0	1,0	1,0	1,0	1,0	1,0	1,0	1,0	1,0
p-CO2 [bar]	1,0	1,0	1,0	1,0	1,0	1,0	1,0	1,0	1,0	1,0
p-P1 [bar]	2,4	2,6	2,3	2,3	2,4	2,3	2,3	2,4	2,3	2,4
p-D [bar]	1,9	2,0	1,8	1,8	1,8	1,7	1,8	1,8	1,8	1,9
p-VD2 [bar]	1,9	2,0	1,8	1,8	1,8	1,7	1,7	1,8	1,8	1,8
p-VD1 [bar]	2,0	2,1	1,8	1,8	1,9	1,8	1,8	1,9	1,9	1,9
Delta p VD[bar]	0,1	0,1	0,1	0,1	0,1	0,1	0,1	0,1	0,1	0,1
p-P2 [bar]	1,4	1,3	1,3	1,3	1,3	1,3	1,3	1,3	1,3	1,3
p-P3 [bar]	1,9	2,0	1,8	1,8	1,9	1,7	1,8	1,8	1,9	1,9
y-CO2 1 [%v/v]	11,0	9,0	5,5	4,7	2,5	1,5	2,0	1,5	2,3	2,0
y O2 1 [%v/v]	0,0	0,0	0,0	0,0	0,0	0,0	0,0	0,0	0,0	0,0
y-CO2 2 [%v/v]	0,0	0,0	0,0	0,0	0,0	0,0	0,0	0,0	0,0	0,0
y -O2 2 [%v/v]	0,0	0,0	0,0	0,0	0,0	0,0	0,0	0,0	0,0	0,0
y-CO2 Rezi [%v/v]	16,8	16,1	14,6	15,0	14,6	15,0	15,3	14,9	15,5	14,7
y - O2 Rezi [%v/v]	0,0	0,0	0,0	0,0	0,0	0,0	0,0	0,0	0,0	0,0
ideal CO2 (MFC)	1,7	5,6	41,5	88,1	59,8	91,3	89,2	78,4	76,3	81,6
real CO2 (MFC)	0,2	0,2	10,4	22,2	16,7	25,6	25,0	19,2	18,1	19,3
ideal N2 (MFC)	93,7	89,8	73,5	26,3	67,4	35,9	38,0	32,5	31,4	26,1
real N2 (MFC)	96,5	95,6	105,9	93,6	112,6	103,0	103,5	93,1	90,9	89,7
GS-TB	0,0	0,0	0,0	0,0	0,0	0,0	0,0	0,0	0,0	0,0

GS-AK	0,0	0,0	0,0	0,0	0,0	0,0	0,0	0,0	0,0	0,0
GS-AS	1,0	1,0	1,0	1,0	1,0	1,0	1,0	1,0	1,0	1,0
GS-VD-P	0,0	0,0	0,0	0,0	0,0	0,0	0,0	0,0	0,0	0,0
GS-VD-HF	0,0	0,0	0,0	0,0	0,0	0,0	0,0	0,0	0,0	0,0
Ideal P2 [l/h]	140,0	140,0	140,0	140,0	140,0	140,0	140,0	140,0	140,0	140,0
Ideal P1 [l/h]	140,0	140,0	140,0	140,0	140,0	140,0	140,0	140,0	140,0	140,0
p Recy [bar]	1,0	1,0	1,0	1,0	1,1	1,1	1,1	1,0	1,0	1,0
T Recy [°C]	29,7	32,0	36,8	45,9	41,6	37,2	30,7	30,4	29,4	35,3
V Recy [m^3/h]	32,8	33,1	33,6	36,3	30,0	28,9	27,7	24,8	24,2	23,7
V Recy norm [m^3/h]	28,6	28,6	28,3	28,6	25,0	25,1	24,9	22,0	21,3	20,5
% Comp. Performance	32,0	32,0	32,0	32,0	32,0	32,0	32,0	28,0	23,0	23,0
T-Cool 1	3,3	3,3	3,6	3,0	2,8	2,7	2,4	2,5	2,5	2,6
T-Cool 2	8,4	9,5	13,1	10,4	15,4	12,4	11,1	11,5	12,0	12,3
L/G real [l/m^3]	4,3	4,2	4,2	3,9	4,7	4,9	5,0	5,6	5,8	5,9
L/G norm [l/m^3]	4,7	4,7	4,6	4,4	5,2	5,3	5,4	6,1	6,3	6,5

Measured Parameters	137	138	139	140	141	142	143	144	145
F-L2 [l/h]	140,0	140,0	140,0	139,8	139,9	140,1	140,0	140,0	140,0
F-L1[l/h]	151,3	152,4	164,5	161,3	159,5	156,2	157,2	157,6	156,6
FL ideal normal [l/h]	140,0	140,0	140,0	140,0	140,0	140,0	140,0	140,0	140,0
FL Upper ideal [l/h]	140,0	140,0	140,0	140,0	140,0	140,0	140,0	140,0	140,0
FL Lower ideal[l/h]	140,0	140,0	140,0	140,0	140,0	140,0	140,0	140,0	140,0
Psoll [kWh]	10,6	10,6	10,6	10,6	10,6	10,6	10,6	10,6	10,6
T-Bgein [°C]	43,8	45,3	46,4	49,6	49,0	48,7	36,5	38,7	39,5
T-AS [°C]	45,3	45,5	47,1	49,4	51,0	52,1	51,6	46,4	45,9
T-A1 [°C]	59,9	62,4	65,6	65,0	63,3	63,4	62,5	63,6	66,1
T-A2 [°C]	64,1	64,7	72,8	73,0	68,1	71,3	71,2	72,7	73,9
T-A3 [°C]	56,6	61,8	62,2	73,2	68,1	72,3	72,7	72,3	71,3
T-A4 [°C]	51,4	50,3	53,4	59,5	59,0	63,1	50,1	48,1	42,5
T-Aein [°C]	40,3	41,4	42,9	46,1	45,2	44,9	34,0	35,1	35,3
T-RG [°C]	46,1	44,8	49,1	53,2	52,6	55,8	50,1	46,9	42,6
T-WTr1 [°C]	48,6	50,2	52,6	53,9	54,3	53,5	53,4	51,4	52,5
T-WTr2 [°C]	103,7	104,0	150,0	150,0	150,0	150,0	150,0	43,7	98,7
T-WTl1 [°C]	115,3	115,6	115,9	116,5	116,9	116,5	116,2	115,5	115,7
T-WT2 [°C]	59,9	61,4	62,2	63,3	63,9	63,7	63,6	61,6	62,5
T-VD1 [°C]	119,9	120,8	121,4	121,5	121,7	122,2	122,8	122,1	122,0
T-VD2 [°C]	121,1	120,8	121,4	121,6	121,8	122,5	123,0	122,5	122,2
T-SG [°C]	120,7	120,4	121,1	121,4	121,4	121,8	121,7	120,8	120,7
T-DS [°C]	120,0	120,3	120,7	120,8	120,9	121,1	121,2	120,6	120,4
T-D1 [°C]	116,0	118,7	119,4	119,7	119,9	120,4	120,7	120,2	120,1
T-D2 [°C]	111,5	118,1	119,0	119,3	119,6	119,8	120,0	119,6	119,6
T-D3 [°C]	104,1	114,5	115,5	116,0	116,6	116,6	116,3	115,9	116,2
T-D4 [°C]	103,5	112,9	114,0	114,6	115,4	115,1	114,2	113,6	114,3
T-D5 [°C]	101,2	107,8	109,0	109,6	111,0	110,3	108,7	109,1	109,8
T-D6 [°C]	104,6	107,6	109,1	109,6	111,4	109,8	108,3	108,4	109,3
T-Kond [°C]	26,1	24,8	25,2	25,4	25,5	25,7	25,9	25,7	25,6
T-Dein [°C]	104,4	104,8	106,7	107,1	107,5	107,9	107,8	106,8	106,8
TCO2 [°C]	80,8	87,4	89,3	89,6	91,0	89,8	88,3	88,6	89,1

p-Amb [bar]	1,0	1,0	1,0	1,0	1,0	1,0	1,0	1,0	1,0
p-Bgein [bar]	0,0	0,0	0,0	0,0	0,0	0,0	0,0	0,0	0,0
p-AS2 [bar]	1,0	1,0	1,0	1,0	1,0	1,0	1,0	1,0	1,0
p-AS1 [bar]	1,0	1,0	1,0	1,0	1,0	1,0	1,0	1,0	1,0
Delta p AS [bar]	0,0	0,0	0,0	0,0	0,0	0,0	0,0	0,0	0,0
p-AK [bar]	1,0	1,0	1,0	1,0	1,0	1,0	1,0	1,0	1,0
p-RG [bar]	1,0	1,0	1,0	1,0	1,0	1,0	1,0	1,0	1,0
p-CO2 [bar]	1,0	1,0	1,0	1,0	1,0	1,0	1,0	1,0	1,0
p-P1 [bar]	2,6	2,5	2,6	2,6	2,5	2,5	2,6	2,6	2,6
p-D [bar]	2,1	2,0	2,0	2,0	2,0	2,0	2,1	2,0	2,0
p-VD2 [bar]	2,1	2,0	2,0	2,0	2,0	2,0	2,1	2,0	2,0
p-VD1 [bar]	2,2	2,1	2,1	2,1	2,1	2,1	2,1	2,1	2,0
Delta p VD[bar]	0,1	0,1	0,1	0,1	0,1	0,1	0,1	0,1	0,1
p-P2 [bar]	1,3	1,3	1,3	1,3	1,3	1,3	1,3	1,3	1,3
p-P3 [bar]	2,1	2,0	2,0	2,0	2,0	2,1	2,1	2,0	2,0
y-CO2 1 [%v/v]	7,1	4,6	2,6	2,5	3,4	3,5	2,6	1,6	1,5
y O2 1 [%v/v]	0,0	0,0	0,0	0,0	0,0	0,0	0,0	0,0	0,0
y-CO2 2 [%v/v]	0,0	0,0	0,0	0,0	0,0	0,0	0,0	0,0	0,0
y -O2 2 [%v/v]	0,0	0,0	0,0	0,0	0,0	0,0	0,0	0,0	0,0
y-CO2 Rezi [%v/v]	15,3	13,8	14,9	14,7	14,2	14,7	15,2	15,4	15,6
y - O2 Rezi [%v/v]	0,0	0,0	0,0	0,0	0,0	0,0	0,0	0,0	0,0
ideal CO2 (MFC)	35,6	18,9	49,9	57,0	70,6	82,1	82,4	83,0	71,2
real CO2 (MFC)	7,3	2,1	7,7	8,8	13,0	17,2	17,3	15,5	11,1
ideal N2 (MFC)	59,6	65,7	21,7	14,6	14,0	13,1	12,8	1,6	0,4
real N2 (MFC)	89,1	82,5	64,9	63,8	72,6	79,2	79,2	70,3	61,5
GS-TB	0,0	0,0	0,0	0,0	0,0	0,0	0,0	0,0	0,0
GS-AK	0,0	0,0	0,0	0,0	0,0	0,0	0,0	0,0	0,0
GS-AS	1,0	1,0	1,0	1,0	1,0	1,0	1,0	1,0	1,0
GS-VD-P	0,0	0,0	0,0	0,0	0,0	0,0	0,0	0,0	0,0
GS-VD-HF	0,0	0,0	0,0	0,0	0,0	0,0	0,0	0,0	0,0
Ideal P2 [l/h]	140,0	140,0	140,0	140,0	140,0	140,0	140,0	140,0	140,0
Ideal P1 [l/h]	140,0	140,0	140,0	140,0	140,0	140,0	140,0	140,0	140,0

p Recy [bar]	1,0	1,0	1,0	1,0	1,0	1,0	1,0	1,1	1,0
T Recy [°C]	37,4	36,0	37,0	40,3	41,7	43,5	43,3	36,8	35,8
V Recy [m^3/h]	34,6	30,5	26,2	26,9	31,8	35,4	35,0	29,5	24,7
V Recy norm [m^3/h]	28,5	25,3	21,8	21,8	25,4	28,3	28,6	25,3	21,2
% Comp. Performance	32,0	32,0	32,0	32,0	32,0	32,0	32,0	32,0	32,0
T-Cool 1	3,1	3,1	3,0	3,0	3,1	3,0	3,2	3,3	3,3
T-Cool 2	9,7	12,0	12,4	12,7	13,2	12,8	12,8	12,9	13,1
L/G real [l/m^3]	4,0	4,6	5,3	5,2	4,4	4,0	4,0	4,7	5,7
L/G norm [l/m^3]	4,6	5,2	6,0	5,9	5,1	4,5	4,5	5,2	6,2

Annex C: Parameters of every operation unit and input stream for every run

The following annex presents the required input and main outputs of every operation unit from the open loop flow sheet for each run. The specified parameters are highlighted in blue, and the black-written parameters are part of the outputs for every unit.

Heat Exchangers - Specifications and main outputs: First Experimental Campaign										
	127		128		129		130		131	
Name	**WT-1**	**WT-2**	**WT-1**	**WT-2**	**WT-1**	**WT-2**	**WT-1**	**WT-2**	**WT-1**	**WT-2**
Property method	ENRTL-RK	ENRTL-RK	ENRTL-RK	ENRTL-RK	ENRTL-RK	ENRTL-RK	ENRTL-RK	ENRTL-RK	ENRTL-RK	ENRTL-RK
Henry's component list ID	GLOBAL	GLOBAL	GLOBAL	GLOBAL	GLOBAL	GLOBAL	GLOBAL	GLOBAL	GLOBAL	GLOBAL
Electrolyte chemistry ID	MEA-CHEM	MEA-CHEM	MEA-CHEM	MEA-CHEM	MEA-CHEM	MEA-CHEM	MEA-CHEM	MEA-CHEM	MEA-CHEM	MEA-CHEM
Use true species approach for electrolytes	YES	YES	YES	YES	YES	YES	YES	YES	YES	YES
Free-water phase properties method	STEAM-TA	STEAM-TA	STEAM-TA	STEAM-TA	STEAM-TA	STEAM-TA	STEAM-TA	STEAM-TA	STEAM-TA	STEAM-TA
Water solubility method	3	3	3	3	3	3	3	3	3	3
Specified pressure [bar]	2,3	1,3	2,3	1,3	2,3	1,3	2,3	1,3	2,3	1,3
Specified temperature [C]	98,7	37,6	102,4	39,8	102,8	45	103,5	50,3	106,2	45,1
Calculated pressure [bar]	2,30	1,30	2,30	1,30	2,30	1,30	2,30	1,30	2,30	1,30
Calculated temperature [C]	100,00	39,80	102,40	45,80	102,80	45,00	103,50	50,30	100,00	45,10
Calculated vapor fraction	0,00	0,00	0,00	0,00	0,00	0,00	0,00	0,00	0,00	0,00
Calculated heat duty [kW]	7,62	-10,74	7,45	-9,83	7,31	-9,95	7,35	-9,15	6,72	-9,94
Net duty [kW]	7,62	-10,74	7,45	-9,83	7,31	-9,95	7,35	-9,15	6,72	-9,94
First liquid / total liquid	1,00E+00	1,00E+00	1,00E+00	1,00E+00	1,00E+00	1,00E+00	1,00E+00	1,00E+00	1,00E+00	1,00E+00
Total feed stream CO_2 flow [kg/hr]	3,30E-05	0,00E+00	5,07E-05	0,00E+00	5,80E-05	0,00E+00	5,75E-05	0,00E+00	6,21E-05	0,00E+00
Total product stream CO_2 flow [kg/hr]	2,17E-03	0,00E+00	3,01E-03	0,00E+00	3,23E-03	0,00E+00	3,40E-03	0,00E+00	2,63E-03	0,00E+00
Net stream CO_2 production [kg/hr]	2,14E-03	0,00E+00	2,96E-03	0,00E+00	3,18E-03	0,00E+00	3,34E-03	0,00E+00	2,57E-03	0,00E+00
Utility CO_2 production [kg/hr]	0,00E+00	0,00E+00	0,00E+00	0,00E+00	0,00E+00	0,00E+00	0,00E+00	0,00E+00	0,00E+00	0,00E+00
Total CO_2 production [kg/hr]	2,14E-03	0,00E+00	2,96E-03	0,00E+00	3,18E-03	0,00E+00	3,34E-03	0,00E+00	2,57E-03	0,00E+00
Utility usage [kg/hr]		2,30E+03		2,11E+03		2,13E+03		1,96E+03		2,13E+03
Utility cost [$/sec]		1,05E-03		9,59E-04		9,71E-04		8,93E-04		9,70E-04
Utility ID		WT-2		WT-2		WT-2		WT-2		WT-2

Heat Exchangers - Specifications and main outputs: First Experimental Campaign										
	132		133		134		135		136	
Name	**WT-1**	**WT-2**	**WT-1**	**WT-2**	**WT-1**	**WT-2**	**WT-1**	**WT-2**	**WT-1**	**WT-2**

Property method	ENRTL-RK	ENRTL-RK	ENRTL-RK	ENRTL-RK	ENRTL-RK	ENRTL-RK	ENRTL-RK	ENRTL-RK	ENRTL-RK	ENRTL-RK
Henry's component list ID	GLOBAL	GLOBAL	GLOBAL	GLOBAL	GLOBAL	GLOBAL	GLOBAL	GLOBAL	GLOBAL	GLOBAL
Electrolyte chemistry ID	MEA-CHEM	MEA-CHEM	MEA-CHEM	MEA-CHEM	MEA-CHEM	MEA-CHEM	MEA-CHEM	MEA-CHEM	MEA-CHEM	MEA-CHEM
Use true species approach for electrolytes	YES	YES	YES	YES	YES	YES	YES	YES	YES	YES
Free-water phase properties method	STEAM-TA	STEAM-TA	STEAM-TA	STEAM-TA	STEAM-TA	STEAM-TA	STEAM-TA	STEAM-TA	STEAM-TA	STEAM-TA
Water solubility method	3	3	3	3	3	3	3	3	3	3
Specified pressure [bar]	2,3	1,3	2,3	1,3	2,3	1,3	2,3	1,3	2,3	1,3
Specified temperature [C]	104	39,1	103,6	35	103,6	35,5	104,7	40,31	106	45,1
Calculated pressure [bar]	2,30	1,30	2,30	1,30	2,30	1,30	2,30	1,30	2,30	1,30
Calculated temperature [C]	104,00	39,10	103,60	35,00	103,60	35,50	104,70	40,31	106,00	45,10
Calculated vapor fraction	0,00	0,00	0,00	0,00	0,00	0,00	0,00	0,00	0,00	0,00
Calculated heat duty [kW]	7,14	-10,84	7,53	-11,47	7,32	-11,39	7,19	-10,66	7,00	-9,94
Net duty [kW]	7,14	-10,84	7,53	-11,47	7,32	-11,39	7,19	-10,66	7,00	-9,94
First liquid / total liquid	1,00E+00	1,00E+00	1,00E+00	1,00E+00	1,00E+00	1,00E+00	1,00E+00	1,00E+00	1,00E+00	1,00E+00
Total feed stream CO_2 flow [kg/hr]	5,67E-05	0,00E+00	3,89E-05	0,00E+00	4,53E-05	0,00E+00	3,85E-05	0,00E+00	4,99E-05	0,00E+00
Total product stream CO_2 flow [kg/hr]	2,70E-03	0,00E+00	2,29E-03	0,00E+00	2,36E-03	0,00E+00	1,84E-03	0,00E+00	2,15E-03	0,00E+00
Net stream CO_2 production [kg/hr]	2,64E-03	0,00E+00	2,25E-03	0,00E+00	2,31E-03	0,00E+00	1,81E-03	0,00E+00	2,10E-03	0,00E+00
Utility CO_2 production [kg/hr]	0,00E+00	0,00E+00	0,00E+00	0,00E+00	0,00E+00	0,00E+00	0,00E+00	0,00E+00	0,00E+00	0,00E+00
Total CO_2 production [kg/hr]	2,64E-03	0,00E+00	2,25E-03	0,00E+00	2,31E-03	0,00E+00	1,81E-03	0,00E+00	2,10E-03	0,00E+00
Utility usage [kg/hr]		2,32E+03		2,46E+03		2,44E+03		2,28E+03		2,13E+03
Utility cost [$/sec]		1,06E-03		1,12E-03		1,11E-03		1,04E-03		9,70E-04
Utility ID		WT-2		WT-2		WT-2		WT-2		WT-2

Pump - Specifications and main outputs: Fist experimental campaign

	127	128	129	130	131	132	133	134	135	136
Name	**P-1**	**P-1**	**P-1**	**P-1**	**P-1**	**P-1**	**P-1**	**P-1**	**P-1**	**P-1**
Property method	ENRTL-RK	ENRTL-RK	ENRTL-RK	ENRTL-RK	ENRTL-RK	ENRTL-RK	ENRTL-RK	ENRTL-RK	ENRTL-RK	ENRTL-RK

Henry's component list ID	GLOBAL	GLOBAL	GLOBAL	GLOBAL	GLOBAL	GLOBAL	GLOBAL	GLOBAL	GLOBAL	GLOBAL
Electrolyte chemistry ID	MEA-CHEM	MEA-CHEM	MEA-CHEM	MEA-CHEM	MEA-CHEM	MEA-CHEM	MEA-CHEM	MEA-CHEM	MEA-CHEM	MEA-CHEM
Use true species approach for electrolytes	YES	YES	YES	YES	YES	YES	YES	YES	YES	YES
Free-water phase properties method	STEAM-TA	STEAM-TA	STEAM-TA	STEAM-TA	STEAM-TA	STEAM-TA	STEAM-TA	STEAM-TA	STEAM-TA	STEAM-TA
Water solubility method	3	3	3	3	3	3	3	3	3	3
Specified discharge pressure [bar]	2,41	2,41	2,41	2,41	2,41	2,41	2,41	2,41	2,41	2,41
Fluid power [kW]	5,66E-03	5,64E-03	5,61E-03	5,57E-03	5,58E-03	5,67E-03	5,68E-03	5,69E-03	5,69E-03	5,67E-03
Calculated brake power [kW]	1,91E-02	1,91E-02	1,90E-02	1,88E-02	1,89E-02	1,92E-02	1,92E-02	1,92E-02	1,92E-02	1,92E-02
Electricity [kW]	1,91E-02	1,91E-02	1,90E-02	1,88E-02	1,89E-02	1,92E-02	1,92E-02	1,92E-02	1,92E-02	1,92E-02
Volumetric flow rate [cum/hr]	1,40E-01	1,40E-01	1,39E-01	1,38E-01	1,38E-01	1,41E-01	1,41E-01	1,41E-01	1,41E-01	1,41E-01
Calculated discharge pressure [bar]	2,41E+00	2,41E+00	2,41E+00	2,41E+00	2,41E+00	2,41E+00	2,41E+00	2,41E+00	2,41E+00	2,41E+00
Calculated pressure change [bar]	1,45E+00	1,45E+00	1,45E+00	1,45E+00	1,45E+00	1,45E+00	1,45E+00	1,45E+00	1,45E+00	1,45E+00
NPSH available [J/kg]	21,86	21,93	21,84	21,92	21,77	20,91	20,51	20,55	19,33	19,79
Head developed [J/kg]	139,02	138,91	138,84	138,75	138,82	139,73	139,81	139,87	140,65	140,70
Pump efficiency used	2,96E-01	2,96E-01	2,96E-01	2,96E-01	2,96E-01	2,96E-01	2,96E-01	2,96E-01	2,96E-01	2,96E-01
Net work required [kW]	1,91E-02	1,91E-02	1,90E-02	1,88E-02	1,89E-02	1,92E-02	1,92E-02	1,92E-02	1,92E-02	1,92E-02
Total feed stream CO_2 flow [kg/hr]	2,62E-05	3,94E-05	4,46E-05	4,42E-05	4,74E-05	4,21E-05	2,97E-05	3,41E-05	2,81E-05	3,55E-05
Total product stream CO_2 flow [kg/hr]	3,30E-05	5,07E-05	5,80E-05	5,75E-05	6,21E-05	5,67E-05	3,89E-05	4,53E-05	3,85E-05	4,99E-05
Net stream CO_2 production [kg/hr]	6,77E-06	1,13E-05	1,34E-05	1,33E-05	1,47E-05	1,46E-05	9,28E-06	1,12E-05	1,04E-05	1,43E-05
Utility CO_2 production [kg/hr]	0,00E+00	0,00E+00	0,00E+00	0,00E+00	0,00E+00	0,00E+00	0,00E+00	0,00E+00	0,00E+00	0,00E+00
Total CO_2 production [kg/hr]	6,77E-06	1,13E-05	1,34E-05	1,33E-05	1,47E-05	1,46E-05	9,28E-06	1,12E-05	1,04E-05	1,43E-05
Utility usage [kW]	1,91E-02	1,91E-02	1,90E-02	1,88E-02	1,89E-02	1,92E-02	1,92E-02	1,92E-02	1,92E-02	1,92E-02
Utility cost [$/sec]	1,86E-06	1,85E-06	1,85E-06	1,83E-06	1,83E-06	1,87E-06	1,87E-06	1,87E-06	1,87E-06	1,86E-06
Utility ID	PUMP	PUMP	PUMP	PUMP	PUMP	PUMP	PUMP	PUMP	PUMP	PUMP

Columns - Specifications and main outputs: Fist experimental campaign										
	127		128		129		130		131	
Name	**ABI**	**GAIL**	**ABI**	**GAIL**	**ABI**	**GAIL**	**ABI**	**GAIL**	**ABI**	**GAIL**
Property method	ENRTL-RK	ENRTL-RK	ENRTL-RK	ENRTL-RK	ENRTL-RK	ENRTL-RK	ENRTL-RK	ENRTL-RK	ENRTL-RK	ENRTL-RK
Henry's component list ID	GLOBAL	GLOBAL	GLOBAL	GLOBAL	GLOBAL	GLOBAL	GLOBAL	GLOBAL	GLOBAL	GLOBAL
Electrolyte chemistry ID	MEA-CHEM	MEA-CHEM	MEA-CHEM	MEA-CHEM	MEA-CHEM	MEA-CHEM	MEA-CHEM	MEA-CHEM	MEA-CHEM	MEA-CHEM
Use true species approach for electrolytes	YES	YES	YES	YES	YES	YES	YES	YES	YES	YES
Free-water phase properties method	STEAM-TA	STEAM-TA	STEAM-TA	STEAM-TA	STEAM-TA	STEAM-TA	STEAM-TA	STEAM-TA	STEAM-TA	STEAM-TA
Water solubility method	3	3	3	3	3	3	3	3	3	3
Number of stages	20	20	20	20	20	20	20	20	20	20
Condenser	NONE	PARTIAL-V	NONE	PARTIAL-V	NONE	PARTIAL-V	NONE	PARTIAL-V	NONE	PARTIAL-V
Reboiler	NONE	KETTLE	NONE	KETTLE	NONE	KETTLE	NONE	KETTLE	NONE	KETTLE
Number of phases	2	2	2	2	2	2	2	2	2	2
Free-water	NO	NO	NO	NO	NO	NO	NO	NO	NO	NO
Top stage pressure [bar]	0,96	1,8	0,96	1,8	0,96	1,8	0,96	1,8	0,96	1,8
Specified distillate rate [kmol/hr]		12,4		12,4		12,4		12,4		12,4
Calculated molar reflux ratio	5,92	9,70	5,78	9,76	5,60	9,74	5,31	9,64	5,38	9,57
Calculated bottoms rate [kmol/hr]	6,12	5,53	6,08	5,51	6,04	5,47	5,97	5,41	5,98	5,42
Calculated boilup rate [kmol/hr]	1,18	0,91	1,19	0,91	1,20	0,91	1,20	0,91	1,20	0,90
Calculated distillate rate [kmol/hr]	1,04	0,62	1,07	0,62	1,11	0,61	1,17	0,61	1,16	0,61
Condenser / top stage temperature [C]	39,73	118,17	46,22	117,82	48,62	117,72	55,21	117,74	52,06	117,83
Condenser / top stage pressure [bar]	0,96	1,80	0,96	1,80	0,96	1,80	0,96	1,80	0,96	1,80
Condenser / top stage heat duty [kW]	0,00	3,51	0,00	3,06	0,00	2,96	0,00	2,82	0,00	3,83
Condenser / top stage subcooled duty [kW]		-2,72		-2,65		-2,62		-2,59		-2,60
Condenser / top stage reflux rate [kmol/hr]	6,17	6,05	6,18	6,01	6,21	5,97	6,23	5,91	6,25	5,88

Reboiler pressure [bar]	0,96	1,81	0,96	1,81	0,96	1,81	0,96	1,81	0,96	1,81
Reboiler temperature [C]	48,17	120,12	51,45	120,07	52,55	120,08	52,49	120,12	53,33	120,08
Reboiler heat duty [kW]	0,00	10,68	0,00	10,68	0,00	10,68	0,00	10,68	0,00	10,68
Total feed stream CO_2 flow [kg/hr]	7,42	0,00	7,42	0,00	7,42	0,00	7,42	0,00	7,42	0,00
Total product stream CO_2 flow [kg/hr]	0,96	1,82	0,60	2,06	0,48	2,14	0,45	2,16	0,44	2,10
Net stream CO_2 production [kg/hr]	-6,46	1,82	-6,82	2,06	-6,94	2,14	-6,98	2,15	-6,98	2,10
Utility CO_2 production [kg/hr]	0,00	0,00	0,00	0,00	0,00	0,00	0,00	0,00	0,00	0,00
Total CO_2 production [kg/hr]	-6,46	1,82	-6,82	2,06	-6,94	2,14	-6,98	2,15	-6,98	2,10
Condenser utility usage [kW]		0,80		0,42		0,34		0,22		1,23
Condenser utility cost [$/sec]		7,74E-05		4,04E-05		3,32E-05		2,14E-05		1,19E-04
Condenser utility ID		PROWATER		PROWATER		PROWATER		PROWATER		PROWATER
Reboiler utility usage [kW]		10,68		10,68		10,68		10,68		10,68
Reboiler utility cost [$/sec]		1,04E-03		1,04E-03		1,04E-03		1,04E-03		1,04E-03
Reboiler utility ID		REBOILER		REBOILER		REBOILER		REBOILER		REBOILER
Basis for specified distillate to feed ratio	MOLE	MOLE	MOLE	MOLE	MOLE	MOLE	MOLE	MOLE	MOLE	MOLE
Basis for specified bottoms to feed ratio	MOLE	MOLE	MOLE	MOLE	MOLE	MOLE	MOLE	MOLE	MOLE	MOLE
Basis for specified boilup ratio	MOLE	MOLE	MOLE	MOLE	MOLE	MOLE	MOLE	MOLE	MOLE	MOLE
Calculated molar boilup ratio		0,165		0,165		0,166		0,168		0,167
Calculated mass boilup ratio	0,24	0,13	0,24	0,13	0,24	0,13	0,24	0,13	0,24	0,13

Columns - Specifications and main outputs: Fist experimental campaign

	132		133		134		135		136	
Name	**ABI**	**GAIL**	**ABI**	**GAIL**	**ABI**	**GAIL**	**ABI**	**GAIL**	**ABI**	**GAIL**
Property method	ENRTL-RK	ENRTL-RK	ENRTL-RK	ENRTL-RK	ENRTL-RK	ENRTL-RK	ENRTL-RK	ENRTL-RK	ENRTL-RK	ENRTL-RK

Henry's component list ID	GLOBAL	GLOBAL	GLOBAL	GLOBAL	GLOBAL	GLOBAL	GLOBAL	GLOBAL	GLOBAL	GLOBAL
Electrolyte chemistry ID	MEA-CHEM	MEA-CHEM	MEA-CHEM	MEA-CHEM	MEA-CHEM	MEA-CHEM	MEA-CHEM	MEA-CHEM	MEA-CHEM	MEA-CHEM
Use true species approach for electrolytes	YES	YES	YES	YES	YES	YES	YES	YES	YES	YES
Free-water phase properties method	STEAM-TA	STEAM-TA	STEAM-TA	STEAM-TA	STEAM-TA	STEAM-TA	STEAM-TA	STEAM-TA	STEAM-TA	STEAM-TA
Water solubility method	3	3	3	3	3	3	3	3	3	3
Number of stages	20	20	20	20	20	20	20	20	20	20
Condenser	NONE	PARTIAL-V	NONE	PARTIAL-V	NONE	PARTIAL-V	NONE	PARTIAL-V	NONE	PARTIAL-V
Reboiler	NONE	KETTLE	NONE	KETTLE	NONE	KETTLE	NONE	KETTLE	NONE	KETTLE
Number of phases	2	2	2	2	2	2	2	2	2	2
Free-water	NO	NO	NO	NO	NO	NO	NO	NO	NO	NO
Top stage pressure [bar]	0,96	1,8	0,96	1,8	0,96	1,8	0,96	1,8	0,96	1,8
Specified distillate rate [kmol/hr]		12,4		12,4		12,4		12,4		12,4
Calculated molar reflux ratio	6,66	9,63	6,79	9,58	6,80	9,60	7,95	9,40	7,67	9,38
Calculated bottoms rate [kmol/hr]	6,11	5,52	6,14	5,54	6,14	5,54	6,13	5,51	6,09	5,48
Calculated boilup rate [kmol/hr]	1,08	0,91	1,07	0,91	1,07	0,91	0,92	0,92	0,93	0,92
Calculated distillate rate [kmol/hr]	0,93	0,63	0,91	0,63	0,91	0,63	0,78	0,64	0,81	0,64
Condenser / top stage temperature [C]	40,63	118,36	35,35	118,62	35,32	118,57	40,59	119,14	46,75	119,06
Condenser / top stage pressure [bar]	0,96	1,80	0,96	1,80	0,96	1,80	0,96	1,80	0,96	1,80
Condenser / top stage heat duty [kW]	0,00	2,94	0,00	3,07	0,00	3,06	0,00	3,00	0,00	2,77
Condenser / top stage subcooled duty [kW]		-2,74		-2,79		-2,79		-2,87		-2,85
Condenser / top stage reflux rate [kmol/hr]	6,19	6,04	6,17	6,07	6,17	6,07	6,17	6,06	6,19	6,03
Reboiler pressure [bar]	0,96	1,81	0,96	1,81	0,96	1,81	0,96	1,81	0,96	1,81
Reboiler temperature [C]	55,57	120,16	52,73	120,21	54,17	120,19	56,22	120,37	58,62	120,36
Reboiler heat duty [kW]	0,00	10,68	0,00	10,68	0,00	10,68	0,00	10,68	0,00	10,68
Total feed stream CO_2 flow [kg/hr]	6,60	0,00	6,60	0,00	6,60	0,00	5,59	0,00	5,59	0,00
Total product stream CO_2 flow [kg/hr]	0,33	1,69	0,64	1,50	0,58	1,54	0,27	1,14	0,13	1,21
Net stream CO_2 production [kg/hr]	-6,28	1,69	-5,96	1,50	-6,03	1,54	-5,32	1,14	-5,46	1,21
Utility CO_2 production [kg/hr]	0,00	0,00	0,00	0,00	0,00	0,00	0,00	0,00	0,00	0,00
Total CO_2 production [kg/hr]	-6,28	1,69	-5,96	1,50	-6,03	1,54	-5,32	1,14	-5,46	1,21
Condenser utility usage [kW]		0,20		0,28		0,28		0,13		0,08

Condenser utility cost [$/sec]		1,95E-05		2,69E-05		2,67E-05		1,28E-05		7,39E-06
Condenser utility ID		PROWATER		PROWATER		PROWATER		PROWATER		PROWATER
Reboiler utility usage [kW]		10,68		10,68		10,68		10,68		10,68
Reboiler utility cost [$/sec]		1,04E-03		1,04E-03		1,04E-03		1,04E-03		1,04E-03
Reboiler utility ID		REBOILER		REBOILER		REBOILER		REBOILER		REBOILER
Basis for specified distillate to feed ratio	MOLE	MOLE	MOLE	MOLE	MOLE	MOLE	MOLE	MOLE	MOLE	MOLE
Basis for specified bottoms to feed ratio	MOLE	MOLE	MOLE	MOLE	MOLE	MOLE	MOLE	MOLE	MOLE	MOLE
Basis for specified boilup ratio	MOLE	MOLE	MOLE	MOLE	MOLE	MOLE	MOLE	MOLE	MOLE	MOLE
Calculated molar boilup ratio		0,165		0,165		0,165		0,167		0,168
Calculated mass boilup ratio	0,22	0,13	0,21	0,13	0,21	0,13	0,18	0,13	0,18	0,13

The specifications for mixers and splitters are kept constant during all runs. Therefore, just one set of input parameters are annexed:

Mixer - Specifications and main outputs: Fist experimental campaign	
Name	**MIX-2**
Property method	ENRTL-RK

Henry's component list ID	GLOBAL
Electrolyte chemistry ID	MEA-CHEM
Use true species approach for electrolytes	YES
Free-water phase properties method	STEAM-TA
Water solubility method	**3**
Specified pressure [bar]	**0**
Outlet temperature [C]	110
Calculated outlet pressure [bar]	1,3
Vapor fraction	0
First liquid /Total liquid	1
Total feed stream CO_2 flow [kg/hr]	0
Total product stream CO_2 flow [kg/hr]	0
Net stream CO_2 production [kg/hr]	0

Splitters - Specifications and main outputs: Fist experimental campaign

Name	SPLIT-1	SPLIT-2
Property method	ENRTL-RK	ENRTL-RK
Henry's component list ID	GLOBAL	GLOBAL
Electrolyte chemistry ID	MEA-CHEM	MEA-CHEM

Use true species approach for electrolytes	YES	YES
Free-water phase properties method	STEAM-TA	STEAM-TA
Water solubility method	3	3
First outlet stream		0,87
First specified split fraction		0,87
First calculated split fraction	0,20	0,87
Second outlet stream	0,80	
Second specified split fraction	0,80	
Second calculated split fraction	0,80	0,13
Total feed stream CO_2 flow [kg/hr]	0,96	3,55E-03
Total product stream CO_2 flow [kg/hr]	0,96	3,55E-03
Net stream CO_2 production [kg/hr]	0	0

Annex D: Specifications and results of every process stream for each run

The full specifications and results of every process stream could be found in the digital attachment

Annex E: Concentration profiles and validation graphs for every run

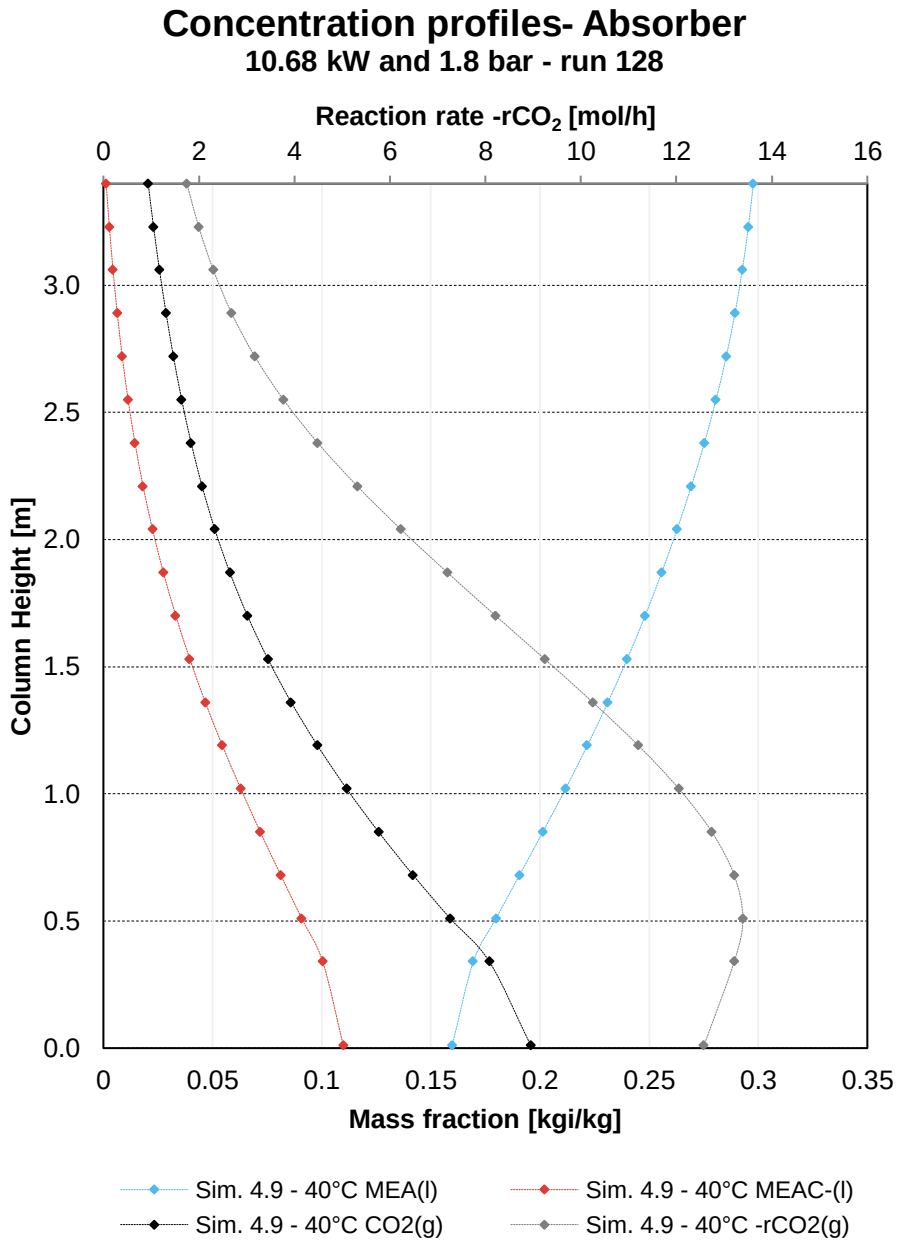

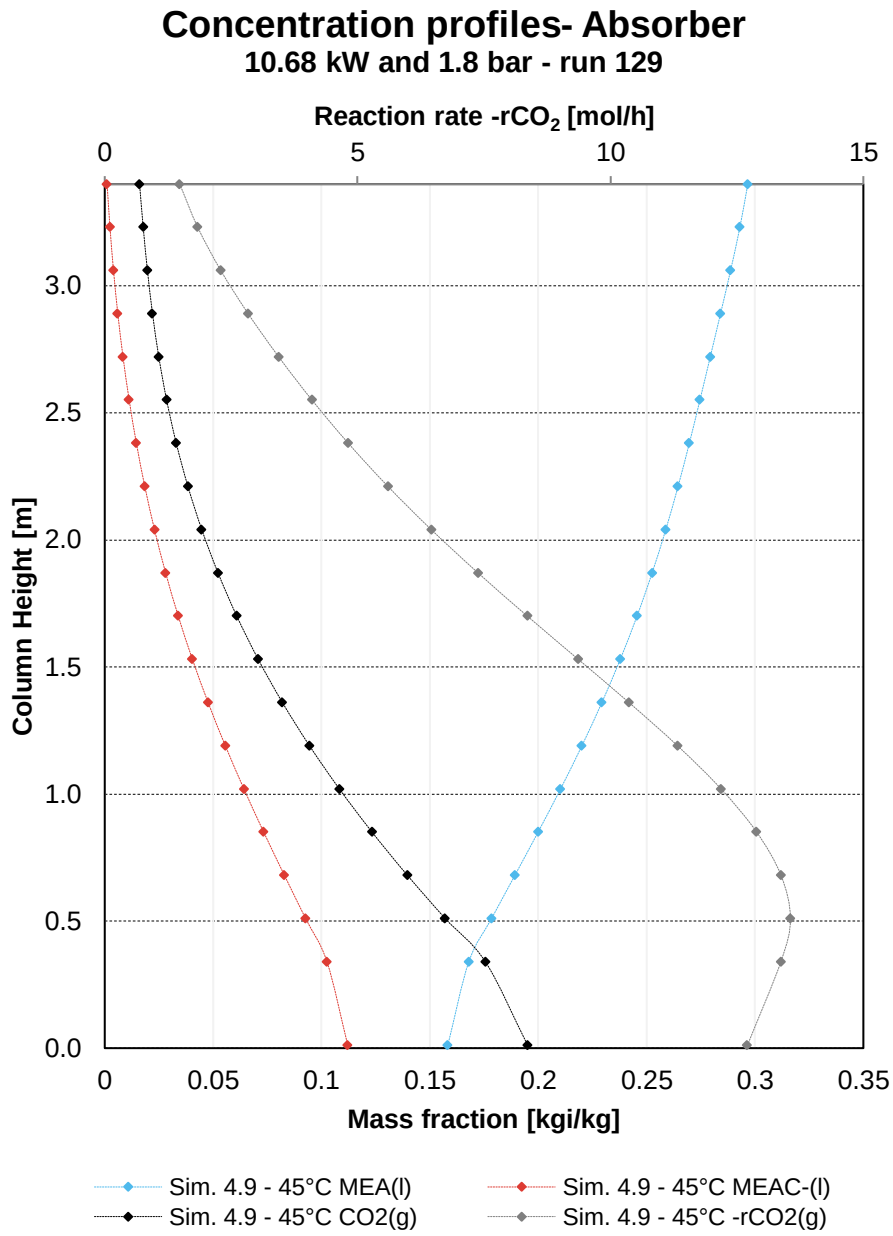
Concentration profiles- Absorber
10.68 kW and 1.8 bar - run 129
Reaction rate -rCO2 [mol/h]
0
5
10
15
Column Height [m]
3.0
2.5
2.0
1.5
1.0
0.5
0.0
0
0.05
0.1
0.15
0.2
0.25
0.3
0.35
Mass fraction [kgi/kg]
Sim. 4.9 - 45°C MEA(l)
Sim. 4.9 - 45°C MEAC-(l)
Sim. 4.9 - 45°C CO2(g)
Sim. 4.9 - 45°C -rCO2(g)

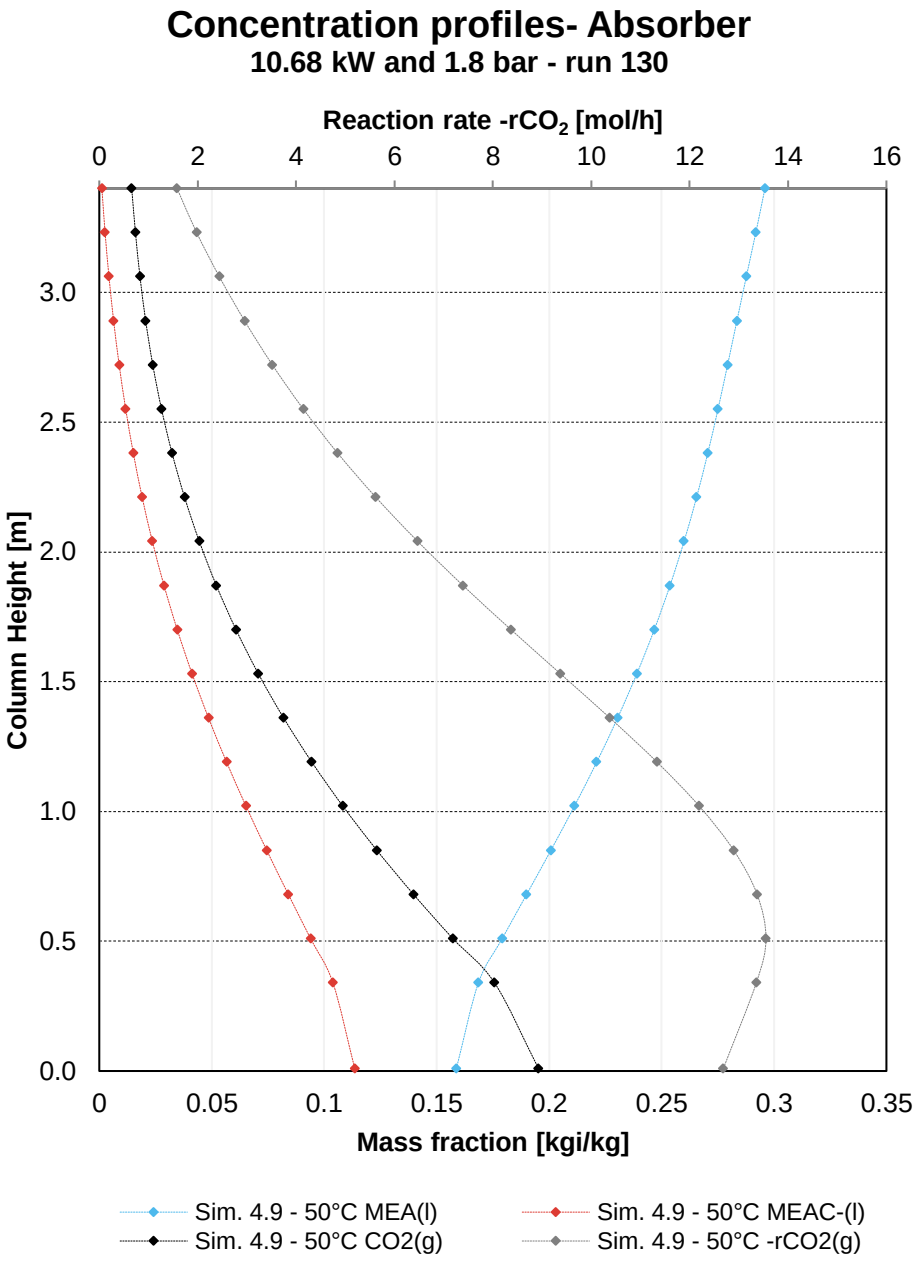
Concentration profiles- Absorber
10.68 kW and 1.8 bar - run 130
Reaction rate -rCO2 [mol/h]
0
2
4
6
8
10
12
14
16
Column Height [m]
3.0
2.5
2.0
1.5
1.0
0.5
0.0
0
0.05
0.1
0.15
0.2
0.25
0.3
0.35
Mass fraction [kgi/kg]
Sim. 4.9 - 50°C MEA(l)
Sim. 4.9 - 50°C MEAC-(l)
Sim. 4.9 - 50°C CO2(g)
Sim. 4.9 - 50°C -rCO2(g)

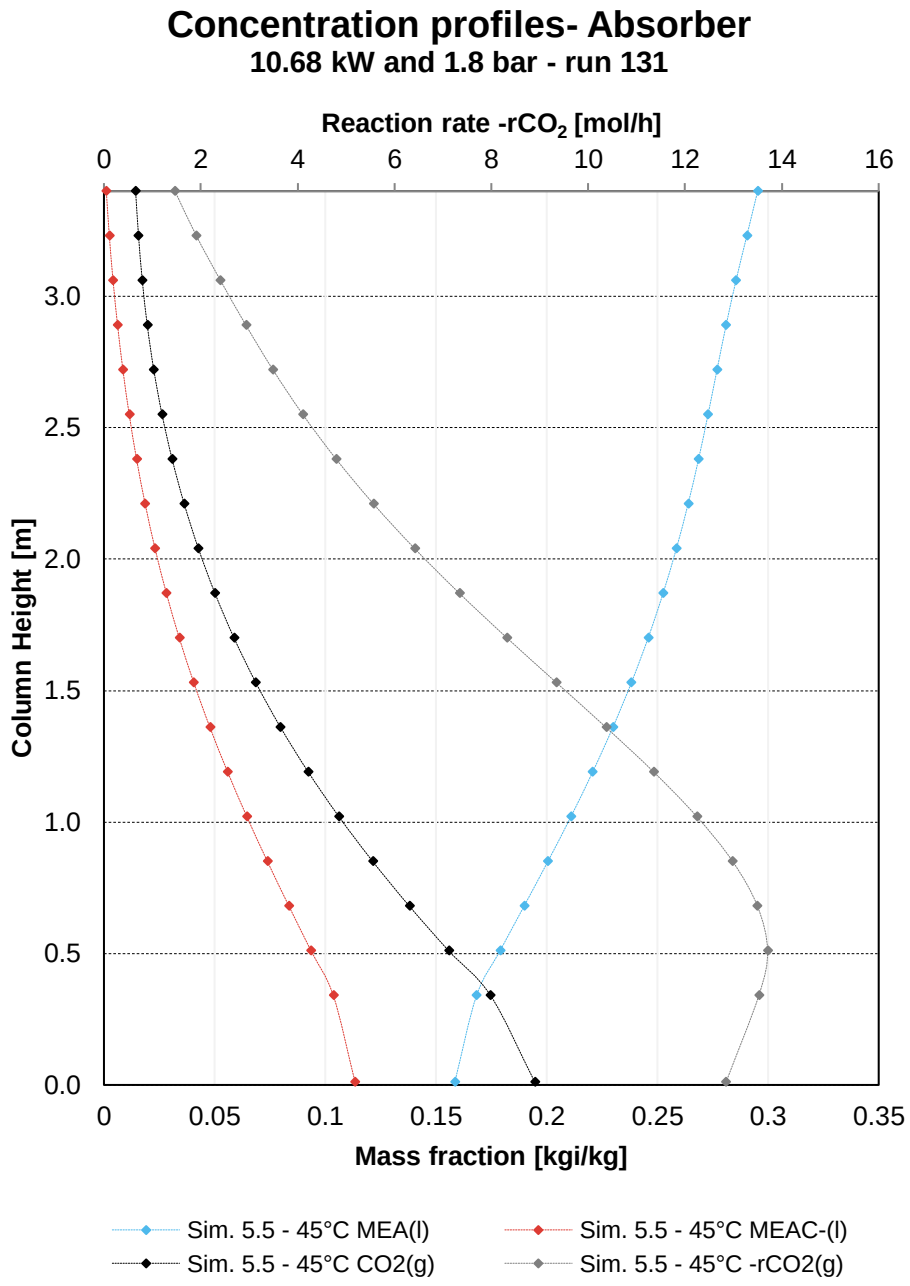
Concentration profiles- Absorber
10.68 kW and 1.8 bar - run 131
Reaction rate -rCO2 [mol/h]
0
2
4
6
8
10
12
14
16
Column Height [m]
0.0
0.5
1.0
1.5
2.0
2.5
3.0
0
0.05
0.1
0.15
0.2
0.25
0.3
0.35
Mass fraction [kgi/kg]
Sim. 5.5 - 45°C MEA(l)
Sim. 5.5 - 45°C MEAC-(l)
Sim. 5.5 - 45°C CO2(g)
Sim. 5.5 - 45°C -rCO2(g)

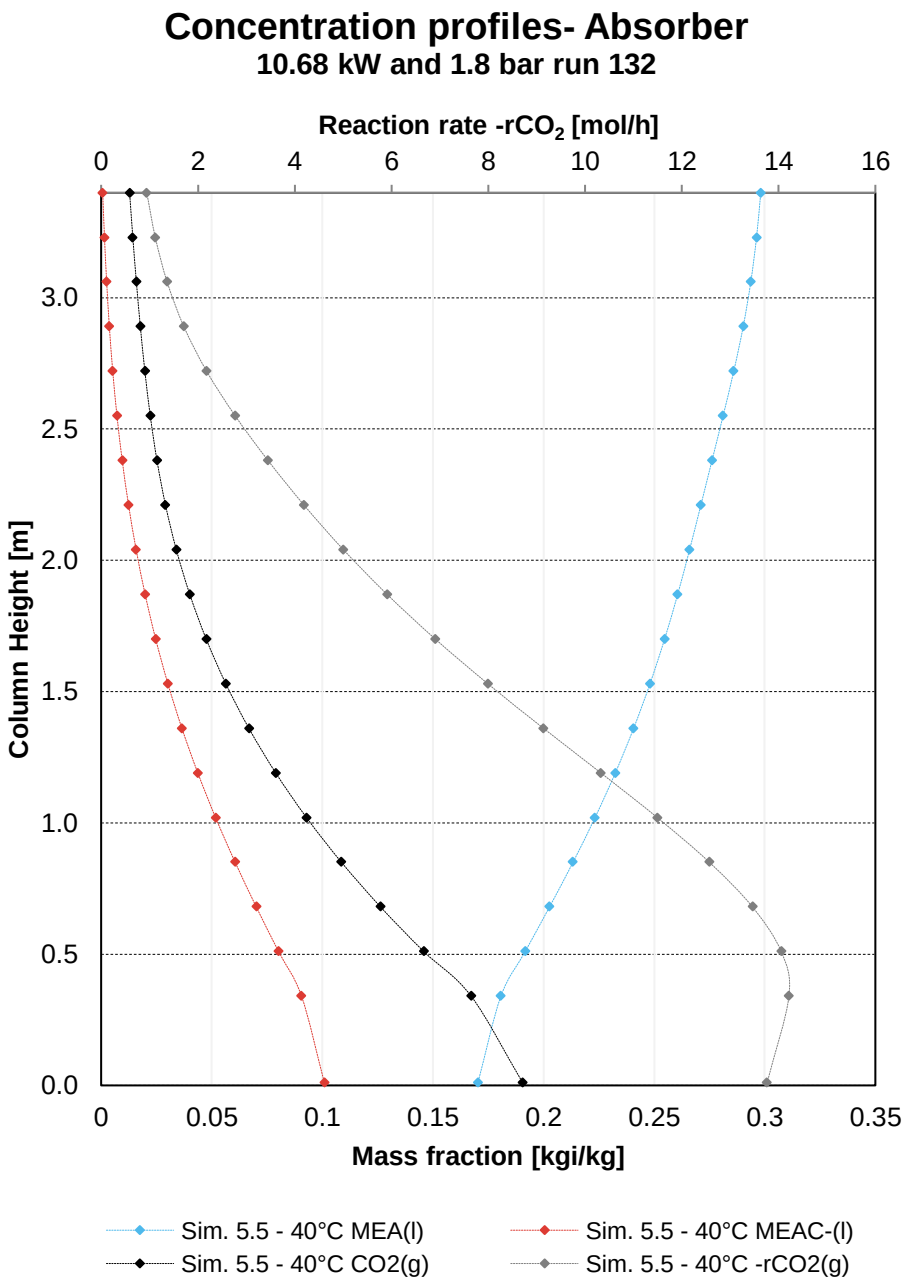
Concentration profiles- Absorber
10.68 kW and 1.8 bar run 132
Reaction rate -rCO2 [mol/h]
0
2
4
6
8
10
12
14
16
Column Height [m]
0.0
0.5
1.0
1.5
2.0
2.5
3.0
0
0.05
0.1
0.15
0.2
0.25
0.3
0.35
Mass fraction [kgi/kg]
Sim. 5.5 - 40°C MEA(l)
Sim. 5.5 - 40°C MEAC-(l)
Sim. 5.5 - 40°C CO2(g)
Sim. 5.5 - 40°C -rCO2(g)

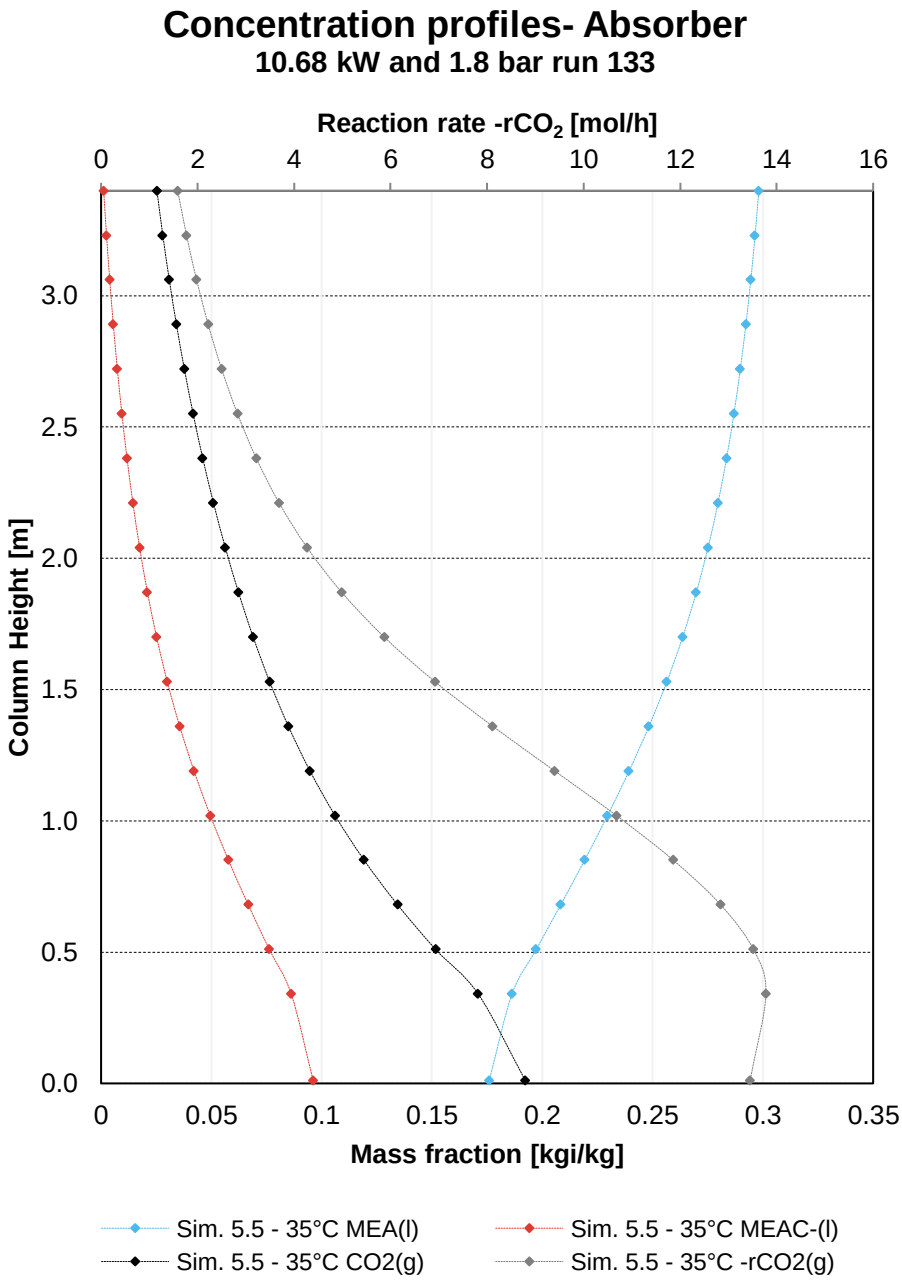
Concentration profiles- Absorber
10.68 kW and 1.8 bar run 133
Reaction rate -rCO2 [mol/h]
0
2
4
6
8
10
12
14
16
Column Height [m]
0.0
0.5
1.0
1.5
2.0
2.5
3.0
0
0.05
0.1
0.15
0.2
0.25
0.3
0.35
Mass fraction [kgi/kg]
Sim. 5.5 - 35°C MEA(l)
Sim. 5.5 - 35°C MEAC-(l)
Sim. 5.5 - 35°C CO2(g)
Sim. 5.5 - 35°C -rCO2(g)

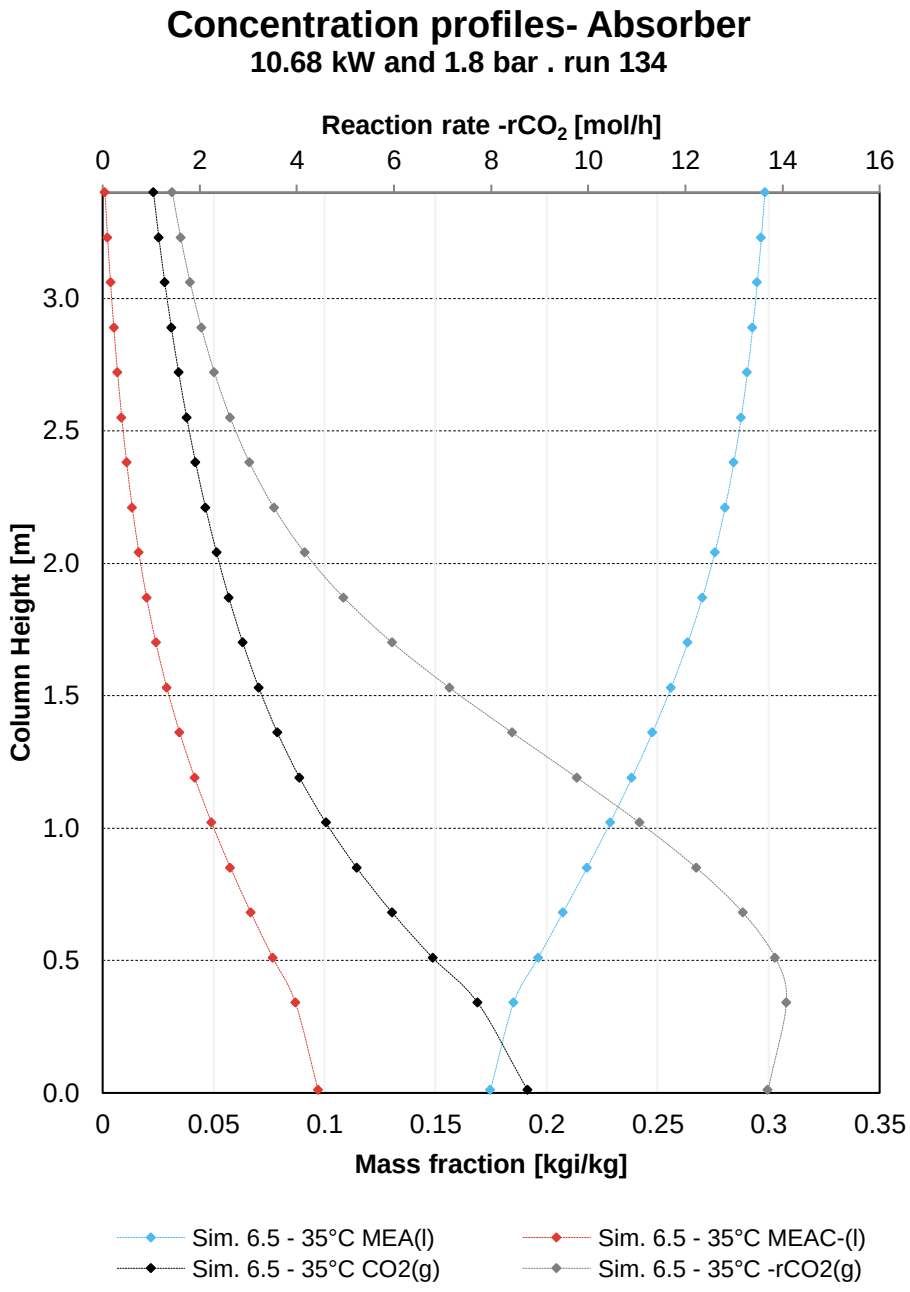
Concentration profiles- Absorber
10.68 kW and 1.8 bar . run 134
Reaction rate -rCO2 [mol/h]
0
2
4
6
8
10
12
14
16
Column Height [m]
0.0
0.5
1.0
1.5
2.0
2.5
3.0
0
0.05
0.1
0.15
0.2
0.25
0.3
0.35
Mass fraction [kgi/kg]
Sim. 6.5 - 35°C MEA(l)
Sim. 6.5 - 35°C MEAC-(l)
Sim. 6.5 - 35°C CO2(g)
Sim. 6.5 - 35°C -rCO2(g)

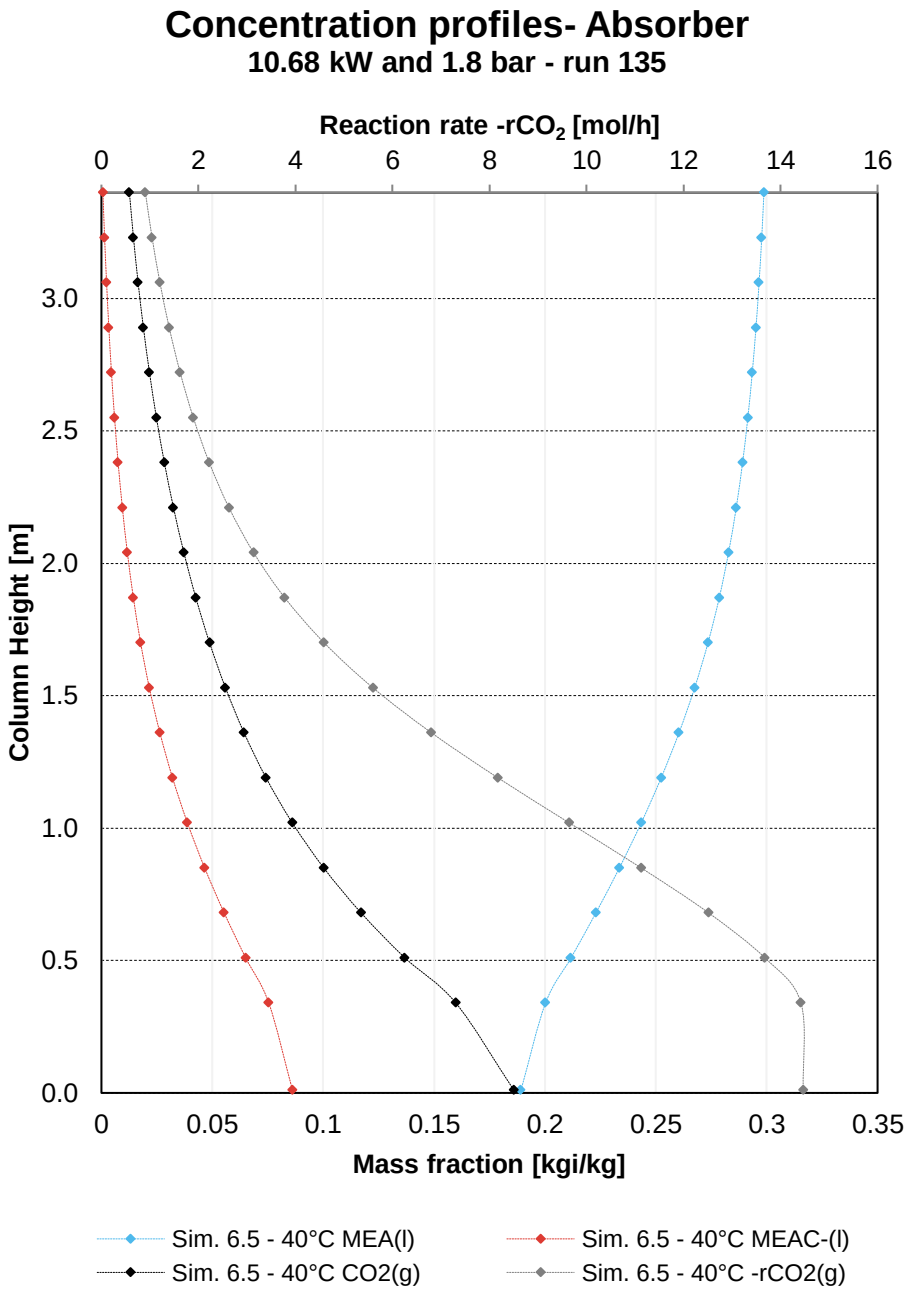
Concentration profiles- Absorber
10.68 kW and 1.8 bar - run 135
Reaction rate -rCO2 [mol/h]
0
2
4
6
8
10
12
14
16
Column Height [m]
0.0
0.5
1.0
1.5
2.0
2.5
3.0
0
0.05
0.1
0.15
0.2
0.25
0.3
0.35
Mass fraction [kgi/kg]
Sim. 6.5 - 40°C MEA(l)
Sim. 6.5 - 40°C MEAC-(l)
Sim. 6.5 - 40°C CO2(g)
Sim. 6.5 - 40°C -rCO2(g)

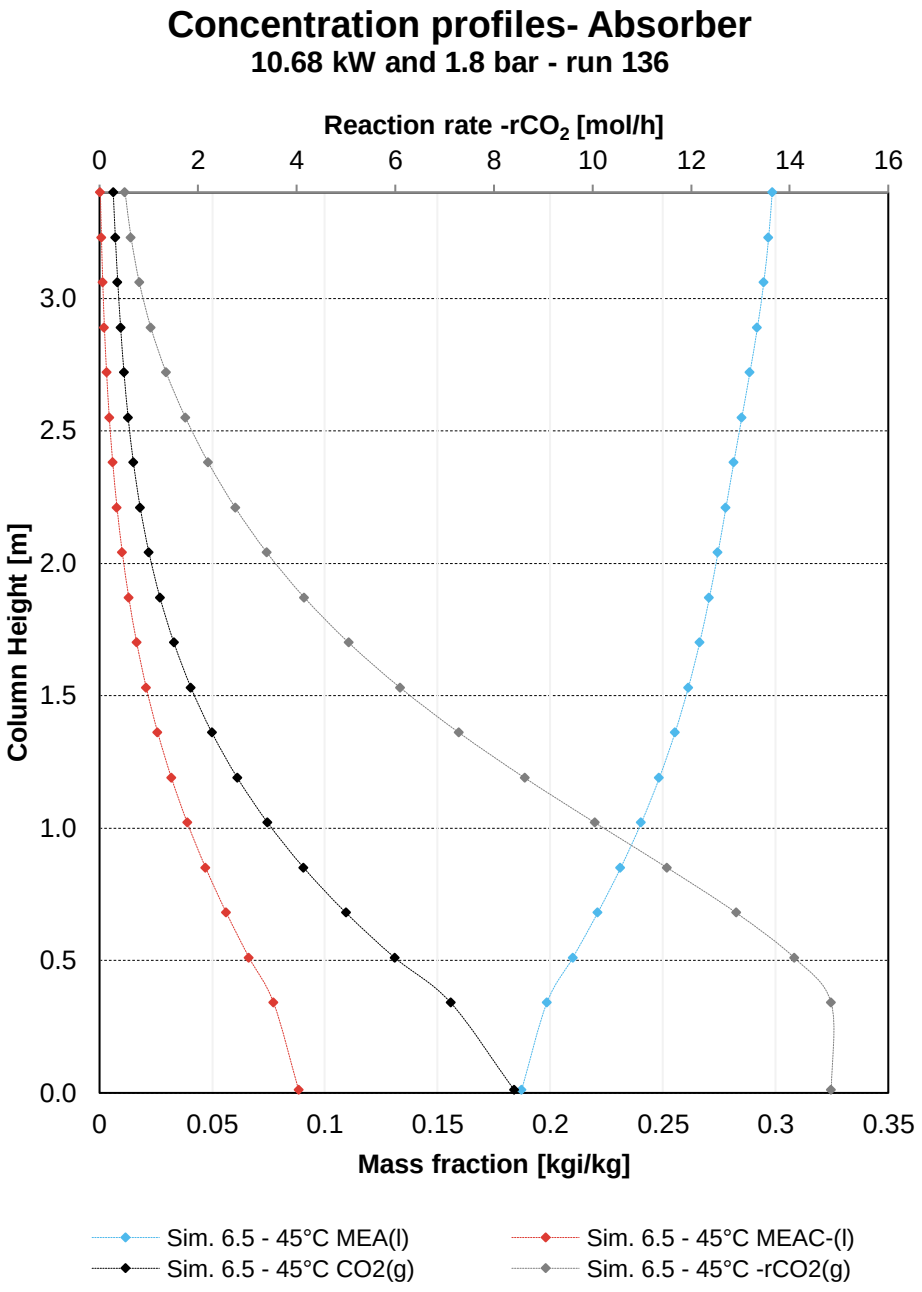
Concentration profiles- Absorber
10.68 kW and 1.8 bar - run 136
Reaction rate -rCO2 [mol/h]
0
2
4
6
8
10
12
14
16
Column Height [m]
3.0
2.5
2.0
1.5
1.0
0.5
0.0
0
0.05
0.1
0.15
0.2
0.25
0.3
0.35
Mass fraction [kgi/kg]
Sim. 6.5 - 45°C MEA(l)
Sim. 6.5 - 45°C MEAC-(l)
Sim. 6.5 - 45°C CO2(g)
Sim. 6.5 - 45°C -rCO2(g)

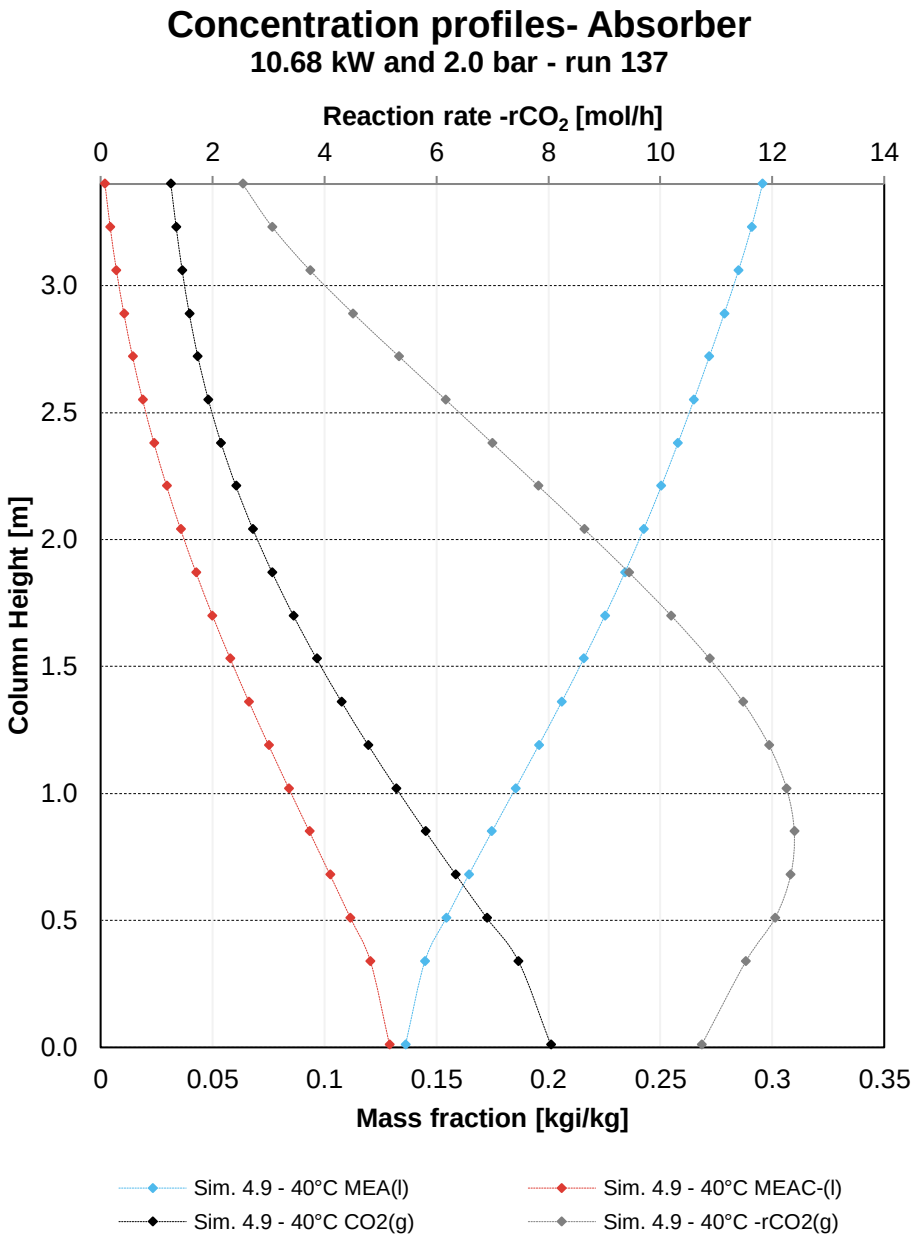
Concentration profiles- Absorber
10.68 kW and 2.0 bar - run 137
Reaction rate -rCO2 [mol/h]
0
2
4
6
8
10
12
14
Column Height [m]
0.0
0.5
1.0
1.5
2.0
2.5
3.0
0
0.05
0.1
0.15
0.2
0.25
0.3
0.35
Mass fraction [kgi/kg]
Sim. 4.9 - 40°C MEA(l)
Sim. 4.9 - 40°C MEAC-(l)
Sim. 4.9 - 40°C CO2(g)
Sim. 4.9 - 40°C -rCO2(g)

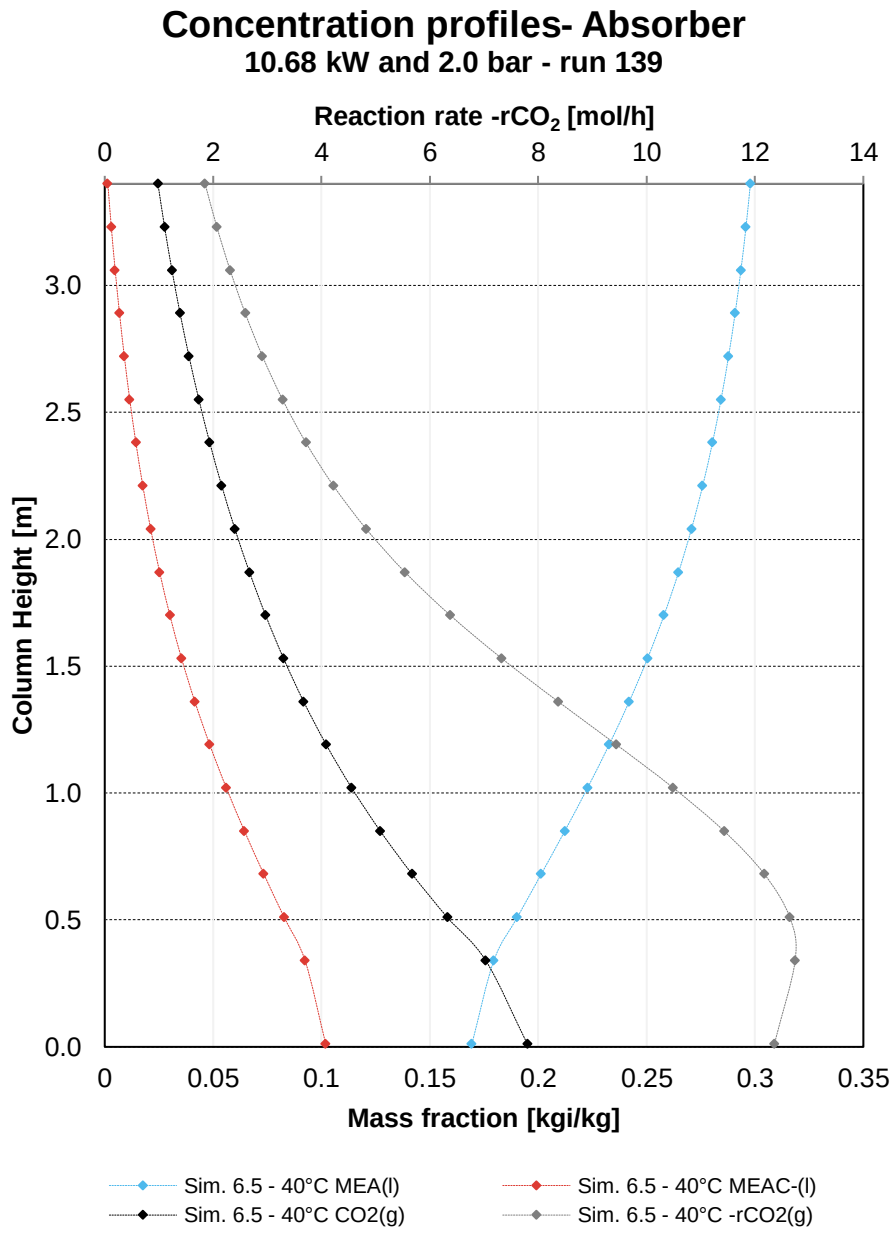
Concentration profiles- Absorber
10.68 kW and 2.0 bar - run 139
Reaction rate -rCO2 [mol/h]
0
2
4
6
8
10
12
14
Column Height [m]
3.0
2.5
2.0
1.5
1.0
0.5
0.0
0
0.05
0.1
0.15
0.2
0.25
0.3
0.35
Mass fraction [kgi/kg]
Sim. 6.5 - 40°C MEA(l)
Sim. 6.5 - 40°C MEAC-(l)
Sim. 6.5 - 40°C CO2(g)
Sim. 6.5 - 40°C -rCO2(g)

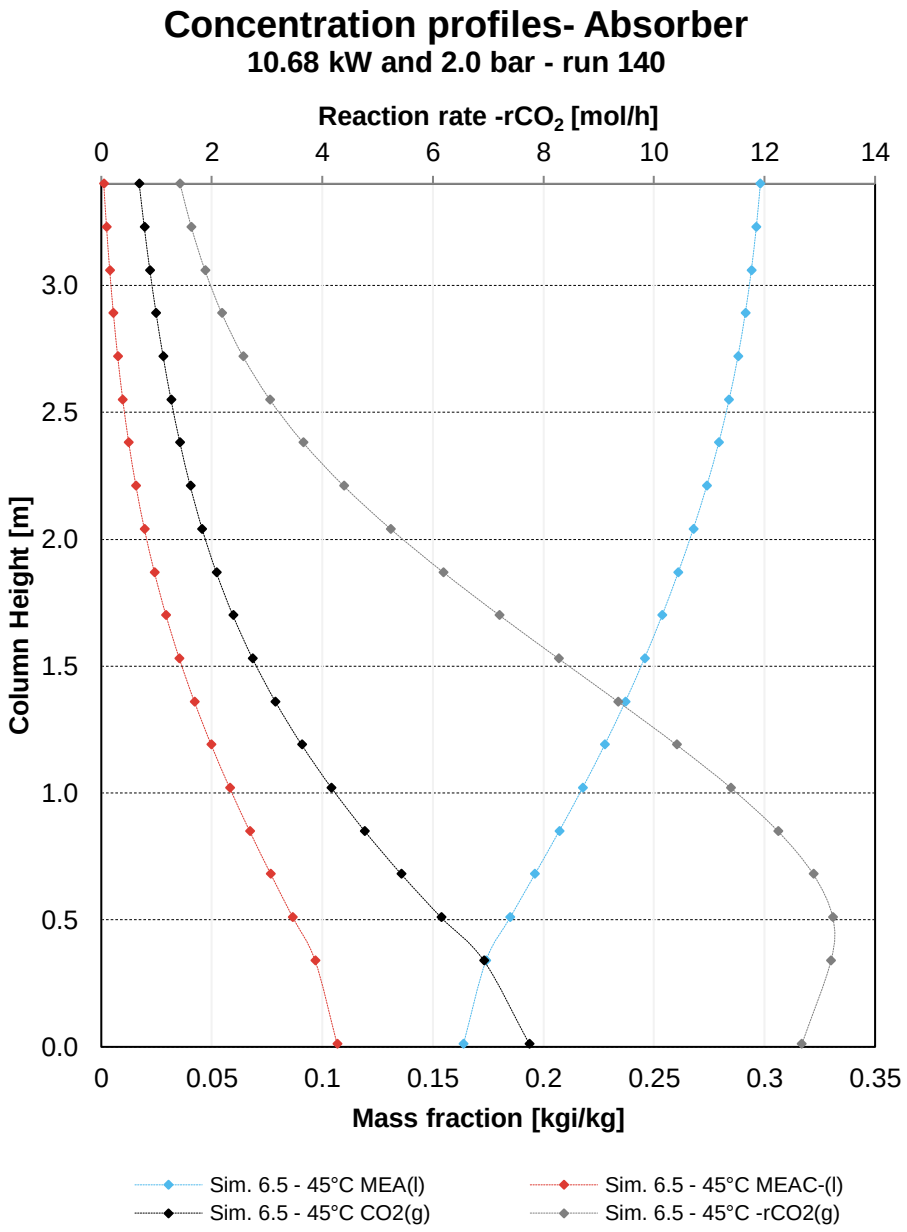
Concentration profiles- Absorber
10.68 kW and 2.0 bar - run 140
Reaction rate -rCO2 [mol/h]
0
2
4
6
8
10
12
14
Column Height [m]
0.0
0.5
1.0
1.5
2.0
2.5
3.0
0
0.05
0.1
0.15
0.2
0.25
0.3
0.35
Mass fraction [kgi/kg]
Sim. 6.5 - 45°C MEA(l)
Sim. 6.5 - 45°C MEAC-(l)
Sim. 6.5 - 45°C CO2(g)
Sim. 6.5 - 45°C -rCO2(g)

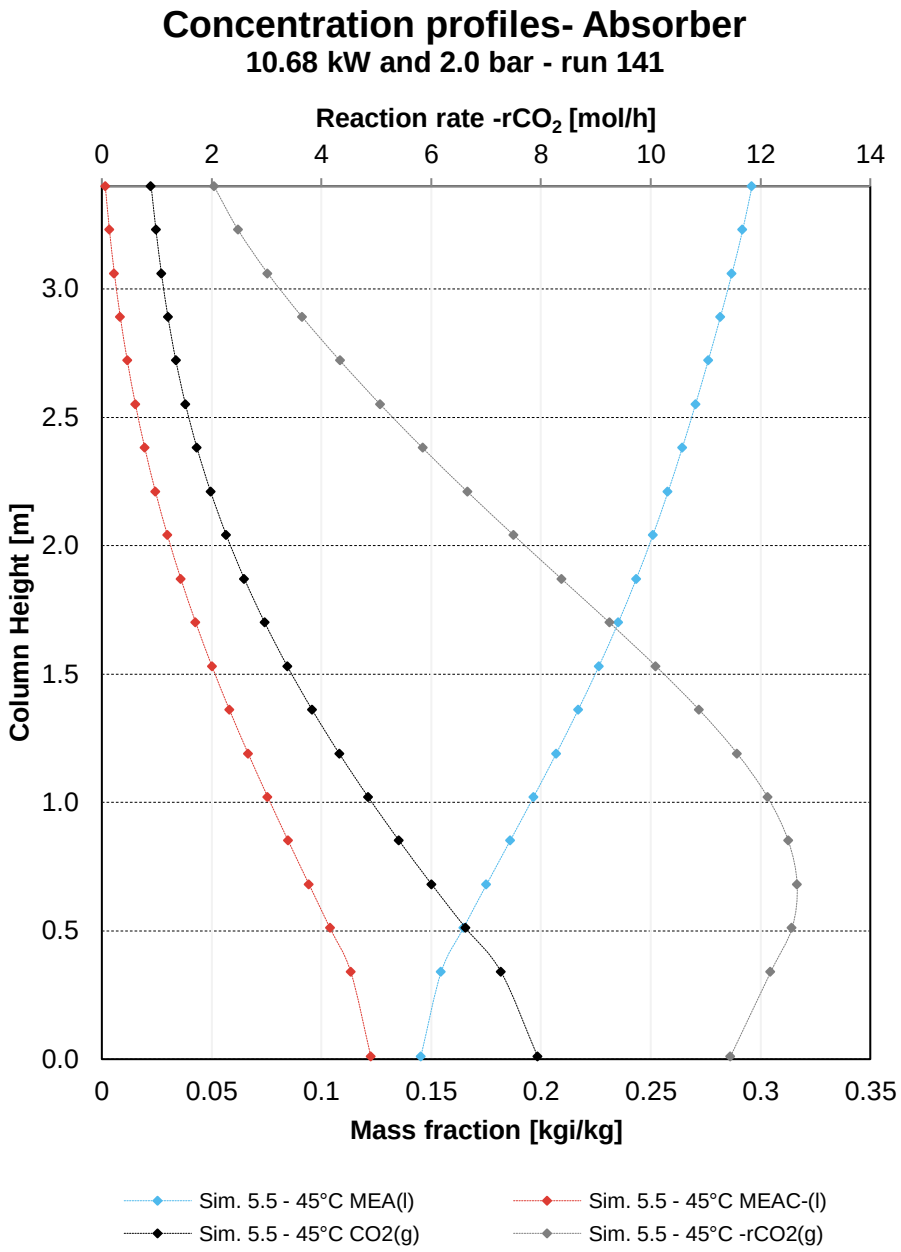
Concentration profiles- Absorber
10.68 kW and 2.0 bar - run 141
Reaction rate -rCO2 [mol/h]
0
2
4
6
8
10
12
14
Column Height [m]
0.0
0.5
1.0
1.5
2.0
2.5
3.0
0
0.05
0.1
0.15
0.2
0.25
0.3
0.35
Mass fraction [kgi/kg]
Sim. 5.5 - 45°C MEA(l)
Sim. 5.5 - 45°C MEAC-(l)
Sim. 5.5 - 45°C CO2(g)
Sim. 5.5 - 45°C -rCO2(g)

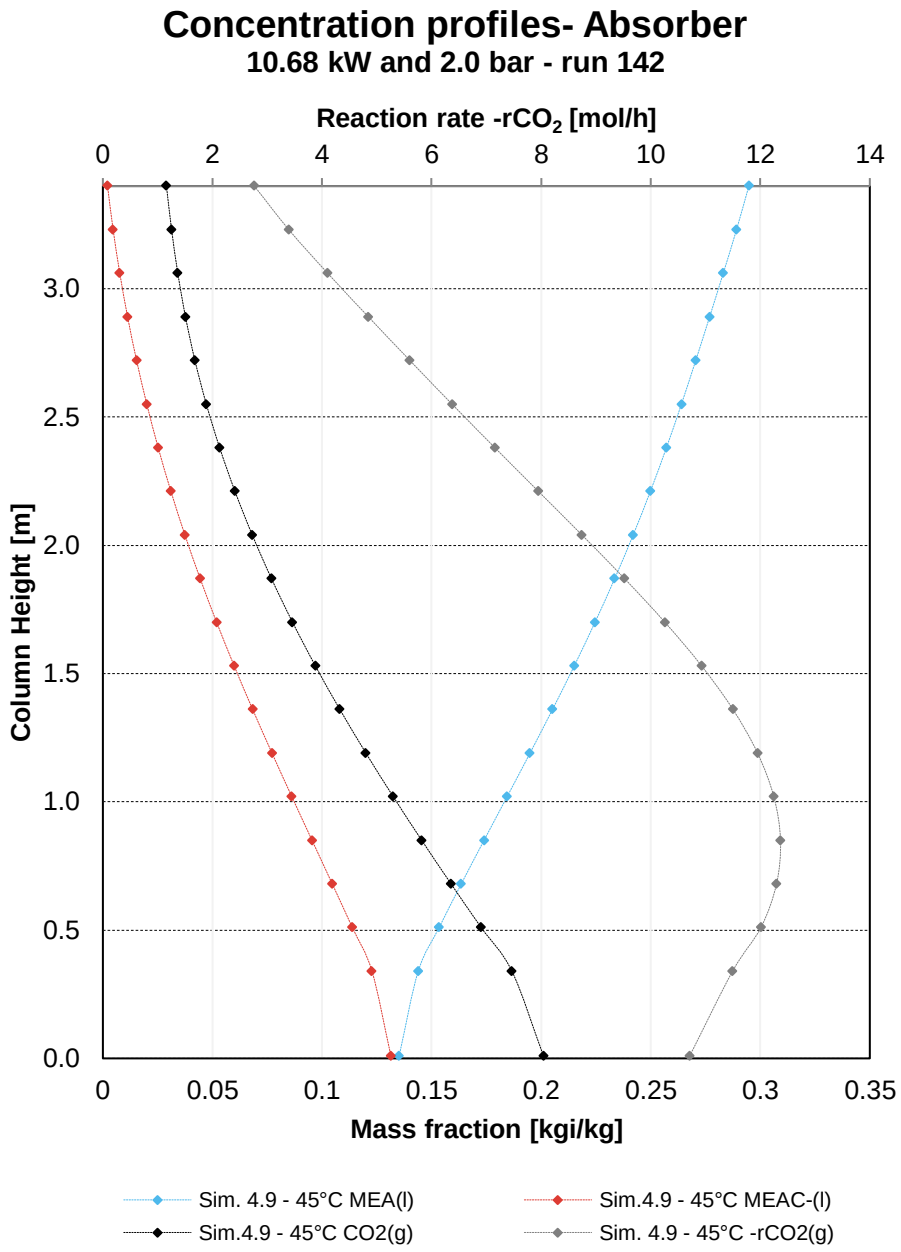
Concentration profiles- Absorber
10.68 kW and 2.0 bar - run 142
Reaction rate -rCO2 [mol/h]
0
2
4
6
8
10
12
14
Column Height [m]
0.0
0.5
1.0
1.5
2.0
2.5
3.0
0
0.05
0.1
0.15
0.2
0.25
0.3
0.35
Mass fraction [kgi/kg]
Sim. 4.9 - 45°C MEA(l)
Sim.4.9 - 45°C MEAC-(l)
Sim.4.9 - 45°C CO2(g)
Sim. 4.9 - 45°C -rCO2(g)

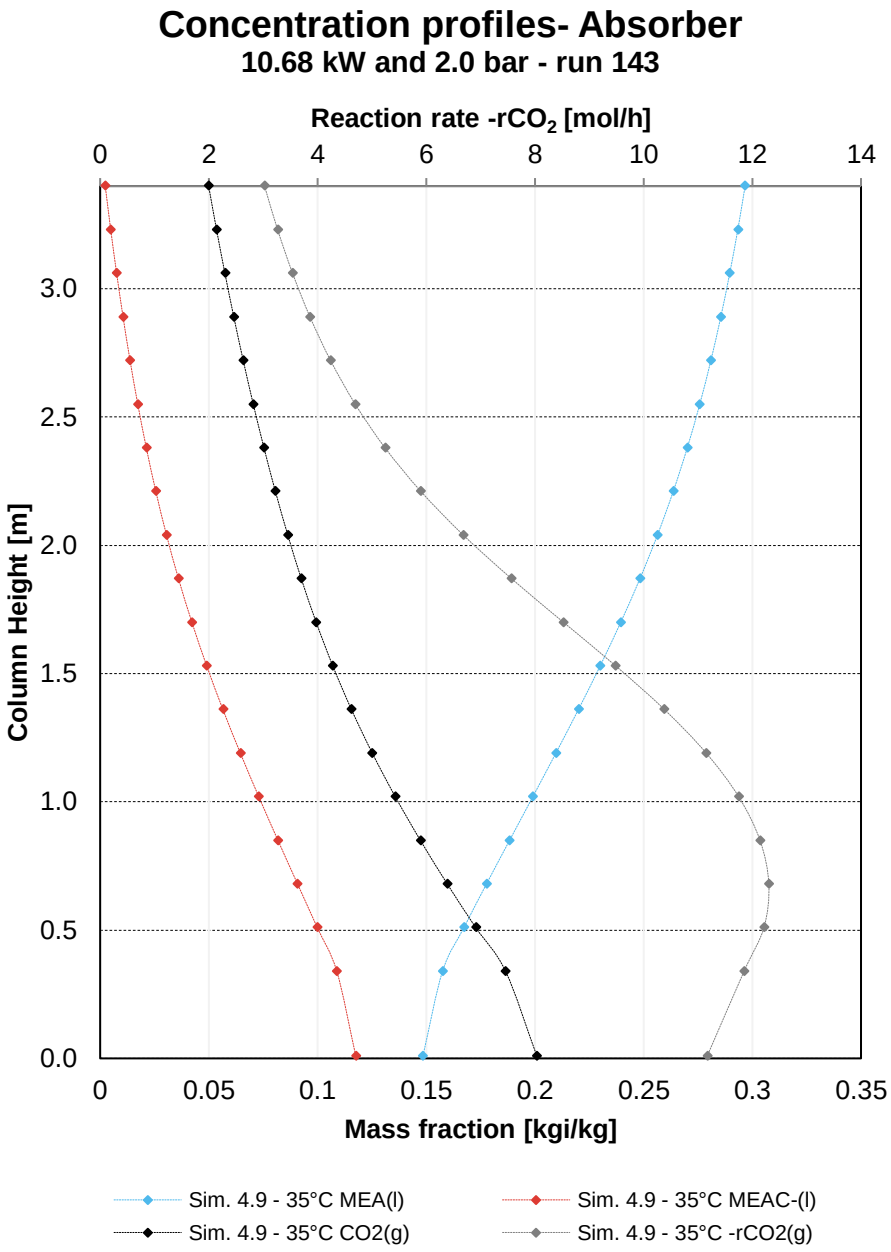
Concentration profiles- Absorber
10.68 kW and 2.0 bar - run 143
Reaction rate -rCO2 [mol/h]
0
2
4
6
8
10
12
14
Column Height [m]
0.0
0.5
1.0
1.5
2.0
2.5
3.0
0
0.05
0.1
0.15
0.2
0.25
0.3
0.35
Mass fraction [kgi/kg]
Sim. 4.9 - 35°C MEA(l)
Sim. 4.9 - 35°C MEAC-(l)
Sim. 4.9 - 35°C CO2(g)
Sim. 4.9 - 35°C -rCO2(g)

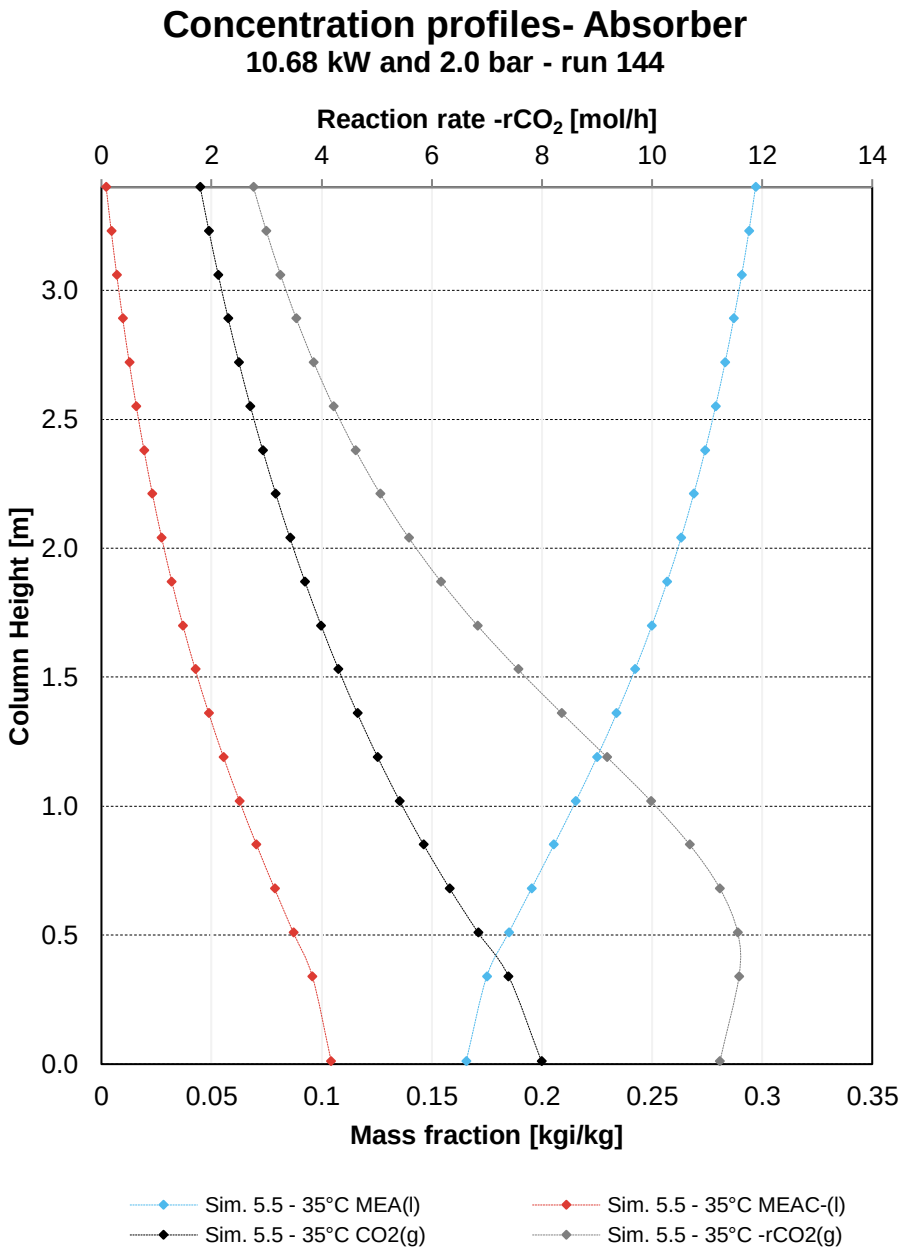
Concentration profiles- Absorber
10.68 kW and 2.0 bar - run 144
Reaction rate -rCO2 [mol/h]
0
2
4
6
8
10
12
14
Column Height [m]
0.0
0.5
1.0
1.5
2.0
2.5
3.0
0
0.05
0.1
0.15
0.2
0.25
0.3
0.35
Mass fraction [kgi/kg]
Sim. 5.5 - 35°C MEA(l)
Sim. 5.5 - 35°C MEAC-(l)
Sim. 5.5 - 35°C CO2(g)
Sim. 5.5 - 35°C -rCO2(g)

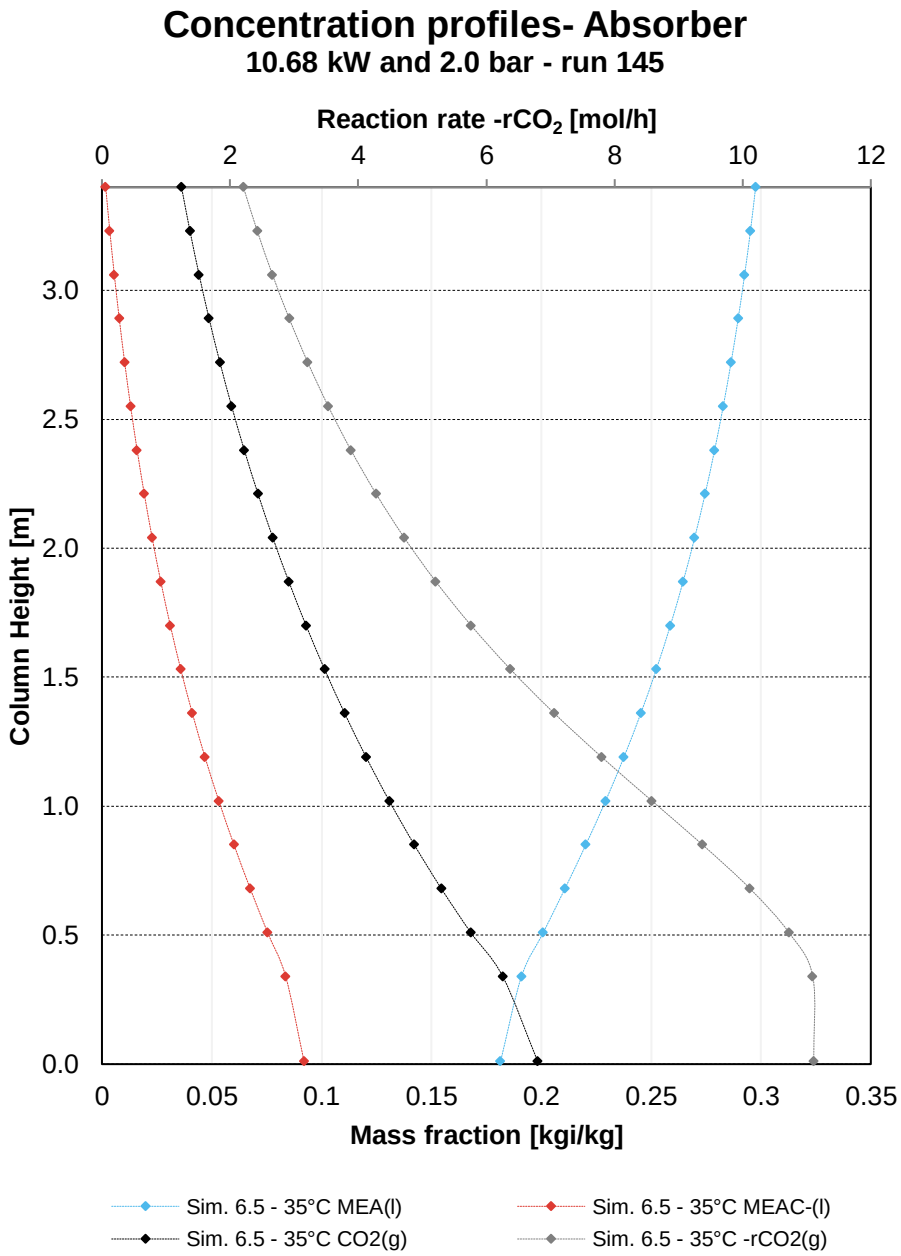
Concentration profiles- Absorber
10.68 kW and 2.0 bar - run 145
Reaction rate -rCO2 [mol/h]
0
2
4
6
8
10
12
Column Height [m]
3.0
2.5
2.0
1.5
1.0
0.5
0.0
0
0.05
0.1
0.15
0.2
0.25
0.3
0.35
Mass fraction [kgi/kg]
Sim. 6.5 - 35°C MEA(l)
Sim. 6.5 - 35°C MEAC-(l)
Sim. 6.5 - 35°C CO2(g)
Sim. 6.5 - 35°C -rCO2(g)

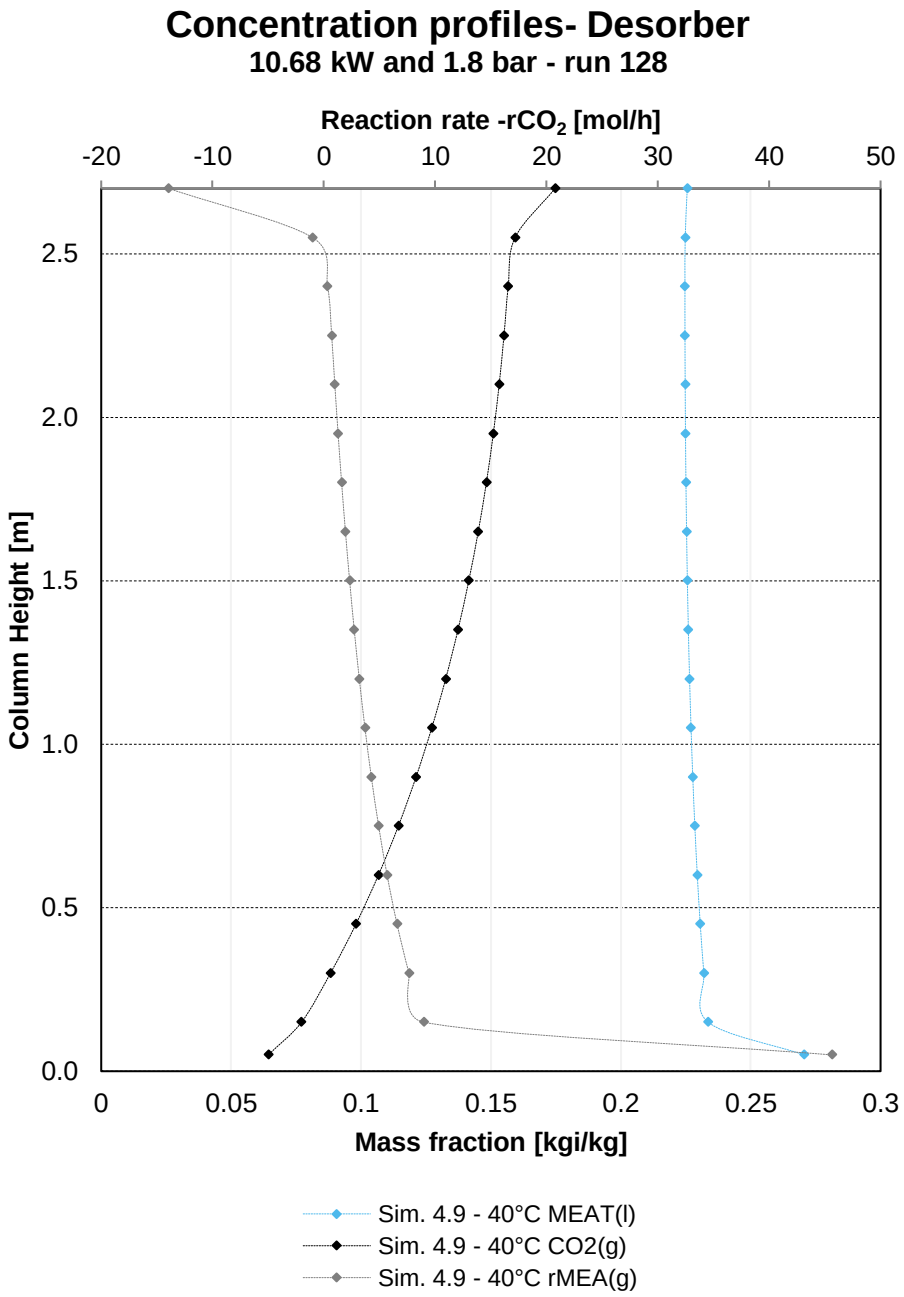
Concentration profiles- Desorber
10.68 kW and 1.8 bar - run 128
Reaction rate -rCO2 [mol/h]
-20
-10
0
10
20
30
40
50
Column Height [m]
0.0
0.5
1.0
1.5
2.0
2.5
0
0.05
0.1
0.15
0.2
0.25
0.3
Mass fraction [kgi/kg]
Sim. 4.9 - 40°C MEAT(l)
Sim. 4.9 - 40°C CO2(g)
Sim. 4.9 - 40°C rMEA(g)

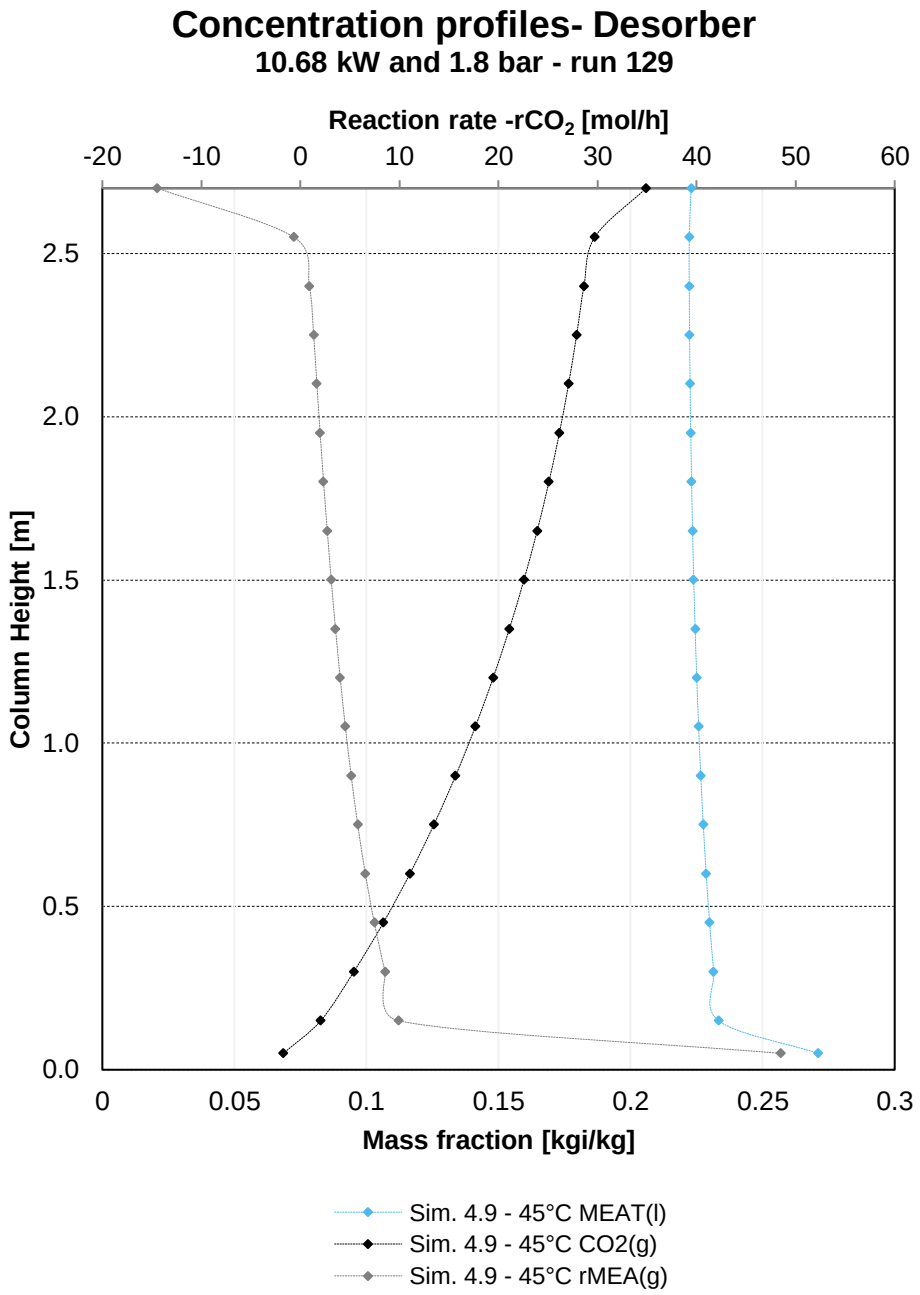
Concentration profiles- Desorber
10.68 kW and 1.8 bar - run 129
Reaction rate -rCO2 [mol/h]
-20
-10
0
10
20
30
40
50
60
Column Height [m]
2.5
2.0
1.5
1.0
0.5
0.0
0
0.05
0.1
0.15
0.2
0.25
0.3
Mass fraction [kgi/kg]
Sim. 4.9 - 45°C MEAT(l)
Sim. 4.9 - 45°C CO2(g)
Sim. 4.9 - 45°C rMEA(g)

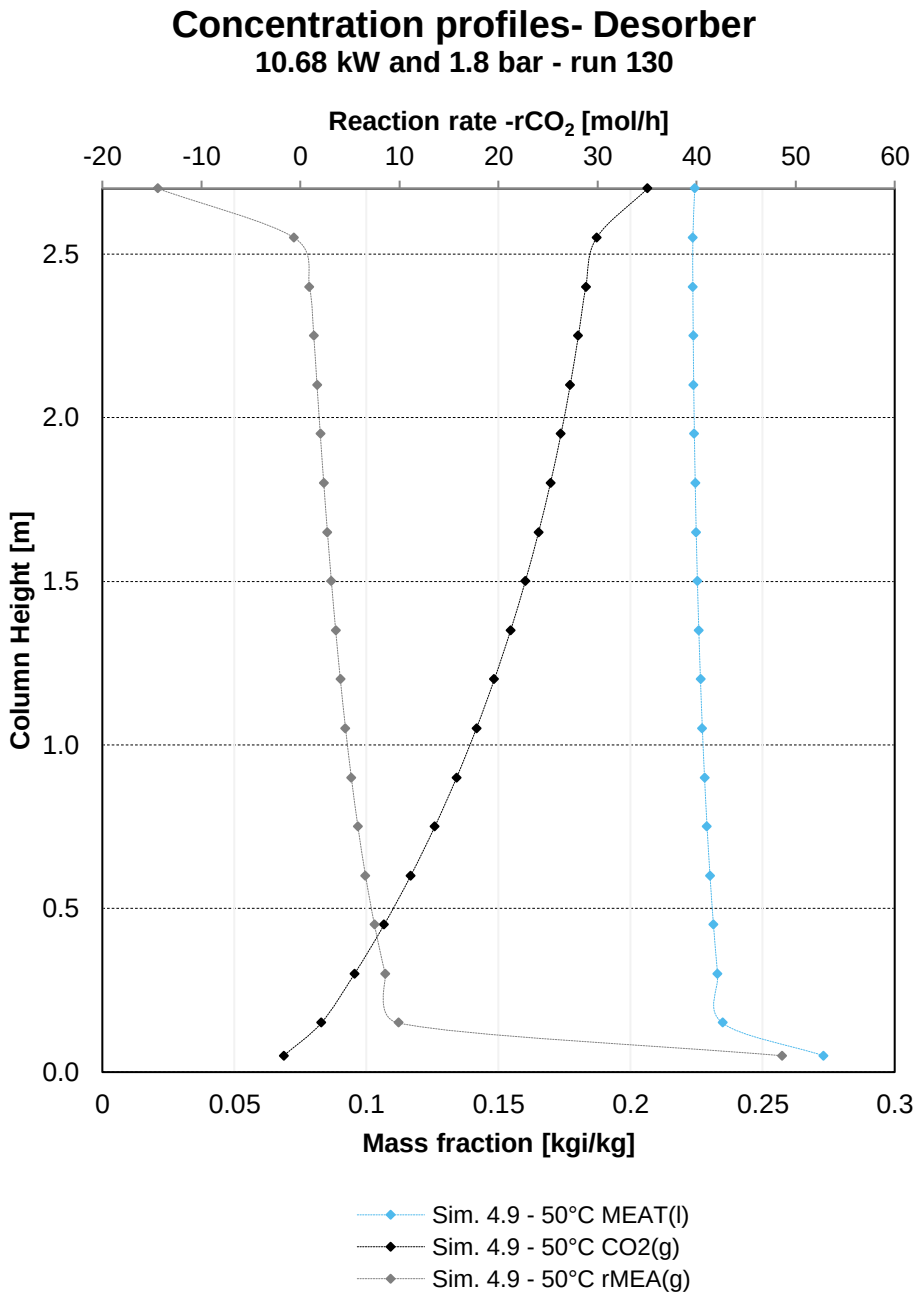
Concentration profiles- Desorber
10.68 kW and 1.8 bar - run 130
Reaction rate -rCO2 [mol/h]
-20
-10
0
10
20
30
40
50
60
Column Height [m]
0.0
0.5
1.0
1.5
2.0
2.5
0
0.05
0.1
0.15
0.2
0.25
0.3
Mass fraction [kgi/kg]
Sim. 4.9 - 50°C MEAT(l)
Sim. 4.9 - 50°C CO2(g)
Sim. 4.9 - 50°C rMEA(g)

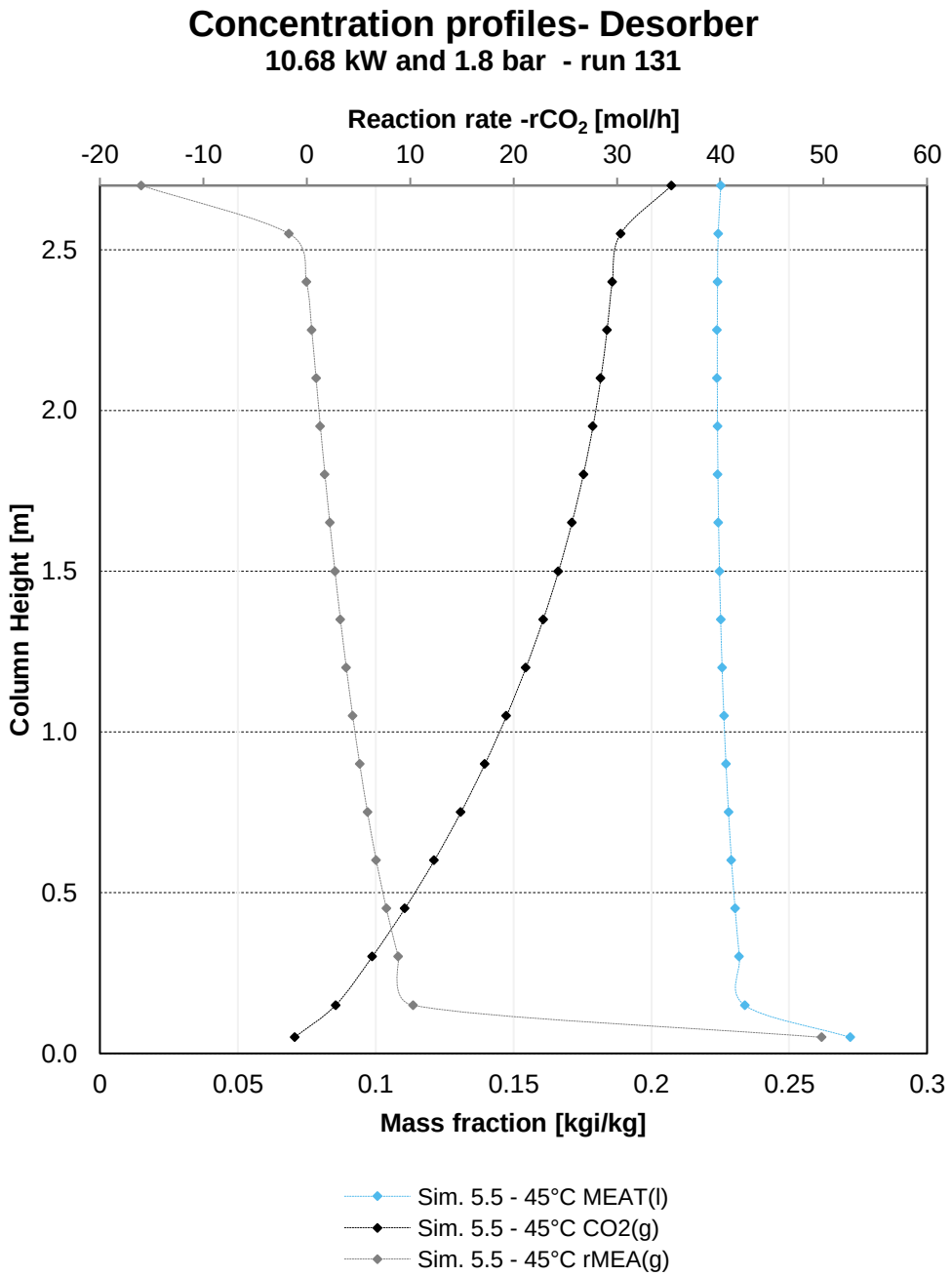
Concentration profiles- Desorber
10.68 kW and 1.8 bar - run 131
Reaction rate -rCO2 [mol/h]
-20
-10
0
10
20
30
40
50
60
Column Height [m]
0.0
0.5
1.0
1.5
2.0
2.5
0
0.05
0.1
0.15
0.2
0.25
0.3
Mass fraction [kgi/kg]
Sim. 5.5 - 45°C MEAT(l)
Sim. 5.5 - 45°C CO2(g)
Sim. 5.5 - 45°C rMEA(g)

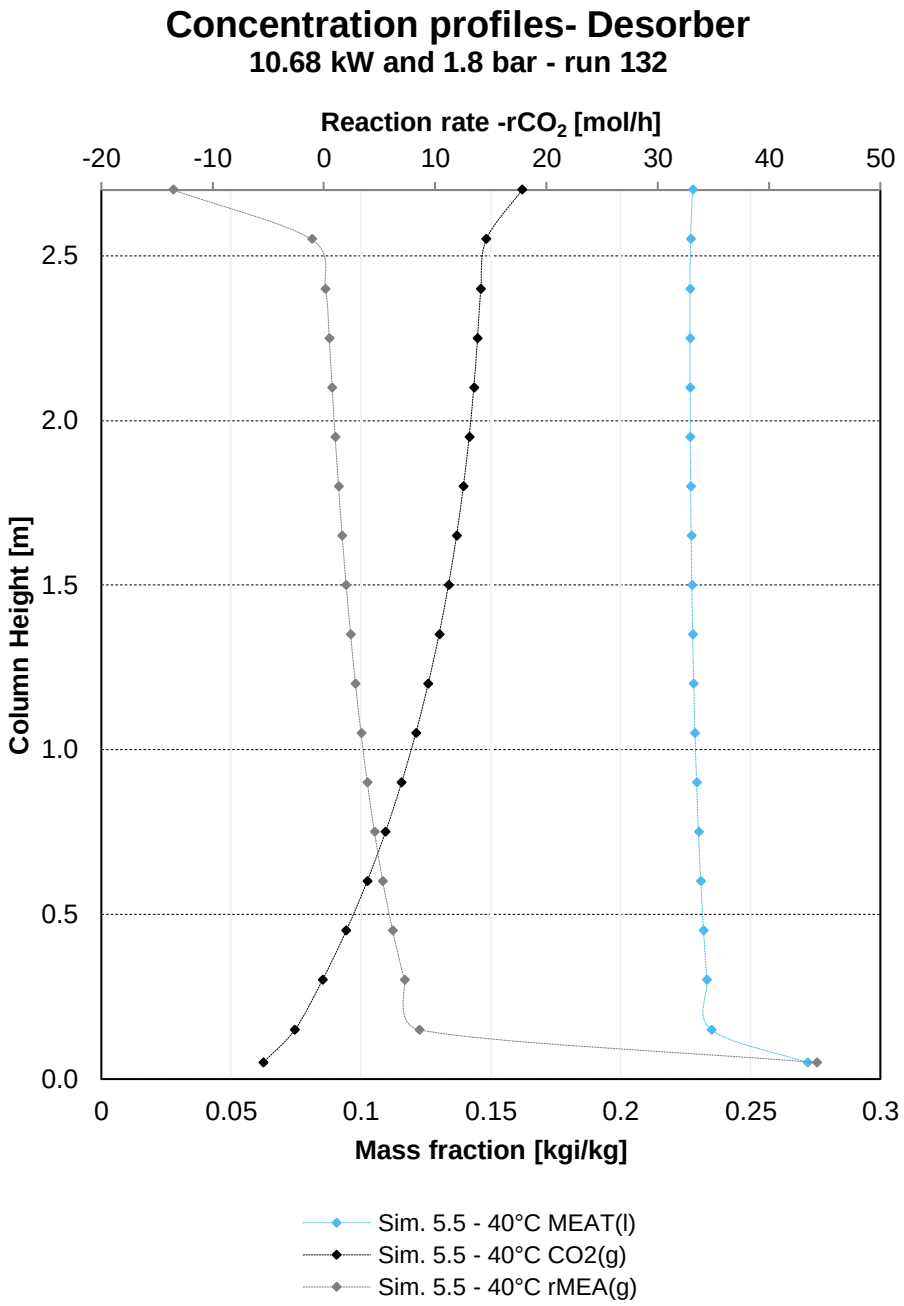
Concentration profiles- Desorber
10.68 kW and 1.8 bar - run 132
Reaction rate -rCO2 [mol/h]
-20
-10
0
10
20
30
40
50
Column Height [m]
0.0
0.5
1.0
1.5
2.0
2.5
0
0.05
0.1
0.15
0.2
0.25
0.3
Mass fraction [kgi/kg]
Sim. 5.5 - 40°C MEAT(l)
Sim. 5.5 - 40°C CO2(g)
Sim. 5.5 - 40°C rMEA(g)

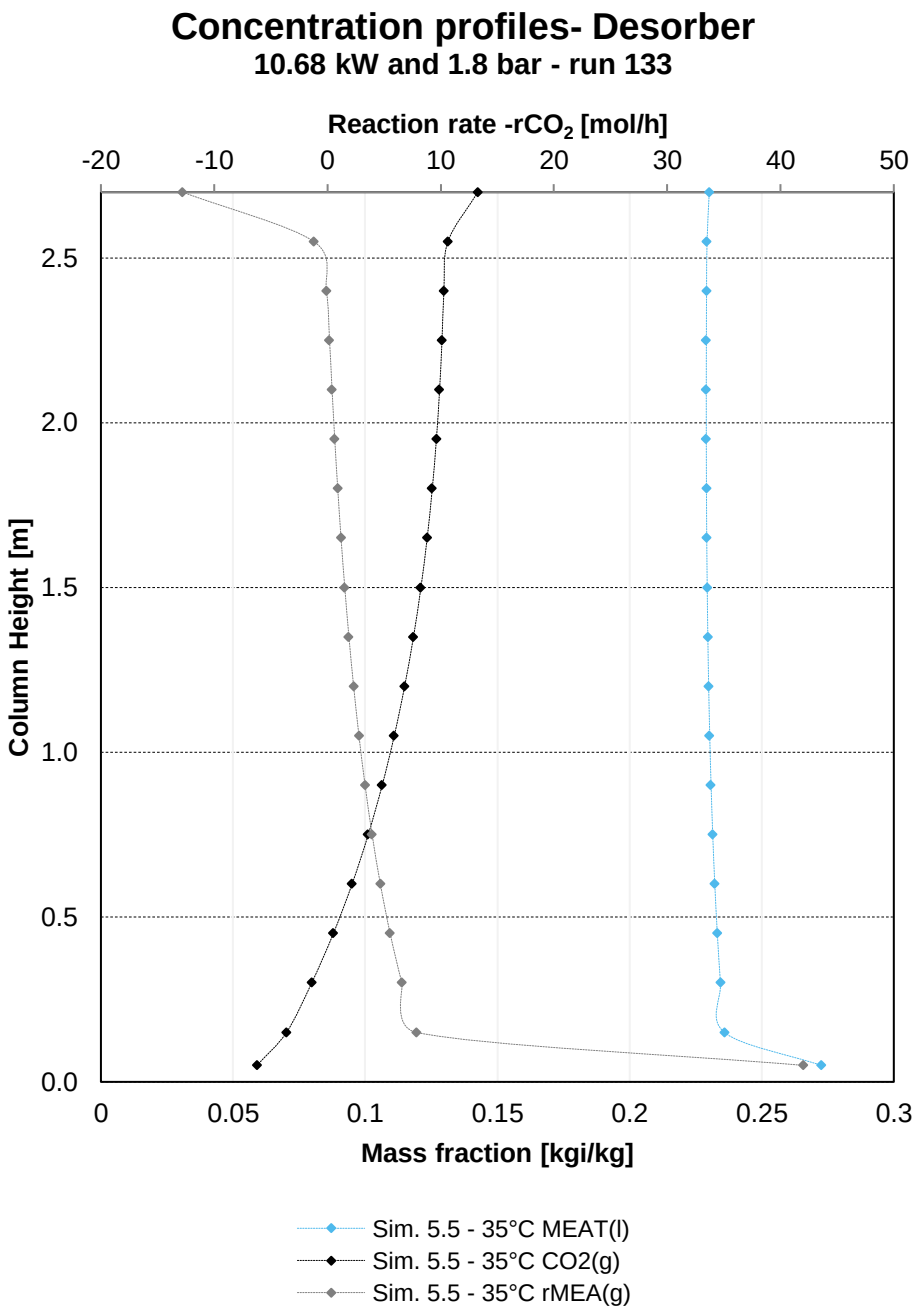
Concentration profiles- Desorber
10.68 kW and 1.8 bar - run 133
Reaction rate -rCO2 [mol/h]
-20
-10
0
10
20
30
40
50
Column Height [m]
0.0
0.5
1.0
1.5
2.0
2.5
0
0.05
0.1
0.15
0.2
0.25
0.3
Mass fraction [kgi/kg]
Sim. 5.5 - 35°C MEAT(l)
Sim. 5.5 - 35°C CO2(g)
Sim. 5.5 - 35°C rMEA(g)

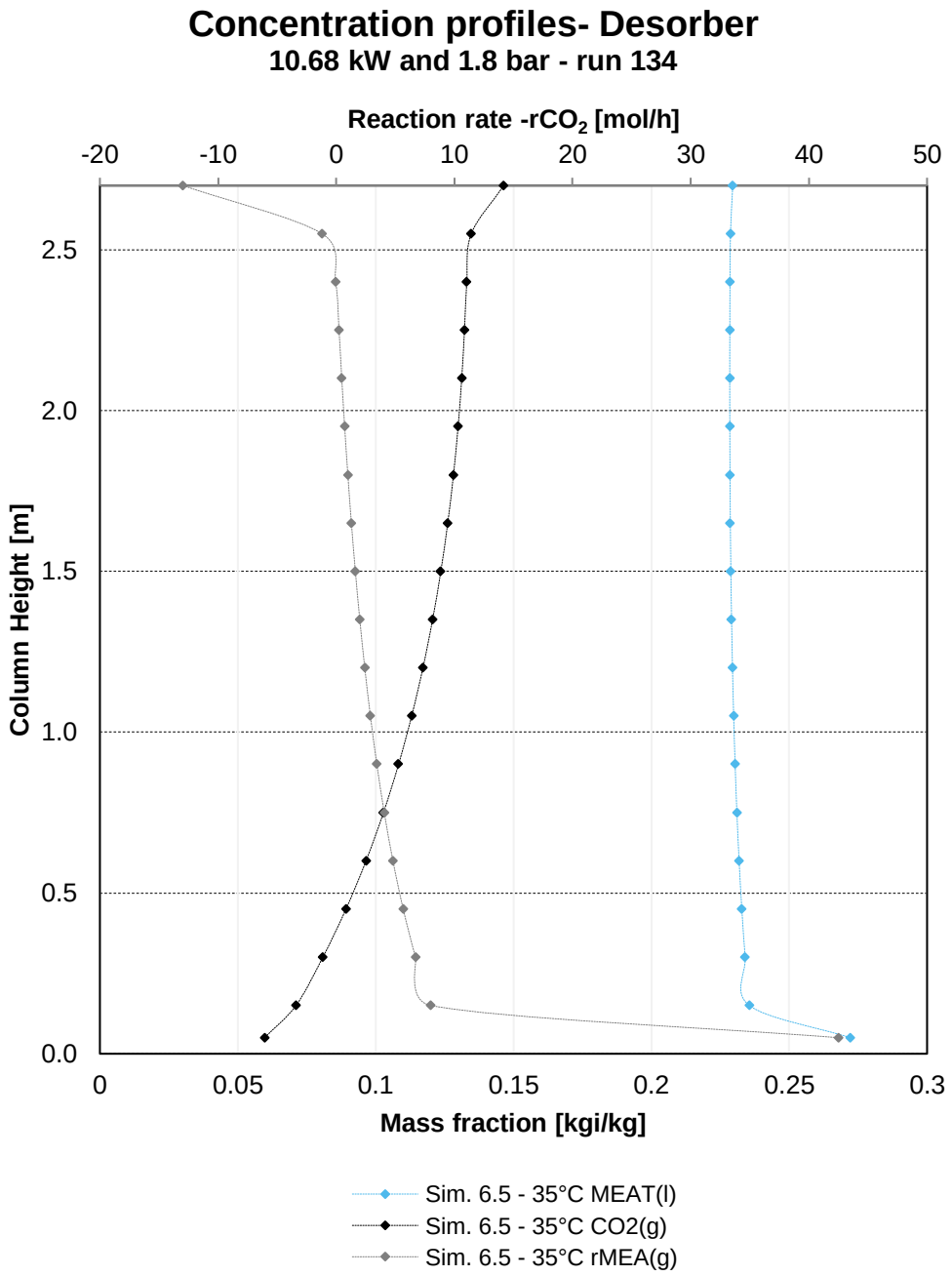
Concentration profiles- Desorber
10.68 kW and 1.8 bar - run 134
Reaction rate -rCO2 [mol/h]
-20
-10
0
10
20
30
40
50
Column Height [m]
0.0
0.5
1.0
1.5
2.0
2.5
0
0.05
0.1
0.15
0.2
0.25
0.3
Mass fraction [kgi/kg]
Sim. 6.5 - 35°C MEAT(l)
Sim. 6.5 - 35°C CO2(g)
Sim. 6.5 - 35°C rMEA(g)

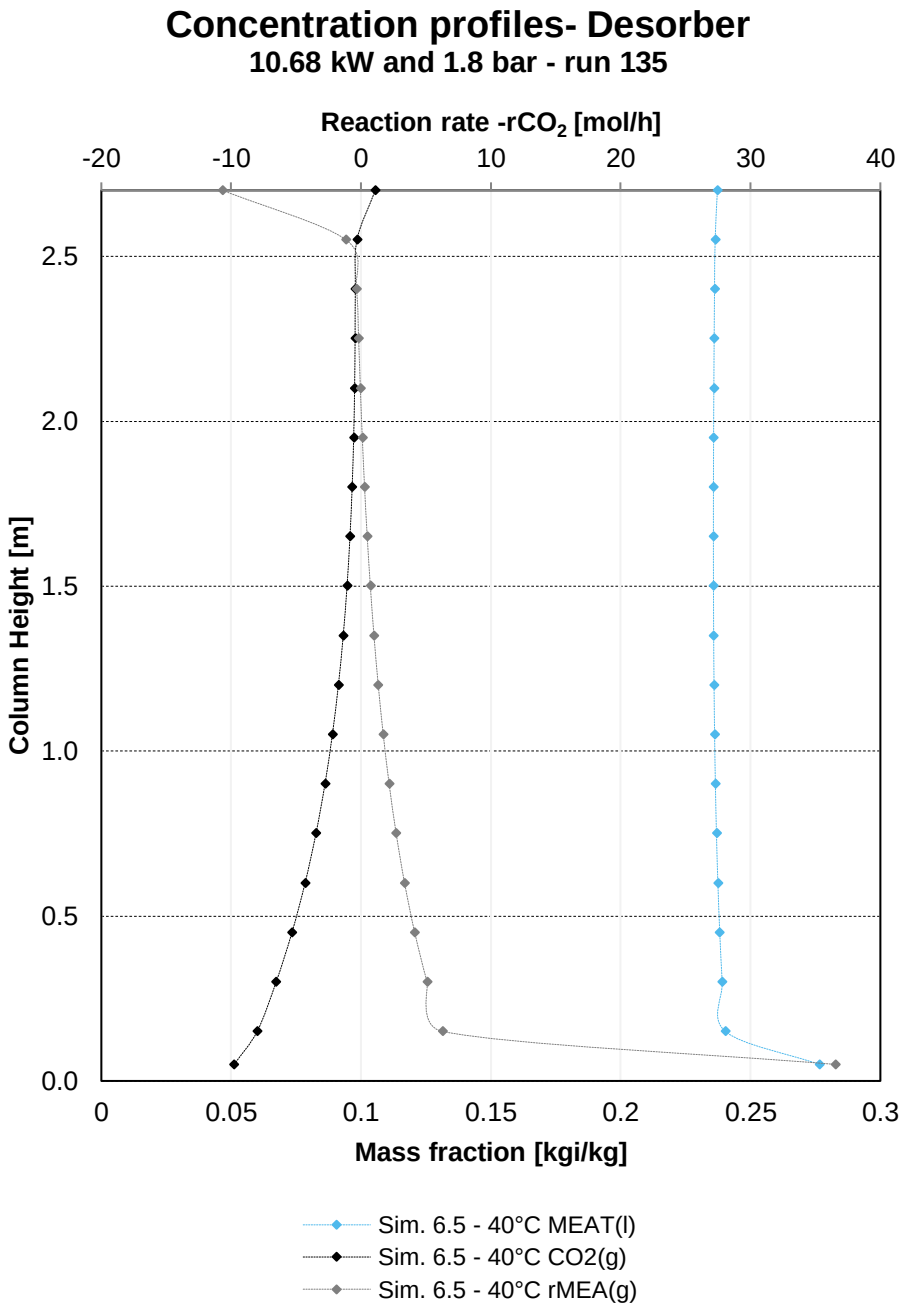
Concentration profiles- Desorber
10.68 kW and 1.8 bar - run 135
Reaction rate -rCO2 [mol/h]
-20
-10
0
10
20
30
40
Column Height [m]
2.5
2.0
1.5
1.0
0.5
0.0
0
0.05
0.1
0.15
0.2
0.25
0.3
Mass fraction [kgi/kg]
Sim. 6.5 - 40°C MEAT(l)
Sim. 6.5 - 40°C CO2(g)
Sim. 6.5 - 40°C rMEA(g)

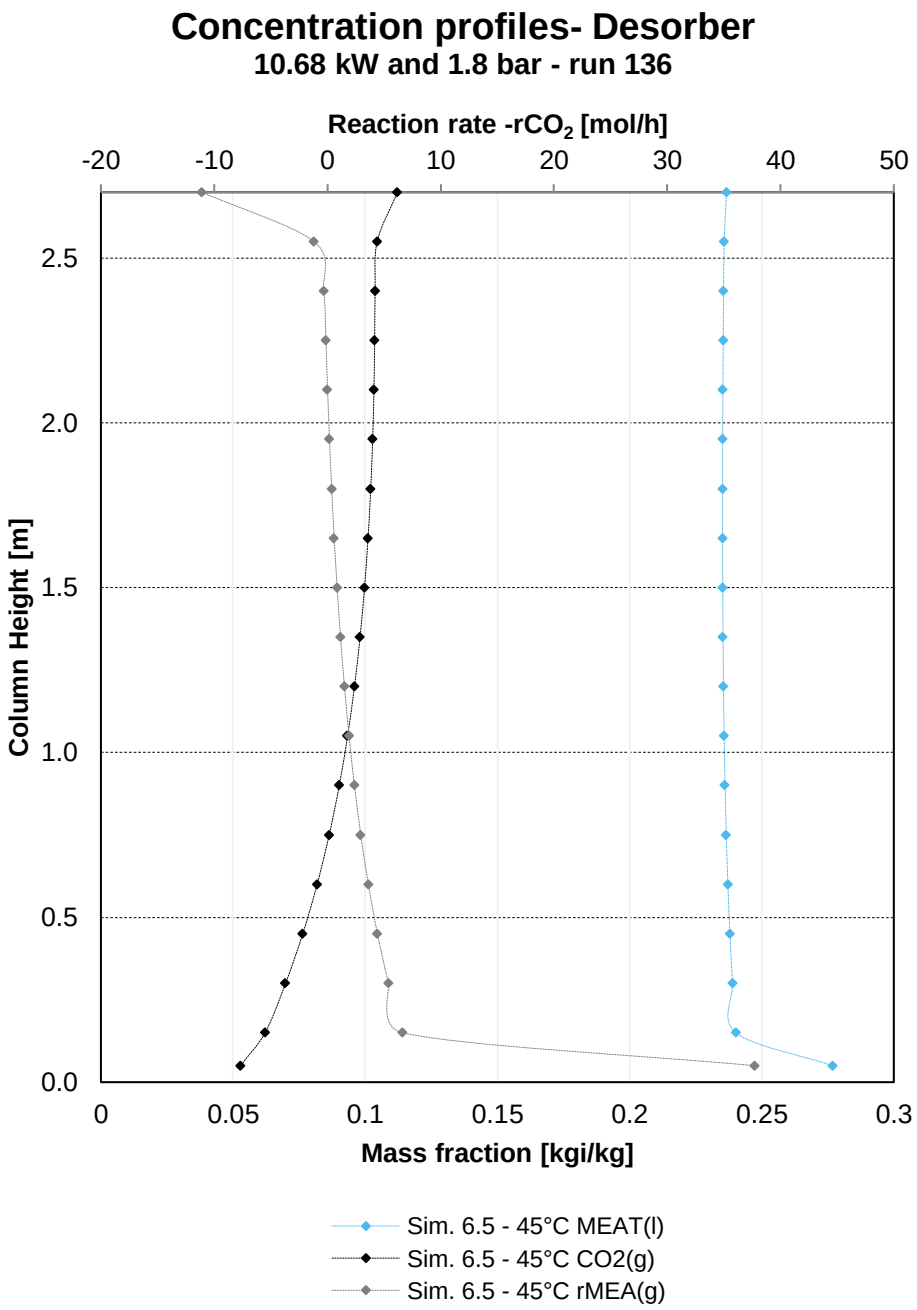
Concentration profiles- Desorber
10.68 kW and 1.8 bar - run 136
Reaction rate -rCO2 [mol/h]
-20
-10
0
10
20
30
40
50
Column Height [m]
2.5
2.0
1.5
1.0
0.5
0.0
0
0.05
0.1
0.15
0.2
0.25
0.3
Mass fraction [kgi/kg]
Sim. 6.5 - 45°C MEAT(l)
Sim. 6.5 - 45°C CO2(g)
Sim. 6.5 - 45°C rMEA(g)

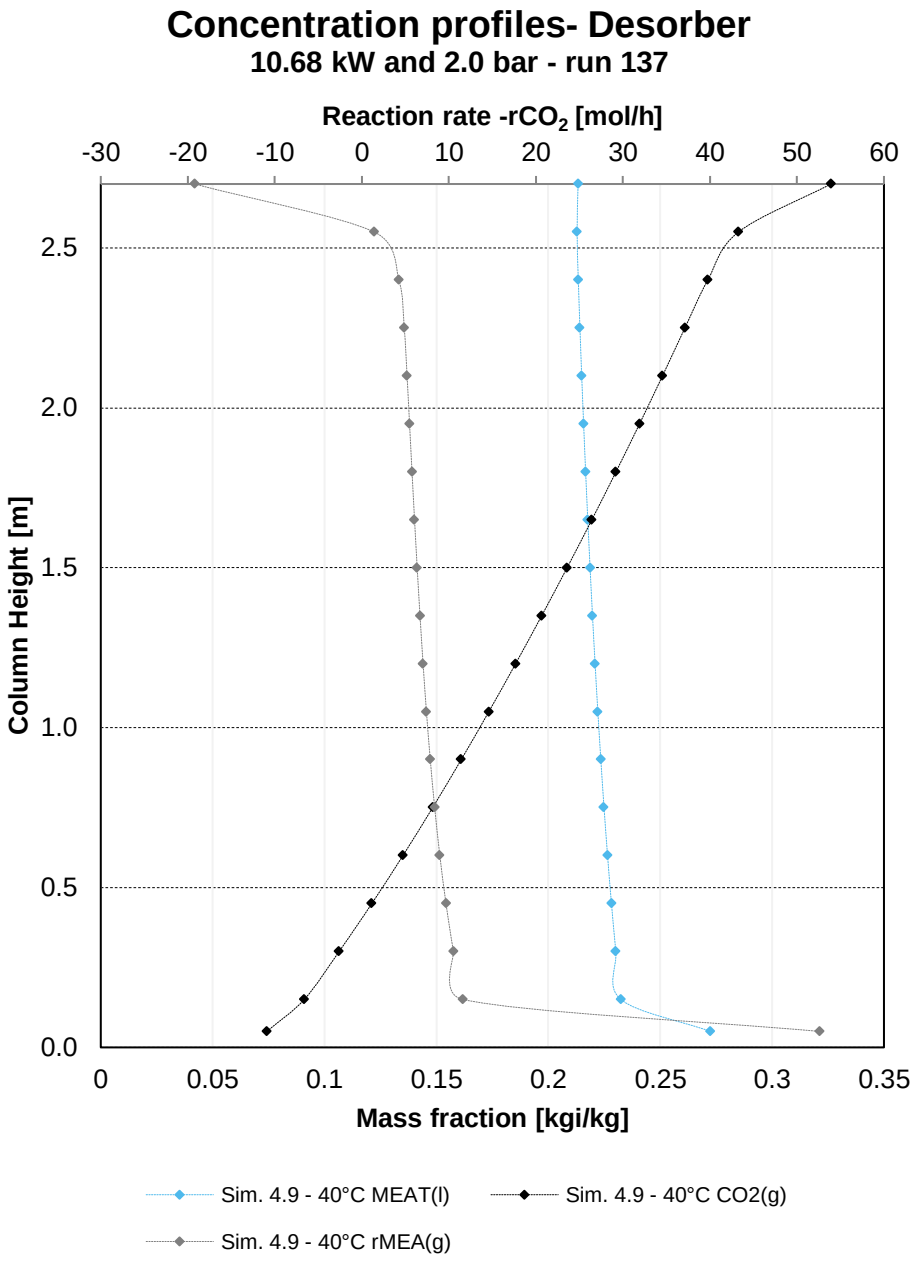
Concentration profiles- Desorber
10.68 kW and 2.0 bar - run 137
Reaction rate -rCO2 [mol/h]
-30
-20
-10
0
10
20
30
40
50
60
Column Height [m]
2.5
2.0
1.5
1.0
0.5
0.0
0
0.05
0.1
0.15
0.2
0.25
0.3
0.35
Mass fraction [kgi/kg]
Sim. 4.9 - 40°C MEAT(l)
Sim. 4.9 - 40°C CO2(g)
Sim. 4.9 - 40°C rMEA(g)

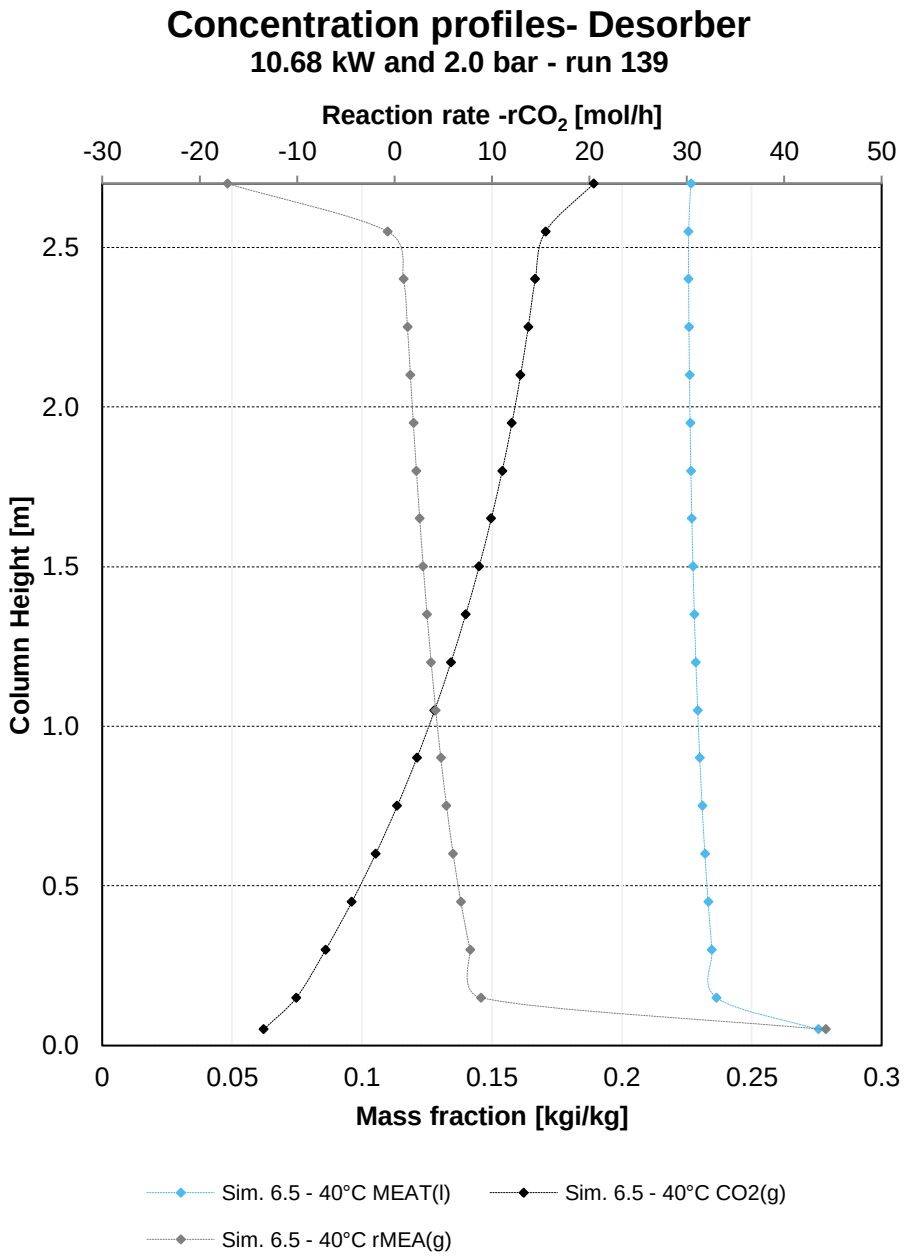
Concentration profiles- Desorber
10.68 kW and 2.0 bar - run 139
Reaction rate -rCO2 [mol/h]
-30
-20
-10
0
10
20
30
40
50
Column Height [m]
0.0
0.5
1.0
1.5
2.0
2.5
0
0.05
0.1
0.15
0.2
0.25
0.3
Mass fraction [kgi/kg]
Sim. 6.5 - 40°C MEAT(l)
Sim. 6.5 - 40°C CO2(g)
Sim. 6.5 - 40°C rMEA(g)

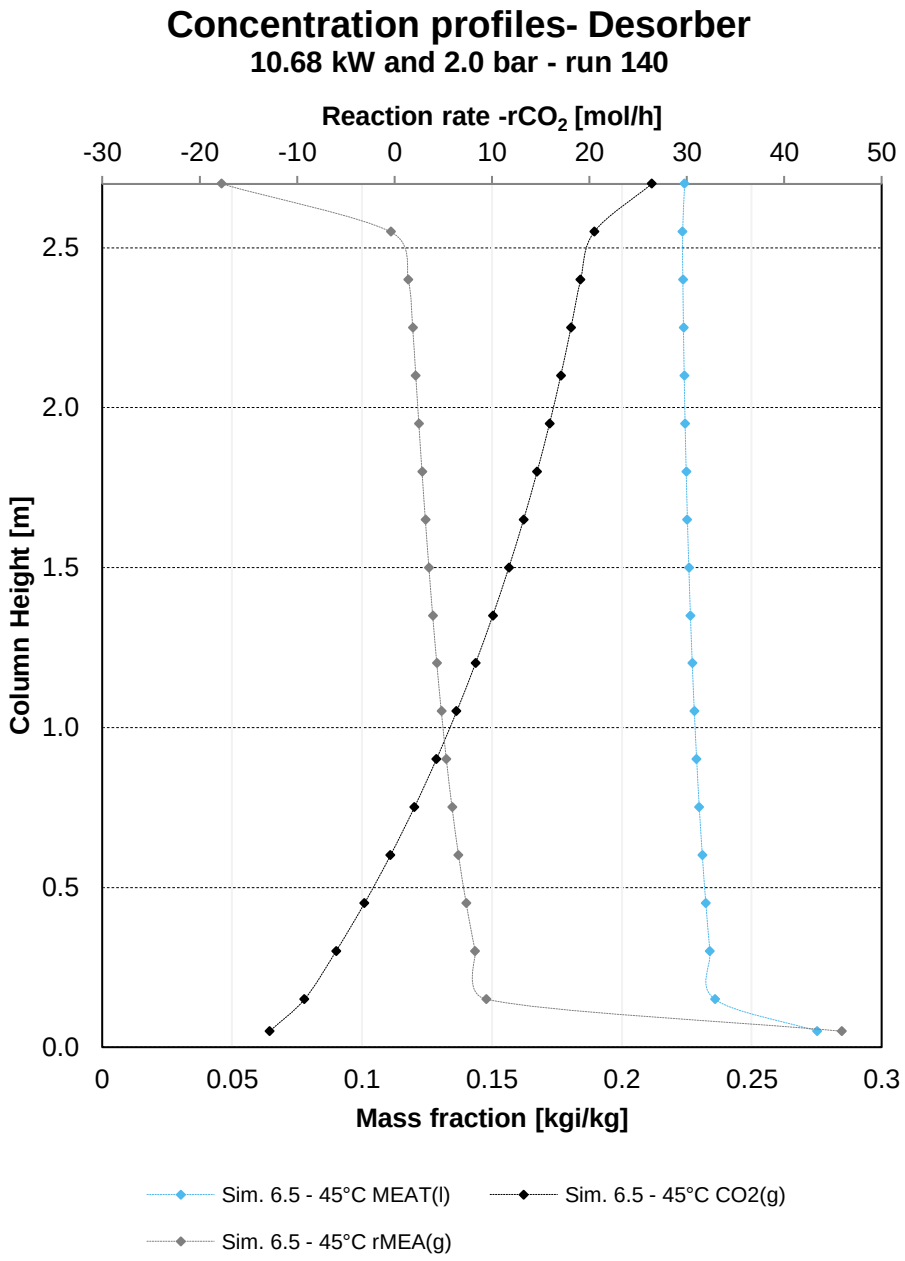
Concentration profiles- Desorber
10.68 kW and 2.0 bar - run 140
Reaction rate -rCO2 [mol/h]
-30
-20
-10
0
10
20
30
40
50
Column Height [m]
0.0
0.5
1.0
1.5
2.0
2.5
0
0.05
0.1
0.15
0.2
0.25
0.3
Mass fraction [kgi/kg]
Sim. 6.5 - 45°C MEAT(l)
Sim. 6.5 - 45°C CO2(g)
Sim. 6.5 - 45°C rMEA(g)

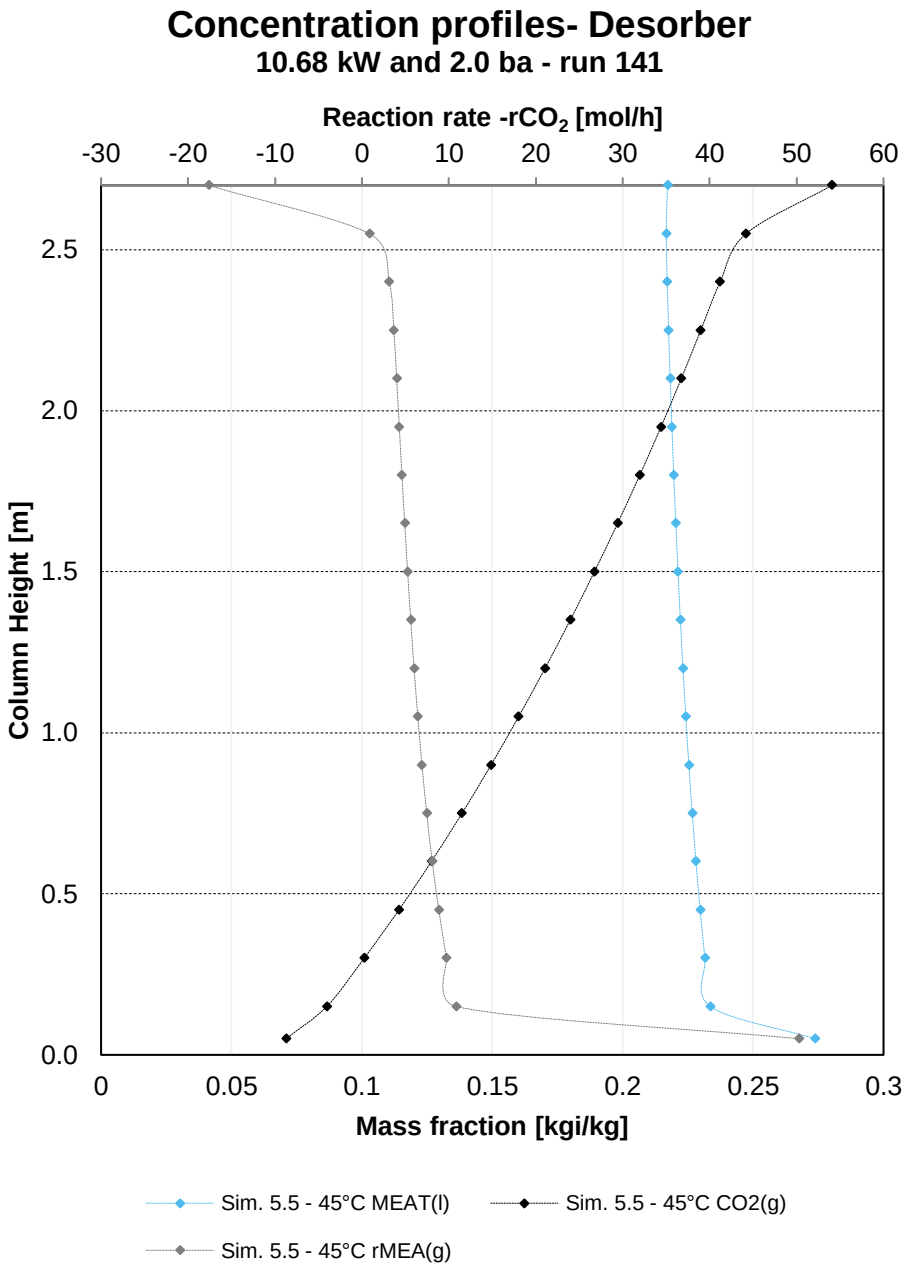
Concentration profiles- Desorber
10.68 kW and 2.0 ba - run 141
Reaction rate -rCO2 [mol/h]
-30
-20
-10
0
10
20
30
40
50
60
Column Height [m]
2.5
2.0
1.5
1.0
0.5
0.0
0
0.05
0.1
0.15
0.2
0.25
0.3
Mass fraction [kgi/kg]
Sim. 5.5 - 45°C MEAT(l)
Sim. 5.5 - 45°C CO2(g)
Sim. 5.5 - 45°C rMEA(g)

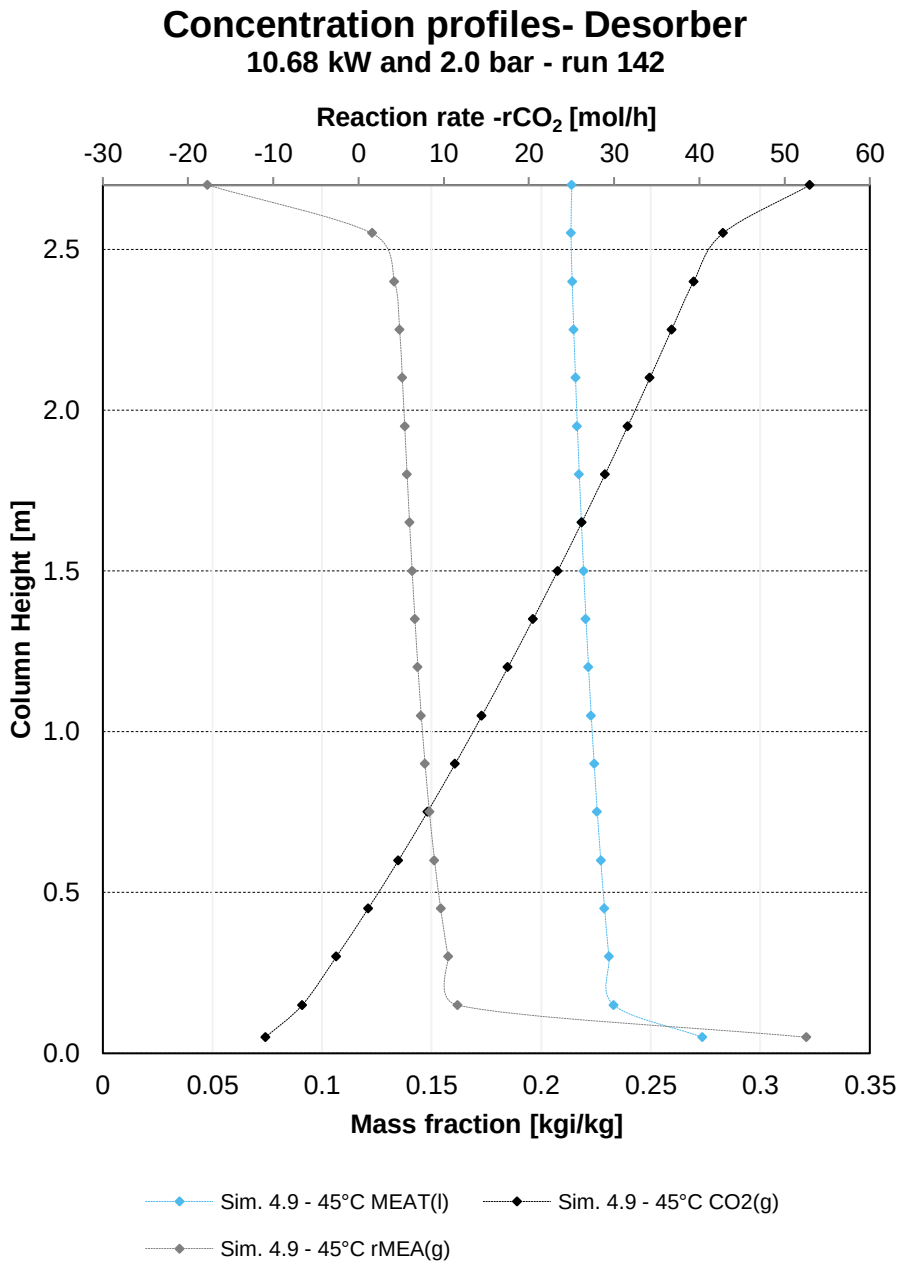
Concentration profiles- Desorber
10.68 kW and 2.0 bar - run 142
Reaction rate -rCO2 [mol/h]
-30
-20
-10
0
10
20
30
40
50
60
Column Height [m]
2.5
2.0
1.5
1.0
0.5
0.0
0
0.05
0.1
0.15
0.2
0.25
0.3
0.35
Mass fraction [kgi/kg]
Sim. 4.9 - 45°C MEAT(l)
Sim. 4.9 - 45°C CO2(g)
Sim. 4.9 - 45°C rMEA(g)

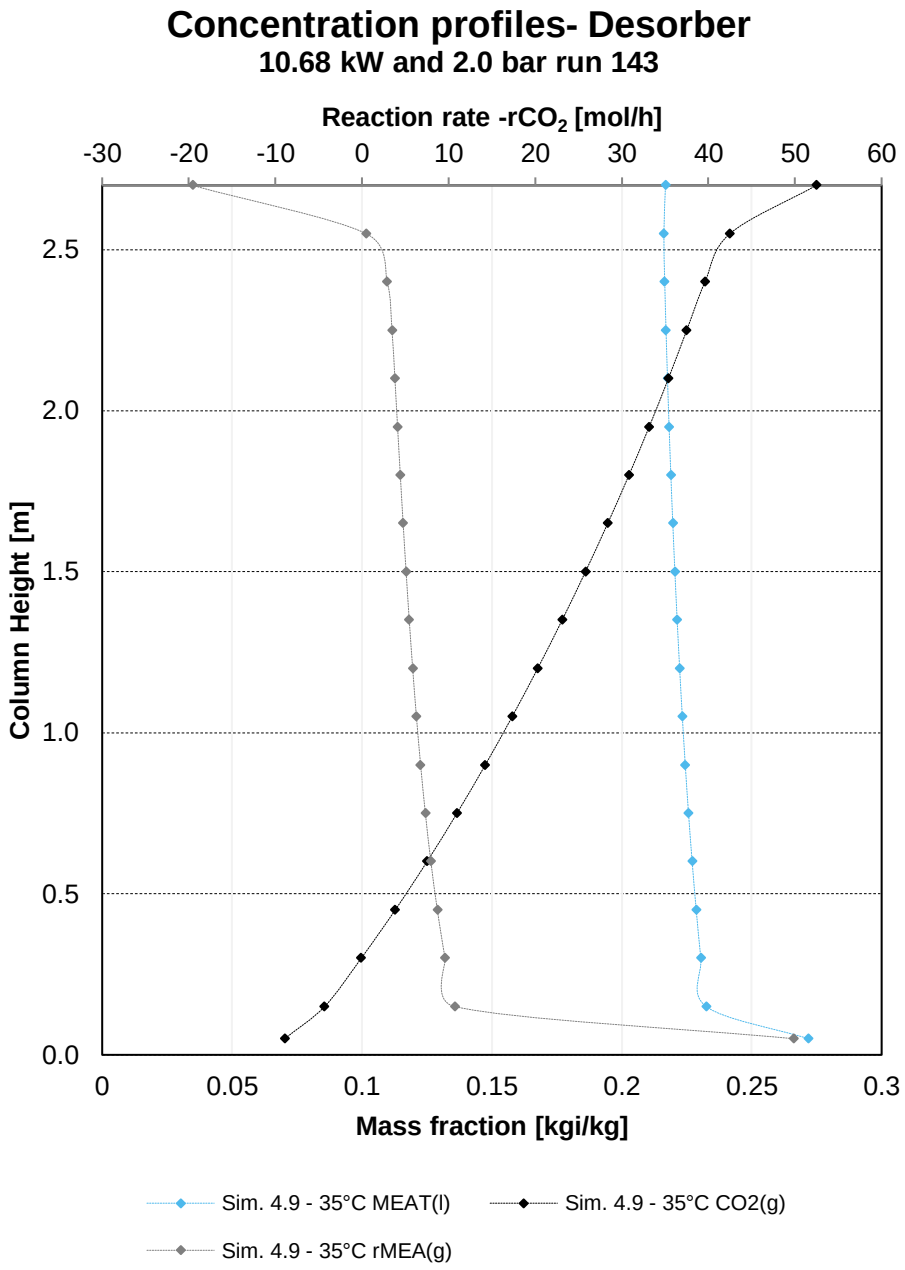
Concentration profiles- Desorber
10.68 kW and 2.0 bar run 143
Reaction rate -rCO2 [mol/h]
-30
-20
-10
0
10
20
30
40
50
60
Column Height [m]
2.5
2.0
1.5
1.0
0.5
0.0
0
0.05
0.1
0.15
0.2
0.25
0.3
Mass fraction [kgi/kg]
Sim. 4.9 - 35°C MEAT(l)
Sim. 4.9 - 35°C CO2(g)
Sim. 4.9 - 35°C rMEA(g)

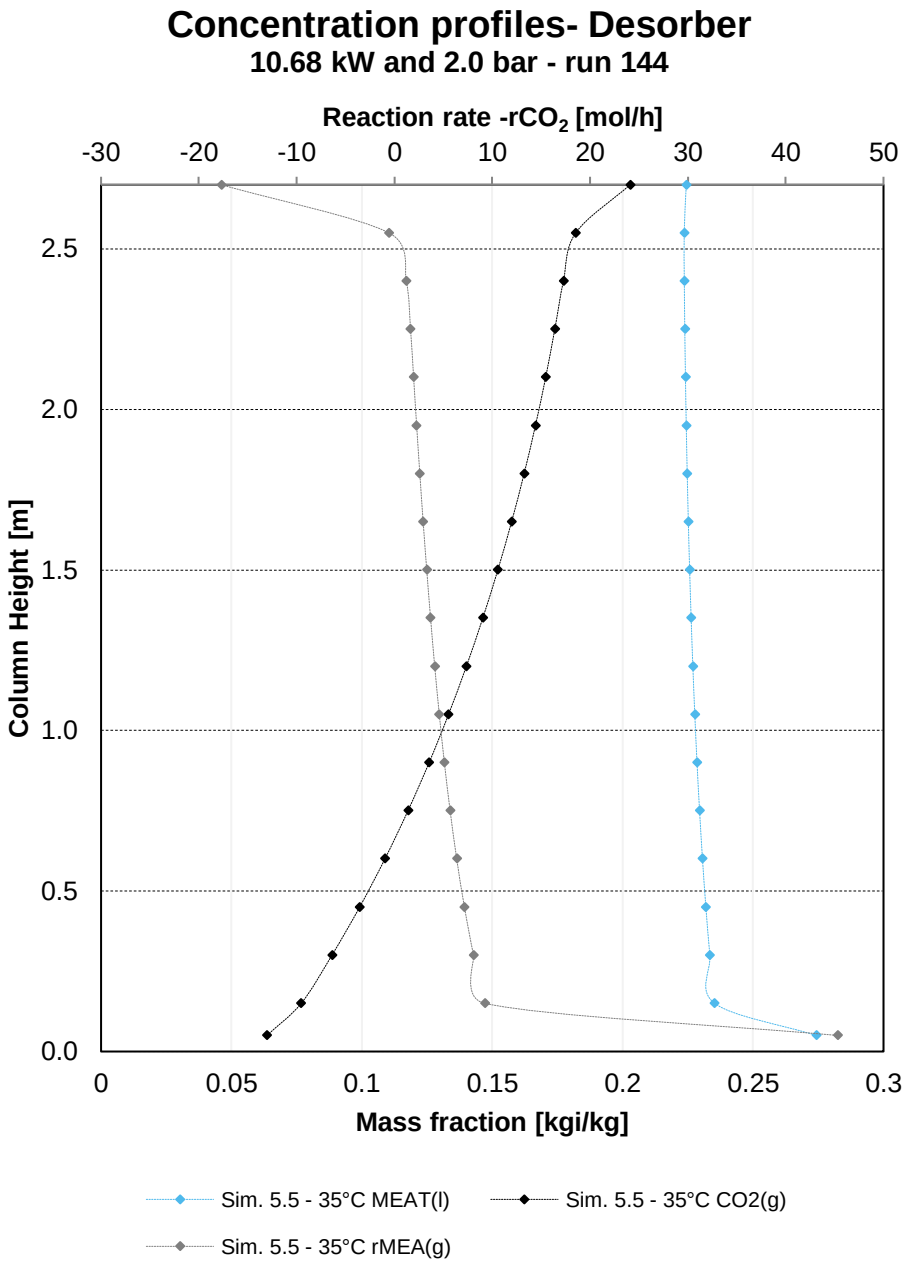
Concentration profiles- Desorber
10.68 kW and 2.0 bar - run 144
Reaction rate -rCO2 [mol/h]
-30
-20
-10
0
10
20
30
40
50
Column Height [m]
2.5
2.0
1.5
1.0
0.5
0.0
0
0.05
0.1
0.15
0.2
0.25
0.3
Mass fraction [kgi/kg]
Sim. 5.5 - 35°C MEAT(l)
Sim. 5.5 - 35°C CO2(g)
Sim. 5.5 - 35°C rMEA(g)

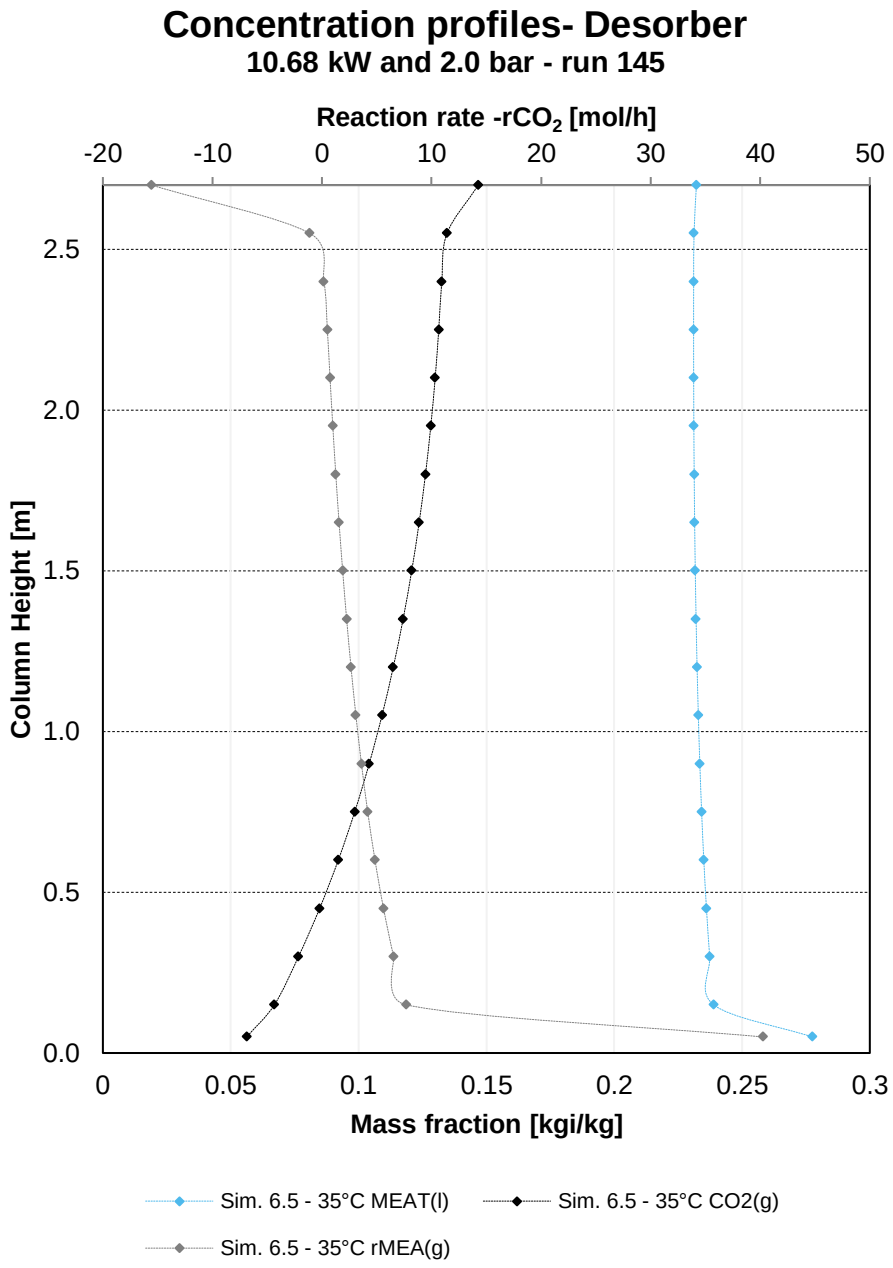
Concentration profiles- Desorber
10.68 kW and 2.0 bar - run 145
Reaction rate -rCO2 [mol/h]
-20
-10
0
10
20
30
40
50
Column Height [m]
0.0
0.5
1.0
1.5
2.0
2.5
0
0.05
0.1
0.15
0.2
0.25
0.3
Mass fraction [kgi/kg]
Sim. 6.5 - 35°C MEAT(l)
Sim. 6.5 - 35°C CO2(g)
Sim. 6.5 - 35°C rMEA(g)

General validation graph
run 128

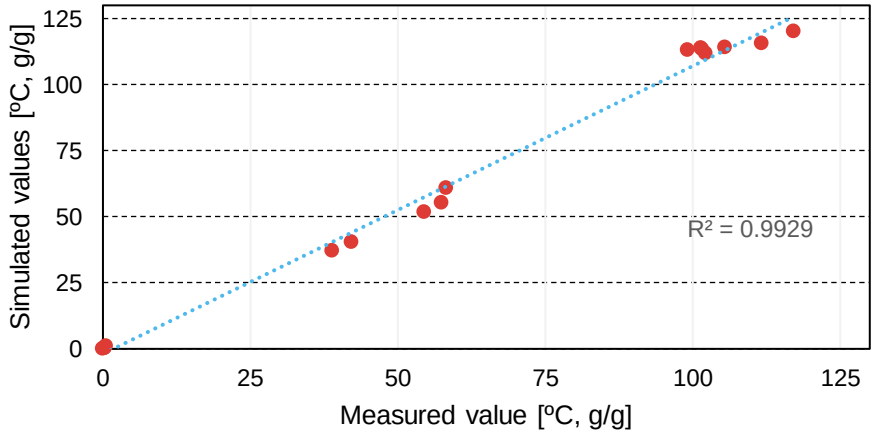

General validation graph
run 129

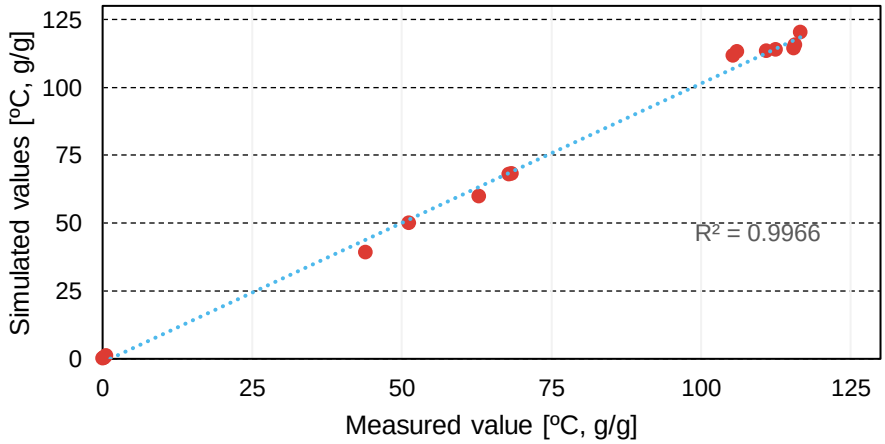

General validation graph
run 130

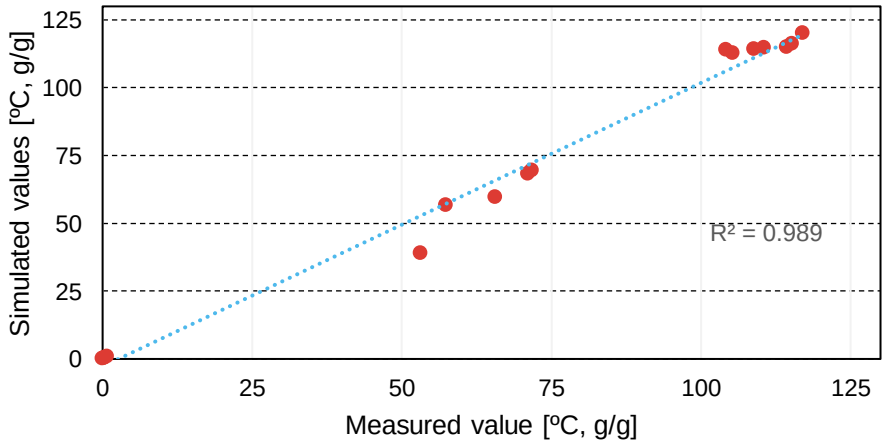

General validation graph
run 131

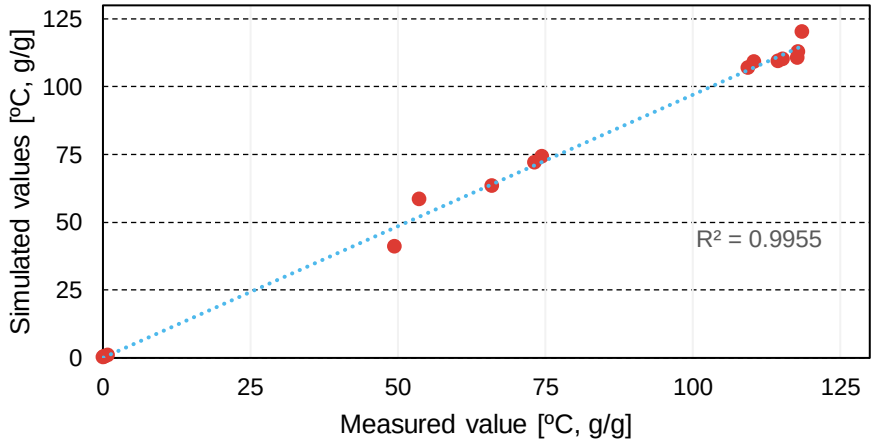

General validation graph
run 132

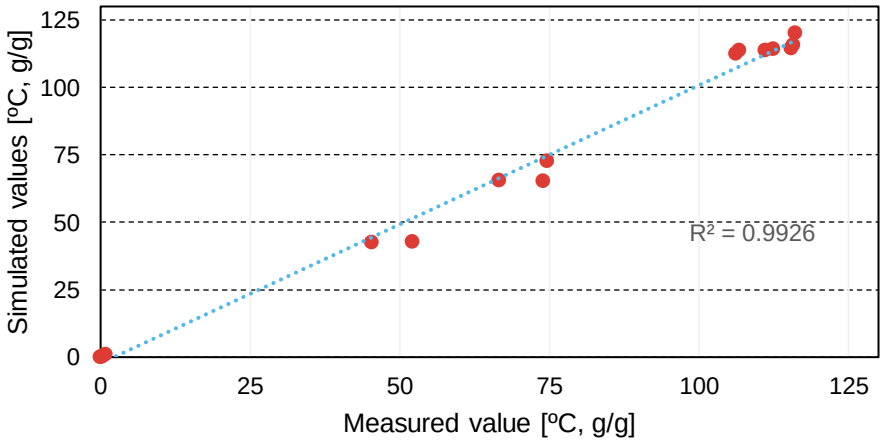

General validation graph
run 133

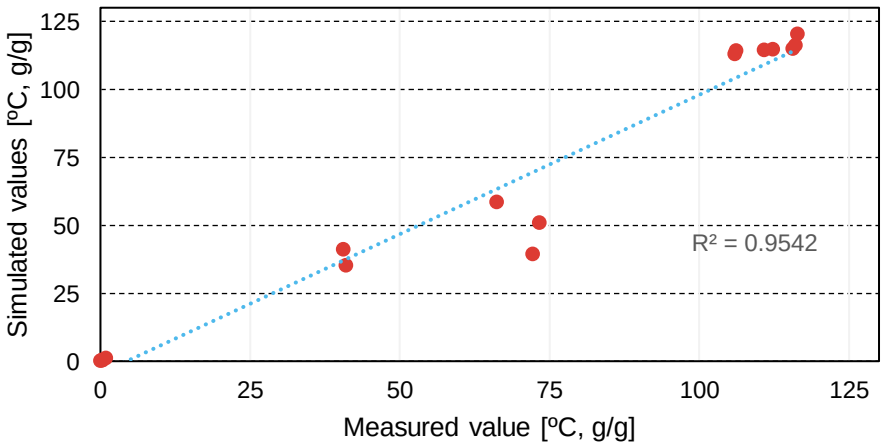

General validation graph run 134

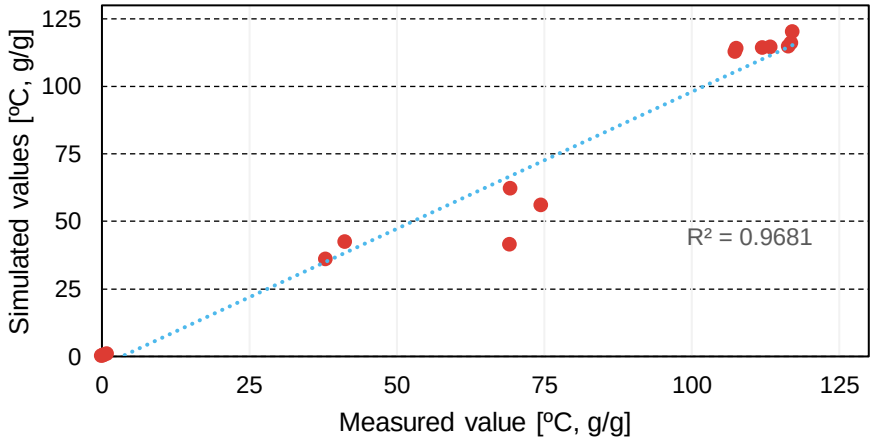

General validation graph run 135

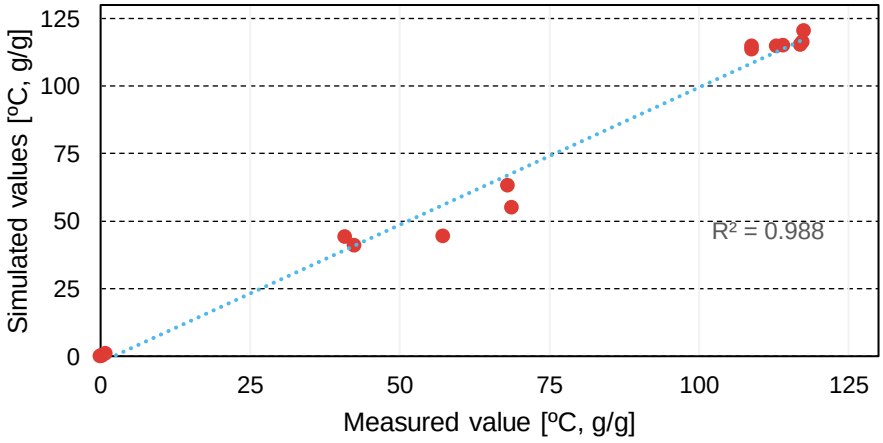

General validation graph run 136

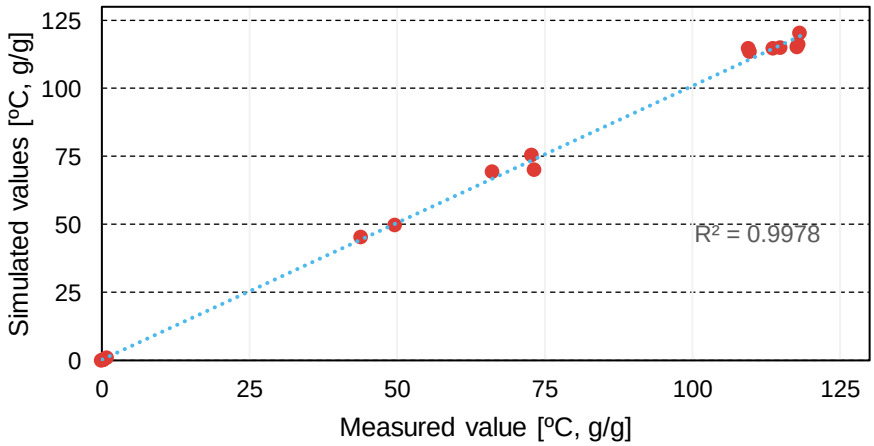

General validation graph
run 137

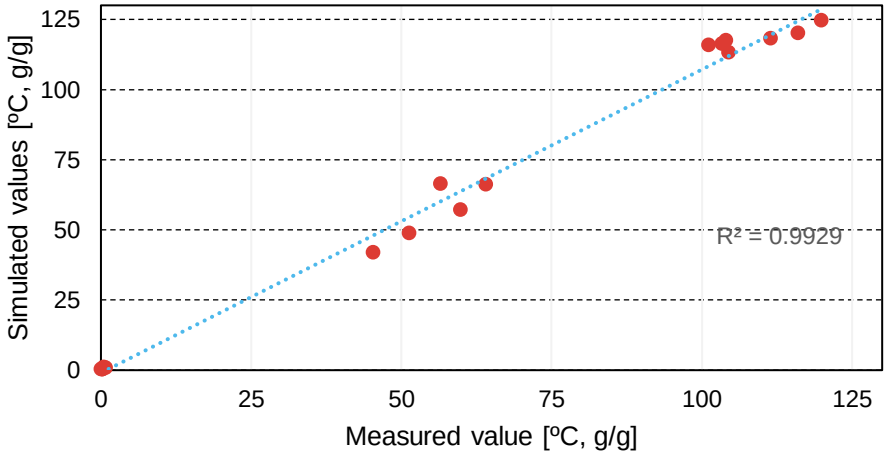

General validation graph
run 139

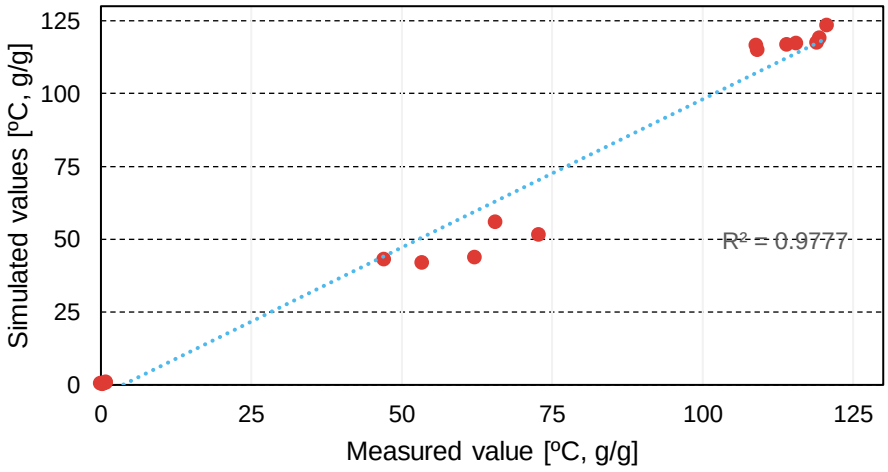

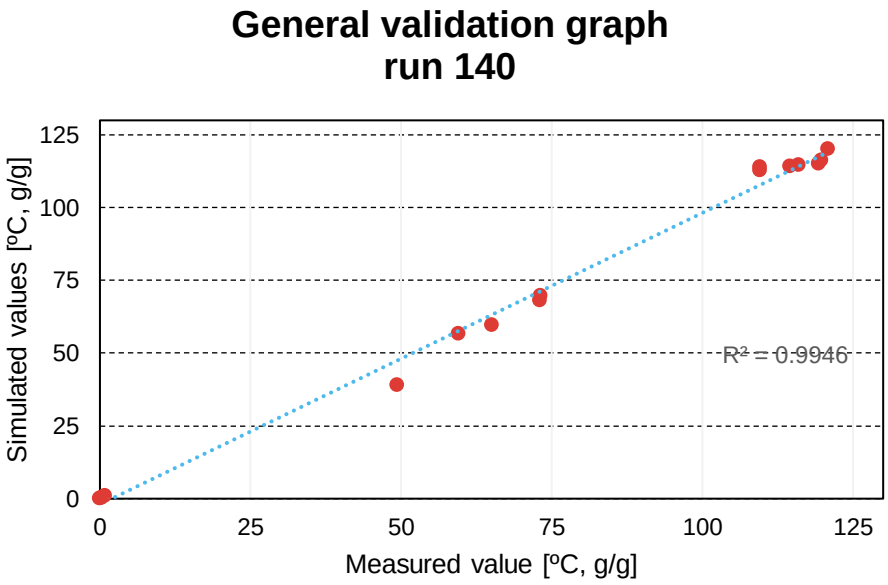
General validation graph
run 140
Simulated values [ºC, g/g]
Measured value [ºC, g/g]
R² = 0.9946
0
25
50
75
100
125

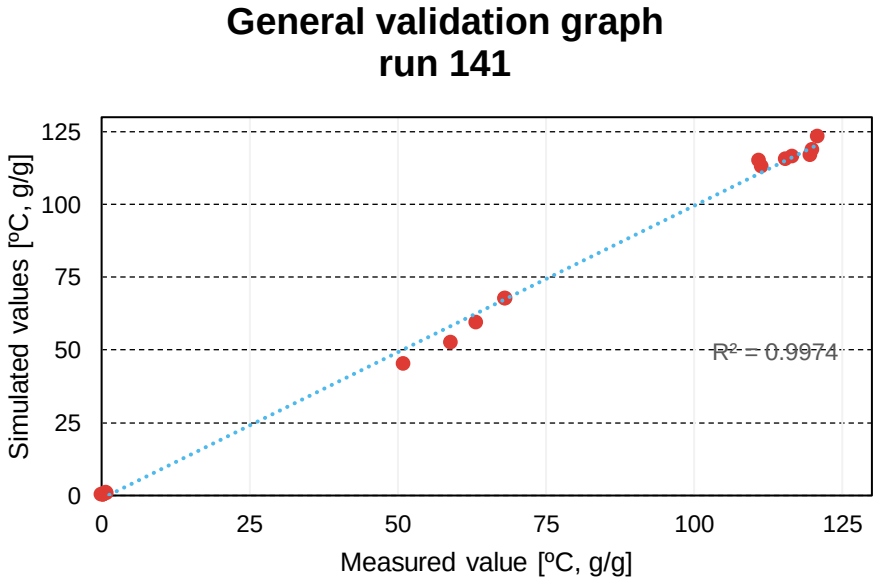
General validation graph
run 141
Simulated values [ºC, g/g]
Measured value [ºC, g/g]
R² = 0.9974
0
25
50
75
100
125

General validation graph
run 142

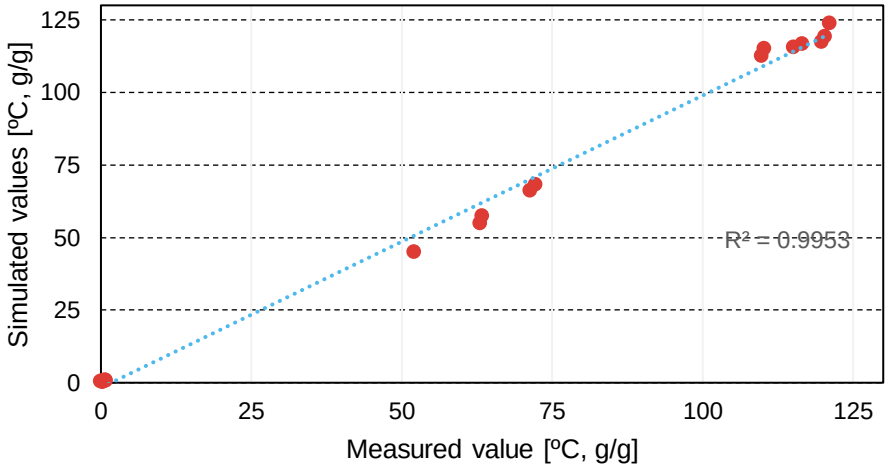

General validation graph
run 143

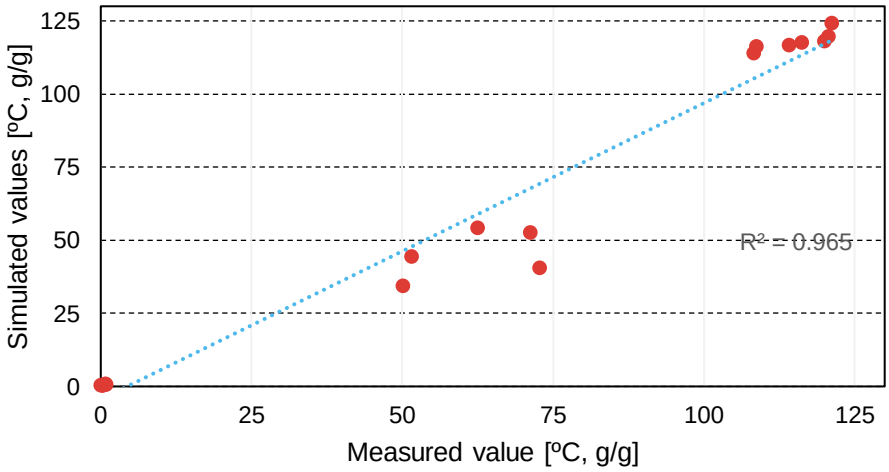

General validation graph
run 144

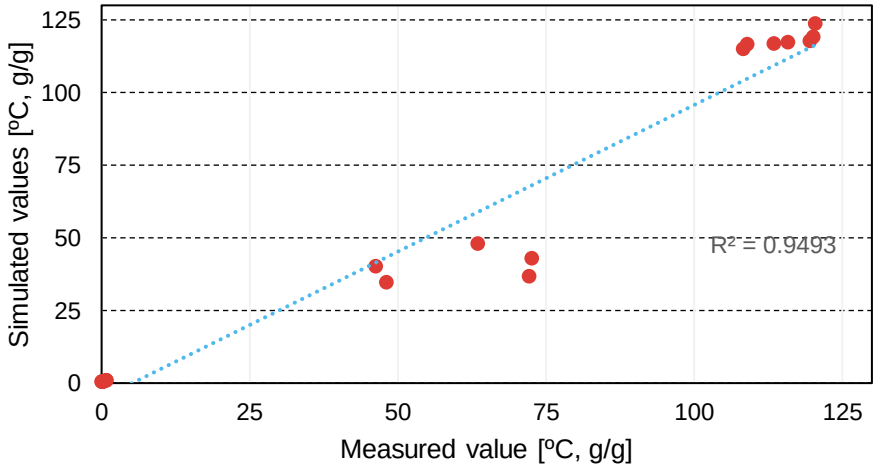

General validation graph
run 145